

Table of Contents

Chapter 1	Introduction.....	1
1.1	Background and motivation	2
1.1.1	Gait Disorder and Rehabilitation	2
1.1.2	Previous work in the author’s research group.....	5
1.2	Research objectives	7
1.3	Thesis outline and contributions	8
Chapter 2	Literature review	10
2.1	Conventional gait rehabilitation approaches	11
2.2	Gait rehabilitation robots.....	13
2.2.1	Previous designs of gait rehabilitation robots	13
2.2.2	Analysis of reviewed designs.....	17
2.3	Control strategies of robotic gait rehabilitation.....	18
2.3.1	Trajectory tracking control	18
2.3.2	Bio-cooperative control	19
2.3.3	AAN control algorithms	20
2.4	Clinical effectiveness of robotic gait rehabilitation training.....	25
2.4.1	Trials with trajectory tracking controlled robots	29
2.4.2	Trials on AAN controlled robots	30
2.5	Approaches to assess gait ability.....	32
2.6	Discussion	35
2.7	Conclusions	38
Chapter 3	Development of a Compliant Gait Rehabilitation Exoskeleton.....	39
3.1	Introduction	40
3.2	Support structure and trunk mechanism.....	41
3.3	Lower Limb Exoskeleton	43

3.3.1	Actuation system of the lower limb exoskeleton	43
3.3.2	Mechanical design of the lower limb exoskeleton.....	48
3.3.3	Pneumatic system.....	50
3.4	Instrumentation.....	52
3.5	Safety and adaptability of GAREX.....	54
3.6	Discussion and conclusions.....	54
Chapter 4	Force Dynamics Model of the Pneumatic Muscle Actuators	56
4.1	Introduction	57
4.2	Modelling the dynamic characteristics of the PM.....	59
4.3	Experimental setup and procedures.....	60
4.4	Result Analysis.....	62
4.5	Discussion and conclusions.....	68
Chapter 5	Joint Space Trajectory and Compliance Control	69
5.1	Introduction	70
5.2	System modelling.....	72
5.2.1	Flow dynamics of the analogue valves	73
5.2.2	Pressure Dynamics of the PM.....	74
5.2.3	Force dynamics of the PM actuation system	75
5.2.4	Load dynamics of the knee joint mechanism.....	75
5.3	SISO trajectory control of the knee joint mechanism	77
5.3.1	Control algorithm development	77
5.3.2	Experimental setup and validation of the SISO SM controller.....	79
5.4	MIMO sliding mode trajectory and compliance controller.....	85
5.4.1	Control algorithm development	85
5.4.2	Experiments on the MIMO SM control system.....	91
5.4.3	Experiments with gait trajectories	97
5.5	Discussion and conclusions.....	101

Chapter 6	MIMO Sliding Mode Control System for GAREX.....	103
6.1	Introduction	104
6.2	Reference gait trajectory generation	105
6.3	MIMO Sliding mode controllers for GAREX.....	112
6.4	From average antagonistic PM pressure to joint compliance	118
6.5	Experimental validation of the MIMO SM control system of GAREX	119
6.5.1	Robotic Gait Training Pilot.....	119
6.5.2	Validation of controllable compliance.....	124
6.6	Discussion and conclusions.....	127
Chapter 7	FLCA Based Assist-as-needed Gait Rehabilitation for GAREX	129
7.1	Introduction	130
7.2	The assessment of active participation.....	131
7.2.1	Interaction torque sensing	131
7.2.2	Relation between interactive torque and subject participating level	132
7.3	Implementation of the FLCA controller.....	135
7.4	Experimental validation	141
7.5	Discussion and conclusions.....	147
Chapter 8	Conclusions.....	149
8.1	Impact and contributions	150
8.1.1	Robotic design of GAREX	150
8.1.2	A complete model of the PM actuated exoskeleton.....	150
8.1.3	Control systems of GAREX.....	151
8.2	Outlook and future work	152
8.3	Publications	153
Appendices.....		155
Appendix A: Ethics Approval.....		155
A-1 Consent Form.....		155

A-2 Advertising poster.....	157
A-3 Participant information sheet.....	158
A-4 Questionnaire.....	162
References.....	164

List of Figures

Figure 1-1 Left: Lokomat, a treadmill based exoskeleton type of gait rehabilitation robot. (Reproduced from [9] © 2011 IEEE). Right: Gait Trainer, an end-effector gait rehabilitation robot. (Reproduced from [10] Copyright © 2007 SAGE Publications)	3
Figure 3-1 Left: computer-Aided Design of the GAREX system. The unactuated DoFs of the trunk mechanism are labelled with the arrows (red: translational DoFs; yellow: rotational DoFs). Right: a health subject walking on the treadmill with the guidance provided by GAREX.	42
Figure 3-2 Illustrations of the joint actuation systems for the hip (left) and knee (right) joints. Variable definitions are listed with arrows showing their positive direction.	45
Figure 3-3 Joint torque versus gait cycle plots for the knee (top) and hip (bottom) joints. The joint torque requirement data of the 57kg healthy subject during normal walking are adopted from [162] The data of the 71kg and 100kg are calculated from the 57kg subject with normalization of body weight. The shaded areas in the plots are indicating the joint torque output capability of both the extension and flexion PMs throughout the gait cycle.....	47
Figure 3-4 Left: the front view of the lower limb exoskeleton with the thigh and shank modules outlined in blue and red respectively. The relative position of the two modules can be adjusted in order to align the rotational axes (marked with dashed lines in the figure) of the knee and hip with the subject's ones. Right: Side view of the lower limb exoskeleton with a healthy subject wearing it.	49
Figure 3-5 The pneumatic flow diagram for one of the actuated exoskeleton joint. The actuated joints of the LLE have identical actuation system configurations. The two actuated joints share the same pneumatic source and main solenoid valve.	51
Figure 3-6 Hardware configuration block diagram. Major components of the instrumentation hardware system are listed with connectors indicating the types of interfaces and directions of data flows.	52
Figure 3-7 Left: CAD drawing of the knee joint mechanism; right: photo showing details of the knee mechanism of GAREX.	53

Figure 4-1 Block diagram of the GAREX system. Three major sub-systems are illustrated with blocks with arrows indicating the connection sequence and media.57

Figure 4-2 The Hill's type of dynamic PM model adapted by Reynolds et al. [165].....59

Figure 4-3 Experimental setup to calibrate the dynamic model parameters of a PM actuator.60

Figure 4-4 The force versus contraction and velocity scatter plot, when the pressure of PM_1 was regulated to 3.2 bar. Red and blue dots represent data during the contraction and stretching of PM_1 respectively62

Figure 4-5 The first order polynomial representation curve fitting result of PM force versus its contracting length and velocity when its pressure was regulated to 3.2 bar. The upper plot is for the contracting process of PM_1 and the lower plot is for the stretching process.....63

Figure 4-6 (A), (B) and (C) are the $F(P)$, $K(P)$ and $B(P)$ versus PM_1 pressure plots respectively. The scatters represent the parameters gathered from the 51 experiments. The red scatters are for the contracting processes of PM_1 and blue ones are for the stretching processes.65

Figure 4-7 (A), (B) and (C) are the $F(P)$, $K(P)$ and $B(P)$ versus PM_1 pressure plots for the 400-mm long PM. The red scatters are for the contracting processes of PM_1 and blue ones are for the stretching processes. The first order linear model parameters are represented using green lines and the modified piecewise model parameters are represented in black lines.....67

Figure 5-1 Schematic drawing of the PM actuated knee joint mechanism. How the angular values are calculated is also illustrated.76

Figure 5-2 Left: structure of the knee joint mechanism; right: a healthy subject participating validation experiment with the mechanism81

Figure 5-3 The control system's square wave trajectory tracking performance. Top: only the knee joint mechanism is controlled to track the desired trajectory Bottom: square wave tracking with the leg of a healthy subject attached to the mechanism.82

Figure 5-4 Sinusoidal trajectory tracking results of SISO SM control system of the knee joint mechanism without human leg attached. (A): Tracking result of a 0.25 Hz sinusoidal desired trajectory. (B) Tracking error of the 0.25 Hz wave trajectory. The root mean square error is

0.0325 radian ($e_{RMS}=0.033$). (C) and (D): Tracking result and error of a 0.5 Hz sinusoidal desired trajectory($e_{RMS}=0.041$).	83
Figure 5-5 Sinusoidal trajectory tracking results of SISO SM control system of the knee joint mechanism without human leg attached. (A) and (B): Tracking result and error of a 1 Hz sinusoidal desired trajectory($e_{RMS}=0.077$). (C) and (D): Tracking result and error of a 1.5 Hz sinusoidal desired trajectory($e_{RMS}=0.124$).	84
Figure 5-6 Sinusoidal trajectory tracking results of SISO SM control system of the knee joint mechanism with human leg attached. (A) and (B): Tracking result and error of a 0.5 Hz sinusoidal desired trajectory ($e_{RMS}=0.087$). (C) and (D): Tracking result and error of a 1 Hz sinusoidal desired trajectory ($e_{RMS}=0.125$).	85
Figure 5-7 SM controller tracking performance. Top-left: knee joint trajectory tracking of a 0.1 Hz sinusoid wave. Top-right: Step responses of the average pressure. Bottom-left: difference between the actual and desired joint angular trajectory. Bottom-right: the controlled valve voltages during the experiment	92
Figure 5-8 Joint trajectory and pressure tracking performances of the MIMO SM controller. The experiment is conducted on the sole knee joint mechanism. ($P_{0d} = 400KPa$). Top: desired (red) versus actual (blue) joint trajectory; middle: the trajectory deviation; bottom: desired versus actual average pressure.	93
Figure 5-9 Joint trajectory and pressure tracking performances of the MIMO SM controller. The experiment is conducted with leg attached.. ($P_{0d} = 400KPa, e_{RMS} =0.1022$).	94
Figure 5-10 Joint trajectory and pressure tracking performances of the MIMO SM controller. The experiment is conducted with leg attached. ($P_{0d} = 300KPa, e_{RMS} =0.1174$).	95
Figure 5-11 Joint trajectory and pressure tracking performances of the MIMO SM controller. The experiment is conducted with leg attached. ($P_{0d} = 200KPa, e_{RMS} =0.1726$)	96
Figure 5-12 A healthy subject participating in a validation experiment with the mechanism	97
Figure 5-13 The MIMO SM controller's simultaneous multivariable tracking performance. Top: knee joint gait trajectory tracking. Bottom: system responses to the steps changes in desired average PM pressure	98

Figure 5-14 Results of the experiments on knee joint trajectory tracking and compliance control with five healthy subjects. (A) (C) (E): the subjects were instructed to relax their right knees during the entire experiments; (B) (D) (F): the subjects were instructed to obstruct the mechanism’s guidance during the time period highlighted in yellow. Average PM pressure was regulated at 360, 270 and 180 KPa for the results plotted in top (A, B), middle (C, D) and bottom (E, F) rows, respectively..... 100

Figure 5-15 Knee joint trajectory versus gait cycle progress plots at different gait cycle frequencies (F_{GC}). The RMS trajectory errors during two gait cycles are also listed again corresponding frequencies. 101

Figure 6-1 The record trajectory data and generated desired trajectory curve of Subject_A’s hip joint when walking at 1.2 km/h. The period of the average gait cycle (T_{GC}) is 2.43 s. The coefficient of determination (R^2) of the regression curve is 0.92..... 107

Figure 6-2 The record trajectory data and generated desired trajectory curve of Subject_A’s knee joint when walking at 1.2 km/h. $T_{GC} = 2.43$ s. $R^2=0.87$ 108

Figure 6-3 The record trajectory data and generated desired trajectory curve of Subject_A’s hip joint when walking at 1.5 km/h. $T_{GC} = 2.06$ s. $R^2=0.92$ 108

Figure 6-4 The record trajectory data and generated desired trajectory curve of Subject_A’s knee joint when walking at 1.5 km/h. $T_{GC} = 2.06$ s. $R^2=0.90$ 109

Figure 6-5 The record trajectory data and generated desired trajectory curve of Subject_A’s hip joint when walking at 1.8 km/h. $T_{GC} = 1.90$ s. $R^2=0.93$ 109

Figure 6-6 The record trajectory data and generated desired trajectory curve of Subject_B’s hip joint when walking at 1.5 km/h. $T_{GC}=1.76$ s. $R^2 = 0.91$ 110

Figure 6-7 The record trajectory data and generated desired trajectory curve of Subject_A’s hip joint when walking at 1.8 km/h. $T_{GC} = 1.90$ s. $R^2=0.91$ 110

Figure 6-8 The record trajectory data and generated desired trajectory curve of Subject_B’s knee joint when walking at 1.5 km/h. $T_{GC}=1.76$ s. $R^2= 0.80$ 111

Figure 6-9 The record trajectory data and generated desired trajectory curve of Subject_C’s hip joint when walking at 1.5 km/h. $T_{GC}=2.5$ s; $R^2= 0.89$ 111

Figure 6-10 The record trajectory data and generated desired trajectory curve of Subject_C's knee joint when walking at 1.5 km/h. $T_{GC}=2.5$ s. $R^2= 0.90$ 112

Figure 6-11 The control system block diagram of GAREX. In the figure $i=F,E$ and $j=h,k$; U_{ij} is the voltage fed into the corresponding analogue valve; m_{ij} is the pneumatic mass flow rate to the corresponding PMs; \bar{P}_{jd} is the average pressure of the antagonistic PMs of the corresponding joint. The subscript d indicates desired value of a property..... 112

Figure 6-12 Illustrated side view drawing of the exoskeleton module for dynamics analysis of the mechanism. The z-axes of the two coordinate systems are both pointing out of the page. 114

Figure 6-13 The comparison between the desired and actual gait trajectories of the two actuated joints during the validation experiments. The trajectories have been normalized to one gait cycle. The red lines are the predefined reference gait trajectory. The blue lines represent the average gait trajectories over the experimental period. The shaded area stands for the standard deviations of the average trajectories over the recorded gait cycles. (A): the hip joint trajectories with average PM pressure of the joint regulated to 160 KPa. (B): the knee joint trajectories with average PM pressure of the joint regulated to 160 KPa. (C) and (D): the hip and joint trajectories when the average PM pressure of both joints were regulated to 240 KPa. 121

Figure 6-14 the same type of plots as in Figure 6-13. (E) and (F): the hip and joint trajectories when the average PM pressure of both joints were regulated to 320 KPa. (G) and (H): the hip and joint trajectories when the average PM pressure of both joints were regulated to 400 KPa. 123

Figure 7-1 The 6-axis load cell for interaction force sensing. 132

Figure 7-2 Experimental results when the subject was actively trying to follow the desired gait pattern. (A) Desired and actual knee joint trajectories versus time plot. (B) Plots of trajectory error and RMS trajectory error over every gait cycle. (C) Plots of interaction torque and RMS interaction torque over every gait cycle..... 133

Figure 7-3 Experimental results when the subject was requested to relax the leg attached to the exoskeleton. (A) Desired and actual knee joint trajectories versus time plot. (B) Plots of trajectory error and RMS trajectory error over every gait cycle. (C) Plots of interaction torque and RMS interaction torque over every gait cycle..... 134

Figure 7-4 Experimental results when the subject was requested to slightly oppose the guidance of exoskeleton. (A) Desired and actual knee joint trajectories versus time plot. (B) Plots of trajectory error and RMS trajectory error over every gait cycle. (C) Plots of interaction torque and RMS interaction torque over every gait cycle. 135

Figure 7-5 The fuzzy compliance adaptive control system block diagram of GAREX. In the figure $i = F, E$ and $j = h, k$; U_{ij} are the input to the plant or the voltages fed into the corresponding analogue valves; τ_{int_k} is the interaction torque of the knee joint; P_j is the average pressure of the antagonistic PMs of the corresponding joint; the subscript d indicates desired value of a property and $\Delta \bar{P}_{kd}$ are the increment to the desired average pressure of the antagonistic PMs of the knee joint. 136

Figure 7-6 The membership functions of the input variables. (A) The RMS value of the interaction torque. (B) The RMS value of the tracking error. (C) The change of the tracking error..... 138

Figure 7-7 The output membership function of the FLCA controller 139

Figure 7-8 The experimental result plots for Subject A. (A) The desired knee joint average PM pressure versus time plots. (B) The GC RMS trajectory error versus time plot. (C) the GC RMS interaction torque versus time plots. 142

Figure 7-9 The experimental result plots for Subject B..... 143

Figure 7-10 The experimental result plots for Subject C..... 145

Figure 7-11 The desired and actual average PM pressures of the knee joint versus time plots for the three experiments conducted by Subject A. (A) “Active” experiment; (B) “Relax” experiment; (C) “Oppose” experiment. 146

List of Tables

Table 2-1 Overview of mechanical design of treadmill based gait rehabilitation robots.	15
Table 2-2 Summary of the effectiveness studies reviewed in this section.	27
Table 3-1 Torque and range of motion design parameters of GAREX	46
Table 3-2 List of key instrumental components of GAREX	52
Table 4-1 Parameters of different dynamic models and regression analysing results of the models, for the 300mm PM used in GAREX.	66
Table 4-2 . Modelling parameters and regression analysing results for the 400-mm long PM manufactured by FESTO	68
Table 5-1 A list of parameters used in the model and SISO SM controller implementation .	80
Table 5-2 Tuning parameters of the MIMO SM controller implemented to the knee joint mechanism	91
Table 6-1 The RMS errors (rad) of both actuated joints under all four experimental conditions	123
Table 6-2 Compliance scores given by the 12 subjects for the experiments with four discrete average PM pressures.	124
Table 6-3 Statistical analysis result of the experiments on compliance. Top half of the table is showing the means and variances of the rated compliance levels for all the controlled average PM pressures. Both the original and logarithm transformed means and variances are listed. The bottom half of the table is illustrating all the possible between groups p-values of the Tukey’s test.	126
Table 7-1 The rule tables for the FLCA. Since there are three input variables, each of the 3x3 table is for one membership function of the $\Delta\theta_{k_RMS}$ input.....	140

Nomenclature

AAN	Assist-as-needed
BWS	Body weight support
BWSTT	Body weight support treadmill training
CAD	Computer-aid-design
DoF	Degree of freedom
EMG	Electromyography
FLCA	Fuzzy logic compliance adaptation
GAREX	GAit Rehabilitation Exoskeleton. The new robot system developed in the research
GRF	Ground reaction force
LLE	Lower limb exoskeleton
MIMO	Multi-input-multi-output
PM	Pneumatic muscle
RCT	Randomized controlled trial
RMS	Root mean square
ROM	Range of motion
SCI	Spinal cord injury
SEA	Series elastic actuation
SISO	Single-input-single-output
SM	Sliding mode
Subscript: E	The variable or constant is related to the extensor PMs of a joint
Subscript: F	The variable or constant is related to the flexor PMs of a joint
Subscript: h	The variable or constant is related to the hip joint
Subscript: k	The variable or constant is related to the knee joint

Co-Authorship Form

This form is to accompany the submission of any PhD that contains published or unpublished co-authored work. **Please include one copy of this form for each co-authored work.** Completed forms should be included in all copies of your thesis submitted for examination and library deposit (including digital deposit), following your thesis Acknowledgements. Co-authored works may be included in a thesis if the candidate has written all or the majority of the text and had their contribution confirmed by all co-authors as not less than 65%.

Please indicate the chapter/section/pages of this thesis that are extracted from a co-authored work and give the title and publication details or details of submission of the co-authored work.

Cao, Jinghui, Sheng Quan Xie, Raj Das, and Guo L. Zhu. "Control strategies for effective robot assisted gait rehabilitation: the state of art and future prospects." *Medical engineering & physics* 36, no. 12 (2014): 1555-1566.

Chapter 2 of the thesis is extracted from the

Nature of contribution by PhD candidate	Conducting research, drafting the paper,
---	--

Extent of contribution by PhD candidate (%)	90%
---	-----

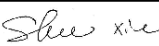
CO-AUTHORS

Name	Nature of Contribution
Xie, Sheng Quan	Contributing the initial idea, supervising paper writing and proofreading
Das, Raj	Idea contribution, proofreading
Zhu, Guoli	Idea contribution, proofreading

Certification by Co-Authors

The undersigned hereby certify that:

- ◆ the above statement correctly reflects the nature and extent of the PhD candidate's contribution to this work, and the nature of the contribution of each of the co-authors; and
- ◆ that the candidate wrote all or the majority of the text.

Name	Signature	Date
Dr Raj Das		20/2/2017
Zhu, Guoli		20/02/2017
Xie, Sheng Quan		23/02/2017

Co-Authorship Form

This form is to accompany the submission of any PhD that contains published or unpublished co-authored work. **Please include one copy of this form for each co-authored work.** Completed forms should be included in all copies of your thesis submitted for examination and library deposit (including digital deposit), following your thesis Acknowledgements. Co-authored works may be included in a thesis if the candidate has written all or the majority of the text and had their contribution confirmed by all co-authors as not less than 65%.

Please indicate the chapter/section/pages of this thesis that are extracted from a co-authored work and give the title and publication details or details of submission of the co-authored work.

J. Cao; S. Q. Xie; R. Das, "MIMO Sliding Mode Controller for Gait Exoskeleton Driven by Pneumatic Muscles," in IEEE Transactions on Control Systems Technology, vol.PP, no.99, pp.1-8

Chapter 5 of the thesis is extracted from this paper

Nature of contribution by PhD candidate	Conducting algorithm development and experiments ; drafting the paper
Extent of contribution by PhD candidate (%)	90%

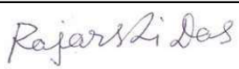
CO-AUTHORS

Name	Nature of Contribution
Xie, Sheng Quan	Proposed the research topic and proofreading
Das, Raj	Helping with the research and paper writing, proofreading.

Certification by Co-Authors

The undersigned hereby certify that:

- ❖ the above statement correctly reflects the nature and extent of the PhD candidate's contribution to this work, and the nature of the contribution of each of the co-authors; and
- ❖ that the candidate wrote all or the majority of the text.

Name	Signature	Date
Dr Raj Das		20/2/2017
Prof. Sheng Quan Xie		23/02/2017

Last updated: 19 October 2015

Co-Authorship Form

This form is to accompany the submission of any PhD that contains published or unpublished co-authored work. **Please include one copy of this form for each co-authored work.** Completed forms should be included in all copies of your thesis submitted for examination and library deposit (including digital deposit), following your thesis Acknowledgements. Co-authored works may be included in a thesis if the candidate has written all or the majority of the text and had their contribution confirmed by all co-authors as not less than 65%.

Please indicate the chapter/section/pages of this thesis that are extracted from a co-authored work and give the title and publication details or details of submission of the co-authored work.

Cao, J., Zhang, M., McDaid, A. and Xie, S.Q., 2017. Design and control of a compliant Robotic Gait Rehabilitation EXoskeleton (GAREX), IEEE Transactions on Mechatronics (Under review)

Chapter 6 of the thesis is extracted from this paper

Nature of contribution by PhD candidate	Conducting the research and drafting the paper.
Extent of contribution by PhD candidate (%)	90%

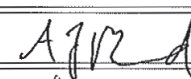
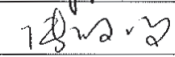
CO-AUTHORS

Name	Nature of Contribution
Xie, Sheng Quan	Research supervision, proofreading, proposing the initial idea.
Zhang, Mingming	Providing suggestions on the experimental design, proofreading
Andrew McDaid	Suggestion on the control and experimental implementations, proofreading

Certification by Co-Authors

The undersigned hereby certify that:

- ❖ the above statement correctly reflects the nature and extent of the PhD candidate's contribution to this work, and the nature of the contribution of each of the co-authors; and
- ❖ that the candidate wrote all or the majority of the text.

Name	Signature	Date
Prof. Sheng Quan Xie		23/02/2017
Dr. Andrew McDaid		28/2/2017
Dr. Mingming Zhang		25/02/2017

Co-Authorship Form

This form is to accompany the submission of any PhD that contains published or unpublished co-authored work. **Please include one copy of this form for each co-authored work.** Completed forms should be included in all copies of your thesis submitted for examination and library deposit (including digital deposit), following your thesis Acknowledgements. Co-authored works may be included in a thesis if the candidate has written all or the majority of the text and had their contribution confirmed by all co-authors as not less than 65%.

Please indicate the chapter/section/pages of this thesis that are extracted from a co-authored work and give the title and publication details or details of submission of the co-authored work.

Cao, Jinghui, Sheng Quan Xie, Mingming Zhang, and Raj Das. "A new dynamic modelling algorithm for pneumatic muscle actuators." In International Conference on Intelligent Robotics and Applications, pp. 432-440. Springer International Publishing, 2014.

Chapter 3 of the thesis is extracted from this paper

Nature of contribution by PhD candidate	Conducting the research and drafting the paper.
Extent of contribution by PhD candidate (%)	90%

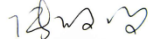
CO-AUTHORS

Name	Nature of Contribution
Xie, Sheng Quan	Proposed the idea, research supervision, proofreading
Zhang, Mingming	Helping the research, proofreading
Das, Raj	Review the experiments and proofreading

Certification by Co-Authors

The undersigned hereby certify that:

- ❖ the above statement correctly reflects the nature and extent of the PhD candidate's contribution to this work, and the nature of the contribution of each of the co-authors; and
- ❖ that the candidate wrote all or the majority of the text.

Name	Signature	Date
Dr Raj Das		20/2/2017
Prof. Sheng Quan Xie		23/02/2017
Dr Mingming Zhang		25/02/2017

Co-Authorship Form

This form is to accompany the submission of any PhD that contains published or unpublished co-authored work. **Please include one copy of this form for each co-authored work.** Completed forms should be included in all copies of your thesis submitted for examination and library deposit (including digital deposit), following your thesis Acknowledgements. Co-authored works may be included in a thesis if the candidate has written all or the majority of the text and had their contribution confirmed by all co-authors as not less than 65%.

Please indicate the chapter/section/pages of this thesis that are extracted from a co-authored work and give the title and publication details or details of submission of the co-authored work.

Cao, Jinghui, Sheng Quan Xie, Andrew McDaid, and Raj Das. "Sliding Mode Control of an Exoskeleton Gait Rehabilitation Robot Driven by Pneumatic Muscle Actuators." In ASME 2015 International Design Engineering Technical Conferences and Computers and Information in Engineering Conference, pp. V009T07A002-V009T07A002. American Society of Mechanical Engineers, 2015. Chapter 3 of the thesis is extracted from this paper

Part of the chapter 5 of the thesis is extracted from this publication.

Nature of contribution by PhD candidate	Conducting majority part of the research and drafting the paper.
---	--

Extent of contribution by PhD candidate (%)	90%
---	-----

CO-AUTHORS

Name	Nature of Contribution
Xie, Sheng Quan	Proposed the idea, research supervision, proofreading
Andrew McDaid	Helping with the control system develop, proofreading
Das, Raj	Review the experiments and proofreading

Certification by Co-Authors

The undersigned hereby certify that:

- ❖ the above statement correctly reflects the nature and extent of the PhD candidate's contribution to this work, and the nature of the contribution of each of the co-authors; and
- ❖ that the candidate wrote all or the majority of the text.

Name	Signature	Date
Dr Raj Das	<i>Rajarsi Das</i>	20/2/2017
Prof. Sheng Quan Xie	<i>Shu xie</i>	23/02/2017
Dr. Andrew McDaid	<i>A McDaid</i>	28/2/2017

Last updated: 19 October 2015

Chapter 1 Introduction

Gait disorders caused by stroke are both common and severe. It urges researchers, clinicians or engineers to develop new rehabilitation methodologies that are effective and more accessible to the patients. The effectiveness of conventional gait rehabilitation trainings is largely dependent on the therapists' experience. Conducting such trainings is also physically intensive for the therapists. As a result, robotic technologies were introduced to the field, which have opened up new developmental possibilities.

Effectiveness is a main driving factor for the gait rehabilitation robot development. Rehabilitation training needs to be compliant with motor learning theories in order to produce effective outcome. In terms of robotic rehabilitation, control strategies are what reflect such theories. As a result, the robotic design needs to accommodate the needs of control strategies development. The ultimate goal of the research is development of a robotic exoskeleton system to facilitate repetitive, task-specific and assist-as-needed gait rehabilitation training. Such goal needs to be tackled systematically. Hence, the main objectives of the thesis are determined in order to propel the developmental process

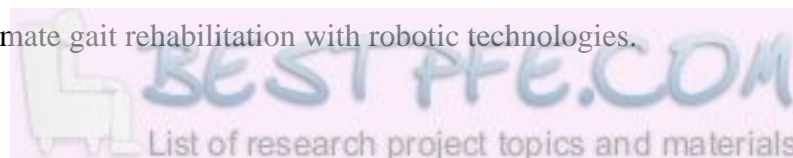
1.1 Background and motivation

1.1.1 Gait Disorder and Rehabilitation

Stroke is sudden blockage of blood vessels in the brain, which can result in damage to the brain tissues and in severe cases even death. About 8800 New Zealanders suffer new stroke annually [1]. This figure in the United States is about 610,000 [2]. With a survival rate at approximately 80%, it is estimated that there are 60,000 stroke survivors in New Zealand and the number in the United State is about 7,000,000. This makes stroke the leading cause of disability in both countries [1-3]. According to World Health Organisation, 15 million people suffer stroke every year globally, among whom about one third die and another one third are left permanently disabled [4].

Majority of the stroke survivors suffer the gait disorder and almost a half of these people cannot walk independently without assistance. Therefore, walking ability recovery or gait rehabilitation has been a popular research field. Bonita and Beaglehole [5], who investigated the motor recovery of the stroke population in Auckland New Zealand, reported that at 6 month post-stroke 62% survivors still suffered motor deficits. Duncan [3] reported that inability to walk is one of the most common problems in the population who suffered acute stroke. Kelly-Hayes et al. also stated that 30% stroke survivors are unable to walk without any assistance [6].

Being both common and severe means there are needs to develop rehabilitation strategies that specifically address the gait disorders. Neural plasticity provides the theoretical foundation that rehabilitation training can lead to the motor function recovery after cortical lesions [7]. Motor learning is thought to be a prerequisite factor in the development of representational plasticity in the central nervous system [8]. Hence, the development of effective gait rehabilitation needs to be compliant with the motor learning principles. In terms of conventional rehabilitation, the task-specific repetitive approach, which is more compliant with modern motor learning principles, has been proven to be superiorly effective in terms of motor function recovery. The most commonly used task specific repetitive approach in gait rehabilitation is body weight support treadmill training (BWSTT). Despite its effectiveness, such training requires two to three therapists and relatively high physical output from the therapists. As a result, the lengths of training sessions are usually short. Furthermore, assistance provided by therapist is experience based, which means consistent optimal gait movement cannot always be achieved. Thus, it is a logical step forward to automate gait rehabilitation with robotic technologies.



Gait rehabilitation robotics has been a popular research topic for the past twenty years. In the early stage of the development, gait rehabilitation robots were designed to automate the conventional BWSTT. There were mainly two types of gait training robots, one is exoskeleton type of robots represented by the Lokomat; the other is end-effector type of robots represented by Gait Trainer (Figure 1-1). Both types of robots were aimed to guide the patients reproduce desired gait patterns like what therapists do during manual BWSTT. Geared electrical motors were typically used to actuate these robots. In terms of control strategies, only trajectory tracking control has been developed in the early stage. The exoskeleton type of robots has controlled trajectories of the actuated joints to reproduce the desired gait pattern. The end-effector robots control position and orientation of the foot plates in the sagittal plane to simulate over ground walking for the training subject. Trunk manipulating and body weight support mechanisms are also adopted in both types of robots to maintain trunk posture of the patient and prevent falling during the rehabilitation training.



Figure 1-1 Left: Lokomat, a treadmill based exoskeleton type of gait rehabilitation robot. (Reproduced from [9] © 2011 IEEE). Right: Gait Trainer, an end-effector gait rehabilitation robot. (Reproduced from [10] Copyright © 2007 SAGE Publications)

The desires for safer and more effective gait rehabilitation have been driving researchers, clinicians and engineers to improve the robotic gait training technology. Such improvements mainly focus on the robotic design and control aspects.

In terms of robotic design, robots with more actuated degrees of freedom have developed to make the rehabilitation training more task specific. Ambulatory training has also been made possible by mobile robotic gait rehabilitation system. Such development has the potential to integrate gait training into daily life activities. Technologies like bio-signal sensing and virtual realities have been brought into robotic gait rehabilitation systems to achieve better training outcomes.

Various control strategies have been developed in order to provide more effective robotic gait rehabilitation. Research indicates that subject's voluntary participation can lead to more effective rehabilitation training [11-13]. However, the conventional trajectory tracking control only guides the patients to reproduce desired gait pattern regardless their voluntary effort. To encourage more active participation and effort by a patient, control strategies have been developed to provide just enough support that the patient needs to sustain periodical gait. Thus, such control strategies are regarded as assist-as-needed (AAN) strategies.

Rehabilitation training needs to be compliant with neurological theories in order to produce effective outcome. In terms of robotic rehabilitation, control strategies are what reflect such theories. Hence, in addition to the basic requirements of automating BWSTT, the robot design should be oriented to the needs of control development. Based on this viewpoint, the development of gait rehabilitation robot should be conducted systematically. The requirements of training strategies are used to shape up the robotic design specifications, so that the robotic platform and control system can work seamlessly together for more effective gait rehabilitation.

Impedance or admittance related controllers enable gait rehabilitation robots to provide needs specific trainings to tailor the patient's individual extent of gait disorders. Such controllers can also change the degree of assistance provided by the robot for the implementation of AAN training strategies [14]. Compliant and back-drivable actuators for robotic gait rehabilitation have been widely researched, not only because of safety and comfort considerations, but also the capability of facilitating impedance/admittance controller development. Compliant actuation can be achieved by adding elastic components in series with conventional stiff actuators [15] or employing intrinsically compliant actuators such as pneumatic actuators [16].

Pneumatic muscle (PM) actuators are one example of the compliance actuators. PMs have high power/force to weight ratio. Their compliance could be adjusted through changing the inflation pressures. As a result, PM actuators have been utilized in various applications of robot-human interaction [17-20], especially rehabilitation robots, due to their intrinsic compliance and high

force/power to weight ratio. The author's research group has been investigating the use of pneumatic muscle actuated lower limb exoskeleton in gait rehabilitation.

1.1.2 Previous work in the author's research group

1.1.2.1 *The Intrinsically Compliant Robotic Orthosis for Gait Rehabilitation*

The robotic gait rehabilitation orthosis prototype was developed by Hussain as a part of his PhD study. The orthosis was a unilateral device with the hip and knee joints of the exoskeleton actuated by PM actuators. Because of the unidirectional actuation of a single PM, each of the exoskeleton's actuated joints had an antagonistic pair of PMs.

Several control strategies were implemented to control the robotic gait rehabilitation orthosis. Both the boundary layer augmented sliding mode controller and chattering free robust variable structure (CVCS) controller were proposed for trajectory and joint compliance control [21, 22]. Based on the CVCS algorithm, control strategies to implement AAN training were also developed [23], [24].

There is still room for further development in terms of robotic design, control system and experimental validation. Firstly, to the aspect of design, the maximum achievable torque was claimed to be 50 Nm for both PM actuated joints of the robot. It was well-known that, under constant pressure, the force generated by a PM decreases as its contraction increases. Hence only stating the maximum capability was not sufficient to satisfy the torque requirement of the robotic gait rehabilitation. Moreover, only straps rather than rigid braces were used to secure patient's leg to the exoskeleton. Unpredictable relative movement would cause misalignment between the exoskeleton joints and subject's anatomical joints, and affect the force transmission from the exoskeleton to the lower limb.

Secondly, to the aspect of modelling and control, the pressure dynamics of the PMs was neglected in the research. The pressure dynamics of PMs and pneumatic flow dynamics of the valves are major sections of the pneumatic actuation system and also subject to nonlinearity. Hence, it is important to take them into account when doing system modelling or controller development. Two attempted joint trajectory controllers by Hussain et al. [21, 22] both had PM pressures as inputs to the controlled plant. However, the on/off solenoid valves used to regulate the pneumatic flow into and out of the PMs only took digital input signals. The process of regulating PM pressure was not reported. Similar problems also applied to the AAN controllers reported in [23] and [24]. These two high level control systems both had robust position sub-

controllers. However, the position controllers' outputs were joint actuating torques. Again, it was not clear how the system converted the digital signals to the valves into such actuating torques.

Thirdly, to the aspect of experimental validation, there was a lack of experimental varieties. Despite that various controllers were proposed, the experimental results of the controllers were mostly presented in the same format, in which the trajectories of a number of healthy subjects over a number of gait cycles (GCs) were averaged into a single trajectory over one or two GCs. The inter/intra-subject variability was rarely presented or discussed. With such data presentation, there were no significant differences between experiments with multiple subjects over a number of GCs and experiments with a single subject over a few GCs. A larger variety of experiments with more detailed results would improve the significance of Hussain's research and help other to reproduce the experimental results as benchmarks to further research.

1.1.2.2 The Human-inspired Robotic Exoskeleton

Kora conducted his master research on the development of Human-inspired Robotic Exoskeleton (HuREx) [25]. It was aimed to develop a more robust lower limb exoskeleton that could advance the design by Hussain. HuREx had a single degree of freedom (DoF) design. Its knee joint was actuated by a pair of antagonistic PMs with 300 mm in length and 40 mm in diameter. Each of the PMs (FESTO DMSP-40-300N-RM-AM) is capable to generate up to 6000N force. With the designed torque lever of 20mm, the actuation system could provide sufficient torque to support and guide the knee joint during walking. Due to the physical dimension of the PMs, they could not be attached to the exoskeleton directly. Bowden cable was utilized to transmit the power from remotely mounted PMs to the actuated knee joint. In terms of physical lower limb interaction, 3D printed parts with glass fibre reinforcement make sure comfortable and strong support from the exoskeleton to leg segments, as well rigid connection between them. An experiment based force-contraction-pressure model was developed as well as a flow dynamics model for the high-speed solenoid valves that regulate the pneumatic flow of the PMs. Based on these models, position and impedance controllers were developed to track the reference trajectories in the joint space.

Although HuREx is more robust than its predecessor, there were still issues to solve before it could be tested in clinical settings, mainly because the actuation system is still not optimized. Although, the PMs were able to provide sufficient torque, their large volumes required higher pneumatic flow rate. Due to the limitation of the pneumatic supply system, HuREx was not

able to track knee joint gait trajectories in the bandwidth required for task specific gait rehabilitation. One of the main motivations of using PMs in lower limb exoskeleton is light weight. The PMs were detached from HuREx and Bowden cables were adopted for power transmission. PM's advantage of being light weight was not reflected in such design. Furthermore, the stretch and friction of the Bowden cables would add more nonlinearity and uncertainty to actuation system.

1.2 Research objectives

The ultimate goal of this thesis is to develop a new PM driven robotic exoskeleton system to facilitate repetitive, task-specific and assist-as-needed gait rehabilitation training. To achieve the ultimate goal, both robust exoskeleton hardware and intelligent control system software need to be developed, followed by extensive experimental validations. The goal was then split into several major research objectives or milestones. The major research objectives are elaborated in the following paragraphs.

The first objective is hardware development of the new GAit Rehabilitation EXoskeleton (GAREX). Although, two previous lower limb robotic exoskeletons for gait rehabilitation had been developed in the author's research group, each of them had its own drawbacks that prevent them to be further developed for clinical applications. The design of GAREX needs to fulfil the requirements of clinical applications, in terms of actuation torque, bandwidth, safety and anthropometric adaptability. Moreover, the robotic design should also provide versatilities for the development of intelligent control strategy.

The second objective is to develop and experimentally validate lower trajectory tracking and compliance control strategies on GAREX. Nonlinearity of the PM and disturbances from the human robot interaction mean that robust trajectory controller is needed to provide safe and comfortable gait rehabilitation. The intrinsic compliance is the main motivation of adopting PMs to drive GAREX. Hence, meanwhile tracking the desired gait trajectories, the control system is also supposed to have the capability of adjusting the joint space compliance, in order vary the assistance level provided by the exoskeleton.

The third objective is to implement an assist-as-needed control algorithm on GAREX and conduct pilot experiments with healthy subjects to investigate the feasibility of bring the AAN

controlled system into the stage of clinical trials. This control algorithm is to reflect the intelligence of the GAREX system, which needs to be able to assess a patient's capability or level of participation. Ideally, the assessment could be performed online during the gait training.

1.3 Thesis outline and contributions

This thesis covers the entire development process of GAREX for robotic gait rehabilitation. The contributions of the thesis are around making utilizing benefits brought by the PM actuators to advance the state of art of robotic gait rehabilitation. The upcoming chapters are organised in the following order.

Chapter 2 presents a thorough literature review focusing on the field of robotic gait rehabilitation. It is hoped, through the literature review, the gaps of the current research can be identified. Therefore, potential contributions and further objectives of this research can be clearly outlined.

The robotic system design of GAREX is presented in Chapter 3. There have not been any clinical studies on PM driven gait rehabilitation robots. Hence, the design of GAREX is oriented to provide task specific gait rehabilitation to stroke patients. Patients' safety is the paramount in design considerations. The torque, range of motion and actuation bandwidth requirements are also satisfied in order to make the training task-specific.

It is highly beneficial to model the complete PM actuation system of GAREX in order to understand their behaviours and facilitate control system development. The task specific gait training requires dynamic operations of the PMs, but there was no dynamic model could be directly applied to the PMs used in GAREX. Chapter 4 thus presents a new experiment based modelling approach for the PM actuators.

Due to the nonlinear and hysteresis nature of the PM actuators, sliding mode controllers, which are robust to nonlinearity and modelling uncertainties, were considered to be suitable for GAREX. Chapter 5 presents the developmental process of a multi-input-multi-output (MIMO) sliding mode (SM) controller which can simultaneously control the joint space trajectory and compliance of the exoskeleton. The experimental validation of the controller on a single actuated joint is also covered in this chapter.

Chapter 6 presents the implementation of the MIMO SM controller to both the actuated joints of GAREX. Extensive experiments reveal that the control system is able to deliver task specific

treadmill based gait rehabilitation training and regulate the amount of assistance provided to the training subject simultaneously.

With the MIMO SM controller developed and validated, the author then investigates how to utilize it to implement the assist-as-need training concept. Hence, Chapter 7 is about the development and pilot studies of the fuzzy logic compliance adaptation control system. The system can adjust the joint space compliance based on the subject's voluntary participation assessment during gait rehabilitation.

Chapter 8 concludes this thesis by highlighting the scientific contributions of the PhD research. Limitations of this research and a discussion on possible future work are also included in this chapter.

Chapter 2 Literature review

This chapter primarily focuses on three major aspects of robotic gait rehabilitation, which are robot design, control strategy and effectiveness study. Before the robotic gait rehabilitation is reviewed, the recovery mechanism behind rehabilitation training and conventional approaches are also reviewed.

In this literature review, the gait rehabilitation robots are categorized into treadmill based, end-effector and ambulatory robots. The focus of this review is on the treadmill based robots since they provide good platforms for investigating new actuation systems and conducting control strategy research. Through the review, it is realized that pneumatic muscle (PM) actuators, which are intrinsically compliant and lightweight, could potentially be ideal actuators for gait rehabilitation exoskeleton.

In the early stage of robotic gait rehabilitation development, control strategies applied to rehabilitation robots were adapted from those applied to traditional industrial robots. However, these strategies were not optimized for the effectiveness of gait rehabilitation. As a result, researchers have been investigating control strategies tailored for the needs of rehabilitation. Among these control strategies, assist-as-needed (AAN) control is one of the most popular research topics in this field. Effectiveness AAN training strategies have gained supports from both motor learning principles and clinical studies. Hence, detailed analysis on AAN control strategies of gait rehabilitation robots is conducted in this chapter,

Clinical studies reviewed are focused on the effectiveness of control algorithms. Through the review, it is noticed that only a few of clinical studies were conducted to compare the effectiveness between different control strategies. It cannot be concluded that any control strategy is superior in terms of effectiveness.

There have not been any clinical studies on PM driven gait rehabilitation robots, mainly due to the robustness of the robotic designs. For the research of more effective robotic gait rehabilitation, the newly developed robotic platform and control strategies need to work seamlessly as a system. Such system also needs extensive experimental validations to achieve the potential for clinical trials or application.

2.1 Conventional gait rehabilitation approaches

Ultimately, development of new rehabilitation techniques should rely on a thorough understanding of underlying recovery mechanism [26]. Gait rehabilitation training or locomotor recovery is a process of neurological rehabilitation. Neural plasticity, which is defined by Sharma et al. [7] as the ability of the central nervous system (CNS) to adapt in response to changes in the environment or lesions. It is also believed to be the basis underlying motor function recovery after cortical lesions, such as stroke and cerebral palsy [7].

‘Rehabilitation, for patients, is foundationally a process of relearning how to move to carry out their needs successfully’ [27]. Motor learning is thought to be a prerequisite factor in the development of representational plasticity in the CNS [8]. General motor learning principles are hypothesized to be still valid for motor recovery [28]. One fundamental principle is that the degrees of performance improvement are dependent on the amount of practice [29]. However, large amount of practice or repetition alone is not enough to induce ideal motor learning outcome [30, 31]. Animal experiment conducted by Plautz et al. [8] indicated that practice needs to be task-related to produce representational plasticity in motor cortex. Introducing training variability in the skill acquisition session improves the overall session performance compared to single task repetition in one session [32]. Motor learning theories have driven the development of both conventional and robotic rehabilitation strategies.

Conventional rehabilitation strategies can be categorised into three groups, which are compensatory approaches, neurofacilitatory approaches and task-specific repetitive approaches. Some neurological lesions, such as stroke, result hemiplegia and hemiparesis. Hemiplegia and hemiparesis only affect limbs on a single side of human body. Compensatory approach involves training patients to utilise their unaffected end effectors (e.g. unaffected hand) or body segments (e.g. unaffected muscles in the hemiplegic side) to achieve the same functional abilities before the injury [33, 34]. For gait rehabilitation, therapists concern less on reproducing a more normal gait pattern after injuries, but more onto teaching patients more stable and functional gait pattern which allows them to walk safely to achieve a certain level of physical independency [35]. Compensatory approach is effective in functional recovery, but it may be associated with reduced joint range and pain in long term [35]. Moreover, patients may tend to rely on compensations for certain tasks instead of using affected effectors. This thus causes a pattern of learned non-use [36, 37], which subsequently limits the gain of motor function of the impaired limb.

Unlike compensation, neurofacilitatory approach focuses on the rejuvenation of lost motor abilities. Bobath therapy, also known as neurodevelopmental therapy (NDT), is one representative concept of the neurofacilitatory approach. Bobath therapy involves tone-inhibiting manoeuvres and gait-preparatory tasks in sitting and standing postures to control spasticity and facilitate normal movement pattern of hemiplegic limbs. The therapy was first developed in 1950s and is still a widely adopted post-stroke physiotherapy approach in Europe [38-40]. Very limited articles have been published to standardise the rehabilitation therapies based on the Bobath concept, with the last publication of Bobath on adult hemiplegia in 1990 [41]. To a great extent, training and applications of the therapy are experience based [40].

Compared to the Bobath approach, the task-specific repetitive approach is more compliant with the modern motor learning concepts described previously. Neuroscientists have proven that repetition plays a major role in inducing and maintaining brain changes [42]. Bayona et al. [31] reviewed the related experiments and concluded that tasks meaningful to animal rather than repetitions alone are more likely to generate functional reorganization. For human, daily practice of task-specific motor activities can also lead to reorganization of the adult primary motor cortex [43, 44]. Randomized controlled trials (RCT) conducted by Langhammer and Stranghelle both concluded that for acute patients task-specific training programme was more effective than Bobath programme [45, 46].

Body weight support treadmill training (BWSTT), which was first developed by Finch and Barbeau in 1986 [47], is a well-researched task-specific repetitive gait rehabilitation approach. Compared to neurofacilitatory approaches, BWSTT enables patients practice complex gait pattern repetitively. Usually during BWSTT, a patient walks on the treadmill with a body weight support (BWS) system attached via harness. Therapists guide patient's legs to follow desired trajectories, as well as promote correct pelvis and trunk movements during gait [39]. Hesse et al. compared BWSTT to conventional physiotherapy according to the Bobath concept on chronic stroke patients. It was concluded that BWSTT is superior with regard to restoration of gait and improvement of over ground walking speed. In terms of intensity, similar investigations also indicated that more gait cycles were achieved by the BWSTT, for the sessions with the same duration [48, 49].

During the BWSTT, patients are trained to produce rhythmic gait cycles. The repetitive movements make the automation of this training process possible. It is a heavy task for therapists, since they have to manually move the patients' paretic legs continuously. Hence, the sustaining

time of each training session is usually short. Due to physical limits of therapists, for patients with excessive spasticity, manual training is nearly impossible [50]. Furthermore, therapists are expected to provide optimal and identical leg swing in every gait cycle, which is largely dependent on therapists' experience. Inter/intra- therapist variances cannot be eliminated in BWSTT. Hence optimal consistency in gait movements cannot always be achieved. Robotic training has provided a solution to these problems. In addition, a variety of technologies can be integrated into robotic training process to make the rehabilitation process more effective and appealing to both the therapist and patients. Such technologies including but not limited to dynamic feedback [51], biological feedback[52], and virtual reality [53].

2.2 Gait rehabilitation robots

2.2.1 Previous designs of gait rehabilitation robots

From the viewpoint of mechanism, gait rehabilitation robots can be allocated to three categories: treadmill training robots, end-effector robots and ambulatory robots. Robots designed for rehabilitating a single lower limb joint not during walking are not included in this section, since repetitive gait pattern is not adopted.

Treadmill training robots automate the process of manual BWSTT training. They are designed to replace therapists for guiding leg movement and patient support. As a result, such robots usually consist of two major mechanisms, the gait driving mechanism and the trunk/pelvis manipulating mechanism. A summary of reviewed treadmill training robots can be retrieved in Table 2-1. More thorough analysis is presented for the gait driving mechanisms, since they have stronger influence on the implementation of control strategies.

End-effector robots are also known as footplate robots. This kind of robots has two separate footplates to support patients who stand on them and move their feet according to certain rules. Gait Trainer [54] was designed to simulate conventional BWSTT by moving patient's feet in fixed trajectories. The footplates were driven by linkage systems and each footplate only had one degree of freedom (DoF). During training, the back and forward footplate movements were to simulate the stance and swing phase of gait cycles, respectively. The ratio was set to 60% stance phase and 40% swing phase per gait cycle. The orientation of the footplates also changed as the progression of the gait cycle to simulate the movement of the actual floor walking. HapticTrainer is an extended version of GaitTrainer by adding the concept of programmable plates. This device follows a modular design with 3 DoFs of each footplate in sagittal plane

and the potential to extend to 6 DoFs, which enable it to simulate feet movements in various walking scenarios [55, 56]. G-EO system is an updated version of HapticTrainer. It also contains two programmable footplates but more compact, which means it is more suitable for clinical usage [57]. Yoon and Ryu [58] developed a footplate robot which could simulate walking on different terrains and also turning movements. Each robotic footplate had 6 DoFs. This design was then further simplified for rehabilitation purposes. Each footplate of this robot was actuated in the sagittal plane with 3 DoFs. This robot also had an upper limb guiding mechanism. The arm swing during gait was simplified into a single-link pendular motion, which is synchronous to the lower limb movements [59, 60].

Ambulatory trainers are a popular type of designs in the scope of robotic gait rehabilitation. Some ambulatory trainers [61, 62] have no leg orthoses. They simply provide a mobile base for BWS, balance training or the ease of access by therapists. KineASSIST is one representative of this kind of robots. It could move in response of the patient's locomotion. Its trunk and pelvic mechanisms permitted the patient's trunk to shift and rotate in any direction. It could also slow and stop patient falling without causing pain. This design benefits confidence building during balance training [61]. Walktrainer [63] and NaTure-Gaits [64, 65] were also ambulatory robotic gait trainers, which had bilateral exoskeletons to guide leg movements. Similar to KineASSIST, these two trainers each had a mobile base for BWS, trunk/pelvis support and exoskeleton mounting. The exoskeletons constrained the training subject's leg movements in the parasagittal planes. The hip, knee and ankle joints of both trainers were actuated by DC motors. For Walktrainer, the powered pelvic orthosis actuated the patient's pelvis in all 6 DoFs with DC motors and linear gearboxes. For NaTure-Gaits, only vertical and lateral translations of the pelvis were actuated.

Table 2-1 Overview of mechanical design of treadmill based gait rehabilitation robots.

Name	Gait driving mechanism		Trunk/pelvic	Other features and comments
	DoFs	Actuation system	mechanism	
LokoMat [50]	1 3 5	Motors and gear reduction units for linear actuation with levers for active DoFs	DoF: A, B	Crane like BWS. Active control of the amount of BWS was also implemented [66]
ALEX [67, 68]	1 2 3 5	linear motor with levers for all active DoF	DoF: A C D E	Developed as a research gait rehabilitation robots for AAN training. Its design was adapted from a passive leg orthosis GBO, which can be gravitational load of leg invariant to its configuration[69].
LOPES[70, 71]	1 2 3 5	Series elastic actuation (SEA) with Bowden cable transmission detached motors and gear units from the gait driven exoskeleton	DoF: A B C	Elastic elements make the actuation system more compliant. Adoption of SEA reduced weight of moving parts without reducing power, thus the force bandwidth increased. These would benefit the implementation of the proposed zero impedance control.
ARTHuR[72, 73]	1 3 5	Two moving coil forcers driven by linear motors can move along a horizontal rail to drive a two-bar linkage attached to patient's ankle	N.A.	As a research tool, ARTHuR does not have proper leg orthosis. The actuation mechanism can drive the foot to reach any point in the sagittal plane by moving the forcers along their rail. The actuation is also backdrivable[74]. A similar system to ARTHuR was developed by Wu et al. [75]
PAM & POGO [16, 76]	1 2 3 5	All actuated DoFs of this system are actuated by pneumatic cylinders	DOF: A B C D E F	Names of the system are short for Pelvis Assistive Manipulator and Pneumatically Operated Gait Orthosis, which explain the function of two mechanisms.
UoA PMbot [19]	1 2 3 4	A pair of PMs is used for one active joint.	DOF: A C	The actuation system is inspired by the human musculoskeletal system. For a specific joint, one PM is for flexion and the other is for extension. PM is light and with controllable compliance.

For clarity, Arabic numbers are used to represent degree of freedoms (DoF) of the gait driving mechanism, and alphabetic characters are used for DoFs of the trunk/pelvic mechanism. The matches are as follow:

1- Hip flexion/extension, 2- Hip ad-/abduction, 3- Knee flexion/extension, 4- Ankle Dorsi-/plantar-flexion, 5- ankle joint is left free to move in all DoF. A- vertical transition; B- forward/backward transition; C- lateral transition; D- rotation about the vertical axis; E- Rotation about the axis perpendicular to the sagittal plane; F- Rotation about the axis perpendicular to the frontal plane. A number or characters in normal font means the specific DoF is actively actuated; in bold font means the DoF is left free to move.

2.2.2 Analysis of reviewed designs

The foot plates of the end-effector robots need to at least partially bear the weight the training patients. Therefore, there were high torque/force requirements for the actuators of such robots. The reviewed end-effector robots were all driven by geared electrical motors which are stiff and non-back-drivable. The foot plates are the only interacting media between the robots and the lower limbs of the patients. Compared to exoskeleton type of robots, patients training on the end-effort robots are less constrained and only the trajectory of the foot are controlled to produce gait like movements. As a result, in the initial phase of the training, one therapist was still needed to assist the knee joint movement [10].

The gait driving mechanism of the treadmill based gait rehabilitation robots are usually in the form of exoskeletons. The reviewed treadmill based (summarized in Table 2-1) robots have exoskeletons that are at least designed with the sagittal plane rotations of the hip and knee joint actuated, so as to guide the patient to reproduce desired gait patterns. In terms of joint actuation, the first two robots listed in Table 2-1 were driven by electrical motors that exert linear actuation with moment arms to the joints. Some gait rehabilitation exoskeletons adopted geared electric motors to directly actuated joint rotations, such as the NaTUre-Gaits by Wang et al. [65] and the three-DoF lower limb exoskeleton by Wu et al. [77].

To meet the torque requirements of gait rehabilitation, the motor units used in these robots were of high inertia and end point impedance (stiffness). Stiff actuation is good for increasing trajectory tracking precision, but it could cause discomfort or injury to patients with spasticity during rehabilitation training [78]. The impedance controller implementations could make such robots to provide compliance patient interaction. However, the implementation added extra layer of development complexity to the robots [78]. Nonetheless, due to the high inertia of the exoskeleton and limited sampling rate of the controllers, only a limited range of impedance could be achieved and the systems was thus prone to stability issues [9, 14].

To make the actuation more compliance and reduce the inertia of the gait driven exoskeleton, the lower extremity powered exoskeleton (LOPES) was developed [70], with serial elastic actuators and Bowden cable power transmission. However, spring stiffness of the SEA system was constant; thus, the extent of high impedance that could be reached was restricted. Friction and extension of Bowden cables during operation was difficult to model. As a result, it could also affect the control precision and bandwidth, reduce power transfer efficiency [19, 79].

Intrinsically compliant pneumatic actuators provide another approach to bring compliance into rehabilitation robotic designs. Pneumatic cylinders were utilized to actuate the hip and knee joints' flexion/extension of the Pneumatically Operated Gait Orthosis (POGO) [80]. To meet the torque requirement of gait rehabilitation, bulky and heavy cylinders may need to be used.

Pneumatic muscle (PM) actuators are intrinsically compliant, lightweight and with high force/power to weight ratio. PMs have been regarded as promising candidates for actuating rehabilitation robots. Hussain et al. [19] developed a treadmill based robotic gait rehabilitation exoskeleton actuated by PMs in the University of Auckland; hence the device is named as 'UoA PMbot' in Table 2-1.

There have not been detailed actuation system analysis reported on this robot in order to satisfy the joint torque and range of motion requirements for task specific gait training [19]. Safety, adaptability to anthropometrics of various patients, and the design of the pneumatic system are all necessary to consider, in order to develop a robust robotic PM driven exoskeleton for clinical application. However, these factors were just superficially mentioned in [19, 81]. Therefore, a new PM driven gait exoskeleton has been developed and the developmental process is elaborated in Chapter 3.

2.3 Control strategies of robotic gait rehabilitation

The reviewed control strategies can generally be divided into three categories: trajectories tracking, bio-cooperative and assist-as-needed (AAN). Trajectory tracking is also known as position control, so robots guide the lower limbs to move along certain reference paths, similar to the way therapists move patient's legs during manual BWSTT.

2.3.1 Trajectory tracking control

The implementations of trajectory tracking control strategies are dependent on the mechanical design. End-effector robots usually guide the patients' feet along the reference trajectories in the parasagittal planes. Open loop control with pre-defined trajectory was implemented on GaitTrainer due to its one DoF linkage driving footplates. The foot trajectory was defined by its hardware design with 60% stance phase and 40% swing phase in every gait cycle. The orientation of the footplates also changed as the progression of the gait cycle to simulate the movement of level treadmill walking [54]. As an extended version of GaitTrainer, both HapticTrainer [55, 56] and G-EO [57] both had two programmable footplates. Each of them

was actuated in all 3 DoFs in the sagittal plane; so they could be programmed to simulate walking on various terrains or even add perturbations to the training process.

Treadmill based or ambulatory robots usually guide the flexion/extension of the hip, knee (and possibly ankle) joints along their individual angular reference trajectories [21, 50, 65]. These reference trajectories are usually adopted from literature [16, 50]. Customization has also been made in order to have more suitable reference trajectories for individual patients. “Teach and reply” is another way to obtain the reference trajectory, which was firstly proposed on research robot ARTHuR [72]. Due to the back-drivability of this robot, patients can walk on treadmill with the robot attached. In this case, the robot was in sensing and recording mode. The recorded movements would be used as reference in the actuation mode. The logic was then achieved on robotic gait rehabilitation system PAM and POGO [82]. Walking with leg orthoses attached for sensing and evaluation has also been reported on a non-backdrivable robot with the actuators removed [83]. Moreover, the desired reference trajectory can also be generated online according to the movement trajectory of the unimpaired limb of hemiparetic patients. This was first implemented on an upper limb robotic device [84]. An algorithm called Complementary Limb Motion Estimation (CLME) was developed for gait rehabilitation. In CLME, the trajectory of the disabled leg is generated online based on the sound leg autonomously. CLME was implemented on LOPES gait rehabilitation robot and evaluation studies were also conducted, which indicated that (1) CLME was able to produce stable gait for the impaired leg; (2) patients can walk more naturally with CLME than with a fixed reference trajectory [85, 86].

Trajectory tracking control strategies were also implemented to PM driven lower limb rehabilitation robots. Due to the nonlinear and hysteresis behaviours of the PM actuators, sliding mode controllers were often adopted to control joint space positions in order to guide the subjects to walk in desired training trajectories [20, 21].

2.3.2 Bio-cooperative control

Although customization has been made in reference trajectory generation, trajectory tracking control still has some limitations. Literature has suggested that physically guiding may decrease motor learning [70, 87]. The reason is that guidance changes the dynamics of the task, such as walking task. Thus, the trained task is not exactly the target task. This does not fully obey the motor learn rationale that training needs to be task specific. Furthermore, guidance reduces the burdens on the participant’s motor system to discover [70] the principles needed to perform the task successfully. Patient’s physical effort is also reduced by pure trajectory tracking training.

Marchel-Crespo and Reinkensmeyer [88] summarized this phenomenon as “Slacking Hypothesis”, which means that a rehabilitation robot could possibly decrease recovery as a decrease in the subject’s motor output, effort, energy consumption and/or attention.

Bio-cooperative control strategies were introduced to control and encourage patient’s participation both physiologically and psychologically. Active and high intensity physical participation of the patient can facilitate the motor learning process during rehabilitation training [13]. Koenig and his colleagues [52] have reported closed loop control of patient’s physical participation using heart rate or weight sum of interaction torque [51] between a patient and the robot as feedback. The algorithm development and related experiments were based on the Lokomat. The controller’s output was either on the virtual environment or treadmill speed. For less impaired and cognitively capable patients, a screen showing virtual environment was used on indicated the desired level of participation. These patients were asked to actively conduct training to match the desired level of participation. For more impaired patients or patients who cannot understand the virtual environment display, treadmill speed was controlled to match the feedback heart rate to the desired value. Higher treadmill speed means more physical effort and thus higher heart rate, vice versa [52].

Virtual reality, as another bio-cooperative control technique, has been proved useful in terms of motivating and challenge patients for longer training duration and cadence [53], modifying patients’ participating level [89, 90], updating subjects with their training performance [91] and generalising training result to real life scenario [89]. Real-time estimation of cognitive load during Lokomat robot training was developed, as well as a virtual task with varying cognitive difficulty levels. The cognitive load has three difficulty levels: under-challenged, challenged and over-challenged. In this virtual task, a question is displayed for the subject. The subject needs to accelerate to answer the question with “yes”, before an object representing the question disappears in the display. Otherwise, the subject decelerates to answer “no”. The closed loop control was achieved by modifying the task according the estimation to keep the subject reasonably challenged. [92, 93].

2.3.3 AAN control algorithms

As the name suggested, in AAN training strategies, the robotic devices only supply as much effort as a patient needs to accomplish training tasks by assessing his/her performance in real-time. In this way, the voluntary participation of the patient is encouraged; whereas, in conven-

tional robotic trajectory tracking gait training, the patients' active participation is not considered. Studies have been conducted on both animals and human to compare active (voluntary) to passive trainings [11-13]. Results of these studies indicated that a subject's voluntary participation leads to more effective training. However, in terms of implementation, the name "assist-as-needed" only suggests a vague concept, since different kinds of assistance could be applied according to specific applications. This thus implies that a review of various implementations of AAN concept in the field of robotic gait rehabilitation could help the researcher to have a better understand the state of arts and benefit its further development. In this section, each reviewed application will be analyzed from two aspects: (1) what is assessed to quantify the need of assistance; (2) how the assistance is provided by a robot.

Mechanical impedance can be treated as the relationship between the force exerted by the actuators and the kinematics. The concept of impedance control was firstly proposed by Hogan [94]. In this case, the mechanical impedance is viscoelastic, so the restoring force was related to the deviation of reference trajectory and the robot's velocity. The impedance controller implemented on Lokomat followed the same idea [9]. However, a dead band was introduced to allow the normal variation of human gait pattern. The robot would only intervene if a set level of trajectory deviation was exceeded. The value of impedance was chosen by the therapists based on their experience and patients' disability level. The challenge of impedance controller implementation was to have the intrinsically stiff actuation system of Lokomat behave compliant. The way to achieve this was to compensate the natural impedance of Lokomat and subject, as well as effects of gravity and friction, using an inverse dynamics model of subject leg and the exoskeleton and a friction model.

Force-field is the type of impedance controller implemented in Active Leg Exoskeleton (ALEX). In this controller, a "virtual wall" was created along the reference trajectory of the patient's foot in the sagittal plane. ALEX generated a field force that drove the subject's foot to move along the reference trajectory. The field force was consisted of tangential, normal and damping components. The magnitude to the force depended on the perpendicular distance of the foot from the desired trajectory. The closer was the foot to the desired trajectory, the larger the tangent force would be. If the foot was within the tunnel confined by the "virtual walls", it would experience no normal force. Once it is out of the tunnel, the normal force would increase exponentially to force the foot back to the desired trajectory [67, 95]. A similar control strategy was implemented on Lokomat [96]. "Virtual walls" were built along the reference trajectory in the joint spaces of knee and hip flexion/extension.

Robot-in-charge, patient-in-charge and therapist-in-charge modes were implemented on LOPES gait training robot [15]. For robot-in-charge mode, the mechanical impedance of the robots is set to high. It guided the legs to move in pre-defined trajectories, which was similar to the trajectory tracking control. For patient-in-charge mode, low impedance value is used, so the robot thus behaved to be fully compliant and exerted virtually zero interaction torque to the subject. In therapist-in-charge mode, the impedance level was adjusted manually to vary the extent of guidance according to the patient's capabilities or training progress [15]. Compared to the actuators of Lokomat, the serial elastic actuation system of LOPES is more compliant, so reference actuating force can be derived directly from the kinematic errors without inverse-dynamics modeling.

For rehabilitation robots driven by PMs, a controller was developed to change the joint space compliance while tracking the reference trajectory [21]. The behaviour of this control system is similar to the impedance control system on the motor driven gait rehabilitation robots. When the compliance is low, the patient will be confined to move along the desired trajectory and it is similar to have high impedance level. On the other side, when the compliance is high, the patient will have more freedom to move around the desired trajectory and it is similar to control the impedance to a low magnitude.

Another form of AAN rehabilitation encourages self-initiated movement by patients [12]. These approaches allow the patient to start moving voluntarily. If the patient is not able to achieve a threshold, the assistance from the robot will be triggered. This strategy has been widely used in upper limb rehabilitation robots. It was also implemented to the robotic gait training system of PAM and POGO [16], in which step time data obtained from foot switch was used as threshold to trigger robotic intervention. Initially, a reference trajectory with normalized timing was pre-defined for the subject using "teach and replay" method. The reference trajectory was to provide force patterns during a gait cycle rather than pursue precise position control. If the recorded timing was out of the range of allowable threshold, the replaying speed of the reference trajectory would change accordingly to synchronize with the subject's stepping timing. The changes happened discretely every gait cycle with a constant decrement or increment in timing each time. A more advanced synchronization algorithm was also reported in the literature. It utilized kinematics of all actuated DoFs of PAM and POGO to estimate subjects' gait timing continuously, so the robot system can synchronize its gait time of the subjects' in the meantime with customized logic expressions [16].

AAN controls have also been developed for footplate type of gait rehabilitation robot. As reviewed previously, Gait Trainer only had one DoF, so the variations of controller implementation would probably be very limited. Two adaptive control algorithms have been presented in literature [97]. The first one featured a one-dimensional window along the footplate trajectory, within which the patient was only slightly guided. Outside the window, a force field is then applied to reduce the trajectory error. The second algorithm improved the first algorithm by having adaptive window size based on a patient's training progress [97]. Yoon and colleagues [59] developed footplate robot with upper limb mechanism. The interacting torque between the subject's upper limbs was used to detect the subject's intention on changing walking velocity. The walking velocity was updated based on an algorithm, which calculated difference between the accumulated time periods when interacting torque was above the upper threshold and when the interacting torque was below the lower threshold. If the time difference is positive, the walking velocity for the next gait cycle would be increased by the amount proportional to the time period difference, and vice versa. This algorithm enabled the gradual change in walking velocity. This adaption algorithm could also be fitted to various walking terrains which were simulated by the end-effector robot.

The AAN controlled strategies reviewed up to this point only utilized gait kinematics or more specifically derivation to the reference trajectory to determine if assistance is needed. The ability, training progress and/or impairment of individual patients have not been considered. Such gaps could potentially be filled by patient-cooperative training, which have advantages of modify training parameters based on individual needs [88] or disability levels [23]. It also encourages the active movements and muscle contractions and induces more physiological and variable sensory input to the CNS [98].

Jezernik et al. [98] developed algorithms to adapt the reference trajectories of lower limb joints according to results from various assessments. For the adaption, a mathematical expression was firstly constructed with adaptable parameters to describe the desired trajectories of the hip and knee joints. Adaption could be achieved by optimizing relevant parameters in the expressions. For assessments, each leg with orthosis was modelled as a double-link pendulum. Force sensors were used to measure actuator forces and leg-exoskeleton interaction forces. With the interaction force measurements, the interaction torques of hip and knee joints were able to be estimated by inverse-dynamics for the swing phase of every gait cycle [99]. A total of three adaption approaches were reported. The first approach was the inverse-dynamics-based joint-

angle adaptation algorithm. The hypothesis of this approach was that minimal interaction appears when the leg and the exoskeleton were completely synchronized. Variations in the interactive torque could be estimated using the deviation from the desired gait pattern which related to the trajectory parameters. Online optimisation of gait pattern parameters could thus be performed to achieve minimum overall interaction torque. The accuracy of this approach heavily relied on the accuracy of mathematical model of leg-exoskeleton combination. In the second approach, the interaction torques in the joint angle spaces were used to estimate the changes of trajectory accelerations desired by the patient, so adaptation to the desired trajectory could be performed to achieve the expected acceleration [99]. This approach was claimed to reduce the dependency on the leg orthosis model. The third approach is based on impedance control. Impedance controller plays a role to link the allowable trajectory deviation and the interaction torque. Active joint torques from the subject would result additional human-exoskeleton interaction torque, which could be estimated by force measurements. Based on the impedance relation, the additional torque reveals how much the patient would like to change the reference trajectories [98]. Therefore, adaptation to the desired trajectories could be performed.

Apart from gait pattern adaptations, impedance magnitude adaptation was also implemented to the Lokomat robotic gait trainer. The impedance adaptation also relied on estimation of the interaction torque between the patient and the orthosis. This interaction torque was treated as an indication of patient's effort. If little effort detected, the controlled impedance would be set to high, which meant the leg movement was forced to follow the reference trajectory. Conversely, if an increase effort was detected, the impedance would be controlled to a lower value. Hence, a greater deviation would be permitted and the patient would have more freedom too. In this impedance adaptive controller, the reference trajectory was fixed [9].

Adaptive impedance control was also implemented on the gait rehabilitation robot developed by a PM driven rehabilitation robot [23]. The logic of the control algorithm was similar to the one reviewed in the last paragraph. The way they used to determine the level of participation was adopted from [100], in which the authors conducted experiments to identify the average interaction torque of the totally active and passive stages. These two extremes were used as reference for the scaling of patients' participation.

Trajectory tracking control systems are the foundation for gait rehabilitation robotics. This control strategy is more suitable for patients with severe gait disorder or at the initial stage of gait rehabilitation. However, such control strategy may not be optimal for providing effective

gait rehabilitation since it could decrease the subject's motor output, effort, energy consumption and/or attention [88].

To solve such problem and improve the effectiveness of robotic rehabilitation, researchers have been attempting different approaches. Among these approaches, impedance related controllers have been implemented in different platforms. For robots with stiff actuators, extra force sensors and modelling work were needed to give the robots compliance behaviours. For the robots driven by SEA, the back-drivable actuators eased the implementation of impedance control, especially the low/zero impedance control mode. However, during impedance control, the actuators act as force/torque source. Stability may become an issue, if the controller cannot react fast and accurate enough to adjust the force/torque based on the robot kinematics.

The robust trajectory tracking controller ensures the stability of the control system of PM driven robotic. The intrinsic compliance of the PM actuators can be utilized to vary the extent of guidance provided the exoskeleton. The challenge is how to control both joint space position and compliance simultaneously. The controllers presented in [21] only had closed-loop control of the position and the compliance was calculated through an open-loop model based on the PMs.

Moreover, the adaptive impedance controller developed to the PM driven robot [23] was similar to the algorithm implemented to the motor driven system [9]. However, due to the process of in-/deflation and nonlinearity, the pneumatic muscles may not be high-precision force source for impedance control. Hence, the bandwidth of such PM based adaptive impedance control system could be very limited. It would be of the researcher's interest to develop adaptive compliance control system based on the variable stiffness property of PM in order to achieve AAN gait rehabilitation.

2.4 Clinical effectiveness of robotic gait rehabilitation training

Effectiveness of gait rehabilitation robots can be studied through computer simulations and trials on either patients or healthy subjects. Among the large variety of studies, those studies with patients are providing stronger evidences from the clinical perspective; thus, only studies with patients are included in this section. To investigate the effects of control strategies on training effectiveness, reviewed studies are categorised according to control algorithms as described in their training protocols. Most of the searched studies are with the trajectory tracking

control algorithm, since devices with trajectory tracking control have been well-researched and even commercially available. All the reviewed studies are summarised in Table 2-2.

Table 2-2 Summary of the effectiveness studies reviewed in this section.

1st Author	Device	Control Strategy	Patient Type	Control group	Number of participants	Primary outcome measures
Schwartz [101]	Lokomat	T.T	Sub-acute stroke	CT	67	FAC
Hidler[102]	Lokomat	T.T	Sub-acute stroke	CT + TS	63	5m-TWS, 6m-TWD
Ng[103]	Lokomat	T.T	Sub-acute stroke	CT	54	EMS, BBS, FAC, 5m-TWS, Barthel Index
Fisher [104]	Auto-ambulator	T.T	Less than 12 months from onset of stroke	CT	20	8m-TWS, 3m-TWD, Tinetti Balance assessment [105]
Peurala [106]	Gait-Trainer	T.T	Chronic stroke	TS	45	10m-TWS 6m-TWD
Peurala [107]	Gait-Trainer	T.T	Acute stroke	1: CT 2: TS	56	FAC
Husemann [108]	Lokomat	T.T	Acute Stroke	CT	30	FAC, 10MWT
Chang [109]	Lokomat	T.T	Sub-acute stroke	CT	37	Cardiopulmonary fitness assessments
Pohl [10]	Gait-Trainer	T.T	Sub-acute stroke	CT+TS	144	FAC, Barthel Index
Hornby [110]	Lokomat	T.T	Ambulatory chronic stroke	TS	48	SSV, FV
Westlake [111]	Lokomat	T.T	Ambulatory chronic stroke	TS	16	SSV, paretic step ratio
Mayr[112]	Lokomat	Impedance control	Stroke with less than 8 months from onset	CT	16	7 measures covering gait function and speed, muscle strength and tone
Jezernik [113]	Lokomat	Trajectory adaption control algorithms	Incomplete SCI	N.A.	6	Adaption of parameters describing gait trajectory; patients questionnaire

1st Author	Device	Control Strategy	Patient Type	Control group	Number of participants	Primary outcome measures
Duschau-Wicke[114]	Lokomat	Impedance control and PCPC	Incomplete SCI	TT	11	Kinematic variability, interaction torque, heart rate, muscle activity
Schück [115]	Lokomat	PCPC	Chronic stroke and chronic SCI	N.A.	Stroke: 2; SCI: 2	10m-TWS
Fleerkotte [116]	LOPES	Impedance control	Incomplete SCI	N.A.	10	Gait kinematics and clinical assessments
Srivastava [117]	ALEX	AAN force field control	Stroke with 3 to 140 months from onset	N.A	9	SSV; 6m-TWD; DGI; TUG and gait kinematics

The numbers in the ‘Number of participants’ column do not count participants who dropped out during a study. In the ‘Control group’ column, ‘XX+XX’ means two types of training applied to the same group; one study by Peurala et al. [107] has two control groups. Abbreviations used in this table are explained as follow: FAC: Functional Ambulation Classification, for the severity of gait impairment in terms of gait function[118]; T.T: trajectory-tracking control or position control; PCPC: patient-cooperative path control [96] CT: conventional therapy; TS: manual task-specific gait training; 5 or 10m-TWS: 5 or 10 meters timed walking speed, fastest comfortable speed a patient can achieve; 6m-TWD: 6 minutes timed walking distances for endurance; DGI: Dynamic gait index [119] SSV and FV: self-selected velocity and fast velocity, both are measures of gait speed; EMS: Elder Mobility Scale[120]; BBS: Berg Balance Scale[121]; TUG: timed up and go test [122]; N.A.: not apply.

2.4.1 Trials with trajectory tracking controlled robots

From Table 2-2, it can be seen that the trials on trajectory tracking control are of great similarity. Effectiveness of robotic gait rehabilitation was compared against either conventional therapy or task specific gait training (manual BWSTT or over-ground walking). Hence, these trials can be analysed as a group.

A number of studies examined the effectiveness of robotic training versus conventional therapy of the same length [101-104, 107]. Alternatively, some studies had the experimental groups to receive robotic training and conventional therapy and the control group to receive only conventional therapy. The total session lengths of the control group and experimental group were equal for all the experiments [10, 108, 109]. Most of the clinical trials indicated that robotic gait training alone or the combination of robotic gait training and conventional therapy is superior to conventional therapy alone in terms of gait function recovery [10, 101, 103, 107, 109]. Trials also reported improvement but no difference in gait function recovery, which was the primary assessing scale of those trials, between experimental and controlled groups [104, 108]. Another trial however reported that conventional therapy was superior to robotic gait rehabilitation in terms of gait speed and endurance [102].

For trials that compared position controlled robotic gait training with task specific gait training by therapists, the experimental and controlled groups received robotic and therapist-based gait training respectively, with same amount of sessions of same lengths [106, 107, 110, 111]. Majority of these trials [106, 107, 111] reported that there was no significant difference between experimental and controlled groups in primary outcomes, which indicates that functional gain in gait ability. One trial [110] with ambulatory stroke patients reported that BWSTT with therapists is more effective than gait training with Lokomat in position control mode.

From RCTs of position controlled robotic gait rehabilitation on patients with gait disorders, the following findings are extracted. Firstly, the robotic gait training based on this sort of control algorithm has been proved to be effective, since majority of the trials indicate that robotic gait trainings are at least as effective as trainings based on conventional therapies alone. Secondly, despite emancipating therapists from intensive work, there is no evidence for that robotic gait training is superior to manually task specific gait training. Thirdly, the training protocols of studies [102, 110], in which traditional rehabilitation approaches were reported to be more effective than the robotic approaches, were investigated. In [102], the conventional therapy was

customized for individual patient involving the hybrid of interventions based on Bobath concept and task specific gait training. Therapists determined the type and dose of interventions based on their understanding of the patient's training progress. In [110], therapists only provided as much as the patient's paretic limb needed to ensure continuous walking rather than guiding the limb to achieve normal walking trajectory. By contrast, in the experimental group, Lokomat guided the patient's limb to reciprocate in the pre-defined trajectories, even though patients were requested to maximise their participation during training. An additional reviewed study conducted by Israel et al. [123] specifically compared the metabolic cost and EMG of leg muscles between position controlled gait training and manual BWSTT. They concluded that subjects with incomplete SCI had reduced muscular activity when doing robotic gait rehabilitation. According to these evidences, it can be interpreted that customization rehabilitation based on patients' ability and assisting only as needed could potentially lead to more effective gait rehabilitation.

2.4.2 Trials on AAN controlled robots

Compared to trajectory tracking control, much fewer clinical studies on robotic gait rehabilitation with AAN control strategies were encountered during the review. Hence, all the trials with patients were considered during the review and they were not limited to RCTs. Since AAN control approaches are still a relatively new research topic, most of the reviewed studies were designed to investigate certain aspects of effectiveness rather than improvement in gait function in general. This is reflected by the assessments used to measure results as shown in Table 2-2. The number of participating patients was also smaller than those of studies with trajectory tracking control. Due to such variety, studies about AAN control are analysed individually with more details than studies based on trajectory controlled robots.

One study investigated the gait function improvement between Lokomat and conventional gait training [112]. Sixteen strokes patients mostly sub-acute were involved and randomly assigned to two groups who conducted ABA or BAB training (A: Lokomat for 3 weeks and B: conventional therapy for 3 weeks). Impedance control strategy was adopted in Lokomat training with therapists reducing the level of assistance as the progress of the training. For conventional training, mostly Bobath concept based exercises were used with ground walking focused less on the quantity, but more on the gait itself. Assessments took place after 3, 6 and 9 weeks to measure the result of each phase. The results indicated that more significant improvement was found in Lokomat training phase in most of the assessments.

Jezernik et al. [113] conducted a clinical study with six SCI subjects to test the performance of trajectory adaption algorithms reported in [99]. In this study, six subjects were trained with two trajectory adaption algorithms, one based on variation in acceleration and the other based on impedance control. Each subject randomly received a total of six trials with both algorithms in three different conditions. The adaptation performance was measured via calculated gait parameters and questionnaire presented to subject after finishing all the trials. Conclusion of the study indicated that (1) adaption took place successfully, but no significant differences in performance were observed between the two adaption algorithms; (2) subjects all prefer the tested gait-pattern algorithm to the position control algorithm and they are motivated and active in training according to the questionnaire.

Duschau-Wicke et al. [114] conducted experiments to compare the extents of patient participation between AAN strategies and position-control strategy. Eleven incomplete spinal cord injury (SCI) patients were involved in the experiments. They were all trained in position mode [50], impedance control mode [9] and patient-cooperative path control mode [96]. For result measurement, higher spatial and temporal kinematic variability, increased heart rate, less human-robot interaction torque and higher muscle activity (detected by EMG) all indicated higher level of participation, vice versa. The result of this study revealed that significant higher participation in patient-cooperative path-control mode than in position control mode in all the measurements; impedance control mode resulted higher spatial variety and less interaction torque but not significant difference in other measurement when compared to position control mode.

Schück et al. [115] conducted a study on the feasibility of patient-cooperative control of Lokomat. Two chronic SCI and two chronic stroke patients took part in the study. Assessments were performed before and after the four-week training period for comparison purposes. The training strategy was adopted from Duschau-Wicke et al. [96]. As the training progressed, the allowable trajectory variance and walking speed increased; the percentage of BWS was decreased by controller and mechanism, as presented in [66]. The results indicated that more muscle activities observed in patient-cooperative training compared to position controlled gait training. No significant improvement could be concluded from the before-after training assessments.

Fleerkotte et al. [116] investigated the effectiveness of an AAN control strategy based on LOPES robotic gait trainer. Ten incomplete SCI patients were involved in the study. Therapist-

in-charge control mode was applied so impedance value could be adapted to the patient's capabilities. During the period of study, all participants received eight weeks training with three sessions per week and a maximum 45 minutes per session. Effectiveness was examined by the comparison of pre- and post- study measurements of gait kinematics, walking ability and lower limb strength. Significant improvements were observed in both clinical walking ability parameters and gait kinematics. The research concluded that the improvements are at least partly resulted from the training strategies of LOPES.

Srivastava et al. [117] conducted trials with 9 post-stroke subjects with the ALEX gait rehabilitation robot with the AAN force field controller [68]. Each subject received 15 training sessions, five daily sessions per week and every other week for three weeks. Each session had a 40 minutes training time with ALEX. Before, immediately after and 6-month post training performance assessments were conducted to investigate the effectiveness of the training. The experimental results indicated that the improvement in over-ground walking pattern and some clinical gait ability measurements after the trials. However, compared to results reported in Hornby [110], the improvement was not superior to trajectory tracking controlled robotic gait rehabilitation training or conventional BWSTT.

2.5 Approaches to assess gait ability

One important factor for AAN strategy is to understand and quantify the patient's ability, impairment or progress in training. As stated previously in this chapter, the implementation of AAN control algorithm ought to address what is assessed to quantify the need of assistance. Most of the reviewed approaches used kinematic parameters, such as the deviation from the reference trajectory to determine if assistance is necessary, and if so, what the appropriate amount is. For algorithms to measure gait kinematics, the review paper by Rueterbories et al. [124] covered methods to sense and analyse gait kinematics in terms of different sorts of sensors. Force sensors were included in the review, but their functions were limited to threshold detection for identifying gait events, such as heel strike or toe off. Only a few researches [9, 23] have used dynamic parameters like interaction torque for assessment. Due to the importance of assessments and the limited number of available approaches, possible gait assessments are reviewed and discussed in this section to investigate whether they can further improve AAN robotic gait training.

A variety of gait assessment methods have been adopted in clinical studies of gait rehabilitation approaches. Among those assessments, functional ambulatory capacity scale is the most widely

used one, which assesses a subject's walking ability [125]. Similar assessments include 10 meter timed walking for gait speed [126], 6 minute timed walking for gait endurance, Rivermead Motor Assessment [127], Barthel Index [128] for patient's mobility in general. These assessments are dedicated to quantify or qualify in terms of gait functions. There are also assessments focusing on the level of impairment such as Fugl-Meyer Assessment [129] and assessing motor power such as Motricity Index [130]. These assessment methods take place separately from the actual training session and are often conducted once after a few sessions. However, for implementation of AAN strategies, assessments are required to be integrated into the training sessions in order to monitor the patient's ability and training progress.

One way to quantify patient's weakness was to use force sensing to identify patient's weakness and gait ability. Through force sensing and inverse-dynamics, the patient's active torque of lower limb joints can be revealed. Literature has reported methods to use such active joint torque as the scale to quantify patient's weakness [131, 132]. From joint torque and kinematic measurement, mechanical power of joints can also be computed as an indication of gait ability [133]. Neckel et al. [115] developed an algorithm to quantify chronic stroke patients' functional weakness of lower limb using an off-shelf 6-axis load cell. In the experiment, the foot of the affect lower limb bound in a foot retainer. The foot retainer was supported by rigid connection to the load cell. The load cell is the only interaction between the affected leg and the global frame. The torso was also constrained to an upright position. Hence, the affected leg of a patient was placed to a fixed configuration, so only static forces and joint torques would be measured and calculated respectively. The algorithm to calculate joint torques from load cell measurements was adopted from [134]. The generic equation used is shown as follow:

$$\begin{bmatrix} F_{i+1} \\ T_{i+1} \end{bmatrix} = \begin{bmatrix} {}^{i+1}R_i & 0_{3 \times 3} \\ {}^{i+1}P_i \times {}^{i+1}R_i & {}^{i+1}R_i \end{bmatrix} \begin{bmatrix} F_i \\ T_i \end{bmatrix} \quad (2-1)$$

where $i=0,1,2,3$ represents the frame of load cell, ankle joint, knee joint and hip joint respectively. ${}^{i+1}R_i$ is a 3×3 rotational matrix from i to $i+1$ and ${}^{i+1}P_i \times {}^{i+1}R_i$ is a 3×3 skew matrix from i to $i+1$. F_i and T_i are 3×3 matrices representing force and torque in a specific frame.

Compared to the static joint torque which is targeted by the previous approach, the dynamic joint torque during walking is more meaningful for the development of AAN control strategies. One approach to estimate patient's active hip and knee joint torque has been developed to help the implementation of impedance control to Lokomat [9]. In this approach, inertial, coriolis

and gravitational moments of the human leg and exoskeleton, as well as the moments caused by human-robot force interaction were all accounted to calculate the torque of knee and hip joints. After the calculation, the passive torque was eliminated from the total joint torque for the active joint torque. This approach was limited to calculating torque during the swing phase of gait, since the ground reaction force was not measured in stance phase. As a result, the estimated torque can only be used as a rough approximation of patient's participating level.

Neckel et al. [132] also reported an approach to calculate dynamic joint torque patterns during trajectory controlled Lokomat training. Compared to the approach in [9], three axial ground reaction forces were measured using a special split belt treadmill with force plates integrated underneath its conveyor belts [135]. This setup, together with load cells to measure leg-exoskeleton interaction forces and the force generated by the passive foot lifter, can measure the lower limb joint torques throughout the gait cycle with detailed computing algorithm described in [136].

Apart from using traditional load cell and force plate, researchers have also integrated force sensing function into the exoskeleton design. del-Ama et al. [137] have designed a lower limb exoskeleton in a way that interaction force between the shank and exoskeleton can be calculated according to the measurement of deformation of the exoskeleton structure. One section of the thigh segment of the exoskeleton was designed to significantly deform in the response to forces in the sagittal plane. Meanwhile the section was stiff to transverse forces. As a result, only interaction torque in the sagittal plane can be sensed.

Ground reaction force (GRF) sensing during human gait has been well researched in the field of biomechanics. It is recognised that it would also benefit the development of gait rehabilitation. The previously described applications either limited the measurement to static forces or using force plate embedded in a treadmill. These were not the solution for future gait rehabilitation training, which could involve assist-as-needed over-ground walking and ambulatory training in other conditions. Force sensing resistors can be integrated into the insole of shoes to measure GRF. These sensors act like on/off switches to measure gait events. This configuration has been used to evaluate hemiplegic gait [138] and assess gait rehabilitation outcome for SCI patients [139]. One kind of wearable GRF sensing was achieved through pressure sensing, such as in [140]. Pressure sensors on the insoles could be placed in shoes of both feet to measure pressure. However, this setup can only measure distributed vertical components of

GRF for level ground walking. Such technology has been adopted in an assistive walking exoskeleton to sense the shift of the centre of pressure; hence the moving intention of the subject can be detected [141]. However, such pressure sensing is not sufficient for computing patient's joint torque during stance phase, since friction forces also generate moments around lower limb joints. Another approach was to mount two 6-axis load cells underneath the shoes, so GRF and centre of pressure can be measured and calculated [142]. Further evaluation [143] also indicated that the instrumented shoes developed in this research had little effect on gait pattern in terms of both GRF measurement and gait kinematics. Liu et al. [144] developed a similar wearable system, which contains a thin and light sole that can be mounted underneath a pair of shoes. Each sole has five small tri-axial force sensors. Forces measured in local coordinate system of individual sensors were then transformed and summed to the global system of each foot for its GRF and centre of pressure.

Apart from the physical interaction between human and robot, subject's level of participation can also be detected via cognitive human robot interaction, which allows bidirectional flow of information between human and robot. Some types of such information are widely investigated such as bioelectricity of brain and muscle activities [145]. EMG is the technique to record and evaluate the electric activity of skeleton muscle. It has been commonly used in evaluating activity of leg muscles during gait training. EMG can also be modelled to control exoskeleton. This was achieved on HAL 5 for identifying moving intention and controlling exoskeleton by healthy subjects only [146]. For stroke patients, EMG by itself is not a reliable method for controlling rehabilitation robotic, because muscle spasms induce strong EMG signals which cannot be distinguished from the signals from voluntary muscle contractions by the system [147]. Furthermore, modelling is also necessary to quantitative connect EMG signal level with patient's moving intention. The modelling accuracy is influenced by inter-/intra-subject difference and fatigue. Therefore, calibrations also need to be conducted for every subject and every training session [88], which also makes EMG not widely adopted in the current stage.

2.6 Discussion

The development of gait rehabilitation robotic devices and control strategies facilitate each other. Initially, with the aim of automating traditional manual rehabilitation training, robotic trainers were developed. Meanwhile, these robots also provided platforms for implementation and testing novel control strategies, for example AAN algorithms. With ongoing research based

theoretical and supportive evidences, AAN strategies have become widely accepted with theory and evidence based supports. Hence, researchers began to attempt various options of AAN implementations in order to seek more effective ones. The trend urges the upgrade of existing trainers and design of new robots for lighter moving parts, more compliant and powerful actuations.

From the viewpoint of robotic design, most of the AAN algorithms reviewed in Section 2.3 have been implemented on treadmill training based exoskeleton robots with only limited number of cases applied to end-effector robotics and ambulatory robots. Compared to exoskeleton robotics, the only interaction between an end-effector robot and a training patient is through the feet. This limits the potential of integrating sensors and thus the implementing sophisticated AAN strategies. As a result, only simple adaptive control algorithm was implemented to Gait Trainer [97]. Due to the lack of sensor feedback from the low limb, information sensed from other body parts rather than lower limbs was used to achieve patient cooperative gait training [59]. Ambulatory robots are more towards integrating rehabilitation into daily life rather than a tool for control strategy research. It is anticipated that control strategies developed on treadmill based a gait rehabilitation exoskeleton can be easily migrated to an ambulatory robot with similar design.

Trajectory tracking control algorithm is the one used in almost all commercially available robotic gait trainers. This control algorithm has been proved to be effective in gait rehabilitation for stroke and SCI patients. However, apart from relieving therapists from physically intensive work of guiding low limb movements and stabilizing the torso, no significant improvement in effectiveness has been observed in clinical studies against manual BWSTT. Moreover, highly repetitive leg movement also reduces the subject's active participation and motivation. Bio-feedback and virtual reality were adopted in robotic gait training to observe subjects' participation level and motivate them. AAN control algorithms have provided options to unravel the limitations of trajectory tracking control and lead to more effective gait training. The reviewed studies achieved AAN control via impedance adaptation based on patients' abilities or the reference trajectory adaptation based on voluntary leg motion. In majority of these cases, trajectory deviation was used as the performance assessment. To have better assessment of the patient's voluntary effort, bio-feedback and human-robot interaction force/torque were also considered.

Gait ability assessments have been reviewed in this section to investigate their feasibility to be integrated into AAN gait training. Among the reviewed approaches, assessments based on human-exoskeleton interaction force and ground reaction force for active joint torque calculation seem to be more applicable in the current stage. This is due to the ease of integration with robotic gait trainers and less dependence on modelling accuracy. New gait ability assessing approaches however, leads to another question ‘how do we design the controller based on new assessment?’ The adaption to trajectory or impedance is still an option here. Additionally, if active joint torque is used as a representation of the gait ability, assistance by robots can be figured out in new approaches.

Clinical studies on robotic gait rehabilitation have been analysed in this chapter from the viewpoint of control algorithm. The primary goal for majority of clinical studies was to validate the robotic training in general, rather than focusing on the underlying control strategies. Most of the reviewed studies were RCTs with gait rehabilitation robots used only trajectory tracking control strategies, with only a limited number used AAN control strategies. On top of the limited research, the participant sizes were also significant lower in AAN studies than in trajectory tracking studies. Some of the AAN studies had no control group, so only pre-/post-experiment measurements could be compared. These studies also had narrower focuses on one or a few impact factors to clinical effectiveness, rather than the clinical effectiveness as a whole. As a result, the experimental and clinical significance provided by studies in AAN strategies were much less stronger than those on trajectory tracking control [148]. This agrees with the fact that AAN control strategies are cutting edge and still under intensive study, whereas commercialization of trajectory controlled robotic gait trainer has been successful. With the current evidence, it is still too early to draw a conclusion that any AAN strategy is superior to other AAN strategies or the conventional position control strategies. In the future, trials with larger patient groups will be needed to perform controlled clinical studies on the effectiveness related aspects of AAN control strategies. The control groups should not only be limited to manual or position controlled robot gait training, but also other implementations of AAN concept.

Based on this literature review, there have not been any clinical studies conducted on PM driven gait rehabilitation robots, regardless the control strategies implemented. The robotic design could be the main barrier for conducting clinical studies, for its capability to meet the torque and bandwidth requirements of task-specific gait rehabilitation. The PM driven gait rehabilitation robot developed by Hussain et al. [19] was primarily used as a research tool for developing

control strategies. The requirements of task specific robotic gait training, such as torque, safety and adaptability, were only briefly discussed.

2.7 Conclusions

In this chapter, the literature review critically analysed current research in the area of gait rehabilitation robots, with the main focus on discussing the robotic design, control strategies and clinical studies on their effectiveness. The literature review helped the author identify further directions of this PhD research.

With respect to the robotic design, a treadmill based robotic exoskeleton is preferred, since it provides more possibilities in control strategy development than end-effector robots and ambulatory robots. The review on robotic design also indicate that compliant actuation systems with low inertia not only improve the safety and comfort of robotic gait rehabilitation, but also simplified the development of mechanical impedance related controller. In this case, the light and intrinsically compliant PM actuators are regarded to be ideal for the gait rehabilitation robot. One major challenge in design, when working with PM actuators, is to have the exoskeleton ready for clinical studies. Comprehensive design needs to be carried out to meet requirements of safety, adaptability, joint torque, range of motion and bandwidth, in order to provide task specific gait training in clinical settings. The detailed robotic design of the gait rehabilitation exoskeleton will be presented in Chapter 3 of this thesis.

In order to extract the robot's full potential, control strategies need to be individually tailored to work seamlessly with a robot's specific mechanical design. The use of PM actuators enables the control of the joint space compliance of the exoskeleton, without an extra layer of complexity on exoskeleton and biomechanics modelling, as in non-drivable exoskeletons. In the case, that a training strategy required varying the mechanical impedance of a PM driven mechanism, Hussain et al. [23] utilized the PM actuators as torque/force sources the same way as electric motors. The extra layer of complexity was not avoided. Moreover, motor torque can be changed instantaneously by changing the current. However, for PM, the force change is a relatively slow process through inflation or deflation. PM's nonlinearity also affects the precision of its force output. Hence, PM is not an actuator for impedance control [14]. In the same scenario, it would be of the author's interest to utilize the PMs' controllable intrinsic compliance to facilitate the development of AAN training strategies.

Chapter 3 Development of a Compliant Gait Rehabilitation Exoskeleton

Pneumatic muscle actuated rehabilitation robotic devices have been widely researched, because of its intrinsic compliance and high power to weight ratio[19, 78, 149]. Task specific gait rehabilitation training imposes strict torque, range of motion and bandwidth requirements to the robotic exoskeleton design. However, the PM's nonlinear and hysteresis behavior, slow pressure dynamics and negative correlation between its force output and contracting length make the development even more challenging. To address such challenges, a new robotic Gait Rehabilitation EXoskeleton (GAREX) has been developed in order to facilitate task specific gait rehabilitation with controlled intrinsic compliance.

GAREX is developed with the potential clinical experiments in mind. Detailed actuation system design analysis is carried out to meet the requirements of task specific robotic gait training. Implementations on mechanical, electronic and software aspects ensure the safety of the training subject, which is of paramount importance. GAREX also has a modular construction to accommodate anthropometrics of most of the population.

3.1 Introduction

An exoskeleton type robot with low inertial moving parts, powerful and compliance actuators would provide a good robotic platform for AAN gait training. Exoskeleton type of gait rehabilitation robots like LokoMat [50] and Active Leg Exoskeleton (ALEX) [68] have geared electric motors or linear motors to provide linear actuation. The linear actuations together with levers produce driving torques to the actuated joints. To some exoskeletons, DC electric motor and gear units are directly mounted to the actuated joints to provide required rotational movements [65, 77]. To meet the torque requirement of gait rehabilitation training, the adopted motor and gear reduction units are usually heavy in weight. Thus, the inertia of the lower limb exoskeleton is significantly increased. As a result, some control strategies such as impedance control may not be easy to implement [15]. Being heavily geared also means high endpoint impedance, high stiffness and non-backdrivable [75]. However, stiff actuators could generate large force in response the patient's undesirable movements or impacts and further lead to discomfort or even safety problems [19].

One approach to reduce the inertia is to detach the motor units from the moving segment of the exoskeleton. Cable systems are often utilized as media between the distally located actuators and the actuated joints [150]. Series elastic actuators [70] provide a solution to the high endpoint impedance meanwhile adding compliance and back-drivability to the actuated exoskeleton joints. LOPES [15] was developed at the University of Twente with both Series elastic actuation (SEA) and Bowden cable power transmission.

Taking the advantages of the combination, both high and low impedance control strategies have been implemented to achieve robot guidance or near transparent patient in charge walking. However, spring stiffness of the SEA system is limited; thus, the extent of high impedance that can be reached is restricted by the mechanical design. Moreover, the utilization of Bowden cable could also affect the control precision and bandwidth, reduce power transfer efficiency, and be prone to wearing [19, 79].

Pneumatic muscle (PM) actuators provides a good option to reduce exoskeleton inertia as well as achieve variable actuation stiffness, due to the actuators' high power to weight ratio[151] and intrinsic compliance [152]. With such properties, PMs have been employed in various rehabilitation robotic applications [19, 78, 153].

To achieve effective robotic gait rehabilitation, the training is required to be as task specific as possible [154]. Hence, the robots need to assist or guide the subjects to walk in or similar to normal gait speed and pattern. Transferring this to the robot development, the following specifications are to be satisfied: (1) multiple actuated DoFs to reproduce gait pattern; (2) sufficient range of motion for the powered joints; (3) sufficient joint actuation torque to guide severely impaired subjects during training; (4) adequate controlled bandwidth to facilitate the training. Moreover, the intrinsic compliance property is one of the main motivations of adapting PMs in rehabilitation robotics. It is equally important to design the actuation system that opens the possibilities for the researcher to control the compliance of the exoskeleton during gait training.

In the past, gait rehabilitation exoskeletons actuated by PMs have been developed. Beyl et al. [153, 155] developed a lower limb exoskeleton actuated by pleated pneumatic artificial muscle. Both torque and trajectory control approaches were investigated. However, with the only actuated DoF at the knee joint, the device's potential use in clinical trials is limited.

Hussain et al. [19] developed a treadmill based robotic gait rehabilitation exoskeleton with two both the hip and knee joints actuated in the sagittal plane. Only the maximum joint torques of the exoskeleton were mentioned instead of detailed torque analysis which may not be sufficient to justify the torque requirement of task specific gait rehabilitation had been met. Moreover, safety and anthropometric adaptability factors about the exoskeleton design were not reported in details too. There are needs to develop a new PM actuated gait rehabilitation robotic exoskeleton with the requirements of task specific training in mind. All the above factors determining the feasibility of applying the gait rehabilitation robots in clinical setting should be thoroughly investigated.

This chapter will firstly briefly describe the support structure and trunk mechanism of a new GAit Rehabilitation Exoskeleton (GAREX). This will be followed by actuation system and mechanism design of the unilateral lower limb exoskeleton. Pneumatic system and instrumentations will be presented next. Lastly, the safety anthropometric adaptability design of the GAREX system will be covered.

3.2 Support structure and trunk mechanism

GARES consists of three major mechanical modules: the support structure, the trunk mechanism, and most importantly the unilateral low limb exoskeleton which are illustrated in Figure 3-1.

The support structure is constructed with MiniTec frames. All the mechanical, pneumatic and electronic components are mounted to the structure. The structure is usually rigidly connected to the rehabilitation treadmill for treadmill based gait rehabilitation experiments. It also has four wheels, so over-ground training with GAREX is also made possible. Due to the modular mechanical design, the trunk mechanism's vertical and horizontal position relative to the support structure can be easily adjusted to suit various patients or switch between treadmill based and over-ground gait training.

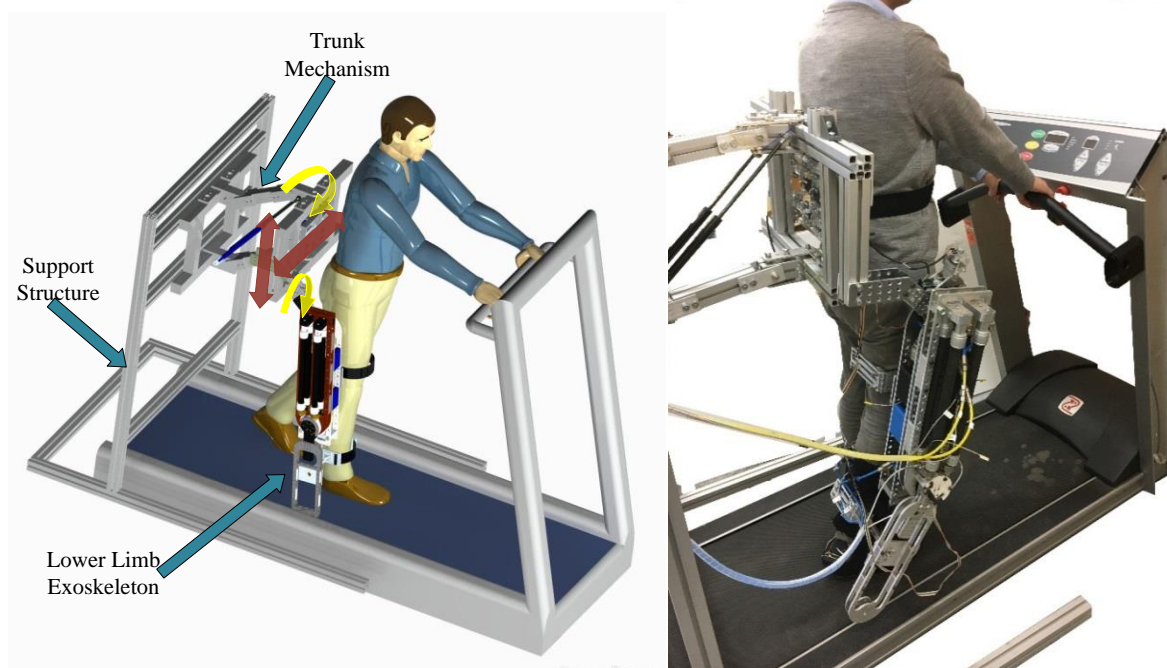


Figure 3-1 Left: computer-Aided Design of the GAREX system. The unactuated DoFs of the trunk mechanism are labelled with the arrows (red: translational DoFs; yellow: rotational DoFs). Right: a health subject walking on the treadmill with the guidance provided by GAREX.

During gait rehabilitation experiments, subject's upper body was attached to the trunk mechanism by means of straps. One of the main functions of the trunk mechanism to have three unactuated or passive degree of freedoms (DoFs), which are vertical and lateral translations as well as the rotation around the vertical axis. During normal walking, the trunk a healthy subject usually has range of motion (ROM) of less than 10cm in both translational DoFs and a less than 20° ROM in the rotational DoF [156]. Hence, the trunk mechanism was designed with 15-cm ROMs for the two translating DoFs and a 30° ROM for the rotational DoF.

Another main function of the trunk mechanism is to suspend the lower limb exoskeleton, so the training patient does not have to bear any weight of the mechanism during training. The suspension is achieved by a pair of air springs whose stiffness was adjusted to an appropriate level via trial and error. The connecting between the trunk mechanism and the lower limb exoskeleton allows two unactuated DoFs of the hip joint which are the abduction and the rotation in the transverse plane. These two DoFs are loaded torsional springs. When the springs are both in neutral position the lower limb exoskeleton is aligned with the sagittal plane. Such design can accommodate the natural movements in these dimensions and meanwhile constraining excessive or unnecessary ad/abduction of hemiplegic gait [157]. Moreover, all the unactuated DoFs of the truck and connection mechanisms can be blocked to suit the requirements of different patients or gait rehabilitation tasks.

3.3 Lower Limb Exoskeleton

The main module of the robotic platform is the lower limb exoskeleton (LLE) which has a unilateral design. In order to help patients to reproduce gait patterns, the sagittal plane rotations of the LLE's hip and knee joints are actuated by PMs, taking the advantages offered by such actuators discussed in the Introduction section of this chapter. The major challenge of LLE design is also from the PM actuation system.

The main design criteria of the LLE are listed as follow:

- 1) *The capability of providing sufficient assisting torque and ROM to facilitate robotic gait rehabilitation.*
- 2) *Compact and light weight design that fit the anthropometric data of majority of the population.*
- 3) *Robust enough for further experiments with human subjects and potential clinical studies.*

3.3.1 Actuation system of the lower limb exoskeleton

Before getting into the design process, it is worthwhile to briefly mention the operation principles of the PM actuators. PMs tend to contract and apply uni-directional pulling actuation to attached objects, when inflated. Hence, it is a common practice to adopt antagonistic configurations of PMs to actuate rotational joints for bi-directional actuation [158-160]. The antagonistic PMs of the exoskeleton are comparable to the extensor and flexor muscle groups of the

human hip and knee joints. Therefore, regarding to the torque requirement of a joint, the extension and flexion PMs were analysed separately. The force generated by a PM actuator is positively correlated to its diameter and inflating pressure and negatively correlated to the contracting percentage with respect to its original length. In other word, there is a trade-off between the ROM and maximum torque at the extreme positions that a certain PM system can provide.

To meet the first design criterion, PMs need to be longer and thicker in order to provide more torque and greater ROM. However, such design could potentially violate the second criterion, because the segment of the exoskeleton cannot be too much longer than the corresponding segment of the human lower limb. Hence, the design problem was simplified into determining the quantity, type, diameter and length of PM actuators for the actuated joints, as well as the moment arms of the antagonistic PMs, so first two criteria mentioned previously could both be satisfied.

The PMs manufactured by FESTO were selected. Compared to in-house manufactured PMs, commercially available PMs would provide better reliability, reduce the inter-PM variance and hence reduce the uncertainty in modelling. The FESTO PMs can be made in three diameters 10, 20 and 40 millimetres and their length can be customized, which provides good design flexibility. In the same situation (pressure, original PM length and contraction percentage), the 40 mm diameter PMs would provide pulling force and hence joint torque. However, due to their bulkiness, mounting them to the exoskeleton would result much longer and thicker exoskeleton segment than actual human lower limb segments. One solution to this problem is to have Bowden cables as transmission and mount the PMs at a remote location [25]. Bowden cable power transmission however conflicts with the one of the initial motivations for employing PMs, which is being light for direct exoskeleton attaching. Nonetheless, the Bowden cable would add modelling uncertainties and reliability issues.

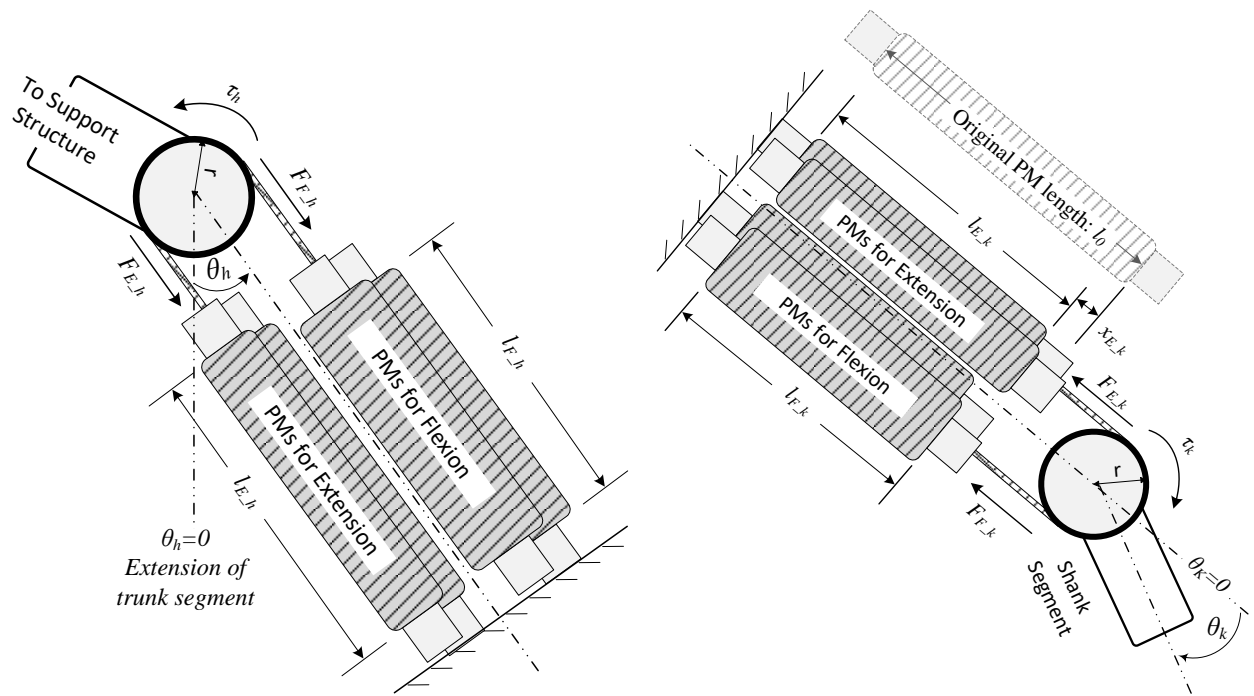


Figure 3-2 Illustrations of the joint actuation systems for the hip (left) and knee (right) joints. Variable definitions are listed with arrows showing their positive direction.

Commonly used cable and pulley based antagonistic PM designs were utilized to the actuated joints. The torque levers of the antagonistic systems are the radii of the pulleys. Compared to the exoskeleton developed by Beyl et al. [20], our design has less moving parts, smaller profiles of joint mechanisms. It is thus easier to implement, more reliable in testing and also simplifies further modelling and controller development processes. In the finalized design, the hip and knee joints of GAREX both have four 20-mm diameter PMs, two for each side of the antagonist, for sufficient torque output. In order to maximise the joint ROM without resulting over-lengthy exoskeleton segments, 300 mm (excluding end fittings) PMs (FESTO: DMSP-20-300N-RM-CM) were selected. The pulley radii or actuating moment arms are 30 mm for both the hip and knee joints. The designed actuation system of GAREX is illustrated in Figure 3-2. The reasoning of choosing such a design will be elaborated in the following paragraphs.

Table 3-1 Torque and range of motion design parameters of GAREX

	Hip	Knee
ROM (θ_{F0} to θ_{E0})	-20° to 40°	-3° to 69°
Linear ROM PM in mm	31.4	37.7
Linear ROM PM in percentage to original length	10.5%	12.6%
Equilibrium position ($x_E = x_F$)	10°	33°
Peak torque at the extreme position	47 Nm	40 Nm
Peak torque at equilibrium position	62 Nm	60 Nm

Based on the gait data published by Perry and Burnfield [161], the actuated ROM of both the hip and knee joints were determined and listed in Table 3-1. Such ROM ensures the exoskeleton can help reproduce a large variety of gait patterns as well as limits the maximum PM contraction in order to meet the torque requirement. It is designed that the extensor PMs are at their original length (no contraction or stretch) when the joint reaches maximum flexion, and vice versa. Hence the contraction of the extension and flexion PM can be expressed as a function of joint angular position as:

$$\begin{cases} x_{Fi} = r_i(\theta_i - \theta_{F0i}) \\ x_{Ei} = r_i(\theta_{E0i} - \theta_i) \end{cases} \quad \text{with } (i = h, k) \quad (3-1)$$

where r_i is the joint radius; θ_i is the joint angular position; θ_{E0i} and θ_{F0i} are the joint angular positions when the extensor or flexor PMs are at their original length; x_{Ei} and x_{Fi} are the length of the extensor and flexor PMs. In this manuscript, the subscripts h and k denote attributes of hip and knee joints respectively. The subscripts E and F denote attributes of extensor and flexor PMs respectively.

In terms of torque requirement, the exoskeleton is designed to provide enough hip and knee joint torque to help a training subject walk in desired gait patterns. The problem can hence be articulated as comparing the torque generation capacity of the actuation system and the maximum possible required torque for both joints throughout a gait cycle. A healthy subject's joint space gait trajectories and joint torques published in [162] is used as reference. It has also been reported in [161] that the joint torque during walking can be normalised by body weight. With this normalisation technique, the walking joint torque requirements for healthy subjects of various body weights can be approximated and plotted in Figure 3-3.

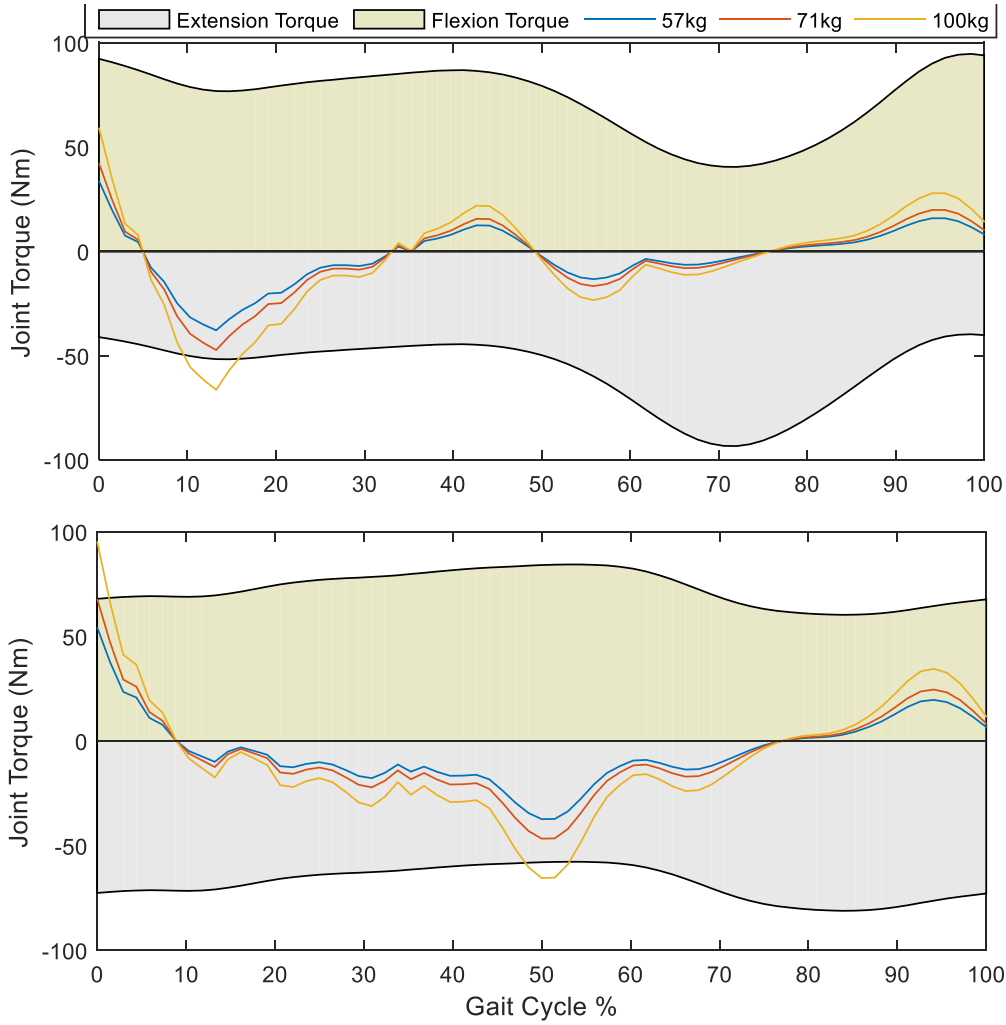


Figure 3-3 Joint torque versus gait cycle plots for the knee (top) and hip (bottom) joints. The joint torque requirement data of the 57kg healthy subject during normal walking are adopted from [162]. The data of the 71kg and 100kg are calculated from the 57kg subject with normalization of body weight. The shaded areas in the plots are indicating the joint torque output capability of both the extension and flexion PMs throughout the gait cycle.

The maximum contractile force (F_{max}) one PM when inflated to maximum pressure (6 bar) can be approximated as a function of its contracting percentage to its original length ($l_0=0.3\text{ m}$), according to the datasheet of the FESTO PM. Thus, the maximum joint actuation torque (τ_{max}) can also be calculated:

$$F_{\max_{ij}} = 16236 \frac{x_{ij}^2}{l_0^2} - 9405 \frac{x_{ij}}{l_0} + 1578 \quad (3-2)$$

$$\tau_{\max_{ij}} = 2r_j F_{\max_{ij}} \text{ with } (i = F, E) \text{ and } (j = h, k) \quad (3-3)$$

By combining the joint trajectory data through a gait cycle with Equation (3-1) and (3-2), the actuators capability of providing extension and flexion torque through the gait cycle can be calculated in (3-3) and illustrated with the shaded areas in Figure 3-3. It can be viewed from the figure that the actuation system is able to fully satisfy hip and knee joint torques requirement of a 71-kg healthy subject during level walking. For the simulated subject with 100 kg body weight, the designed actuation system is still capable to provide sufficient torque for most of the GC except the peak extension torque requirement of the knee joints and the peak flexion and extension torques of the hip joint. By analyzing the plots in Figure 3-3, it is observed that the peak torques all occur within the first 60% of the GC which is the stance phase, when majority of the joint torques are used to support the body weight of the training subject.

Body weight support systems are commonly used in conjunction with robotics exoskeleton and treadmill to provide gait rehabilitation training. The body weight unloading is up to 60% to 80% for patients with severe paralysis [66]. This implies that the exoskeleton only need to bear a fraction of the torque required supporting the body weight. Hence, it can be confidently concluded that the designed actuation system is capable of providing sufficient torque to facilitate robotic gait training for patients of up to 100 kg body weight.

3.3.2 Mechanical design of the lower limb exoskeleton

After selecting the pneumatic actuators, the following step was to design and construct the LLE that integrates with the antagonistic PM actuators.

The LLE also has a modular design. The knee and hip modules each contains its corresponding joint actuation system. The two modules are connected to form the thigh segment of the LLE. The relative position of the two modules can be adjusted to ensure the hip and knee joints of the LLE are aligned with the subject's joints during an experiment. Each of the modules has a rigid leg brace attached. During training, the subject is strapped to the braces via straps. The

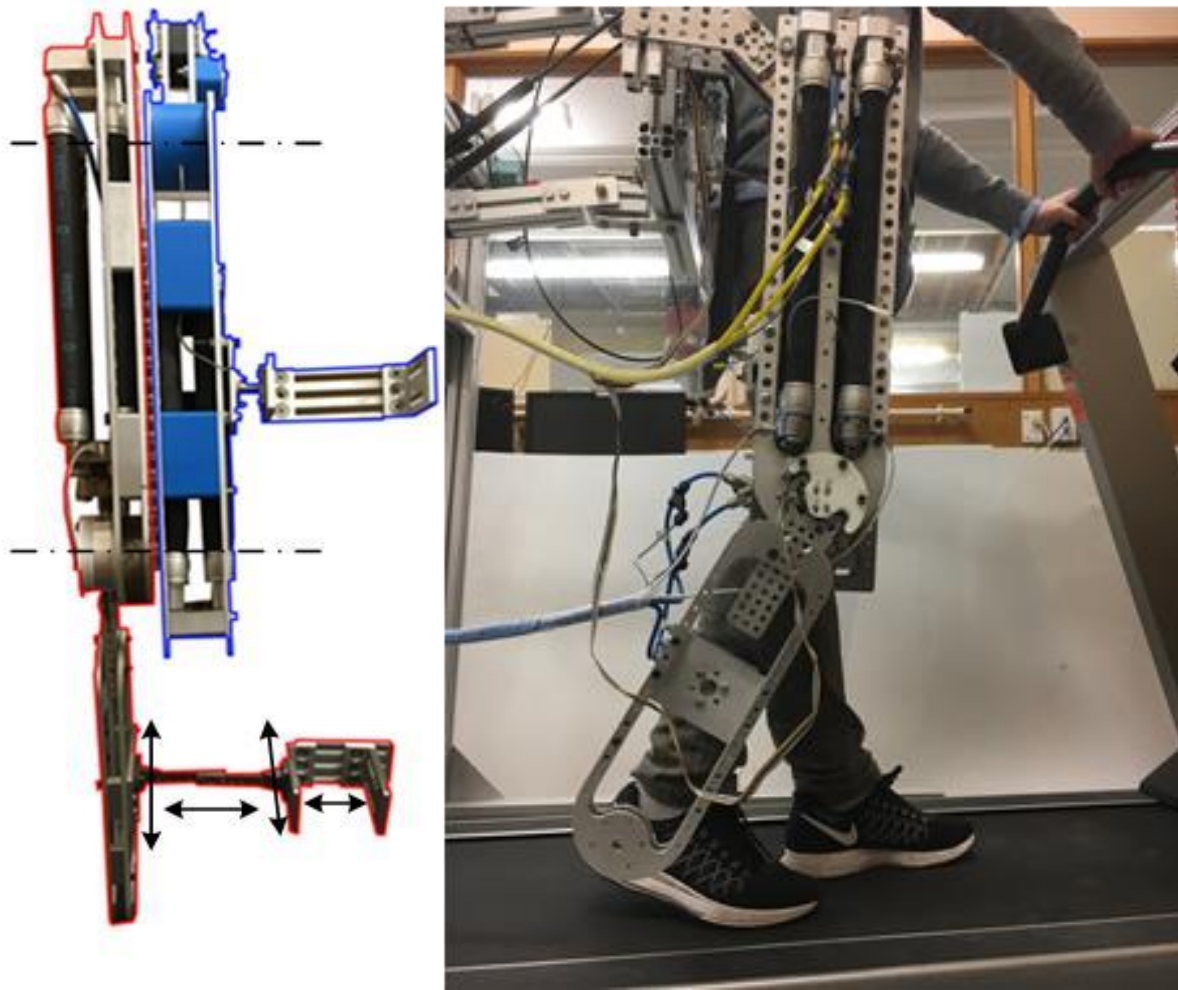


Figure 3-4 Left: the front view of the lower limb exoskeleton with the thigh and shank modules outlined in blue and red respectively. The relative position of the two modules can be adjusted in order to align the rotational axes (marked with dashed lines in the figure) of the knee and hip with the subject's ones. Right: Side view of the lower limb exoskeleton with a healthy subject wearing it.

sizes and positions of the braces are adjustable according to the subject's anthropometric measurements. The braces were designed to be rigid to prevent any relative movement between the exoskeleton and the leg attached to it.

The designs by Hussain et al. [19] and Choi et al.[17] has PMs located at both the thigh and shank segments of the exoskeleton for actuation of the hip and knee joints respectively. On GAREX, all 8 PM actuators were placed to the thigh segment of LLE. Such design transfers the actuators' inertia from the shank to the thigh segment, and thus reduces the torque requirements of both the hip and knee joints for producing the same movement.

In order to accomplish a robust working prototype in a short time frame, most of the parts of the LLE were made of laser cut aluminum plates. Some key structure parts, such as the shafts and bearing houses of the actuated joints, were machined steel parts.

3.3.3 Pneumatic system

One key element of the pneumatic system is the valves controlling the air flow to the PM actuators. Mainly two types of valves have been used on this role. One is pressure controlled proportional valves, which have embedded software to regulate their output pressures to the desired levels. The other type is analogue proportional valve, which effectively changes their orifice areas by changing the spool positions. When used in controlling PM driven mechanism, the pressure regulator type of valves appears to be black boxes in control loops, which leads to simpler the system models by ignoring the details of the pressure characteristics of the PM actuator. However, there could be unpredictable transient behavior of the controlled PM pressure.

To overcome this, four 3/5 analogue valves (FESTO: MPYE-5-1/8-LF-010-B) were adopted in this research, two for each actuated joint, as shown in Figure 3-5. The pneumatic flow through a valve can be controlled by changing the valve's orifice area which depends on the input voltage. Compared to Shen [163] which used a single 3/5 analogue valve for a mechanism driven by an antagonistic pair of PMs, the design in this research can be viewed redundant actuation system if only implementing trajectory control. However, the two-valve design offers more possibilities for developing sophisticated controllers in order to satisfy the requirements of various robotic gait rehabilitation modes.

Similar to the analogue valves, pressure sensors were installed, one for each side of the antagonistic PMs of an actuated joint. The pressure sensors are used for both feedback control and status monitoring. It can also be viewed from Figure 3-5 that a main solenoid valve in between the pneumatic source and the analogue valves for the PMs. The solenoid valve is used to switch the pneumatic flow to the actuation system based a digital signal sent from the control software.

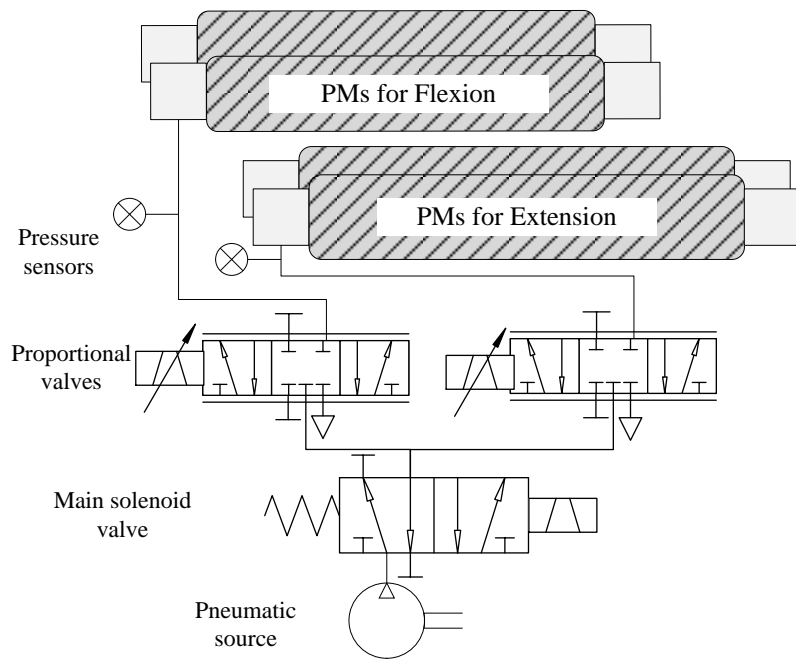


Figure 3-5 The pneumatic flow diagram for one of the actuated exoskeleton joint. The actuated joints of the LLE have identical actuation system configurations. The two actuated joints share the same pneumatic source and main solenoid valve.

3.4 Instrumentation

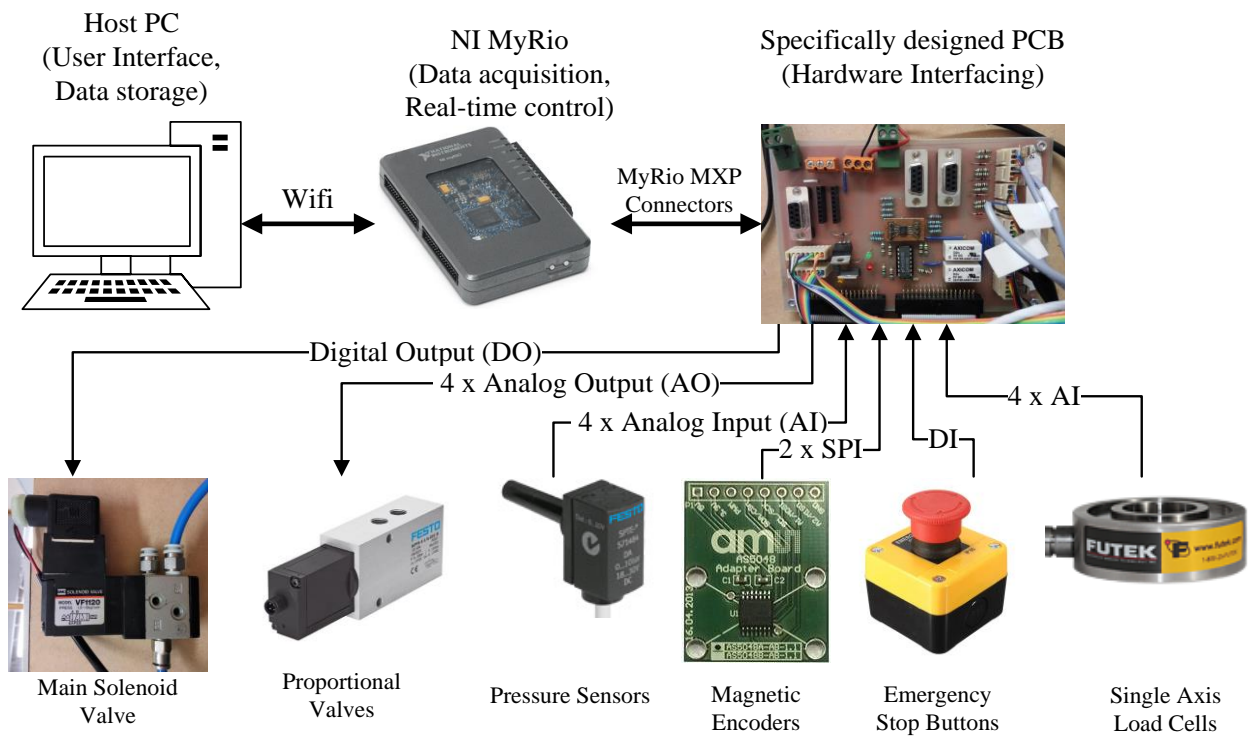


Figure 3-6 Hardware configuration block diagram. Major components of the instrumentation hardware system are listed with connectors indicating the types of interfaces and directions of data flows.

Table 3-2 List of key instrumental components of GAREX

Description	Part Details	Quantity
PM actuators	FESTO: DMSP-20-300N-RM-CM	8
Analogue valves	FESTO: MPYE-5-1/8-HF-010-B	4
Main solenoid valve	SMC: VF1120	1
Pressure sensor	FESTO: SPTE-P10R-S6-V2.5K	4
Single axis load cell	FUTEK: LTH350	2
Angular Encoder	AMS: AS5048B	2
Controller	NI: myRIO-1900	1

All major components including the pneumatic components described in the previous paragraphs are included in the block diagram in Figure 3-6. The block diagram is showing the hardware architecture for the entire GAREX system. MyRIO from National Instrument is used as the main control platform. Inside the myRIO, there is an FPGA module and a micro-processor module. The FPGA has been programmed to conduct hardware interfacing and sensor signal processing at a rate of 1 KHz. The processor could then be utilized to focus on model based controller processing at a rate of 100 Hz. For physical hardware interface, a custom printed circuit board (PCB) was designed. The PCB contains connectors for various components which are illustrated in Figure 3-6, together with amplifying and multiplexing circuit for the sensors

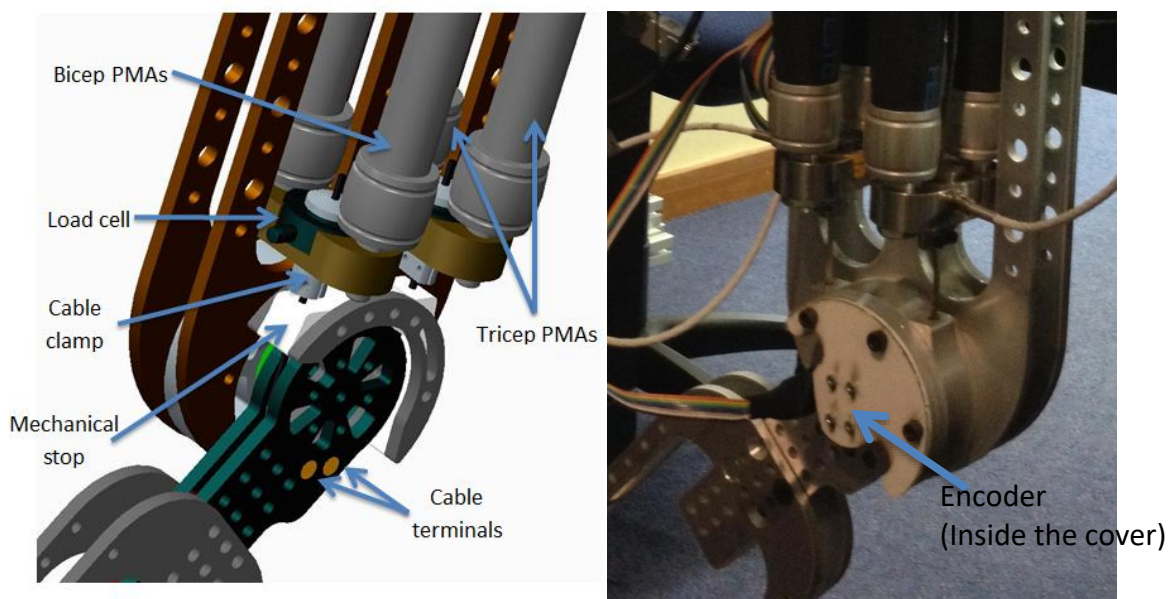


Figure 3-7 Left: CAD drawing of the knee joint mechanism; right: photo showing details of the knee mechanism of GAREX.

and valves. The PCB was also designed with circuits to handle the emergency stop situation which will be discussed later.

For the joint space position feedback, magnetic encoders were mounted to be co-axial with the two actuated joints. The filtered derivatives of the angular positions are computed through the FPGA module for the potential use in controller development. The load cells are also mounted as shown in Figure 3-7 to monitor the pulling forces of the antagonistic PMs at the knee joint and thus the joint's actuation torque. A detailed list of the major components adopted in the hardware configuration is presented in Table 3-2.

3.5 Safety and adaptability of GAREX

The safety is of paramount importance. A variety of features have been designed and implemented to ensure the safety of the patients if any unexpected incident happens.

Mechanical ROM limiting stops shown Figure 3-7 were designed for both the actuated hip and knee joints of the exoskeleton to ensure the exoskeleton cannot move beyond the allowed ROM of corresponding human joints.

Emergency stop buttons are made accessible to both the training patient and the supervising therapist or engineer. Once any of the stops buttons is pressed, three folds of safety actions will take place. In hardware level, relay circuits have been implemented to the custom PCB. The press of a stop button grounds the voltage input to the main solenoid valve, so the pneumatic flow to the actuation system can be cut off. Meanwhile, the analogue signal input to all the proportional valves would be suppressed with a 0V signal, which essentially deflates all the PMs at the valves' full capacity. On the software level, the controller recognises the stop button press; idles all the control process; and sends signals to the valves to cut down pneumatic flow and deflate the PMs, as well as display warning message on the graphical user interface.

To ensure GAREX can provide training to a wide population range, the system was designed to be modular and telescopic. As shown in the left picture of Figure 3-4, the knee and hip modules' relative position can be adjusted to accommodate patients with different lower limb segment lengths. To fit subjects with different builds, the horizontal and vertical position of the exoskeleton module to the trunk manipulation module is designed to be adjustable, as well as the vertical position of the trunk manipulation module relative to the supporting frame. The positions of the leg braces can be adjusted in three directions relative to the thigh or shank segments, which is indicated with the black arrows in the left picture of Figure 3-4. The widths of the leg braces are also adjustable. The adaptability of the design, not only makes the subject more comfortable during the training, but also ensure the subject's thigh and shank segments always align with their corresponding exoskeleton segments. Therefore, the hip and knee joint angles of exoskeleton and attached low limb are regarded to be equal.

3.6 Discussion and conclusions

A new PM driven robotic gait rehabilitation system named GAREX has been designed and built. As reviewed in the last chapter, there have not been clinical studies conducted on PM driven gait rehabilitation robotic system. Hence, GAREX was designed with future clinical

applications in mind. Detailed torque analysis was conducted to verify the system's capability to provide task specific gait training. The system is capable to provide sufficient torques and ROM for the knee and hip joint rotations in the sagittal planes to facilitate gait rehabilitation for patients weighing up to 100 kg.

Position, pressure and force sensors were installed for both control feedback and system monitoring. Safe training was achieved through the multiple software and hardware implementations. The safety system has a redundant design, in unexpected situations, such as emergency stop press or exceeding design ROM, there will be multiple safety actions and any one action alone would ensure the safety of the training subject. Anthropometric adaptability is also a main design consideration. The modular construction of GAREX ensures the system a wide range of adjustments can be made to cater the need of various training subjects.

The requirements of further control strategy development were taken into consideration in the robotic design process. The intrinsically compliant actuation system can be utilized to create a wide range of dynamic environments. Four analogue valves are selected to allow detailed modelling of the entire controlled plant in the following research. Such design also open the possibilities for the researcher to control the intrinsic compliance of the actuation system in order to create a wide range of dynamic environments [164]. Hence, GAREX makes a good platform for develop and validate control strategies.

Chapter 4 Force Dynamics Model of the Pneumatic Muscle Actuators

Pneumatic muscle (PM) actuators have been widely used in wearable robots due to its high power to weight ratio and intrinsic compliance. The task-specific robotic gait rehabilitation imposes bandwidth requirement to the actuation system. The antagonistic PMs that actuate GAREX should at least be able to track 1.5 Hz sinusoidal trajectory with a peak-to-peak displacement at 10% of the PM's original length. Hence a dynamic model is needed to describe the PM's operation. The inflating pressure determines the compliance of a PM. In order to have the exoskeleton to work in a wide range of compliance, the dynamic model needs to cover the entire operating pressure range of the PM. The dynamic model by Reynolds et al. [165] was based on the conventional McKibben PM and only valid for pressures above 2 bar. The FESTO PM adopted in this research is a special type of McKibben PM whose dynamics is not identical to the conventional PMs. As a result, it is necessary for this research to develop an appropriate dynamic model for the adopted PM to host further control development of the robotic gait rehabilitation exoskeleton.

The dynamic model in [165] is used as a benchmark for the model development in this research. Initially, the researcher attempted to characterize the PM based on the benchmark model through experiments in order to find the modelling parameters. For this purpose, an experimental rig was designed and built to investigate the dynamic behaviours of a pneumatic muscle. The rig automates the characterization process by providing motions to the target PM and recording pressure, force, position and velocity data. Experimental results indicated that the benchmark model could not well represent the behaviour of the PMs used in this research. Therefore, based on the benchmark model, the researcher attempted a new model format which is proven to fit better with the experimental data.

4.1 Introduction

The dynamics of the system has to be well understood in order to control the exoskeleton effectively. Based on the design, the hardware system can be simplified into the block diagram shown in Figure 4-1. The PM actuation system can be further divided into models of the pressure dynamics and force dynamics. The pressure dynamics models the relation between the mass flow rate of the analogue valves and the rate of pressure change of the PMs. The force dynamics models the PM's contracting force versus PM pressure and kinematics relationship. This chapter is dedicated to the modelling process of the PM's force dynamics.

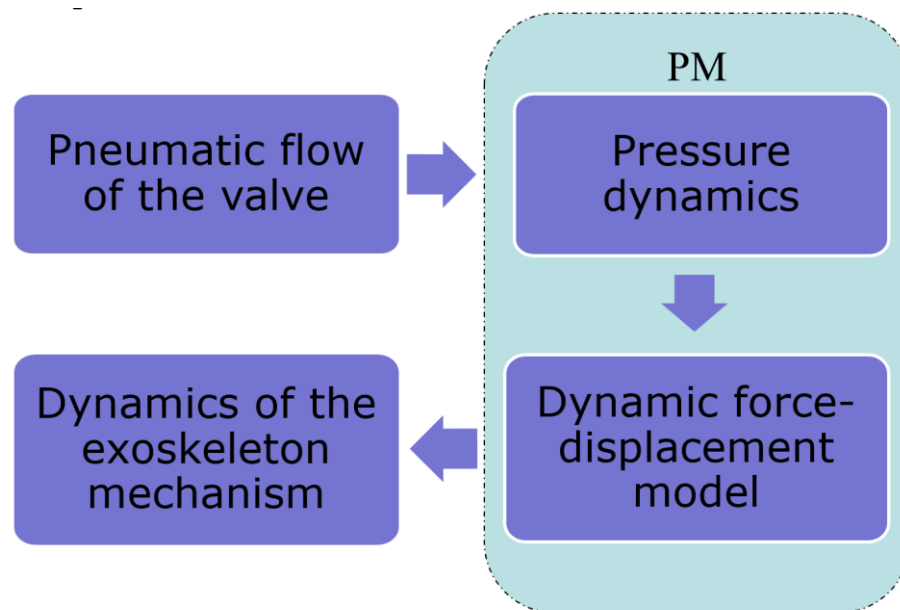


Figure 4-1 Block diagram of the GAREX system. Three major sub-systems are illustrated with blocks with arrows indicating the connection sequence and media.

Pneumatic muscle actuators were firstly invented by Joseph L. McKibben for an orthotic application in 1950s [166]. There were not many further applications or development of PMs until 1980s, when the original PM actuators were redesigned to actuate robotic arms in Japan [167]. In the past two decades, PMs have widely researched in the field of robotic rehabilitation. This is mainly due to their advantages of having high small weight, high strength and high power to weight ratio. PMs are also of controllable compliance, due to the compressibility of air inside the PMs [168]. These advantages make them widely adopted in robot-human interaction applications such as robotic exoskeleton or orthosis [18-20].

Although there are various constructions of PM actuators, the most common one used in research is the McKibben design which consists of a cylindrical flexible airtight tube that fits

inside a sheath with braided thread. When a PM is inflated, it widens and shortens to generate a contracting force and displacement [169]. In spite of the advantages of PMs a major challenge of using PM as actuator is about controlling them precisely. Due to the compliance, elasticity of the material and friction, the PM operation is highly nonlinear and subjects to hysteresis behaviours. Hence, appropriate models of the PMs need to be developed to understand their behaviours and thus control mechanisms driven by them.

A number of researchers have investigated different modelling method of PMs. Chou and Hanaford [151] developed the simple but widely used geometrical model on McKibben PM. Tondu and Lopez [170] further improved the model in [151] by compensating the end deformation (PM is not a cylindrical shape when inflated) and attempting to offset the hysteretic behavior between inflation and deflation of a PM. Another commonly adopted model of PM is the phenomenological model developed by Reynolds et al. [165], which describes the dynamic characteristics of McKibben PMs.

FESTO fluidic muscles adopted in this research is a special type of McKibben PM actuators. FESTO PM's pressure tight rubber tube and braided sheath are integrated into its contraction. Due to the special design, PMs manufactured by FESTO have different properties compared to the conventional McKibben PMs modelled in [151, 165, 170]. At the same pressure, FESTO PMs tend to generate larger forces than conventional McKibben PMs with same diameter and contracting percentage. However, modelling of FESTO muscle has not been extensively researched. Models developed for conventional muscles are adapted to model FESTO muscles with adjusted parameters. Choi et al. [17] adopted the dynamic model to FESTO muscles with adjusted parameters; meanwhile, sliding mode control was implemented to cope with inaccuracy in modelling. Experiment based static models have also been developed to express the force-pressure-contraction relationship [171, 172]. To make better use of the FESTO PMs in dynamic applications such as robotic gait rehabilitation, a more specific dynamic model for FESTO PM still needs to be developed.

This chapter is organised in the following orders. In Section 4.2, a brief review on previous PM modelling approaches and motivation on the development of a new PM model will be presented. Section 4.3 will describe the setup of the testing device and the how the experiments are conducted. Section 4.4 will be devoted to experimental result analysis, proposing the improved dynamic models, as well as model validation.

4.2 Modelling the dynamic characteristics of the PM

The dynamic PM model developed by Reynolds et al. [165] is in a similar format to the well-known Hill's muscle model in biomechanics. It contains parallel force generation, spring and damping elements as shown in Figure 4-2. The dynamic force behavior is represented by the following equation:

$$F(P) + B(P)\dot{x} + K(P)x = L + m\ddot{x} \quad (4-1)$$

where: P is the inflating pressure of the PM actuator; $F(P)$, $B(P)$, $K(P)$ are force, damping and spring elements which are all linearly dependent on pressure (as indicated in (4-2)) and determined experimentally; m is the mass of the load; x , \dot{x} and \ddot{x} are the contracting length, velocity and acceleration of PM respectively; and L is the force exerted on the load.

$$\begin{cases} F(P) = F_0 + F_1P \\ K(P) = K_0 + K_1P \\ B(P) = B_{I0} + B_{I1}P \quad (\text{Inflation}) \\ B(P) = B_{D0} + B_{D1}P \quad (\text{Deflation}) \end{cases} \quad (4-2)$$

The parameters F_i , K_i , B_{Ii} and B_{Di} ($i = 0, 1$) in (4-2) can be determined experimentally. The damping element of the inflation and deflation processes was modelled separately to address the hysteresis behaviour of the PM.

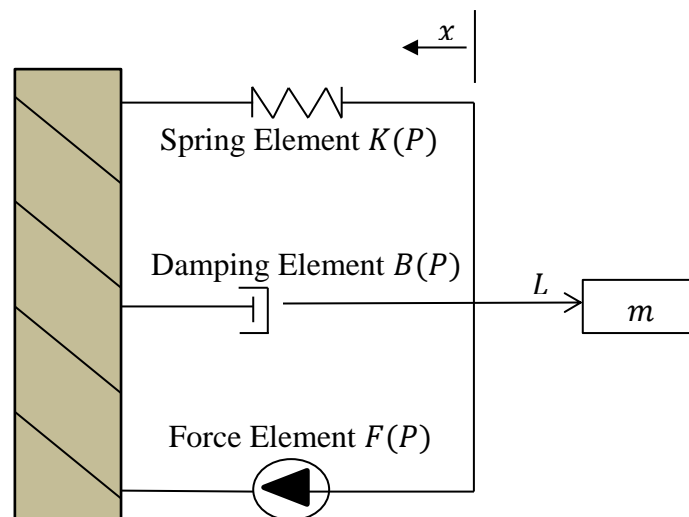


Figure 4-2 The Hill's type of dynamic PM model adapted by Reynolds et al. [165].

The model published in [165] is a good benchmark of the development of a dynamic force model for the specific type of PMs used in this research. Hence an experimental rig was constructed to investigate between the force generated by a PM and its inflating pressure and kinematics. Based on the experimental rig, the research designed an automated experimental process to have the tested PM operate in a wide range of dynamic scenarios and record data. In the data analysis, the research firstly investigated if the model in [165] is able to well present the gathered experimental data. If the fit was not ideal, the researcher would attempt to look for a new or improved dynamic model for the PMs actuating GAREX.

4.3 Experimental setup and procedures

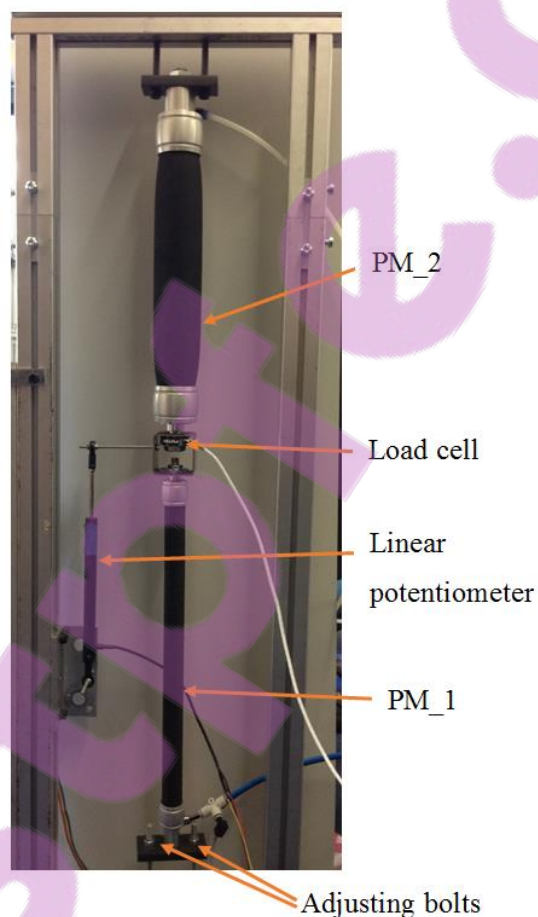


Figure 4-3 Experimental setup to calibrate the dynamic model parameters of a PM actuator.

An experimental rig had been designed and constructed to conduct automated experiments to create various dynamic operating conditions of the tested PM and record force, pressure and kinematic data for further model analysis. The experimental setup is shown in Figure 4-3. The

PM_1 at the bottom was the muscle to be modelled. One of the PMs adopted in the GAREX design was used as PM_1. It is 300 mm in length and 20 mm in diameter. PM_2 (FESTO DMSP-40-300N-RM-CM) was 40 mm in diameter, 300 mm length, which provides motions as required during the experiments. The pressure of PM_1 was controlled by a pressure regulator (FESTO VPPM-6L-L-1-G18-0L6H-A4N). The pneumatic flow rate of PM_2 was manipulated via an analogue valve (MPYE-5-1/8-LF-010-B). A pressure sensor (SPTE-P10R-S6-V2.5K) was also placed next to the pneumatic connection to PM_1 for more accurate pressure measurement. A linear potentiometer (Variomh VLP100) and a load cell (FUTEK LTH350) were used to measure displacement and the interaction force respectively. The assumption of this testing setup was that masses of all moving components are negligible. This is because, in the worst scenario, the product of the entire moving mass (0.3kg) of the rig and the maximum acceleration (3m/s) is less than the noise amplitude of the load cell reading.

A National Instrument myRIO was employed for hardware interfacing and controller processing. The experimental procedures were implemented in a LabVIEW programme. At the beginning of the one experiment, the PM_1 was firstly inflated to a certain pressure, P_1 . By adjusting the two bolts at the bottom of the test rig along the thread rods, an appropriate initial contracting length (x_0), which was usually zero, could be achieved, and at this instant the linear potentiometer had a reading of d_0 . Being appropriate meant the bolts were just in contact with the plate attached to the bottom end of PM_1 and the load cell reading was zero. As a result, the contracting length during the experiment can be calculated using the following equation:

$$x = x_0 - (d - d_0) \quad (4-3)$$

where, x is the instantaneous contracting length of PM_1; d is the instantaneous linear potentiometer reading.

During one set of experiments, the pressure of PM_1 was regulated to the fixed value P_1 , while the PM_2 was inflated and deflated at various rates in order to exert different load to PM_1. At the beginning of one experiment, PM_2 was fully deflated. After the measurement of x_0 was completed, the step inflating voltage was applied to the analogue valve of PM_2. The orifice size of the analogue valve is proportional to the input voltage applied. As a response, PM_2 contracted to stretch PM_1. After the movement was settled and a wait of 3 seconds, another step-down voltage was applied the analogue valve to deflate PM_2. As a result, PM_1 contracted again back to x_0 . It is worth to note that the inflating and deflating orifice areas were of

same magnitude. During this process, kinematics, load cell reading and the pressure of PM_1 were monitored and logged to a data file at a rate of 100 Hz.

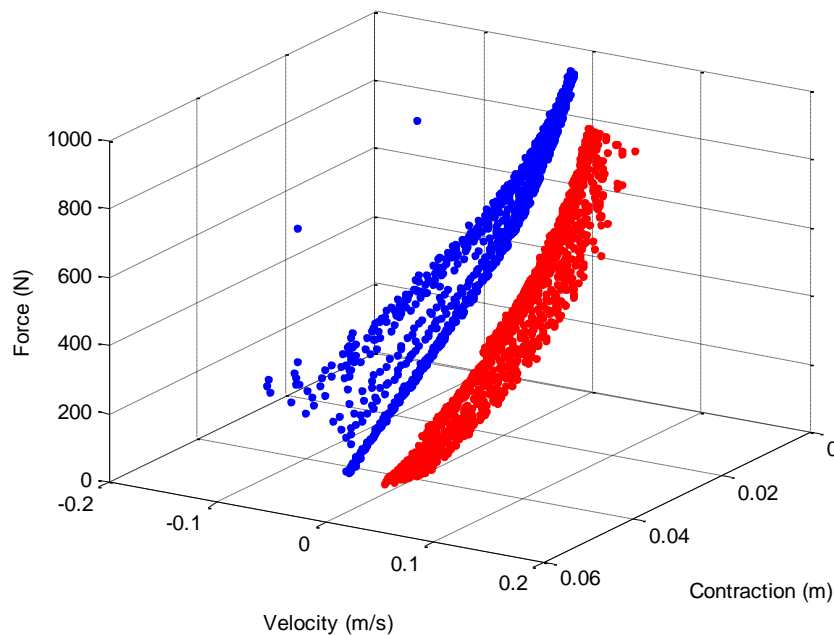
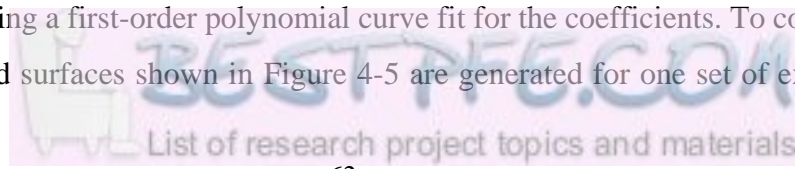


Figure 4-4 The force versus contraction and velocity scatter plot, when the pressure of PM_1 was regulated to 3.2 bar. Red and blue dots represent data during the contraction and stretching of PM_1 respectively

The inflation-settling-deflation process was repeated. The inflating (deflating) orifice areas were increased from 10% to 100% of the maximum opening of the valve in the step size of 10%. Up to this point, the experiment for the selected pressure of PM_1 was completed. Figure 4-4 is showing the gathered data for the set of experimental data when PM_1 is regulated to 3.2 bar. Only dynamic data (velocity magnitude greater than 0.005 m/s) were considered for dynamic modelling. The contracting and stretching data points are separated, so hysteresis can be considered in the proposed model. The same experimental procedure was repeatedly conducted to various pressures of PM_1 ranging from 0.8 to 5 bars, with three experiments for each pressure. A total of 51 valid experiments were conducted.

4.4 Result Analysis

Firstly, the validation of the existing dynamic model proposed in [165] with the newly gathered data was attempted. For a fixed pressure, the $K(P)$, $B(P)$ and $F(P)$ parameters in Equation (4-1) can be calculated using a first-order polynomial curve fit for the coefficients. To cope with the hysteresis, two fitted surfaces shown in Figure 4-5 are generated for one set of experimental



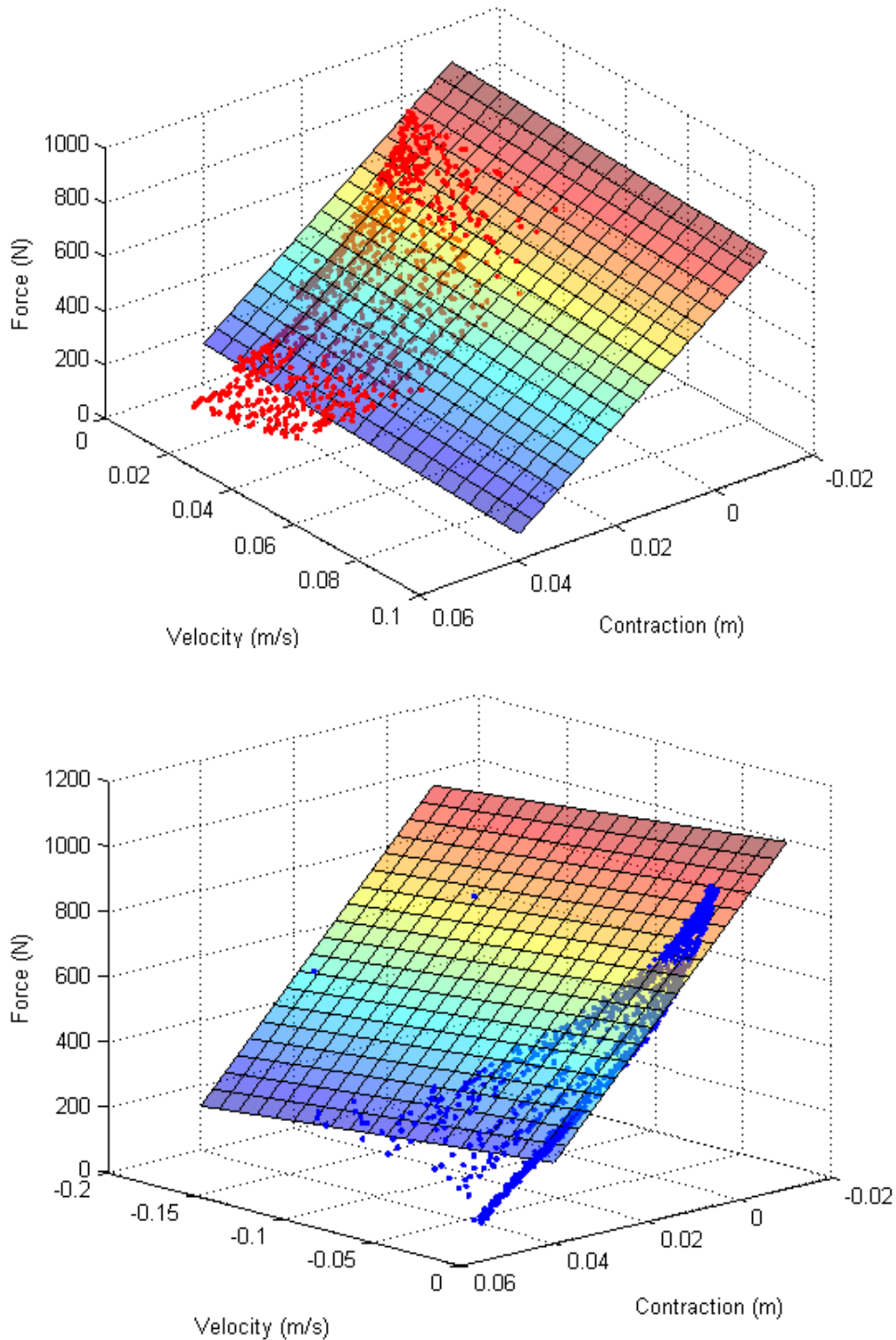


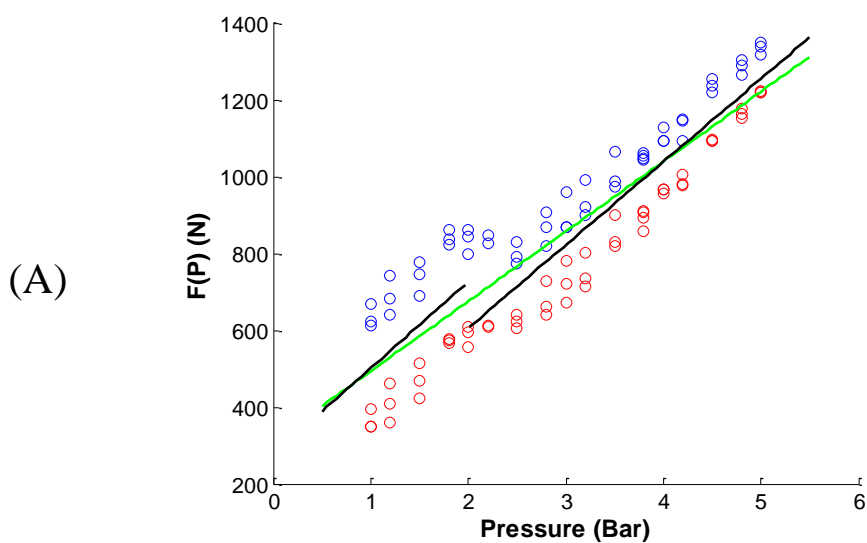
Figure 4-5 The first order polynomial representation curve fitting result of PM force versus its contracting length and velocity when its pressure was regulated to 3.2 bar. The upper plot is for the contracting process of PM_1 and the lower plot is for the stretching process.

results, one for the contracting and the other for the stretching process. The regression results expressed with R^2 for the two fits are 0.941 and 0.913, which indicate good accuracy of the

model at the specific pressure.

For each of the 51 experiments conducted, the data for the contracting and stretching processes of PM₁ were separated. Curve fitting was the conducted for both sets of data in the same method of producing Figure 4-5. As a result, 102 combinations of K(P), B(P) and F(P) could be calculated. These parameter combinations were all plotted against their corresponding PM₁ pressures in order to investigate how the parameters are dependent on PM pressure. The plots are shown in Figure 4-6.

The initial investigation was on the first order linear relationships between PM pressure and the parameters as described in (4-2). The first order linear model is represented using green lines in Figure 4-6. Its modelling coefficients are shown in the third column of Table 4-1. As can be seen from Figure 4-6, the green lines are well correlated to the experimental data except the one for the spring element. To further quantify the how well the dynamic model by Reynolds et al. [165] fits the experimental data. Regression analysis was performed to calculate the R² values (shown in the bottom row of Table 4-1) of the entire population of experimental data. For every valid data point, the force calculated via Equations (4-1) and (4-2) was compared with the measured force. A total of 38,745 and 38217 data points are included in the analysis for stretch and contraction of PM₁ respectively. The result of regression analysis indicates that the model could be improved to better represent the dynamic behavior of the PM. Hence, the researcher attempted to find an improved the dynamic model based on the model published in [165], in order to better represent the force dynamics of the PM adopted in this research.



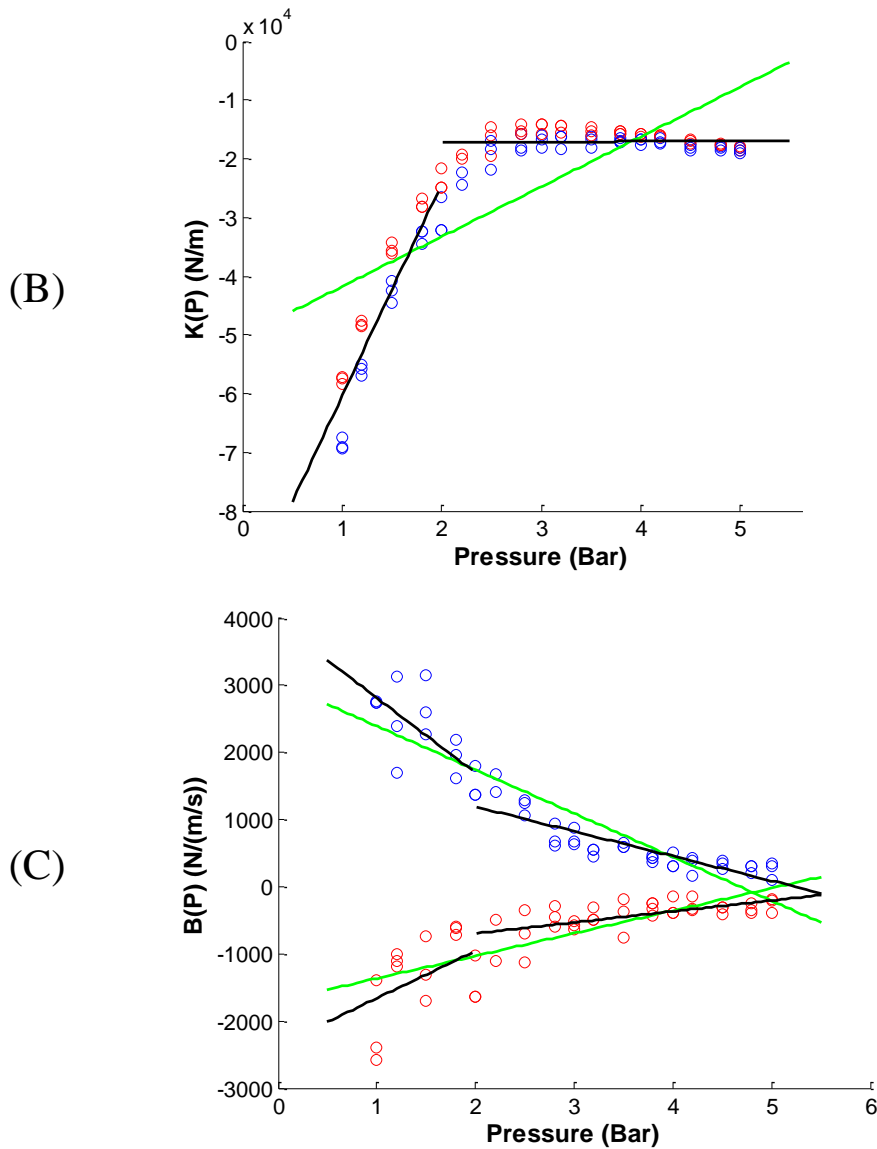


Figure 4-6 (A), (B) and (C) are the $F(P)$, $K(P)$ and $B(P)$ versus PM_1 pressure plots respectively. The scatters represent the parameters gathered from the 51 experiments. The red scatters are for the contracting processes of PM_1 and blue ones are for the stretching processes.

By analyzing the plots in Figure 4-6, it was realized that the spring parameter versus pressure relationships have different trends when the pressure is below or above 2 Bar. The linear representations of $K(P)$, $B(P)$ and $F(P)$ were modified into two-stage piecewise linear functions, which are shown as the black lines in Figure 4-6. The parameters of the piecewise model as well as the R^2 values of the regression analysis are listed in the columns titled “Piecewise Model” of Table 4-1. The R^2 values are calculated in the same way as the ones for the original model. The R^2 values outside the brackets are computed with all three elements from the proposed piecewise model; meanwhile, the ones inside the brackets are computed through a hybrid

Table 4-1 Parameters of different dynamic models and regression analysing results of the models, for the 300mm PM used in GAREX.

Factor	Coefficient	First order linear model	Piecewise Model	
			Below 2 bar	Above 2 bar
Force Element	(N)	311.8	276.8	173.6
	F_1 (N/Bar)	181.9	224.7	216.2
Spring Element	K_0 (N/m)	-39085	-96,524	-17,253
	K_1 (N/m/Bar)	24634	36,121	47.1
Damping Element	Contraction	B_0 (N·s/m)	-1,704	-2,363
		(N·s/m/Bar)	336.5	702.2
	Stretch	B_0 (N·s/m)	3,041	3,930
		B_1 (N·s/m/Bar)	-649.8	-1,117
Regression Analysis	Contraction	R^2	0.9430 (0.9130)	
	Stretch		0.9507 (0.9227)	

model with only the spring element from the piecewise model and the other elements from the original model. The regression analysis indicated that the modified piecewise model and the hybrid model fitted better to the experimental data compared to the original dynamic model. The different between the pure piecewise model and the hybrid model was less obvious.

To exam the generalization of the proposed piecewise dynamic model, a similar experimental process was performed on a different PM manufactured by FESTO with 400mm length and 20mm diameter (FESTO DMSP-20-400N-RM-CM). A total of 56 experiments were conducted with the new targeted PM and the results are presented with Figure 4-7 and Table 4-2, which are in the same formats as Figure 4-6 and Table 4-1 for the 300mm PM. The regression analysing results once again indicated the new piecewise model better can better the experimental data comparing to the original dynamic model.

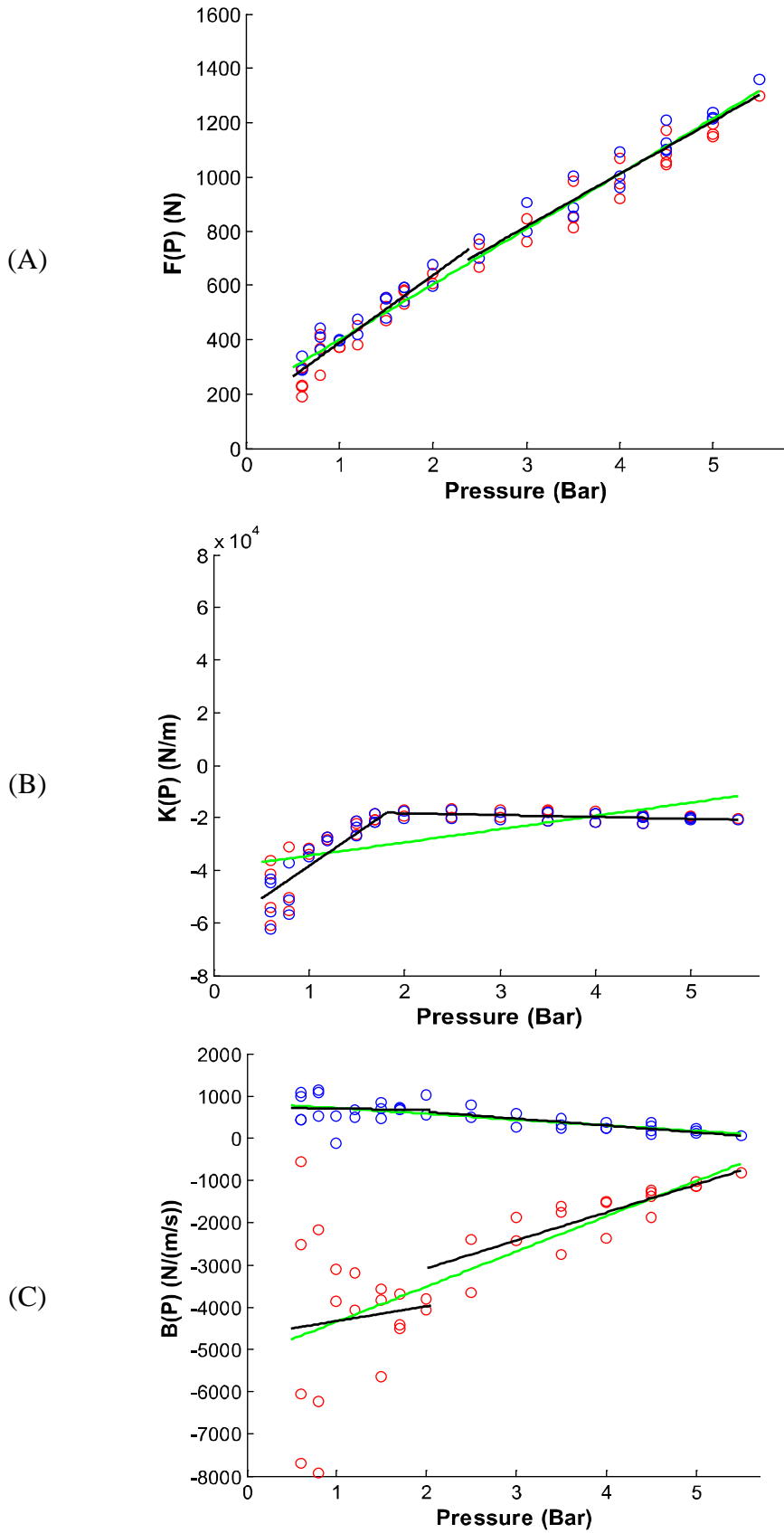


Figure 4-7 (A), (B) and (C) are the $F(P)$, $K(P)$ and $B(P)$ versus PM_1 pressure plots for the 400-mm long PM. The red scatters are for the contracting processes of PM_1 and blue

ones are for the stretching processes. The first order linear model parameters are represented using green lines and the modified piecewise model parameters are represented in black lines.

Table 4-2 . Modelling parameters and regression analysing results for the 400-mm long PM manufactured by FESTO

Factor	Coefficient	First order linear model	Piecewise Model	
			Below 2 bar	Above 2 bar
Force Element	F_0 (N)	254.4	239.5	207.4
	F_1 (N/Bar)	201.7	219.4	213.6
Spring Element	K_0 (N/m)	-50,266	-64,104	-12,188
	K_1 (N/m/Bar)	8,496	24,634	-767.5
Damping Element	Contraction B_0 (N·s/m)	-5,178	-4,680	-4,429
	B_1 (N·s/m/Bar)	831.7	348.9	666.0
Element	Stretch B_0 (N·s/m)	841.3	697.4	964.9
	B_1 (N·s/m/Bar)	-133.8	-12.41	-165.2
Regression Analysis	Contraction R^2	0.0895	0.9679 (0.9671)	
	Stretch	0.6177	0.9746 (0.9742)	

4.5 Discussion and conclusions

A new dynamic modelling approach of PM actuators has been developed based on a dynamic force model based on McKibben PMs published in [165]. Only experiments with pressure 2 Bar and above were reported by Reynolds et al. [165]. Whereas, the new piecewise model proposed in this article are based on extensive experiments with pressures ranging from 0.8 to 5.0 Bar. The piecewise model is preferred by the author, due to its high correlation to experimental data, meanwhile still being in a simple form for the model based control development which will be presented in the next chapter. The proposed models are experimental based and muscle specific. However, the experimental procedures and data processing have been fully automated. As a result, the models can be easily transferred to PMs with different sizes.

Chapter 5 Joint Space Trajectory and Compliance Control

This chapter focuses on a multi-input-multi-output (MIMO) sliding mode (SM) controller. This controller is aimed to simultaneously control the angular trajectory and compliance of the knee joint mechanism of a gait rehabilitation exoskeleton. The MIMO controller is developed based on the model of the entire mechanical system which consists of four sub-system models. They are flow dynamics model of the valves, pressure and force dynamics models of the antagonistic pneumatic muscles, as well as the load dynamics model of the exoskeleton. Single-input-single-output (SISO) sliding mode joint trajectory controller based on the system model is also included in this chapter. The SISO control system helps the author verify the design and modeling work. It is also used as the benchmark for the MIMO control system.

Control systems experiments on the knee joint mechanism of GAREX was conducted to validate the developed SM controllers. The experiment was carried out on sole robot as well as with healthy subjects. The results indicated good multivariable tracking performance of the MIMO SM controller, which provides a good foundation for further development of assist-as-needed training strategies in gait rehabilitation.

5.1 Introduction

As described in Chapter 3, pneumatic muscle (PM) actuators are intrinsically compliant, lightweight and with high force/power to weight ratio. These advantages make PMs suitable for rehabilitation robots, especially exoskeleton type of robots. Ferris et al. [18] developed an ankle-foot orthosis actuated by PM to assist the ankle planar flexion during walking. This orthosis was further developed into a knee-ankle-foot orthosis with the knee flexion/extension and ankle dorsi-/planar-flexion all actuated [149]. A PM actuated upper limb rehabilitation robot, named RUPERT, was developed by a research group from Arizona State University. The robot had four degrees of freedom (DoF) each actuated by a PM actuator [78]. In the author's research group, a robotic exoskeleton for gait rehabilitation had also been developed, with both the hip and knee joints of the exoskeleton powered by antagonistic PM actuators [19]. Despite their advantages, dynamics of PMs is highly non-linear and also subjects to hysteresis; therefore, it becomes a challenging task to model them precisely.

In order to develop more effective controllers, research work on PM modelling had been widely conducted. A review of previous modelling approaches and a new way of modelling the PMs adopted in this research have been covered in Chapter 4 of the thesis. Although modelling of PM has been extensively investigated, researchers [17, 160] still claimed that models tend to be highly nonlinear and subject to uncertainties, mainly due to friction, temperature and change of properties overtime. To cope with these problems, a variety of controllers have been implemented on PM driven mechanisms, which include adaptive pole-placement controller by Caldwell et al. [173], robust and adaptive back-stepping controller by Carbonell et al. [174], fuzzy PD+I controller by Chan et al. [175], neural network based PID controller by Thanh and Ahn [176] and more recently echo state network based predictive controller with particle swarm optimization by Huang et al. [177].

Sliding mode control and its variations have also been implemented in several applications to control mechanisms driven PM actuators, because SM controllers are robust to modelling uncertainties and disturbances. Van Damme et al. [178] applied proxy-based SM control on a 2-DoF serial robotic manipulator actuated by antagonistic pleated PMs. Lilly and Yang [160] applied sliding mode approach to control the trajectory of a single DoF rotational mechanism driven by McKibben PM actuators dynamic model of the PMs was based on the work reported in [165]. Xing et al. [179] developed SM trajectory control with nonlinear disturbance observer to a PM driven mechanism. Chang [158] reported an adaptive self-organizing fuzzy sliding

mode controller for a 2-DoF serial robot manipulator. In [158, 160, 178], the rotational joints were all actuated by antagonistic PMs. Single-input-single-output (SISO) SM approaches were dedicated for trajectory control. It is common that the desired pressures of individual PMs can be calculated by the controllers' output ΔP and a fixed desired average pressure (P_{0d}) of the antagonistic PMs as:

$$\begin{cases} P_{Fd} = P_{0d} + \Delta P \\ P_{Ed} = P_{0d} - \Delta P \end{cases} \quad (5-1)$$

where, P_{Fd} and P_{Ed} are the reference pressures of the muscles for joint flexion and extension respectively. These were fed into the pressure regulators which adjusted the PM pressures to their desired values. Choi et al. [152] implemented both position and compliance control on a PM actuated manipulator. The position control implementation was similar to the work reported by Lilly and Yang [160]. Instead of having fixed average pressure of the antagonistic PMs, an open loop compliance controller was developed. Based on a dynamic model [165] of PM, the magnitude of joint space compliance can be derived from the desired compliance value. It is also noteworthy that the compliance control is independent from the SM trajectory controller.

In [152, 158, 160, 178, 179], the use of pressure regulators, which appears to be black boxes in control loops, simplified the system models by ignoring the details of the pressure characteristics of the PM actuator. Hence, unpredictable errors or time delays could be introduced. Shen [163] eliminated these black boxes by modelling the whole system with four major processes, which were flow dynamics of the valve, pressure and force dynamics of the PM actuators and the load dynamics of a linear antagonistic mechanism. With a single 3/5 analogue valve, the SISO control was made possible by merging the models of four processes and, letting the valve voltage as input and the trajectory as output. This control approach was verified with a linear mechanism actuated by antagonistic PMs. Aschemann and Schindele [180] developed a cascade SM control algorithm to control a linear mechanism. The four major processes similar to [163] were also utilized to model the system. In the outer trajectory control loop, a SM controller was implemented with the force dynamics of the PM actuators and the load dynamics of the mechanism. Equation (5-1) was then used to calculate the reference pressures for the PM actuators from the controller output of the outer loop (ΔP) and the desired average pressure (P_0). For each individual PM, a SM controller was implemented based on the flow dynamics of the valve and the pressure dynamics of the PM actuator. Compared to [152], Aschemann

and Schindele's approach [180], it was able to vary the average pressure, in other word stiffness of the mechanism, while tracking the desired trajectory. However, substantial difference in time constant between the pressure SM controller and trajectory SM controller was needed to decouple the cascaded controller into two SISO controllers [181]. Hence, the bandwidth of the trajectory control was limited.

In Chapter 2, an extensive review of previous work in the field of robotic gait rehabilitation has been conducted. From the literature review, goals of research are to make the robot assisted gait training more task-specific or close to real walking and also to have robot only assist patients as much as they need. In terms of control strategies, the intrinsic compliance property of PMs can be utilized to adjust the level of assistance provided by the exoskeleton. Hence, controller of the exoskeleton should be able to control the joint space trajectory and the compliance of the exoskeleton simultaneously. Similar ideas has been implemented in [152] and [180]; however these two approaches are both subject to certain limitations, which have been discussed in the previous paragraph.

The main contribution of this chapter is the novel application of a centralized multi-input-multi-output (MIMO) SM controller to an antagonistic PM actuated joint mechanism for robotic gait rehabilitation. As a chapter focusing on the control strategy, only the knee joint mechanism of GAREX is used for model development and experimental validations. Firstly, the knee joint mechanism of the skeleton along with the modelling work of the robotic system is introduced. This is followed by the development and validation of a SISO SM joint trajectory controller. There were two reasons of developing the SISO controllers. One is to validate the design and implementation of the mechanism and instrumentations. The other was for benchmarking the MIMO SM controller to be developed and presented in the fourth section of the chapter. Extensive experiments of the MIMO controller are then presented, which are followed by the discussion and conclusions.

5.2 System modelling

A block diagram of the PM driven antagonistic robotic system has been presented in Figure 4-1. In this section the entire plant is divided into four sequential sub-systems which are each modelled individually.



5.2.1 Flow dynamics of the analogue valves

Pneumatic mass flow through the 3/5 analogue valve is modelled as dimensional compressible flow through an orifice. The effective area of the orifice is controlled by the voltage signals applied to the valves. The mass flow rate through a valve is described as a function of the valve's opening area:

$$\dot{m}_i(P_u, P_d) = A_i \cdot \Lambda_i(P_u, P_d) \quad (i = E, F) \quad (5-2)$$

where:

$$\Lambda(P_u, P_d) = \begin{cases} \sqrt{\frac{\gamma}{RT} \left(\frac{2}{\gamma+1}\right)^{(\gamma+1)/(\gamma-1)}} C_f P_u & \text{if } \frac{P_d}{P_u} \leq C_r \text{ (choked)} \\ \sqrt{\frac{2\gamma}{RT(\gamma-1)}} \sqrt{1 - \left(\frac{P_d}{P_u}\right)^{(\gamma-1)/\gamma}} \left(\frac{P_d}{P_u}\right)^{1/\gamma} C_f P_u & \text{otherwise (unchoked)} \end{cases} \quad (5-3)$$

In the two equations above, $A_{(E,F)}$ is the equivalent valve area for the PMs on the respective side; P_u and P_d are the upstream and downstream pressures respectively; C_f is the discharge constant and C_r is the pressure ratio that divides the flow into choked and unchoked flow through the orifice; γ is the ratio of specific heats for air, R is the universal gas constant, T is the gas temperature,

During the inflating process of the PM actuator, the pneumatic supply pressure (P_s) is regarded as the upstream pressure and the downstream pressure is equal to the pressure inside the PM actuator, expressed with (5-4).

$$\begin{cases} P_u = P_s \\ P_d = P_i \end{cases} \quad (i = E, F) \quad (5-4)$$

During the deflating process, the pressure of inside the PM is regarded as the upstream pressure and the atmospheric pressure (P_{atm}) is regarded as the downstream pressure:

$$\begin{cases} P_u = P_i \\ P_d = P_{atm} \end{cases} \quad (i = E, F) \quad (5-5)$$

It is noteworthy that the equivalent area of a valve is constrained by the maximum opening area A_{\max} . The applied voltage to the valve (U_i) which is the actual input to the physical system, is calculated using a linear piecewise function of the controller output A_i as:

$$U_i = \begin{cases} 178592A_i + 5.255 & (0.02A_{\max} \leq A_i \leq A_{\max}) \\ 10^6 A_i + 5 & (-0.02A_{\max} \leq A_i \leq 0.02A_{\max}) \\ 178592A_i + 4.745 & (-A_{\max} \leq A_i \leq -0.02A_{\max}) \end{cases} \quad (i = E, F) \quad (5-6)$$

Ideally, a 5V voltage input to the valve would idle the pneumatic flow through the valve and the equivalent valve opening area would be proportional to $(U_i - 5)$. However, in the actual operation, the proportional relationship is only valid if the input voltage is approximately more than 0.3V away from the ideal idle voltage. Through trial and error, (5-6) was constructed to present the valve input voltage to equivalent opening areas conversion.

5.2.2 Pressure Dynamics of the PM

The PM actuation system block in Figure 4-1 can be further divided into models of the pressure dynamics and force dynamics. The pressure dynamics models the relation between the mass flow rate and the rate of pressure change of a PM actuator. The force dynamics models the PM's contracting force versus PM pressure and kinematics relationship.

For the pressure dynamics model, it is assumed that pneumatic flow into and out of the PM is an adiabatic process [163]. Thus, the rate of change of pressure in PM can be described by the physics based model as:

$$\dot{P}_i = \frac{(\gamma R T \dot{m}_i - \gamma P \dot{V}_i)}{V_i} \quad (5-7)$$

$$V_i = 2(a_1 x_i^2 + a_2 x_i + a_3) \quad (i = E, F) \quad (5-8)$$

$$\dot{V}_i = 4a_1 x_i \dot{x}_i + 2a_2 \dot{x}_i \quad (5-9)$$

where γ and R are the ratio of specific heats and universal gas constant of air; T is the gas temperature; \dot{m} is the pneumatic mass flow rate of the PMs which is positive for flow into the PMs; and V is the volume of air inside the two PMs of each side of the antagonistic pair. V is modelled as a function of muscle contraction length (x) in (5-8) and its time derivative is expressed with (5-9).

5.2.3 Force dynamics of the PM actuation system

A new approach to model the force dynamics of PM actuators has been presented in Chapter 4 of this thesis. The newly developed model is thus adopted as part of the robotic system. Based on the model, the actuation torque provided by the antagonistic PMs can be expressed as:

$$\tau = 2r[F(P_F) + B(P_F)\dot{x}_F + K(P_F)x_F - (F(P_E) + B(P_E)\dot{x}_E + K(P_E)x_E)] \quad (5-10)$$

where the force, spring and damping parameters $F(P)$, $K(P)$, $B(P)$ are expressed as:

$$\begin{cases} F(P_i) = 311.8 + 181.9P_i \\ K(P_i) = -96524 + 36121P_i & (P \leq 2bar) \\ K(P_i) = -17253 - 47.1P_i & (P > 2bar) \\ B(P_i) = -1704 + 336.5P_i & (Inflation) \\ B(P_i) = 3041 + -649.8P_i & (Deflation) \end{cases} \quad (i = E, F) \quad (5-11)$$

Equation (5-11) is in the form of the hybrid model described in Section 4.4. Compared to the pure piecewise representation of all the three modelling parameters, the hybrid representations are easier for controller implementation and still fit well to the PM's behaviours. The constants in the equation are adapted from Table 4-1.

5.2.4 Load dynamics of the knee joint mechanism

Detailed information about the mechanism design of the GAREX system has been reported in Chapter 3 of this thesis. For the purpose of control development, only the knee joint mechanism of the exoskeleton is utilized for case study in this chapter. In a short summary, the knee joint is powered by four PM actuators. Each of the PM actuators is 20 mm in diameter and 300 mm in length (excluding the metal fittings in both ends). The antagonistic PMs actuate the flexion and extension of the rotational knee joint via 3 mm diameter steel cables with a 30-mm moment arm. Major components of the knee joint mechanism are illustrated in Figure 5-1. Two 3/5 analogue valves are utilized, so the pneumatic flow of each side of the antagonistic PMs is adjusted by one valve. Subscripts E and F are utilized to denote the parameters for the extension and flexion PMs, respectively. A pair of pressure sensors is also used to measure the PM pressures (P_E , P_F). It is assumed that all the dynamics of the two PMs to flexion/extension side are identical. A magnetic encoder is mounted along the joint axis to measure the angular position of the joint (θ_k), whose value is zero when the centre lines of thigh and shank segments coincide and increases as the joint flexes. The interface between the electrical-pneumatic system

and the PC based control platform was implemented using National Instrument myRIO platform. The FPGA inside MyRIO was programmed to handle the hardware interfacing and signal filtering.

In terms of the kinematics analysis, the following assumptions were made: the driving cables are always in tension and the stretch of the cables is neglected. Therefore, the contracting length of the PM actuators can thus be expressed as:

$$\begin{cases} x_F = r(\theta_k - \theta_{F0}) \\ x_E = r(\theta_{E0} - \theta_k) \end{cases} \quad (5-12)$$

where, r is the effective radius of the pulley or the joint moment arm of the PM actuators; $\theta_{E0} = 80^\circ$ and $\theta_{F0} = 0^\circ$ are the knee joint positions when the extensor and flexor PMs have no contraction or extension, respectively. Detailed illustration can be found in the schematic drawing of Figure 5-1.

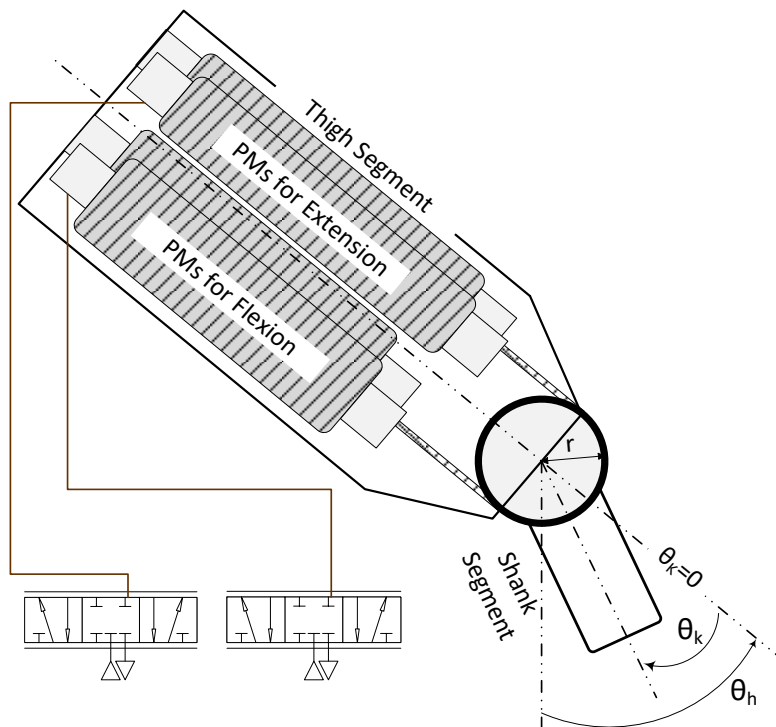


Figure 5-1 Schematic drawing of the PM actuated knee joint mechanism. How the angular values are calculated is also illustrated.

The dynamics of the knee joint mechanism can be described by the following equation:

$$J\ddot{\theta}_k + \xi\dot{\theta}_k + G\sin(\theta_h - \theta_k) = \tau \quad (5-13)$$

where, J is mass polar moment of inertia of the shank segment; ξ is friction coefficient of the actuation system which can be neglected; τ is the net torque provided by the antagonistic PM actuators; G is the maximum joint torque produced by gravity and θ_h is angle between center-line of the thigh segment and the vertical direction shown in Figure 5-1. The moving mass of them PMs is less than 5% of the mass of the shank segment. Therefore, only the polar moment of inertia of the shank segment is considered to determine J , which can be estimated from the computer-aided-design of the exoskeleton.

5.3 SISO trajectory control of the knee joint mechanism

5.3.1 Control algorithm development

Up to this stage, the modelling work of different modules of the system has been completed. With equations (5-2), (5-7), (5-10) and (5-13), the link between of valve areas as the system's and the mechanism's kinematics as the system's output has been constructed. In order to control the joint trajectory of the mechanism, a SISO SM controller, which encompasses all the modelling uncertainties, has been developed. To apply the SM controller to the redundantly actuated system with two individual inputs to the valves and one joint space trajectory output, the conversion from two inputs to single input is having equal and opposite valve orifice areas for the analogue valves. The input (u) of the plant can be expressed as:

$$u = A_F = -A_E \quad (5-14)$$

To develop the SM controller, a complete state-space model with valve area as input and joint kinematics as output has been developed. The state-space variables are expressed in (5-15). To link the state-space variables with the plant's input (u), the time derivative of (5-10) is calculated and expressed explicitly to $\ddot{\theta}_k$ in (5-16).

$$\mathbf{x} = [\theta_k \quad \dot{\theta}_k \quad \ddot{\theta}_k]^T \quad (5-15)$$

$$\begin{aligned} \ddot{\theta}_k = & (2r(F_{F1}\dot{P}_F + B_{F1}\dot{P}_F\dot{x}_F + B_F(P_F)\ddot{x}_F + K_{F1}x_F\dot{P}_F + K_F(P_F)\dot{x}_F \\ & - (F_{E1}\dot{P}_E + B_{E1}\dot{P}_E\dot{x}_E + B_E(P_E)\ddot{x}_E + K_{E1}x_E\dot{P}_E + K_E(P_E)\dot{x}_E)) - G\dot{\theta}\sin(\theta_h - \theta_k)) / J \end{aligned} \quad (5-16)$$

Hence, the derivatives of the state-space variables can be calculated by substituting equations (5-2), (5-7), (5-12) and (5-14) to (5-16):

$$\dot{\mathbf{x}} = \begin{bmatrix} \dot{\theta}_k \\ \ddot{\theta}_k \\ g(\theta_k, \dot{\theta}_k, \ddot{\theta}_k) + h(\theta_k, \dot{\theta}_k, \ddot{\theta}_k)u \end{bmatrix} \quad (5-17)$$

where, $g(\theta_k, \dot{\theta}_k, \ddot{\theta}_k)$ and $h(\theta_k, \dot{\theta}_k, \ddot{\theta}_k)$ are functions of the joint kinematics calculated by extracting input u from the expression of $\ddot{\theta}$.

Based on this nonlinear state space model, a standard integral SM controller could be implemented according to [182]. We firstly expressed the trajectory tracking error vector $\tilde{\mathbf{x}}$ of the state variables in (5-18) with \mathbf{X}_d being the vector of desired values of the state space variables.

$$\tilde{\mathbf{x}} = \mathbf{x} - \mathbf{x}_d = \begin{bmatrix} \tilde{\theta}_k & \dot{\tilde{\theta}}_k & \ddot{\tilde{\theta}}_k \end{bmatrix}^T \quad (5-18)$$

The integral sliding surface is defined as:

$$\sigma = \left(\frac{d}{dt} + \lambda\right)^3 \left(\int_0^t \tilde{\theta} dt\right) \quad (5-19)$$

where, λ is a positive tuning constant of the SM controller, known as bandwidth.

The control action of the SM controller is the sum of the continuous equivalent control element u_{eq} , which helps the reaching of the sliding surface for desired motions, and discontinuous robust element u_{rob} , which makes sure that the desired motions are sustained by sticking to the sliding surface (5-20). By letting $\dot{\sigma} = 0$, the expression of u_{eq} can be derived as (5-21).

$$\mathbf{u} = \mathbf{u}_{eq} + \mathbf{u}_{rob} \quad (5-20)$$

$$u_{eq} = \frac{\ddot{\theta}_{kd} - \hat{g}(\mathbf{x}) - 3\lambda\ddot{\tilde{\theta}}_k - 3\lambda^2\dot{\tilde{\theta}}_k - \lambda^3\tilde{\theta}_k}{\hat{h}(\mathbf{x})} \quad (5-21)$$

where $\hat{g}(\mathbf{x})$ and $\hat{h}(\mathbf{x})$ are the estimated values of $g(\mathbf{x})$ and $h(\mathbf{x})$ from our model. It is assumed that uncertainties of the estimations are bounded by the following rules:

$$\beta^{-1} \leq \frac{h(\mathbf{x})}{\hat{h}(\mathbf{x})} \leq \beta \quad (5-22)$$

$$|g(\mathbf{x}) - \hat{g}(\mathbf{x})| \leq G(x) \quad (5-23)$$

To guarantee the sliding motion, the robust control action u_{rob} is calculated as:

$$u_{rob} = -\frac{q}{\hat{h}(\mathbf{x})} \text{sgn}(\sigma) \quad (5-24)$$

To ensure the stability of the controller, the following condition has to be satisfied.

$$q \geq \beta(G(\mathbf{x}) + \eta) + (\beta - 1)\hat{h}(\mathbf{x})|u_{eq}| \quad (5-25)$$

During the implementation of the controller, the sign function of the robust control action (5-24) was replaced by a saturation function with a narrow boundary layer along the sliding surface. It was aimed to eliminate chattering caused by the finite frequency of the controller processing that leads high frequency switch along the sliding surface.

$$u_{rob} = -\frac{q}{\hat{h}(\mathbf{x})} \text{sat}\left(\frac{\sigma}{\phi}\right) \quad (5-26)$$

where ϕ is the thickness of the boundary layer.

5.3.2 Experimental setup and validation of the SISO SM controller

Modelling work and controller design were conducted with MATLAB. The MUPAD application within MATLAB was utilized to perform symbolic calculation for the model. The symbolic calculation results were converted to MATLAB functions. These functions were then used in the control simulated system in Simulink. The control strategy of the knee joint of the exoskeleton was programmed in LABVIEW and run by a National Instrument myRIO platform. The algorithms developed in MATLAB can be reused with the Mathscript frame in LABVIEW. All the parameters used in the simulation and experiments are listed in Table 5-1. It is also worth to notice that the pressures used in (5-10) and (5-11) are relative pressures (with the unit of 'Bar') to the atmospheric pressure. All other pressures appearing in this chapter are absolute pressures (with the unit of 'KPa').

Table 5-1 A list of parameters used in the model and SISO SM controller implementation

	Value	Unit		Value	Unit
A_{max}	2.837×10^{-5}	m^2	r	0.03	m
a_1	-0.01172	m	G	20	N
a_2	2.803×10^{-3}	m^2	θ_{r0}	0	rad
a_3	9.21×10^{-5}	m^3	θ_{e0}	1.40	rad
J	0.1	kgm^2	λ	23	rad/s
C_r	0.528		ϕ	10000	m/s^2
γ	1.4		η	1	
P_{atm}	101	KPa	β	1.36	
P_s	505	KPa	$G(\mathbf{x})$	$ \hat{g}(\mathbf{x}) $	
R	287	J/(kgK)			

To conduct experiments with the controller, the knee joint mechanism of GAREX was mounted to an aluminum stand with its thigh segment in horizontal position (Figure 5-2). The trajectory experiments were performed with and without human limb attached to the mechanism. Both squared and sinusoidal reference trajectories at various frequencies were used to characterize the performance of the controller implemented. For experiments without human leg attached, the mechanism only actuated the shank segment of the exoskeleton. The other experiments were conducted with human leg attached, in which the mechanism needed to drive the human shank and the shank segment of the exoskeleton as a combined rigid body. It was also assumed that the subject's knee joint was aligned with the knee joint of the mechanism. All the experiments with leg attached were conducted with the help of one healthy subject (male, height: 1.85m, weight: 100kg). A written consent has been obtained from the subject. The ethics approval for experiments with health subjects had been granted University of Auckland Human Participants Ethics Committee (Ref. 014970). The experimental setup was shown in the right picture of Figure 5-2. The one of the subject's lower limbs was securely strapped to the leg holders of the knee joint mechanism. The knee joint rotational axes of the human limb and the mechanism were aligned. During the experiments, the subject was asked to relax the leg and let the mechanism to guide its movements.



Figure 5-2 Left: structure of the knee joint mechanism; right: a healthy subject participating validation experiment with the mechanism

The comparisons between desired and actual trajectories, when the sliding model control system was tracking a squared wave with and without human leg attached, are shown in the two plots of Figure 5-3. The experimental results indicate that the controller was able to track the square wave with fast and stable responses and small steady state errors for both the upper and lower target positions during experiments with and without the subject. The steady state errors could be resulted from 1) the intrinsic compliance of PM actuation system; 2) the open loop relation from the voltage applied to the valve to its orifice area (5-6). Moreover, there was an unknown leakage pneumatic flow rate when the analogue valve spool is in its idle position. Though, it had been attempted to address such leakage rate with the second equation of (5-6), it was still difficult to model it exactly. It is also noticed that there are large magnitude oscillations in the transient responses, which is due to the sudden and high amplitude changes in of the time derivatives of the reference trajectory. This phenomenon is regard not to be a concern, since target trajectories for rehabilitation need to be smooth to prevent injury and discomfort.

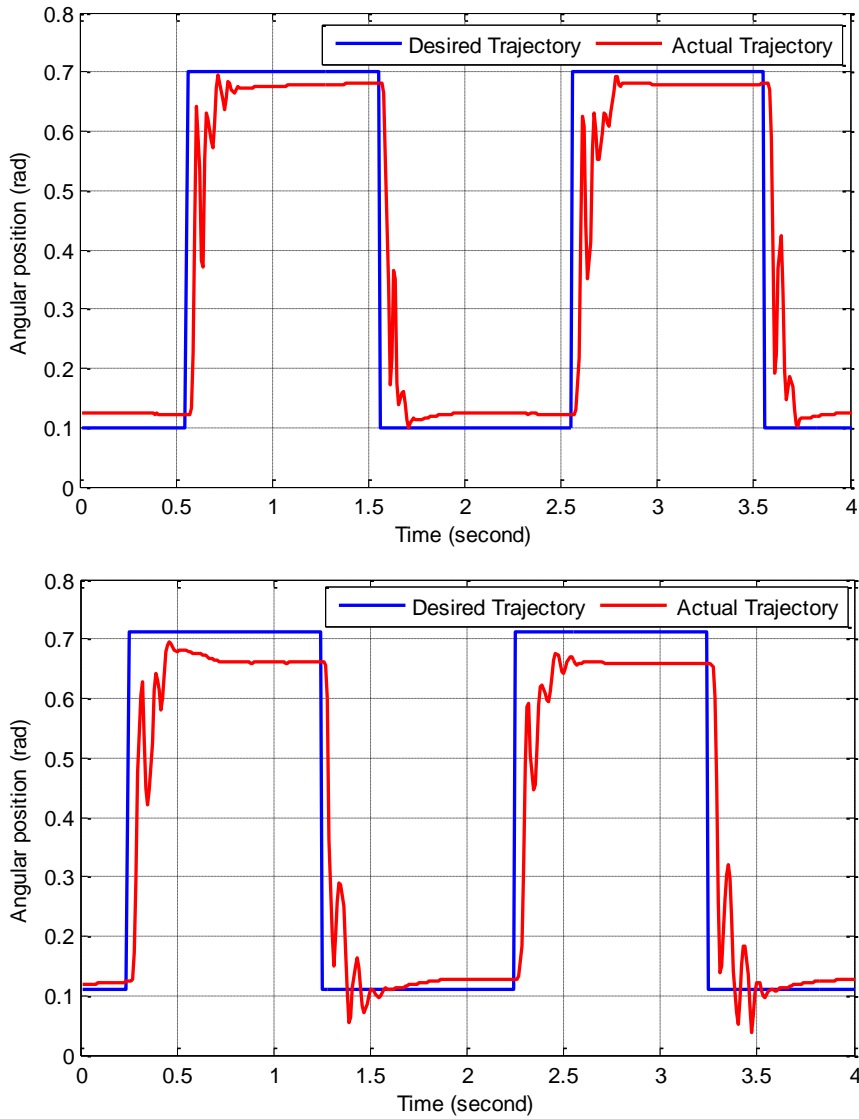


Figure 5-3 The control system’s square wave trajectory tracking performance. Top: only the knee joint mechanism is controlled to track the desired trajectory Bottom: square wave tracking with the leg of a healthy subject attached to the mechanism.

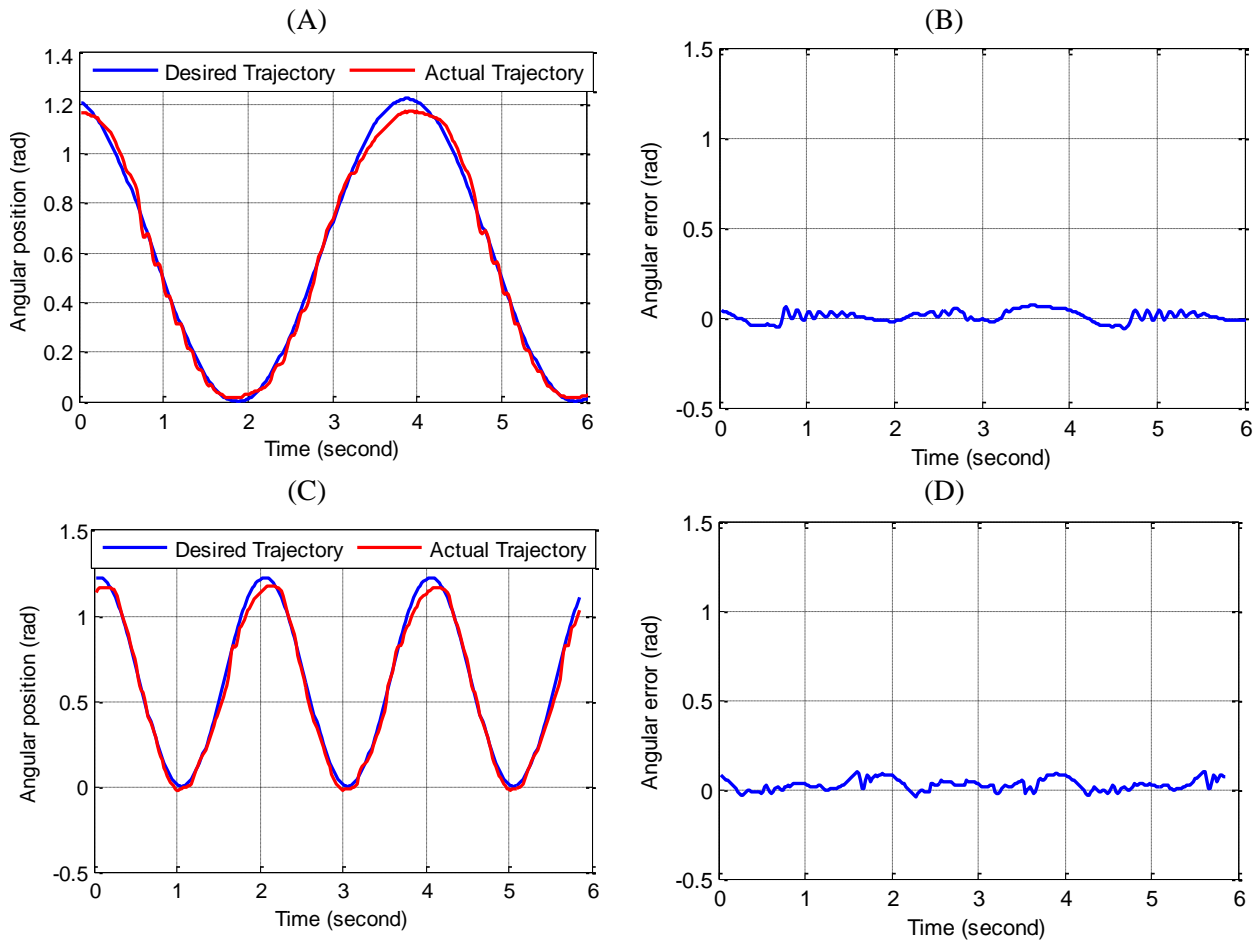


Figure 5-4 Sinusoidal trajectory tracking results of SISO SM control system of the knee joint mechanism without human leg attached. (A): Tracking result of a 0.25 Hz sinusoidal desired trajectory. (B) Tracking error of the 0.25 Hz wave trajectory. The root mean square error is 0.0325 radian ($e_{RMS}=0.033$). (C) and (D): Tracking result and error of a 0.5 Hz sinusoidal desired trajectory($e_{RMS}=0.041$).

The next set of experiments was to make the mechanism track sinusoidal trajectories with magnitude and frequency similar to the joint space gait trajectory of the knee joint during gait rehabilitation. Again, the experiments were conducted both with and without human leg attached. Figure 5-4 and Figure 5-5 are showing the results of the experiments without human participation, in which the trajectory tracking result and error plots are presented with sinusoidal frequencies of 0.25, 0.5, 1 and 1.5 Hz. The root mean square errors (e_{RMS}) were also calculated for each of the experimental conditions in order to assess the controller's performance.

It can be seen from the figures that the control system was able to track the desired sinusoidal trajectories in all the experimental conditions regardless whether being the mechanism alone

or attached with human leg. The trajectory tracking accuracy decreases as the controlled frequency goes up. Compared to experiments with the mechanism alone, there are higher inertial load and more uncertainties and disturbances for the experiments with human leg attached. Hence, as same frequencies, experiments with the subject resulted less accurate tracking.

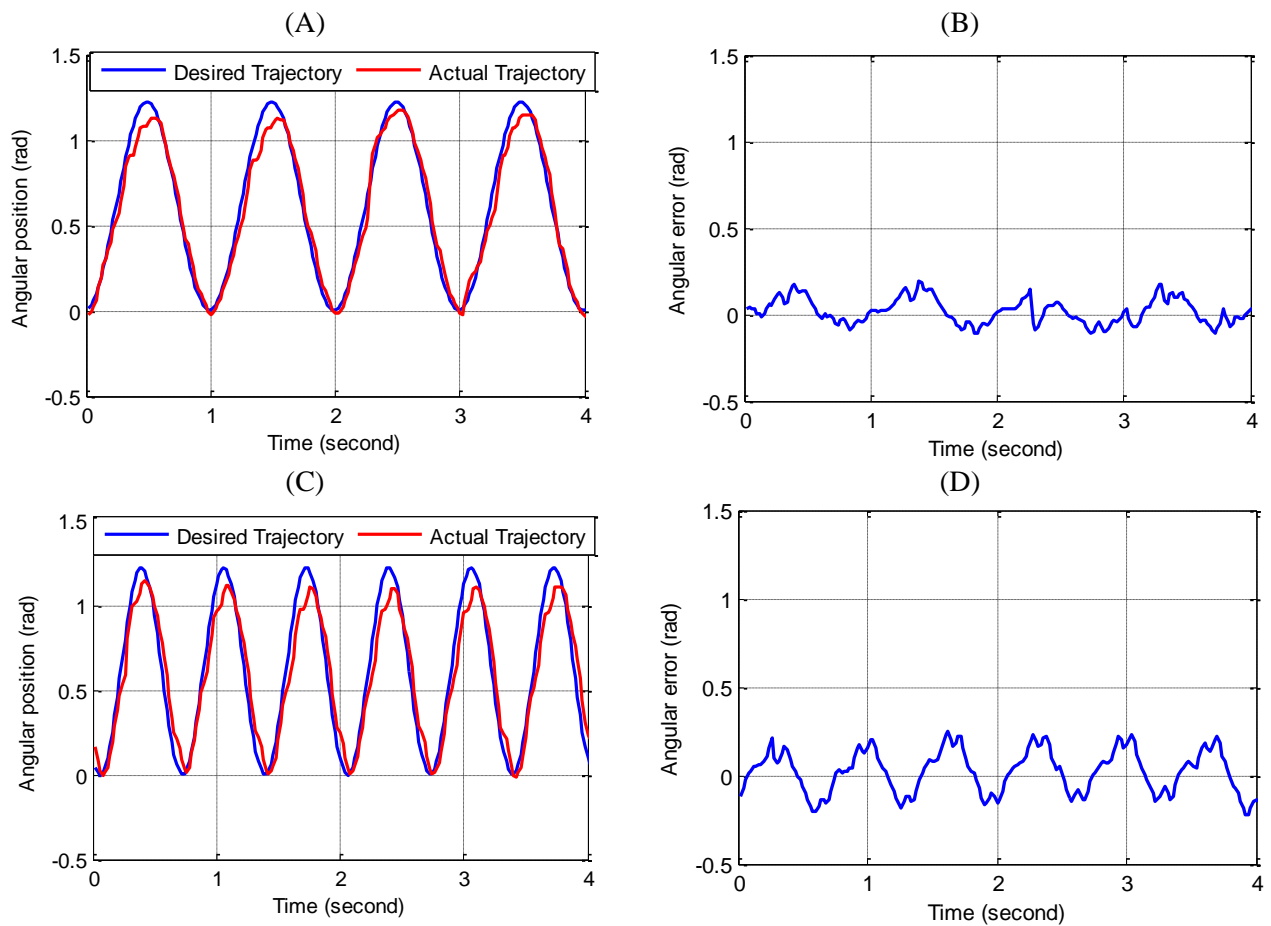


Figure 5-5 Sinusoidal trajectory tracking results of SISO SM control system of the knee joint mechanism without human leg attached. (A) and (B): Tracking result and error of a 1 Hz sinusoidal desired trajectory ($e_{RMS}=0.077$). (C) and (D): Tracking result and error of a 1.5 Hz sinusoidal desired trajectory ($e_{RMS}=0.124$).

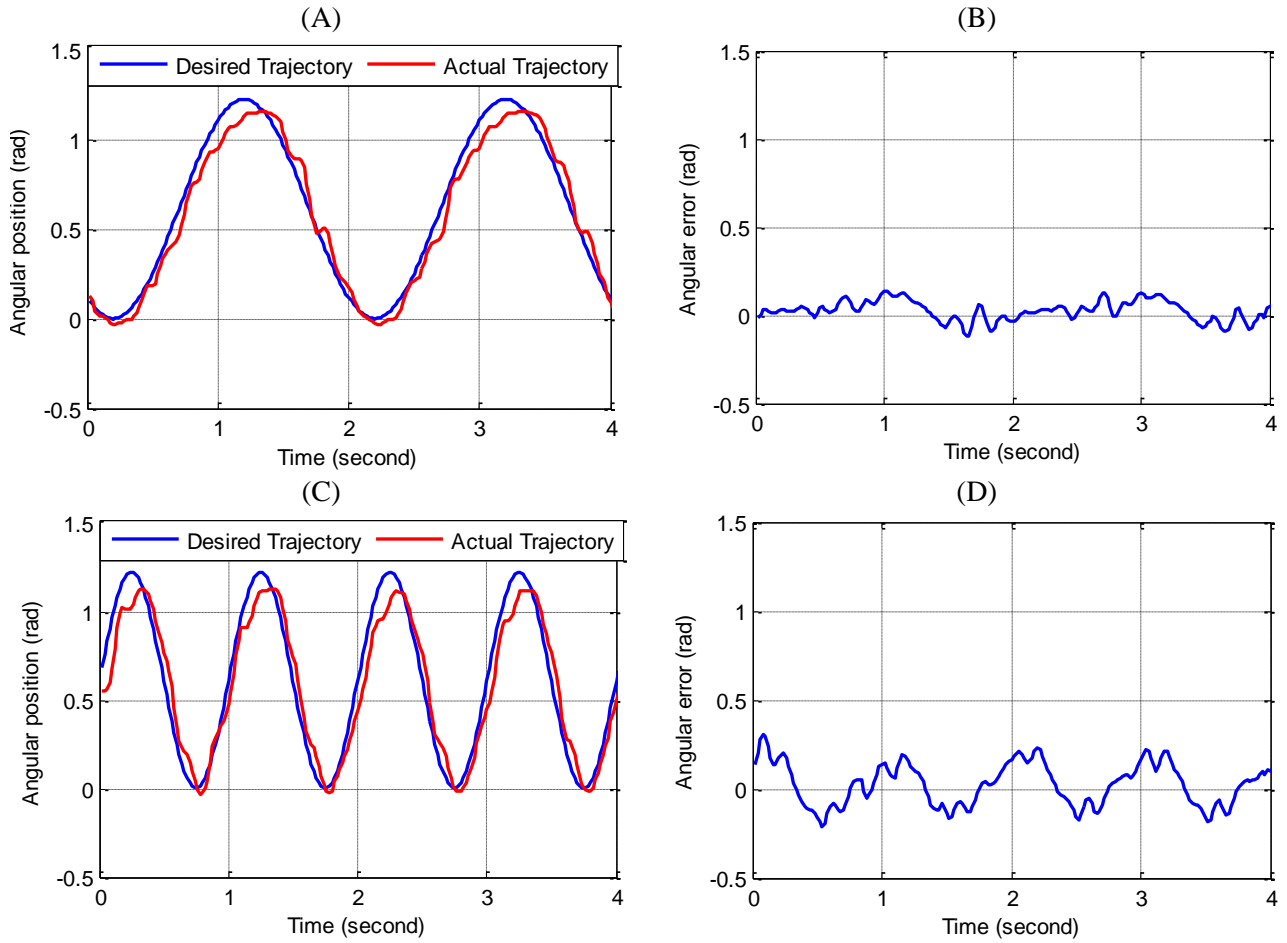


Figure 5-6 Sinusoidal trajectory tracking results of SISO SM control system of the knee joint mechanism with human leg attached. (A) and (B): Tracking result and error of a 0.5 Hz sinusoidal desired trajectory ($e_{RMS}=0.087$). (C) and (D): Tracking result and error of a 1 Hz sinusoidal desired trajectory ($e_{RMS}=0.125$).

5.4 MIMO sliding mode trajectory and compliance controller

5.4.1 Control algorithm development

Both the SISO controller described in Section 5.3 and the MIMO controller of this section were developed on the knee mechanism of GAREX. Hence, the MIMO sliding mode controller is also based on the system model presented in Section 5.2. Unlike the single variable controller which has equal and opposite valve orifice areas for either side of the antagonist, the MIMO control manipulates both the plant inputs in order to tracking the joint space trajectory and adjusting the compliance of the mechanism simultaneously.

For the MIMO SM control system, the two model outputs are the position and the average pressure of the antagonistic PMs of exoskeleton's knee joint. The two inputs are the equivalent areas of the two valves. A state-space model representation of the system was also constructed

for the ease of MIMO SM control implementation. The SS variable (\underline{x}), system input (\underline{u}) and output (\underline{y}), vectors are given in the following three equations.

$$\underline{x} = [\theta_k \quad \dot{\theta}_k \quad P_F \quad P_E]^T = [x_1 \quad x_2 \quad x_3 \quad x_4]^T \quad (5-27)$$

$$\underline{u} = [A_F \quad A_E]^T \quad (5-28)$$

$$\underline{y} = \begin{bmatrix} y_1(\underline{x}) \\ y_2(\underline{x}) \end{bmatrix} = \begin{bmatrix} x_1 \\ \frac{x_3 + x_4}{2} \end{bmatrix}^T \quad (5-29)$$

By combining (5-2) to (5-12), the nonlinear state-space model can be written in the form of:

$$\dot{\underline{x}} = f(\underline{x}) + g(\underline{x}) \times \underline{u} \quad (5-30)$$

$$\text{or } \dot{\underline{x}} = f(\underline{x}) + \sum_{k=1}^2 g_k(\underline{x}) \times u_k \quad (5-31)$$

where

$$f(\underline{x}) = \begin{bmatrix} \dot{\theta}_k \\ \left(\begin{array}{l} 2r(F(P_F) + r(\theta_{F0} - \theta_k)K(P_F) - r\dot{\theta}_k B(P_F)) / J \\ -2r(F(P_E) - r(\theta_{E0} - \theta_k)K(P_E) + r\dot{\theta}_k B(P_E)) / J \end{array} \right) \\ \frac{0.5K P_F (4ar^2 \dot{\theta}_k (\theta_{F0} - \theta_k) - 2a_2 r \dot{\theta}_k)}{V_F} \\ \frac{0.5K P_E (4ar^2 \dot{\theta}_k (\theta_{E0} - \theta_k) + a_2 r \dot{\theta}_k)}{V_E} \end{bmatrix} \quad (5-32)$$

$$g(\underline{x}) = \begin{bmatrix} 0 & 0 \\ 0 & 0 \\ \frac{K R T \Lambda_F}{V_F} & 0 \\ 0 & \frac{K R T \Lambda_E}{V_E} \end{bmatrix} \quad (5-33)$$

$$V_F = 2a_3 + 2a_1 r^2 (\theta_{F0} - \theta_k)^2 - 2a_2 r (\theta_{F0} - \theta_k) \quad (5-34)$$

$$V_E = 2a_3 + 2a_1 r^2 (\theta_{F0} - \theta_k)^2 - 2a_2 r (\theta_{F0} - \theta_k) \quad (5-35)$$

A coordinate transformation [183] is performed with the following equation to make the system outputs and their derivatives as new state variable vector (\underline{z}).

$$\underline{z} = \mu(\underline{x}) = \begin{bmatrix} y_1(\underline{x}) \\ L_f y_1(\underline{x}) \\ L_f^2 y_1(\underline{x}) \\ y_2(\underline{x}) \end{bmatrix} = \begin{bmatrix} x_1 \\ x_2 \\ \dot{x}_2 \\ \frac{x_3 + x_4}{2} \end{bmatrix} \quad (5-36)$$

where the expression of $L_f(y_i)$ stands for the directional derivative of scalar y_i with respect to vector $f(\underline{x})$, which has the following properties:

$$L_f(y_i) = \frac{\partial y_i}{\partial x_1} f_1(\underline{x}) + \dots + \frac{\partial y_i}{\partial x_n} f_n(\underline{x}) \quad \text{with } (i = 1, 2) \quad (5-37)$$

$$L_f^k(y_i) = L_f(L_f^{k-1}(y_i)) \quad \text{with } (i = 1, 2) \quad (5-38)$$

Based on (5-31), the time derivative of output y_i is calculated in (5-39) and the time derivative of the new state space variable vector is calculated with (5-40) to (5-45).

$$\begin{aligned} \frac{dy_i}{dt} &= \frac{\partial y_i}{\partial \underline{x}} \frac{\partial \underline{x}}{\partial t} = \frac{\partial y_i}{\partial \underline{x}} [f(\underline{x}) + g_1(\underline{x})u_1 + g_2(\underline{x})u_2] \\ &= L_f(y_i) + L_{g_1}(y_i)u_1 + L_{g_2}(y_i)u_2 \end{aligned} \quad \text{with } (i = 1, 2) \quad (5-39)$$

$$(5-40)$$

$$L_f^3(y_1(\underline{x})) = \frac{\partial \ddot{\theta}_k}{\partial \theta_k} f_1(\underline{x}) + \frac{\partial \ddot{\theta}_k}{\partial \dot{\theta}_k} f_2(\underline{x}) + \frac{\partial \ddot{\theta}_k}{\partial P_F} f_3(\underline{x}) + \frac{\partial \ddot{\theta}_k}{\partial P_E} f_4(\underline{x}) \quad (5-41)$$

$$\text{where } \frac{\partial \ddot{\theta}_k}{\partial \theta_k} = -\frac{2r^2 (K_F(P_F) + K_F(P_F))}{J}$$

$$\frac{\partial \ddot{\theta}_k}{\partial \dot{\theta}_k} = -\frac{2r^2 (B_F(P_F) + B_E(P_E))}{J}$$

$$\frac{\partial \ddot{\theta}_k}{\partial P_F} = \frac{2r (F_{F1} - B_{F1} \dot{\theta}_k r + K_{F1} (\theta_{F0} - \theta_k) r)}{J}$$

$$\frac{\partial \ddot{\theta}_k}{\partial P_E} = -\frac{2r(F_{E1} + B_{E1}\dot{\theta}_k r - K_{E1}(\theta_{E0} - \theta_k)r)}{J}$$

$$L_{g_1} L_f^2 (y_1(\underline{x})) = \frac{\partial \ddot{\theta}_k}{\partial P_F} \bullet g_{31}(\underline{x}) > 0 \quad (5-42)$$

$$L_{g_2} L_f^2 (y_1(\underline{x})) = \frac{\partial \ddot{\theta}_k}{\partial P_E} \bullet g_{42}(\underline{x}) < 0 \quad (5-43)$$

$$L_f (y_2(\underline{x})) = \frac{(f_3(\underline{x}) + f_4(\underline{x}))}{2} \quad (5-44)$$

$$L_{g_1} (y_2(\underline{x})) = \frac{g_{31}(\underline{x})}{2} > 0; \dots \quad (5-45)$$

To apply the SM control to the modelled system, two sliding surface variables (σ_1, σ_2) are firstly defined:

$$\sigma_1 = \lambda^2 (\theta_k - \theta_{kd}) + 2\lambda (\dot{\theta}_k - \dot{\theta}_{kd}) + (\ddot{\theta}_k - \ddot{\theta}_{kd}) \quad (5-46)$$

$$\sigma_2 = \frac{P_F}{2} + \frac{P_E}{2} - P_{0d} \quad (5-47)$$

where σ_1 represents the sliding surface for the joint space trajectory; σ_2 is for the average pressure; λ is a tuning parameter of the sliding surface; $\theta_k, \dot{\theta}_{kd}, \ddot{\theta}_{kd}$ are desired knee joint angular position, velocity and acceleration respectively; P_{0d} is the desired average pressure of the antagonistic PM actuators.

With the selected sliding surfaces, the control law can be designed in order to drive the state-space trajectories to the sliding surface. Once reached, the trajectories are forced to stay on the sliding surfaces by the controller. A classic controller design [182] is described as:

$$\frac{1}{2} \frac{d}{dt} \sigma_i^2 = \sigma_i \dot{\sigma}_i \leq -\eta_i |\sigma_i| \quad (5-48)$$

in which η_i is strictly positive. The time derivatives of (5-46) and (5-47) can be expressed in the vector form of:

$$\begin{aligned} \begin{bmatrix} \dot{\sigma}_1 \\ \dot{\sigma}_2 \end{bmatrix} &= \begin{bmatrix} \lambda^2(\dot{\theta}_k - \dot{\theta}_{kd}) + \lambda(\ddot{\theta}_k - \ddot{\theta}_{kd}) - \ddot{\theta}_{kd} + L_f^3(y_1(\underline{x})) \\ L_f(y_2(\underline{x})) - \dot{P}_{0d} \end{bmatrix} + \begin{bmatrix} L_{g_1} L_f^2(y_1(\underline{x})) & L_{g_2} L_f^2(y_1(\underline{x})) \\ L_{g_1}(y_2(\underline{x})) & L_{g_2}(y_2(\underline{x})) \end{bmatrix} \begin{bmatrix} u_1 \\ u_2 \end{bmatrix} \\ &= \mathbf{H} + \mathbf{S} + \mathbf{Q}\underline{u} \end{aligned} \quad (5-49)$$

$$\text{with } \mathbf{H} = \begin{bmatrix} h_1 \\ h_2 \end{bmatrix} = \begin{bmatrix} L_f^3(y_1(\underline{x})) \\ L_f(y_2(\underline{x})) \end{bmatrix} \quad (5-50)$$

$$\mathbf{Q} = \begin{bmatrix} q_1 & q_2 \\ q_3 & q_4 \end{bmatrix} = \begin{bmatrix} L_{g_1} L_f^2(y_1(\underline{x})) & L_{g_2} L_f^2(y_1(\underline{x})) \\ L_{g_1}(y_2(\underline{x})) & L_{g_2}(y_2(\underline{x})) \end{bmatrix} \quad (5-51)$$

$$\mathbf{S} = \begin{bmatrix} \lambda^2(\dot{\theta}_k - \dot{\theta}_{kd}) + \lambda(\ddot{\theta}_k - \ddot{\theta}_{kd}) - \ddot{\theta}_{kd} \\ -\dot{P}_{0d} \end{bmatrix} \quad (5-52)$$

Hence, the SM control law can be applied. The control action vector (\underline{u}) contains two components:

$$\underline{u} = \mathbf{Q}^{-1}(\underline{u}_{eq} + \underline{u}_{rob}) \quad (5-53)$$

where, \underline{u}_{eq} is a continuous equivalent control element, which helps reaching of the sliding surfaces for desired motions; is the discontinuous robust element, which makes sure that the desired motions are sustained by sticking to the sliding surface. By zeroing $\dot{\sigma}$, the expression of \underline{u}_{eq} and \underline{u}_{rob} can be derived as:

$$\underline{u}_{eq} = -\mathbf{H} - \mathbf{S} \quad (5-54)$$

$$\underline{u}_{rob} = - \begin{bmatrix} k_1 \text{sgn}(\sigma_1) \\ k_2 \text{sgn}(\sigma_2) \end{bmatrix} \quad (5-55)$$

Based on (5-42), (5-43) and (5-45), matrix \mathbf{Q} is non-singular. Here, it is necessary to remind that all the modelling parameter mentioned previous are based on the ideal situations. All the uncertainties of the model are contained by ideal matrices \mathbf{H} and \mathbf{Q} . Hence, for any instant, the actual representation derivatives of the sliding surfaces are given as:

$$\begin{bmatrix} \dot{\sigma}_1 \\ \dot{\sigma}_2 \end{bmatrix} = \mathbf{H} + \mathbf{S} + \mathbf{Q}\underline{u} \quad (5-56)$$

$$\mathbf{H} = \begin{bmatrix} h_1 \\ h_2 \end{bmatrix}; \quad \mathbf{Q} = \begin{bmatrix} q_1 & q_2 \\ q_3 & q_4 \end{bmatrix} \quad (5-57)$$

where \mathbf{H} and \mathbf{Q} are the instantaneous actual values of the model estimated \mathbf{H} and \mathbf{Q} . The estimation errors of these matrices are bounded by the known function in the following ways:

$$|h_i - h_i| \leq H_i \quad \text{with } (i=1,2) \quad (5-58)$$

$$\forall i = 1, 2, 3, 4 \quad \beta^{-1} \leq \frac{q_i}{q_i} \leq \beta \quad (5-59)$$

$$\beta = \left(\frac{q_{i_max}}{q_{i_min}} \right)_{max}^{1/2} \quad (5-60)$$

To ensure the control law (5-53) satisfy the design criteria stated by (5-48). Equation (5-53) is substituted into (5-56), for $i = 1, 2$:

$$\dot{\sigma}_i = (1 - \zeta_i) s_i + (h_i - \zeta_i h_i) - \zeta_i k_i \text{sgn}(\sigma_i) \quad (5-61)$$

$$\zeta_1 = \frac{q_1 q_4 - q_2 q_3}{q_1 q_4 - q_2 q_3} > 0 \quad (5-62)$$

$$\zeta_2 = \frac{q_1 q_4 - q_2 q_3}{q_1 q_4 - q_2 q_3} > 0 \quad (5-63)$$

Hence, (5-61) is substituted into (5-48) and the following relationship can be generated:

$$\zeta_i k_i \geq \text{sgn}(\sigma_i) \left((1 - \zeta_i) s_i + (h_i - \zeta_i h_i) \right) + \eta_i \quad (5-64)$$

In order to ensure (5-64) is valid, k_i needs to be selected to satisfy the following condition:

$$k_i \geq \left| \left(\zeta_i^{-1} - 1 \right) s_i + \left(\zeta_i^{-1} - 1 \right) h_i + \zeta_i^{-1} (h_i - h_i) \right| + \zeta_i^{-1} \eta_i \quad (5-65)$$

Due to the use of switch functions $\text{sgn}(\sigma_i)$ in (5-55), the system is prone to high frequency chattering along the sliding surfaces. The solution to this problem is replacing the switching element along the sliding surface with piece-wise saturation function with a boundary layer [182, 184]. Hence the robust control element can now be expressed as:

$$\underline{u}_{rob} = - \begin{bmatrix} k_1 \text{sat}\left(\frac{\sigma_1}{\phi_1}\right) \\ k_2 \text{sat}\left(\frac{\sigma_2}{\phi_2}\right) \end{bmatrix} \quad (5-66)$$

where, ϕ_i , ($i = 1, 2$) are the boundary layer thicknesses for their corresponding sliding surfaces.

5.4.2 Experiments on the MIMO SM control system

In terms of implementation, the MIMO SM controller is based on the same hardware platform SISO controller. The modelling parameters have already been listed in Table 5-1. The MIMO SM was tuned experimentally. The tuning parameters of the MIMO SM controller are listed in

Table 5-2 Tuning parameters of the MIMO SM controller implemented to the knee joint mechanism

Parameter	Value	Unit
k_1	1×10^7	
k_2	50000	
λ	8	rad/s
ϕ_1	320000	m/s ²
ϕ_2	8	KPa/s ²

The main contribution of this chapter is on the novel application of the MIMO SM controller to a PM driven gait rehabilitation robots. Hence, extensive experiments haven been conducted in order to validate the system's performance. The experiments were conducted with two different experimental setups. One setup was identical to the experimental setup of the SISO controller, described in Section 5.3.2. Therefore, the performance of the SISO controller could be used to benchmark the MIMO one. The other experimental setup was to investigate the control

system's capability on facilitating the task space robotic gait rehabilitation. Gait like trajectories rather than sinusoidal ones were utilized for evaluation.

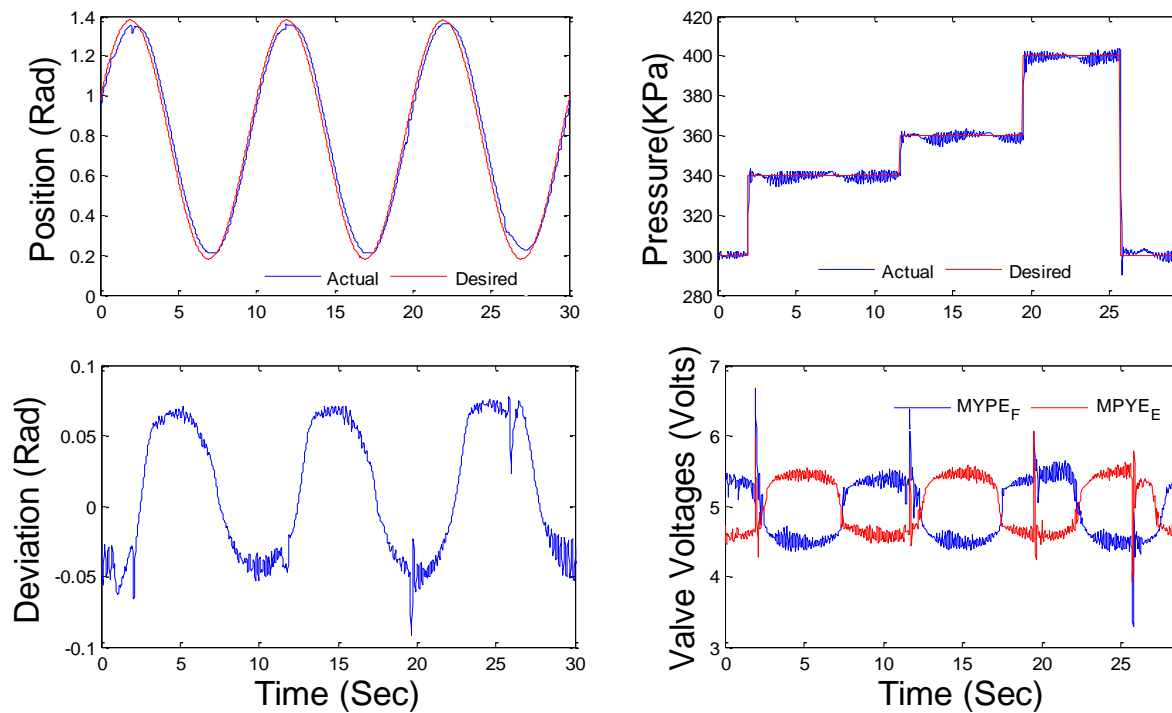


Figure 5-7 SM controller tracking performance. Top-left: knee joint trajectory tracking of a 0.1 Hz sinusoid wave. Top-right: Step responses of the average pressure. Bottom-left: difference between the actual and desired joint angular trajectory. Bottom-right: the controlled valve voltages during the experiment

5.4.2.1 Experiments with sinusoidal trajectories

The first experiment was conducted without leg attached. It was designed to have the knee joint mechanism follow a reference sinusoid trajectory while maintaining its average pressure of the PM actuators. Step changes of the desired average pressure were also adapted to study the system's behavior. Result of the experiment is displayed in Figure 5-7. The figure indicates both the trajectory and pressure tracking are effective. The step changes of the desired average pressure were quickly reacted by the controller's actions shown in the bottom-right plot of the figure. This result indicated good step response behavior of the pressure tracking together with some oscillations in the joint trajectory. It was observed that the oscillation amplitude is positive correlated to step size of the reference pressure. Therefore, such oscillations can be significantly reduced by specifying the maximum change rate of the reference pressure. It is notable that the peak to peak amplitude of the reference sinusoid trajectory is ranging from 0.2 to 1.4

radius for all the experiments described in this manuscript. This was specially selected to simulate the actual knee joint range of motion during gait [156]. Meanwhile, the frequency of the reference sinusoid wave was varied in different experiments to examine the performance of the system.

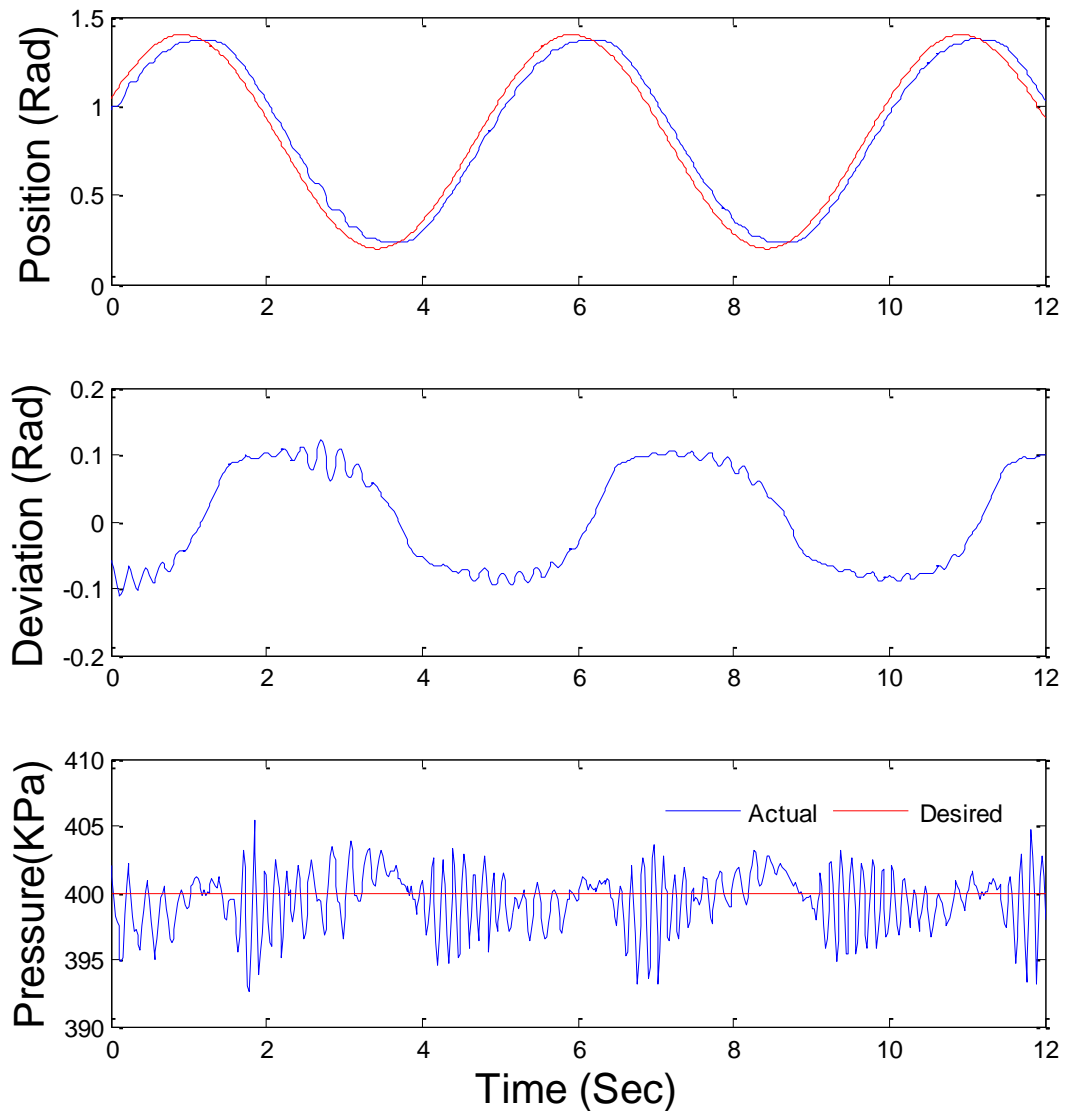


Figure 5-8 Joint trajectory and pressure tracking performances of the MIMO SM controller. The experiment is conducted on the sole knee joint mechanism. ($P_{0d} = 400KPa$). Top: desired (red) versus actual (blue) joint trajectory; middle: the trajectory deviation; bottom: desired versus actual average pressure.

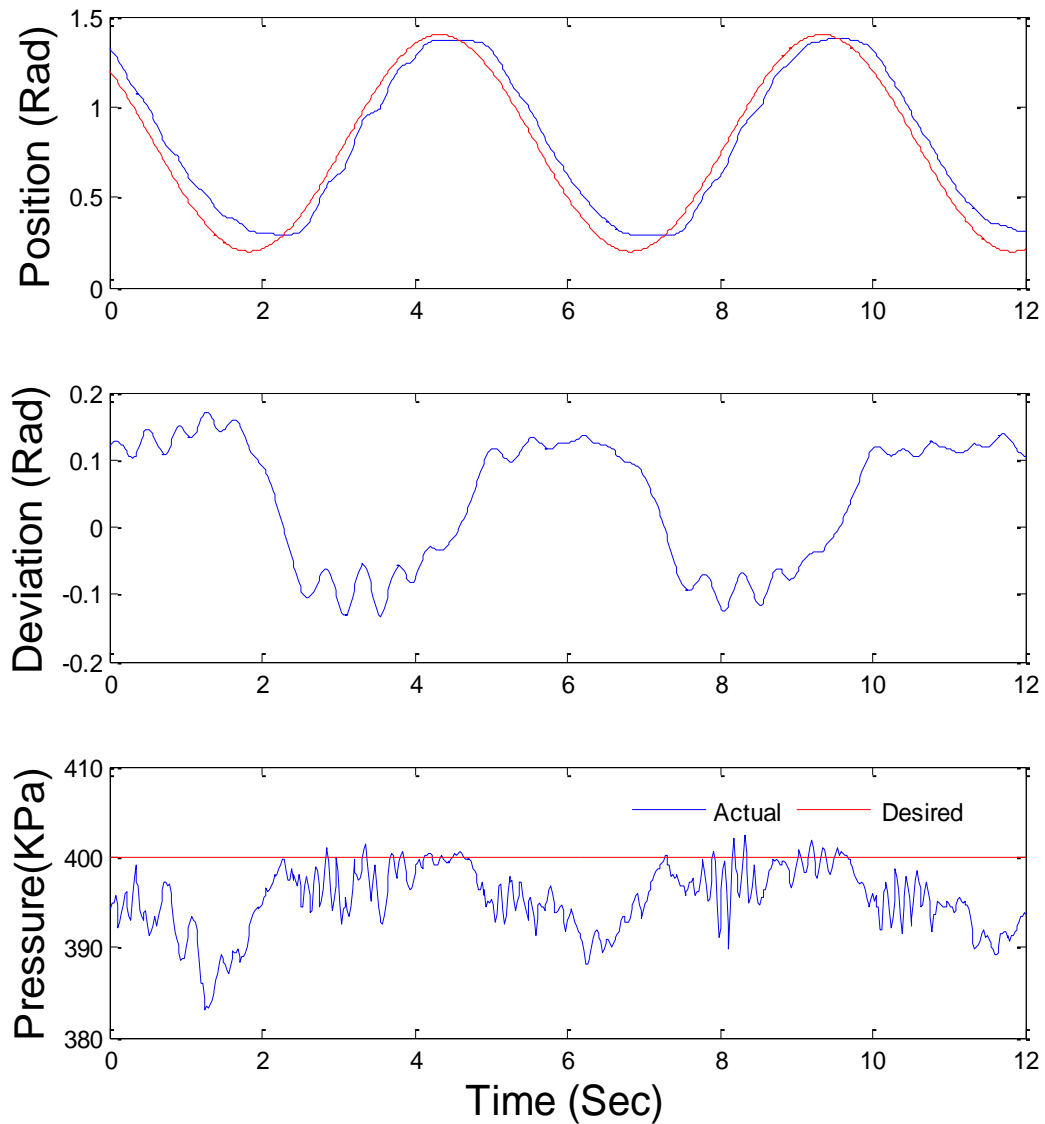


Figure 5-9 Joint trajectory and pressure tracking performances of the MIMO SM controller. The experiment is conducted with leg attached.. ($P_{0d} = 400\text{KPa}$, $e_{RMS} = 0.1022$).

The multivariable tracking performances are also compared between with and without leg situations. For the experiment with human leg attached, the subject was fitted to the exoskeleton as in the right picture of Figure 5-2. He was asked to relax the leg strapped to the exoskeleton and just let the exoskeleton guide his shank movement. Both sets of experiments were conducted with the identical 0.2Hz reference joint trajectory and 400KPa average pressure and the experimental results are illustrated in Figure 5-8 and Figure 5-9. The plots of Figure 5-8 are for the experiment without leg attached and the plots in Figure 5-9 the right are for the other experiment. A few comments can be made on the results shown in these two figures. Firstly, the

added human leg can be treated as disturbance the system (especially in terms of the un-modelled inertia of the moving part). With the presence of such disturbance, the controller was still able to provide good tracking performance. Compared to the without leg experiment, the increase in errors for the joint trajectory and pressure tracking was not significant. The change of compliance due to the change of the average pressure was investigated in the next set of experiments, whose results are shown in Figure 5-10 and Figure 5-11.

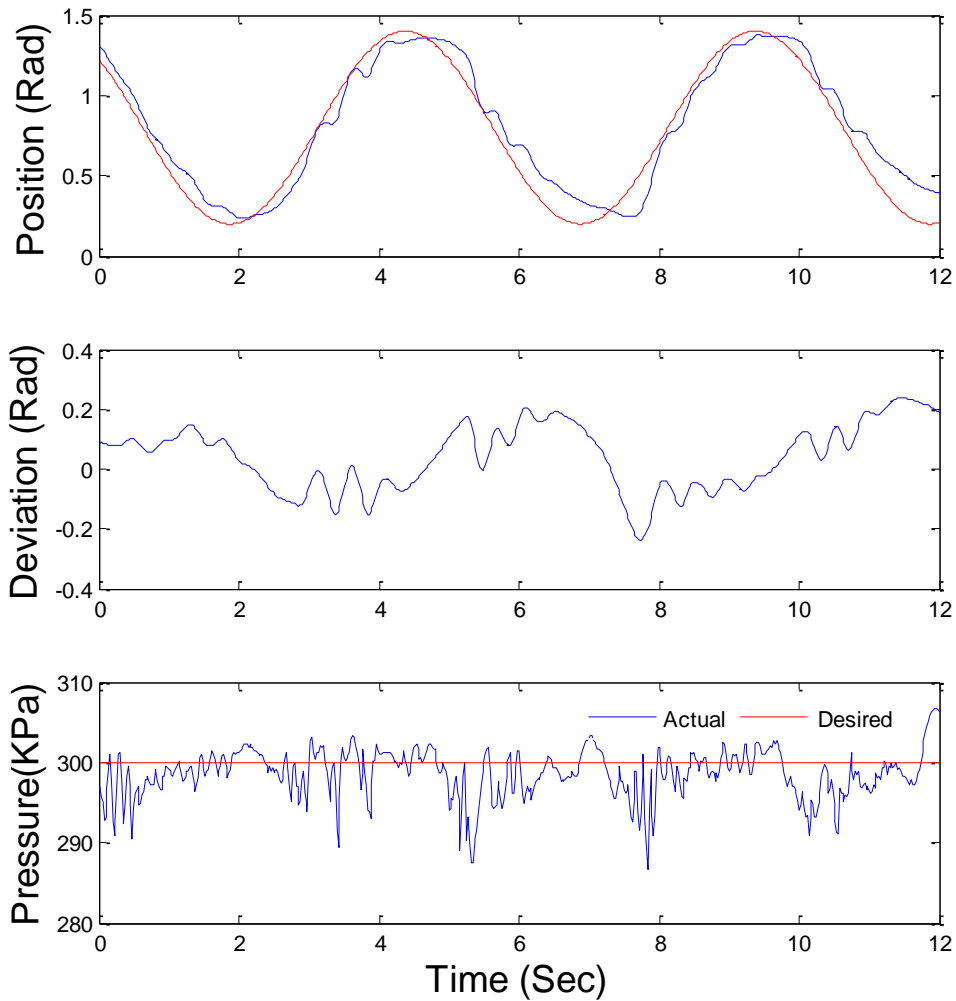


Figure 5-10 Joint trajectory and pressure tracking performances of the MIMO SM controller. The experiment is conducted with leg attached. ($P_{0d} = 300\text{KPa}$, $e_{RMS} = 0.1174$).

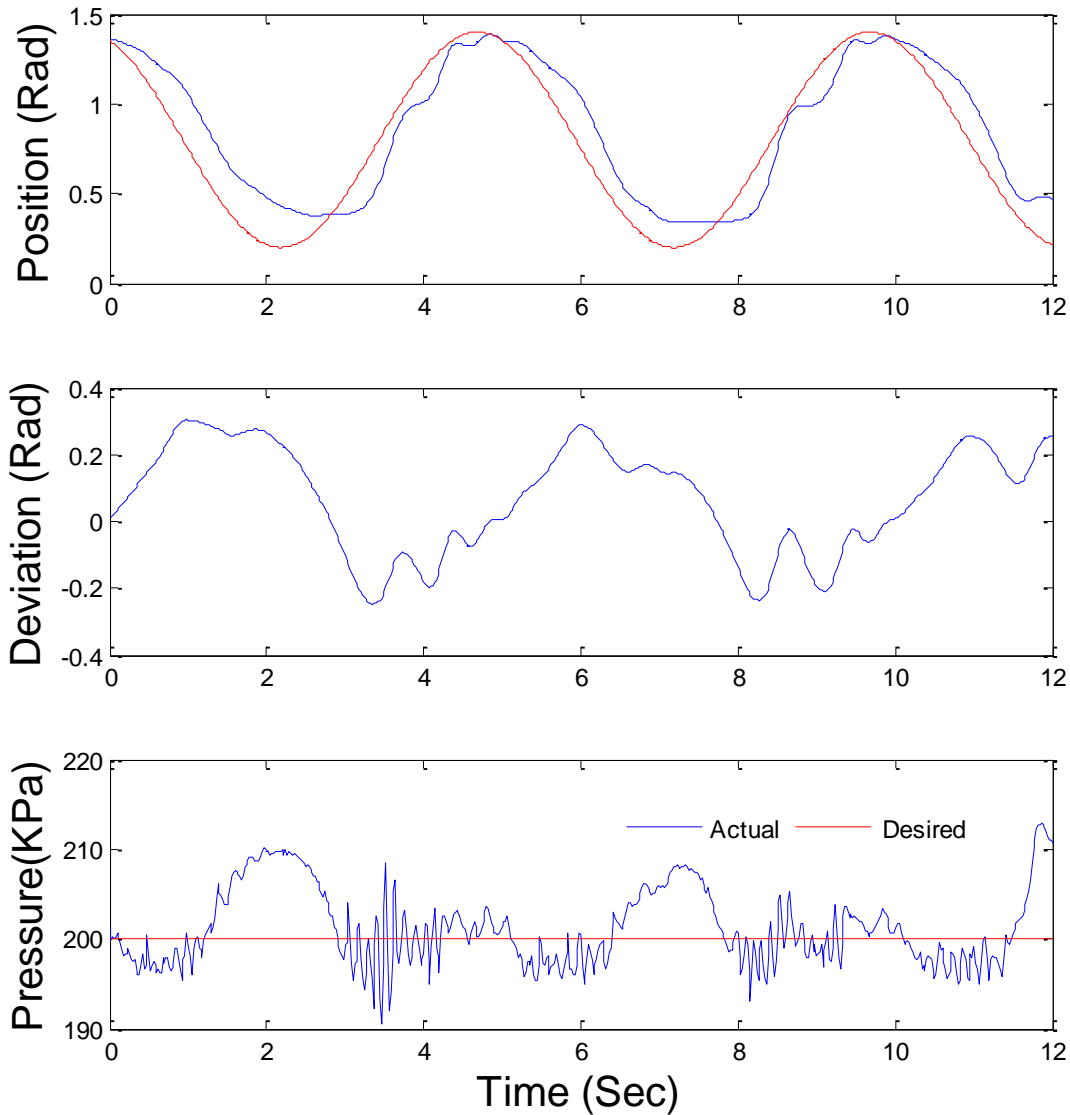


Figure 5-11 Joint trajectory and pressure tracking performances of the MIMO SM controller. The experiment is conducted with leg attached. ($P_{od} = 200\text{KPa}$, $e_{RMS} = 0.1726$)

The experiments shown in Figure 5-10 and Figure 5-11 were conducted with the subject under the same conditions to the experiment shown in Figure 5-9. The experiment of Figure 5-9 had the reference average pressure of 400KPa and the ones of Figure 5-10 and Figure 5-11 were 300KPa and 200KPa respectively. By analysing the three sets of plots, larger joint deviations, which is expressed in terms of root-mean-square trajectory error (e_{RMS}), were observed as average pressure decreased. This further means the control of the actuation system's intrinsic compliance can be achieved. The behaviours are comparable to controller simulated variable impedance or virtual tunnels reported on motor driven gait rehabilitation exoskeletons [95, 96].

5.4.3 Experiments with gait trajectories

All the experiments reported in this section were conducted with subjects, who were healthy and with no lower limb injury. Written consents were obtained from all the participants. The main objective of the controller is to tracking both the knee joint trajectory and the average PM pressure; hence it was validated primarily. When conducting the experiments, the subjects were asked to stand upright with their right legs strapped to the GAREX's lower limb exoskeleton (Figure 5-12). It was ensured the shank and thigh segments of the subjects' legs and the mechanism were aligned; meanwhile the human's and mechanism's knees were also aligned to be coaxial, so the human's and mechanism's knee joint positions were equal. When conducting the experiments, only the knee mechanism was actuated. The hip mechanism was left unactuated.

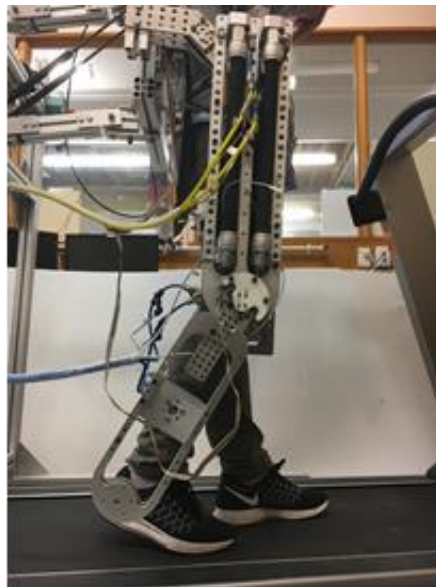


Figure 5-12 A healthy subject participating in a validation experiment with the mechanism

Instead of using sinusoidal reference trajectories, a healthy subject's knee joint trajectory during level walking was adapted as the position control reference in this study. The first experiment conducted was to validate the main objective, which is the tracking performance of both the knee joint trajectory and the average PM pressure of the MIMO SM controller. A male subject (Height: 178cm, weight: 75kg) participated in this experiment. The subject was instructed to relax the leg attached to the mechanism and let the mechanism guide the knee joint movement. The reference knee trajectory was set to 5 seconds per gait cycle; meanwhile, step changes to the reference average pressure were also applied. The experimental results are

shown in Figure 5-13. The figure indicates both the trajectory and pressure tracking were effective. The controller was tuned so that the step changes of the desired average pressure can be reacted quickly enough without affecting the trajectory control performance. This tuning setup resulted a longer rising time, but no overshoot in the average pressure when the reference changed from 200 KPa to 320 KPa and then to 360 KPa. Such controller behavior is thought to be acceptable, as sudden changes in compliance level are unlikely to happen during robotic rehabilitation training. It is observed that the trajectory control accuracy increased as the average pressure increased, which also indicates a decrease in the actuators' compliance.

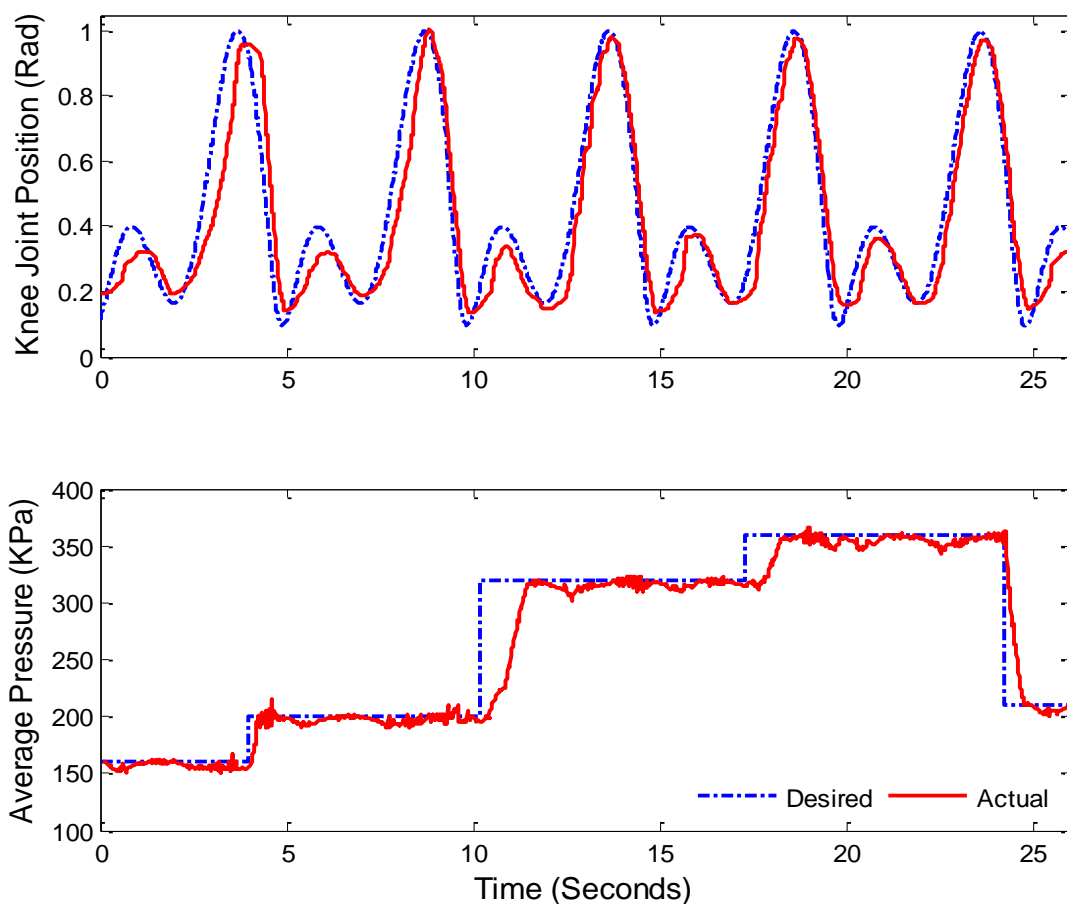


Figure 5-13 The MIMO SM controller's simultaneous multivariable tracking performance. Top: knee joint gait trajectory tracking. Bottom: system responses to the steps changes in desired average PM pressure

To validate relationship between the mechanism compliance and the average PM pressure and further investigate the potential of applying the MIMO SM controller in robotic gait rehabilitation training, a set of experiments were conducted with five healthy subjects (S1: male, 185

cm, 100 kg; S2: male, 178 cm, 73 kg; S3: male, 179 cm, 93 kg; S4: male, 170 cm, 62 kg; S5: female, 167 cm; 55 kg). These five subjects were requested to conduct two groups of experiments. The first group of experiments were conducted in three discrete average PM pressures (180, 270 and 360 KPa). The subjects were fitted to the mechanism and instructed to follow the process in the same manner as the experiment described in the last paragraph. During the second group of experiments, instead of fully relaxing their right knees during the entire experiment, the subjects were instructed to obstruct the mechanism's knee joint guidance at certain period of a gait cycle. The period is approximately from the beginning of swing phase to the point when maximum flexion is reached. During this period the subjects were instructed to obstruct with great effort but without feeling any discomfort. The results of this set of experiments are illustrated in Figure 5-14.

The three subplots (A, C and E) in the left column of Figure 5-14 are for the first group of experiments. The subplots (B, D and F) in the right columns are for the second group. The periods when the subjects were requested to obstruct are highlighted in yellow. The plots in the top, middle and bottom rows are of experiments when the average PM pressure was regulated to 360, 270 and 180KPa respectively.

From Figure 5-14 (A, C and E), it can be observed that the MIMO SM controller is capable of tracking the desired knee joint trajectory at different average PM pressures with different subjects. The tracking accuracy decreases with the average PM pressure. Such changes in tracking accuracy could be interpreted as a result of changes in compliance. Such interpretation was validated in the second group of experiments whose results are shown in Figure 5-14 (B, D and F).

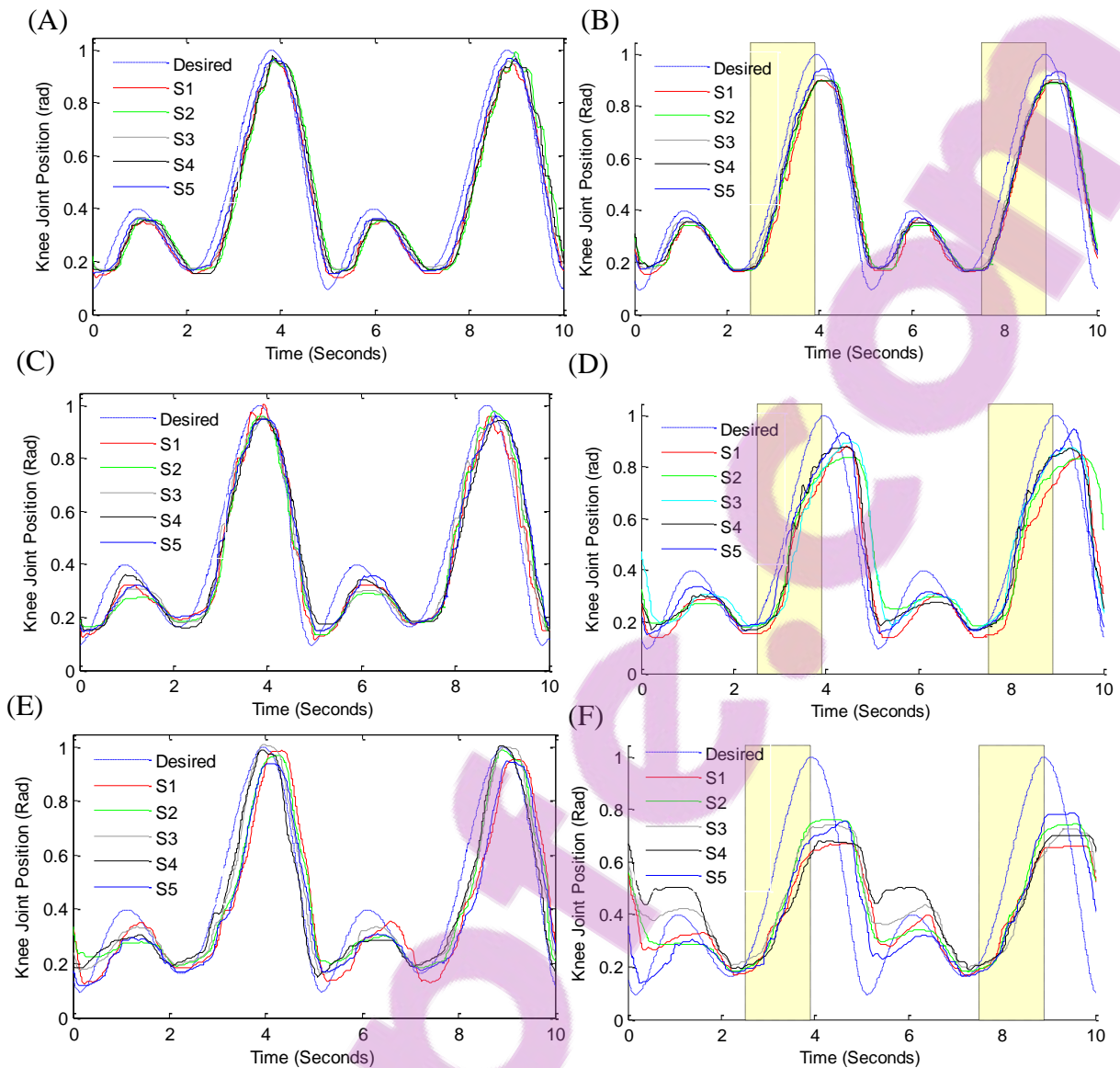


Figure 5-14 Results of the experiments on knee joint trajectory tracking and compliance control with five healthy subjects. (A) (C) (E): the subjects were instructed to relax their right knees during the entire experiments; (B) (D) (F): the subjects were instructed to obstruct the mechanism's guidance during the time period highlighted in yellow. Average PM pressure was regulated at 360, 270 and 180 KPa for the results plotted in top (A, B), middle (C, D) and bottom (E, F) rows, respectively.

The final experiment was designed to explore the bandwidth of the SM controlled system. As mentioned in the introduction section, the gait rehabilitation training needs to be task specific. Hence, the controller and the hardware system need to be able to operate at a bandwidth that is similar to the average gait cycle frequency (0.67Hz) of stroke survivors [185]. The experiment

was conducted with the same male subject and with the same setup as those of the first experiment. During the experiment, the subject was instructed to relax his right leg and let the mechanism guide the knee joint movement at discrete frequencies varying from 0.2 to 0.7 Hz with 0.1 Hz increment. The average PM pressure was regulated at 360 KPa for this experiment. The experimental result is shown in Figure 5. It can be seen that the control system is stable and effective at all the frequencies, although the trajectory tracking performance worsens as demonstrated by an increase in the RMS trajectory error with the frequency. One major contribution of the increase in RMS trajectory error is the increase in the phase delay between the actual and desired trajectory, which could be caused by the intrinsic compliance of the PM actuation system, although, the compliance was controlled to a low level during the experiment.

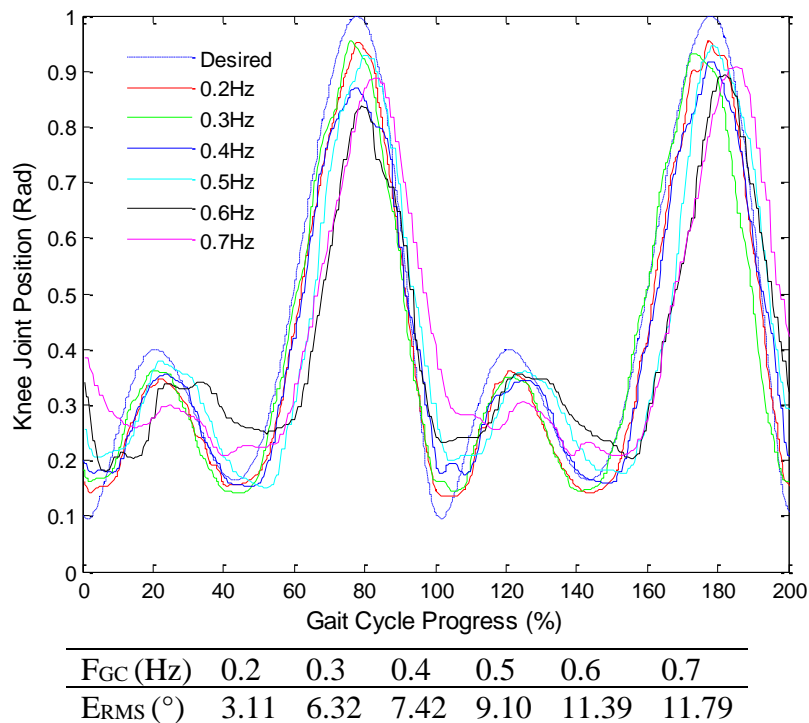


Figure 5-15 Knee joint trajectory versus gait cycle progress plots at different gait cycle frequencies (F_{GC}). The RMS trajectory errors during two gait cycles are also listed again corresponding frequencies.

5.5 Discussion and conclusions

Based on the complete model of the exoskeleton system, SISO and MIMO sliding mode controllers were developed and experimentally evaluated on the knee mechanism of the exoskeleton. The experimental results indicate that stable controller performances were achieved, in spite of nonlinear nature of the actuation system, frequency change in reference trajectories and disturbance introduced by the subject. Both SM controllers were able to track the desired

trajectories with good precision. The MIMO SM controller was also able to regulate the average pressure of the antagonistic PMs, while tracking the desired trajectory.

A new experimental approach was designed and conducted with five healthy subjects to investigate how the change in average pressure of the antagonistic PMs would affect the joint compliance. The experiment results supported the hypothesis that the average pressure is negatively correlated to the compliance of the knee joint mechanism.

From the experimental results presented in this chapter, it can be easily observed that the SISO SM controller generally achieved better angular trajectory tracking performances than the MIMO controller. Controller tuning is one main cause of such differences. When turning the SISO controller, the only objective was to improve trajectory tracking, providing stability of the robotic system. For the MIMO controller, good trajectory tracking was still the main goal of the controller tuning, because of the nature of gait rehabilitation. However, in order to enable the ability of adjusting joint compliance, the trajectory performance was slightly sacrificed.

Compared to the SISO SM controller, a non-integral rather than integral sliding surface were adopted during the MIMO SM controller implementation, although integral control surfaces might lead to better trajectory tracking performances. The reason for such a decision is the safety of future gait rehabilitation applications of the system. During rehabilitation training, the active input of a subject may result in the accumulation of trajectory errors. Controller with integral sliding surfaces may react to the accumulation of trajectory errors with sudden movement or a short period of high frequency oscillation. This may cause discomfort or even injuries to the subject.

Chapter 6 MIMO Sliding Mode Control System for GAREX

A newly proposed multi-input-multi-output sliding mode control algorithm for antagonistic pneumatic muscle driven mechanism is presented in Chapter 5. Followed on from what has been discussed, this chapter focuses on the integration of the MIMO SM controllers to both actuated joints of GAREX. Based on the dynamics modelling of the exoskeleton mechanism with two actuated DoFs, the MIMO SM control system of GAREX is able to comfortably facilitate robotic gait rehabilitation training at the speed of 1.5 km/h.

One prerequisite of conducting robotic gait rehabilitation with GAREX is to acquire reference gait trajectories that can be used in the control system. Unactuated GAREX is fully back-drivable and can also be used as a tool for record joint space gait trajectories when subjects are walking with it. Algorithm was also developed to convert the recorded joint space trajectories into periodical gait cycle trajectories that can be directly applied to the MIMO SM controllers.

Two sets of experiments are conducted. The first set was conducted by one healthy subject. The results indicate that the GAREX system is able to guide the subject to walk on the treadmill in the desired gait pattern with a range of joint compliances. The second set of experiments is designed to investigate if the change in joint compliance can further change the level of assistance received by the training subject. A total of 12 healthy subjects participated in this set of experiments. They were asked to rate the levels of assistance received when training with four different knee joint compliance levels. Statistical analysis demonstrates that the system's compliance can be effectively adjusted in order to change the assistance magnitude provided by GAREX

6.1 Introduction

As described in Chapter 2, the impedance related controllers have been commonly adopted in order to implement the AAN concept. Riener et al. [9] developed an impedance controller on Lokomat. A dead band with no control effort was also introduced to allow normal variation around the reference gait trajectories. Active Leg Exoskeleton developed by Banala et al. [67, 95] was implemented with a force-field controller, which created a "virtual tunnel" along the desired foot trajectory in the sagittal plane. The closer the foot is to the desired trajectory; the larger the tangential force will be applied to drive the foot along the desired trajectory. The foot would experience no normal correction force if within the "virtual tunnel". Once it was out of the "virtual tunnel", the normal force would increase exponentially to force the foot back to the desired trajectory.

Due to the compressibility of air, the compliance of a PM can be controlled by regulating its inside pressure. Such a feature has been utilized in PM actuated robotics to control the compliance of the mechanism. It is feasible to have a PM actuated robot track certain reference trajectories while maintaining the mechanical compliance to a certain level. Such a control strategy has similar behavior to impedance controllers [9, 67, 95]. High joint compliance is comparable to having low mechanical impedance and vice versa. The advantage of such control strategies for PM actuated robots is that the system has direct trajectory control; whereas, impedance controller control systems directly manipulate the force that drives the mechanism back to the reference position. However, due to limited sampling times and sensor noise, during actual experimental validations, impedance controllers may become unstable when trying to achieve higher impedances [186]. Choi et al. [152] implemented the compliance control strategy on a PM actuated manipulator. A joint space SM controller was used for trajectory tracking and the compliance was calculated via an open loop conversion from the average PM pressure of the joint based on a dynamic model of the PM. Since there is no control feedback in the developed control system, the joint compliance could only be predicted instead of controlled via feedback. The same control scheme was also adopted by Hussain et al. [22] for the PM actuated gait rehabilitation robot. The magnitudes of the joint space compliances were calculated from models of the PM and the robotic mechanism. It was also not clear how the change in joint space compliance would affect gait rehabilitation trainings.

In the previous chapters of this thesis, the system modelling and sliding mode controllers of the knee joint mechanism have been presented. A logical step forward was to implement the

MIMO SM controller to both of the actuated joints of GAREX to enable task specific gait training at different compliance levels of the actuated joints.

This chapter is organized in the following order. The experiment based reference gait trajectory generation method will be presented first, as it is important to have suitable desired trajectories for the upcoming pilots of the control system. The next section is about the implementation of the MIMO SM controller on GAREX. Lastly the experimental validations of the system with healthy subjects are presented.

6.2 Reference gait trajectory generation

Experiments were conducted to record healthy subjects' hip and knee joint trajectories as potential reference trajectories for upcoming controller system development. To conduct such experiments, a subject was strapped to GAREX, which had been adjusted according to the subject's anthropometric data. It was ensured the hip and knee joints of the subject and the exoskeleton were coaxial and their thigh and shank segments were also aligned, so the angular positions of the exoskeleton were assumed to be equal to the ones of the attached limb.

During the experiments, the subject was asked to walk on the treadmill with the unactuated lower limb exoskeleton attached. When the exoskeleton was unactuated, the connecting cables of both sides of the antagonistic PM actuation system were never in tension; hence, no torque was exerted on the hip or knee joints by the PM actuation systems. The gravity of the lower limb exoskeleton module was compensated by the air spring suspension system of the trunk mechanism as mentioned in Section 3.2. It was aimed to minimize the disturbance of the subject, so he/she could feel like free walking on the treadmill.

The goal of the experiment was to record periodical joint space trajectories by the subject during free walking. In terms of instrumentation, the hip and knee joint encoders were utilized to measure the angular positions throughout the experiments. In order to extract the periodic trajectories over a gait cycle, it was necessary to identify the starting instant of every gait cycle. In biomechanics, the heel strike or initial contact between the foot and the walking surface is usually regarded as the starting point of a gait cycle of the respective lower limb [156]. Hence, it is a common practice to utilize ground reaction force or pressure sensors to the identification. However, due to the time constraint of the research, such sensors were not implemented to the system. Instead, the researcher monitoring the experiment visually identified the instant of heel strikes and toggled a hand-held switch at the starting point of every gait cycle. The system

recorded the digital input from the switch as well as the encoder readings for post-experiment analysis.

The post experiment analysis was conducted through MATLAB. Based on the toggle switch input, the average gait cycle length in seconds could first be calculated. Then, the effective recorded joint space trajectories could be sliced to fit into the gait cycle length. The sliced data are presented as blue scatters in Figure 6-1 to Figure 6-10

A sum of four sinusoidal functions in the format of (6-1) was decided to represent experimental data.

$$\theta_d(t) = \sum_{i=1}^4 a_i \sin(b_i t + c_i) \quad (6-1)$$

where, t is the time elapsed since the start of the gait cycle; a_i , b_i and c_i ($i=1,2,3,4$) are the curve fitting parameters calculated from the experimental data; $\theta_d(t)$ is the function describing the fitted desired joint space trajectory.

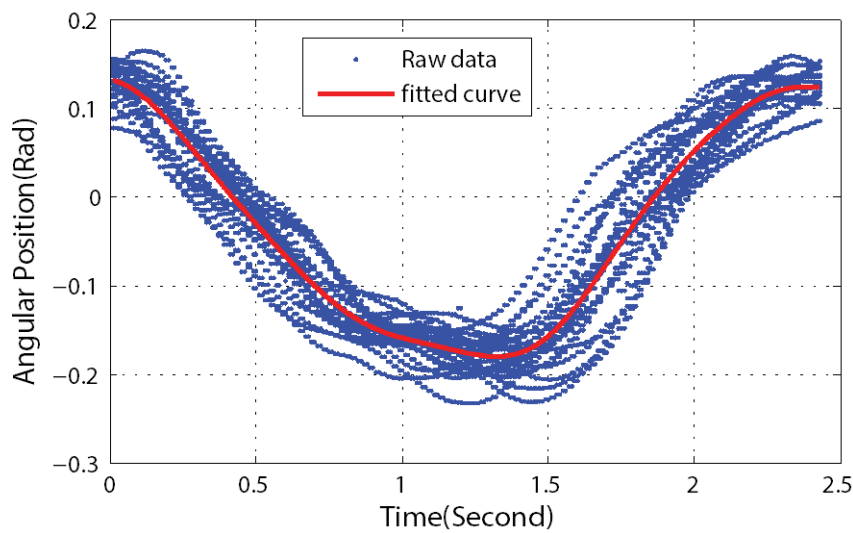
The selected format not only can well fit to the raw data, but also in simple form for real-time application in control systems. The derivatives of the reference trajectory functions are smooth and can be calculated analytically. Parameters of (6-1) were computed from the sliced experimental data using the curve fitting toolbox of MATLAB.

Experiments were conducted to acquire the gait trajectories of three male subjects (Subject_A: 188 cm, 80 kg; Subject_B: 172 cm, 68 kg; Subject_C: male, 185 cm, 100 kg) when walking at various walking speed. The slice raw data of the experiments and the best fitted gait trajectory of a gait cycle are plotted in the following 10 figures. The curve fitting parameters used to describe the generated reference trajectory are listed before each figure. Regression analysis results expressed using coefficients of determination are also listed in the figure captions. Figure 6-1 to Figure 6-7 are for the experimental results of Subject_A. Three experiments were conducted at difference walking speed (1.2 km/h, 1.5 km/h and 1.8 km/h) and the results are plotted for both the hip and knee joints. For comparison reasons, the experimental results of Subject_B and Subject_C walking at 1.5 km/h are also shown in Figure 6-6 to Figure 6-10.

It can be seen from the figures that regression analysis results indicate the developed method was able to generate a reference trajectory to well present the recorded gait patterns. All the

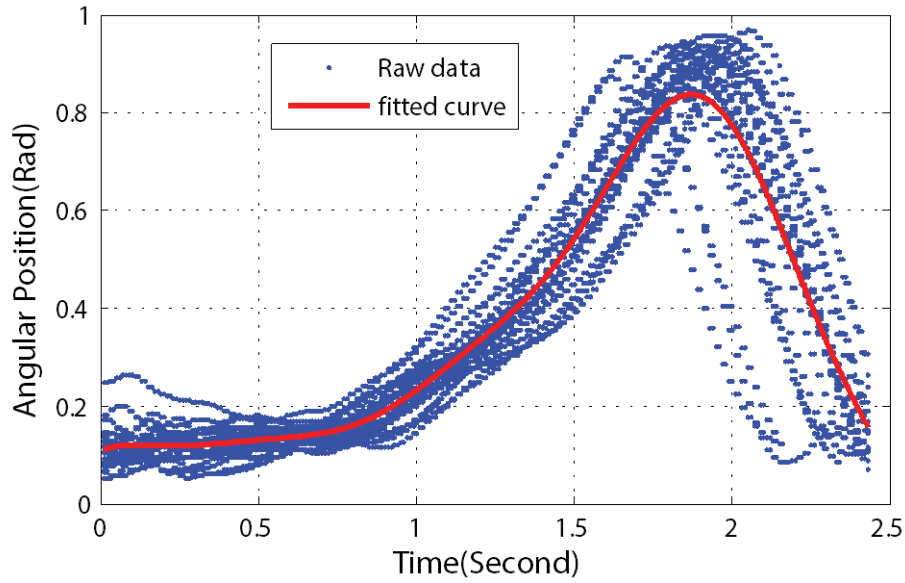
generated reference trajectories were stored for future applications. In the upcoming experiments of the GAREX system, for a specific experimental subject, the researcher could select a reference trajectory recorded by someone who has similar build as the training subject.

Because the starting moments of the gait cycles were identified by the researcher, more uncertainties were introduced than using ground reaction force sensors. Due to such uncertainties, the raw data show some phase differences in the recorded gait cycles shown in all the plots. Such phase differences are regarded as the main affecting factor for the curve fitting quality. For 1.5 km/h walking speed, less phase differences are observed in the knee joint result of Subject_A (Figure 6-4) than Subject_B (Figure 6-8). Hence, the better regression result was obtained from Subject's result.



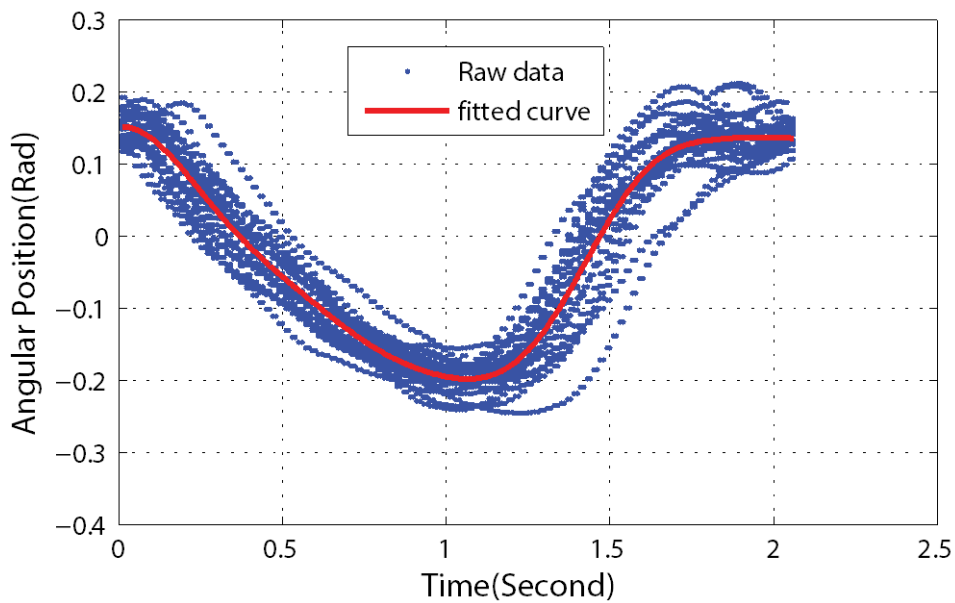
a_1	b_1	c_1	a_2	b_2	c_2
0.155	2.45	1.82	0.0382	0.264	5.06
a_3	b_3	c_3	a_4	b_4	c_4
0.0146	6.43	-5.09	0.00439	10.6	-4.58

Figure 6-1 The record trajectory data and generated desired trajectory curve of Subject_A's hip joint when walking at 1.2 km/h. The period of the average gait cycle (T_{GC}) is 2.43 s. The coefficient of determination (R^2) of the regression curve is 0.92.



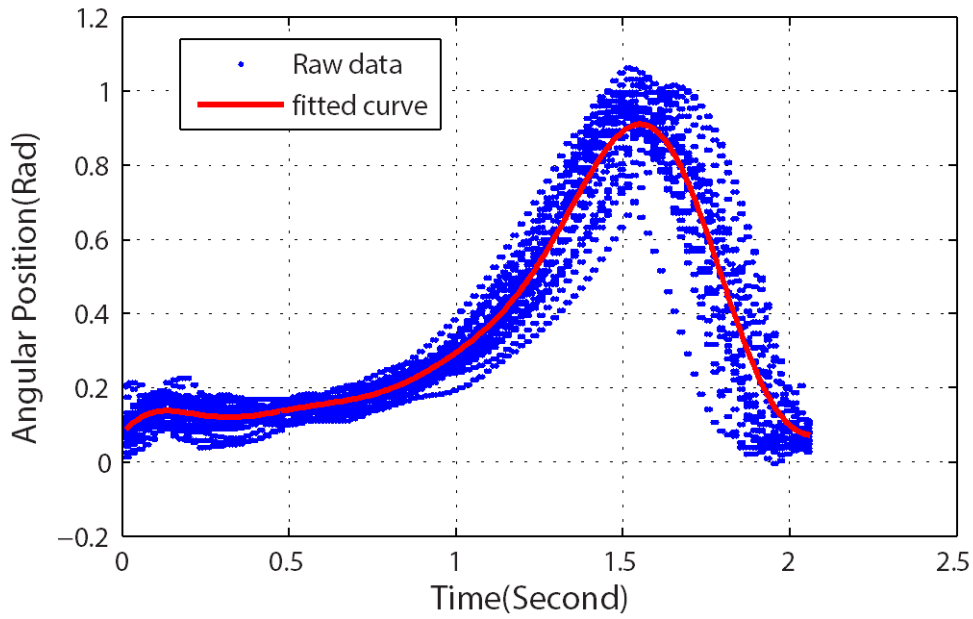
a_1	b_1	c_1	a_2	b_2	c_2
0.744	1.58	-0.473	0.455	2.69	1.99
a_3	b_3	c_3	a_4	b_4	c_4
0.124	7.35	-4.81	0.104	7.91	-2.09

Figure 6-2 The record trajectory data and generated desired trajectory curve of Subject_A's knee joint when walking at 1.2 km/h. $T_{GC} = 2.43$ s. $R^2=0.87$.



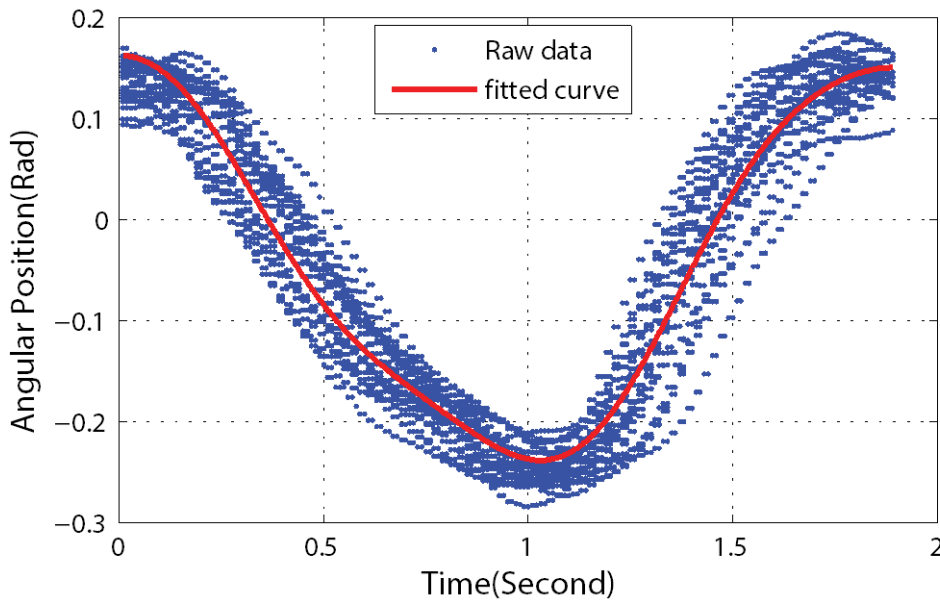
a_1	b_1	c_1	a_2	b_2	c_2
0.0163	3.29	1.50	0.446	0.995	4.28
a_3	b_3	c_3	a_4	b_4	c_4
0.0237	7.89	-4.77	0.00579	12.0	-4.69

Figure 6-3 The record trajectory data and generated desired trajectory curve of Subject_A's hip joint when walking at 1.5 km/h. $T_{GC} = 2.06$ s. $R^2=0.92$.



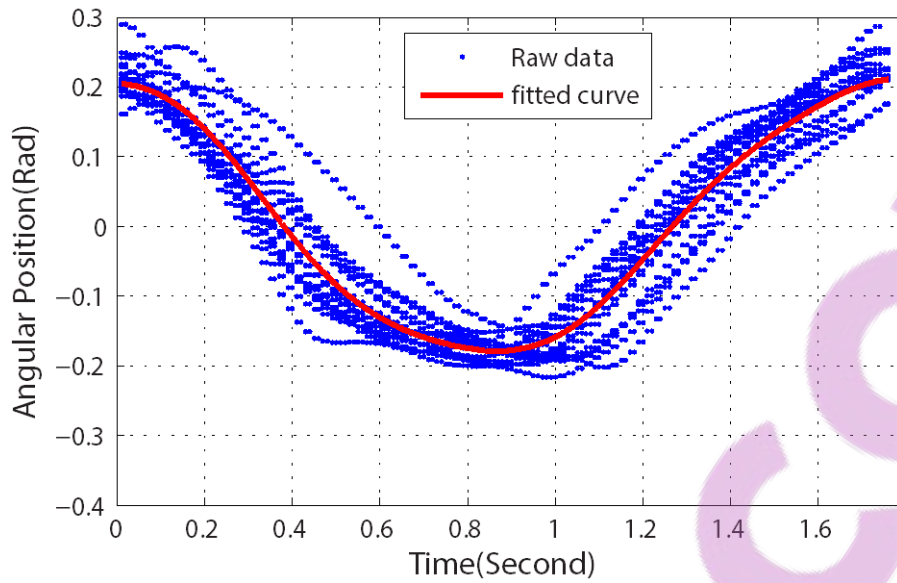
a_1	b_1	c_1	a_2	b_2	c_2
0.57	1.52	-0.448	0.256	4.38	0.995
a_3	b_3	c_3	a_4	b_4	c_4
0.514	9.18	-5.48	0.461	9.45	-2.54

Figure 6-4 The record trajectory data and generated desired trajectory curve of Subject_A's knee joint when walking at 1.5 km/h. $T_{GC} = 2.06$ s. $R^2=0.90$.



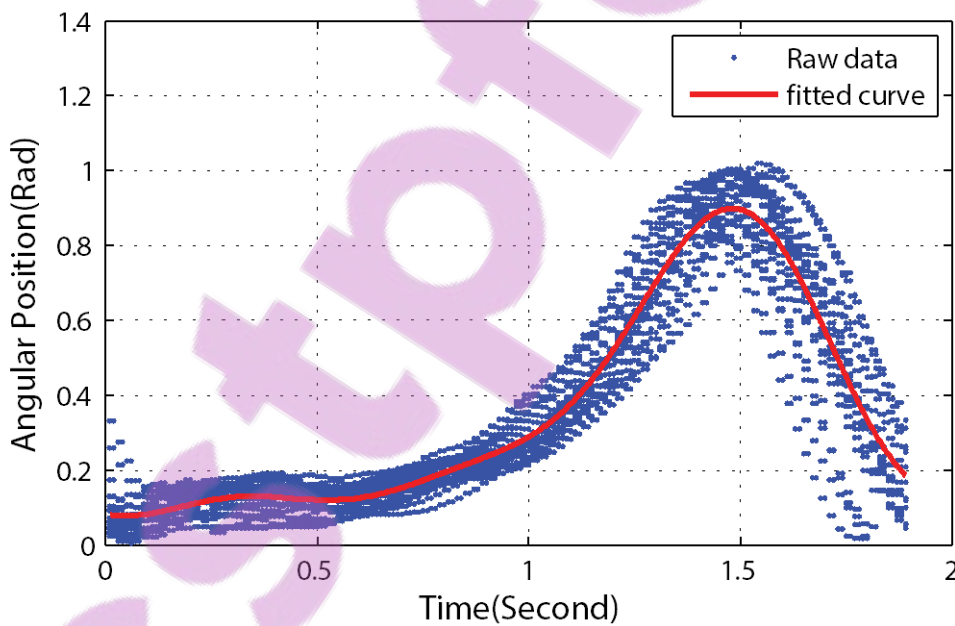
a_1	b_1	c_1	a_2	b_2	c_2
0.57	1.52	-0.448	0.256	4.38	0.995
a_3	b_3	c_3	a_4	b_4	c_4
0.514	9.18	-5.48	0.461	9.45	-2.54

Figure 6-5 The record trajectory data and generated desired trajectory curve of Subject_A's hip joint when walking at 1.8 km/h. $T_{GC} = 1.90$ s. $R^2=0.93$.



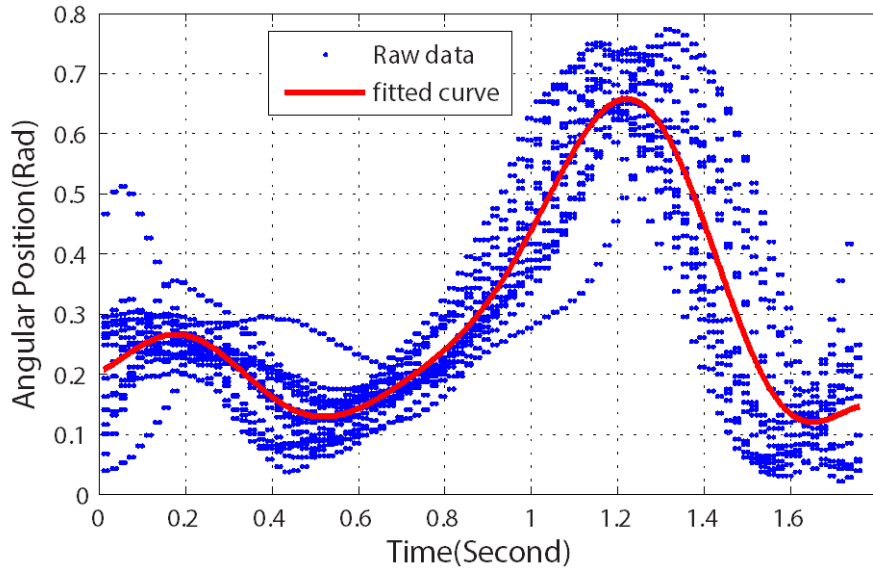
a_1	b_1	c_1	a_2	b_2	c_2
8.19	3.54	1.40	0.0282	5.40	2.82
a_3	b_3	c_3	a_4	b_4	c_4
7.99	3.53	-1.74	0.00933	11.0	-0.392

Figure 6-6 The record trajectory data and generated desired trajectory curve of Subject_B's hip joint when walking at 1.5 km/h. $T_{GC}=1.76$ s. $R^2 = 0.91$.



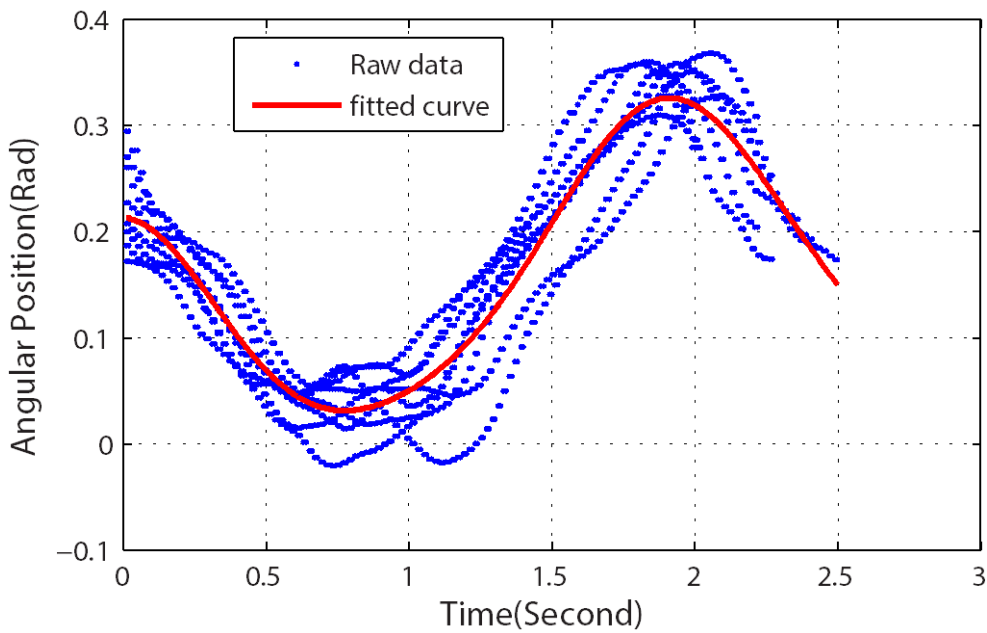
a_1	b_1	c_1	a_2	b_2	c_2
0.655	1.77	-0.193	0.451	3.15	2.42
a_3	b_3	c_3	a_4	b_4	c_4
1.04	8.44	-3.20	0.995	8.60	-0.153

Figure 6-7 The record trajectory data and generated desired trajectory curve of Subject A's hip joint when walking at 1.8 km/h. $T_{GC} = 1.90$ s. $R^2=0.91$.



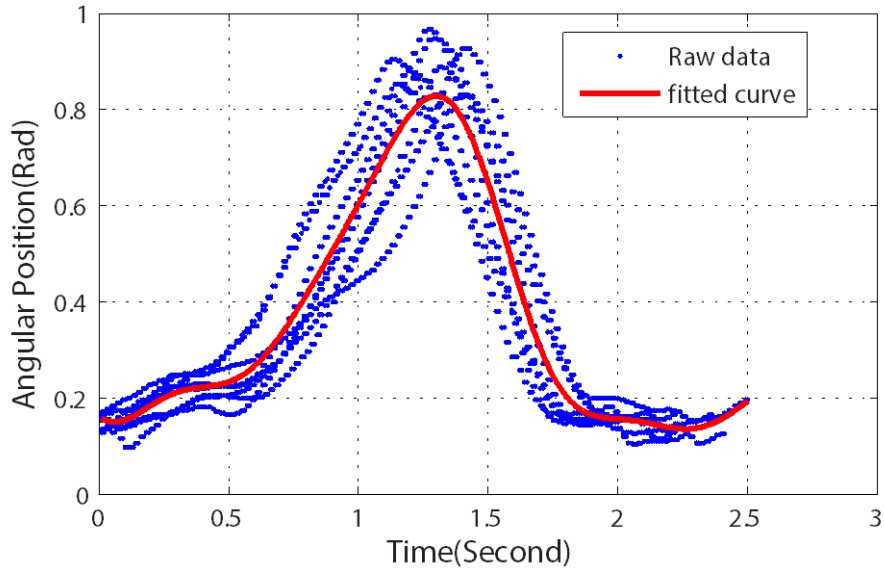
a_1	b_1	c_1	a_2	b_2	c_2
27.7	2.11	0.809	18.28	9.29	-1.99
a_3	b_3	c_3	a_4	b_4	c_4
27.57	2.13	3.94	18.23	9.3	1.15

Figure 6-8 The record trajectory data and generated desired trajectory curve of Subject_B's knee joint when walking at 1.5 km/h. $T_{GC}=1.76$ s. $R^2=0.80$.



a_1	b_1	c_1	a_2	b_2	c_2
0.223	0.947	0.0605	0.422	2.80	0.3539
a_3	b_3	c_3	a_4	b_4	c_4
0.457	2.91	3.05	0.0126	6.58	1.71

Figure 6-9 The record trajectory data and generated desired trajectory curve of Subject_C's hip joint when walking at 1.5 km/h. $T_{GC}=2.5$ s; $R^2=0.89$.



a_1	b_1	c_1	a_2	b_2	c_2
0.457	0.584	0.971	0.0846	6.90	-1.15
a_3	b_3	c_3	a_4	b_4	c_4
0.291	3.48	-2.72	0.0245	10.7	-0.896

Figure 6-10 The record trajectory data and generated desired trajectory curve of Subject_C's knee joint when walking at 1.5 km/h. $T_{GC}=2.5$ s. $R^2=0.90$.

6.3 MIMO Sliding mode controllers for GAREX

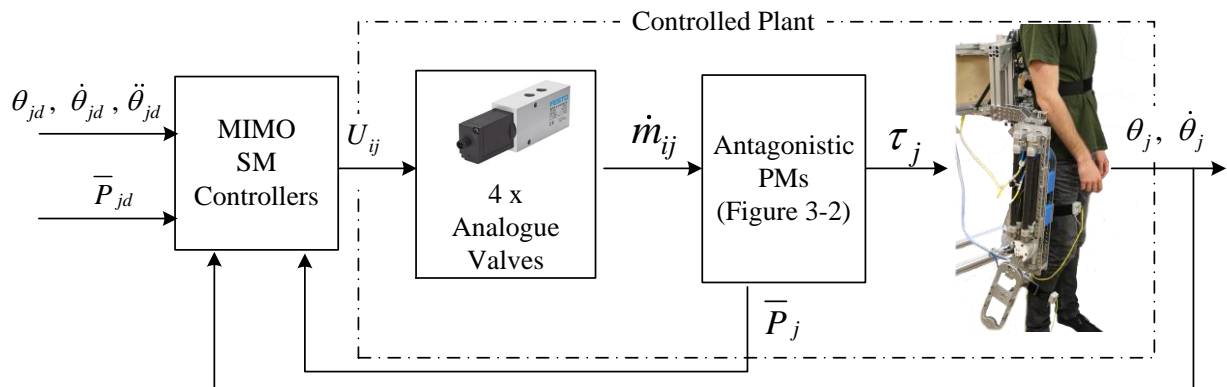


Figure 6-11 The control system block diagram of GAREX. In the figure $i=F,E$ and $j=h,k$; U_{ij} is the voltage fed into the corresponding analogue valve; \dot{m}_{ij} is the pneumatic mass flow rate to the corresponding PMs; \bar{P}_{jd} is the average pressure of the antagonistic PMs of the corresponding joint. The subscript d indicates desired value of a property.

Block diagram of the MIMO SM control system of GAREX is shown in Figure 6-11. This control system needs to control the trajectory and compliance of GAREX's hip and knee joints

simultaneously. In terms of modelling, the valves and PM actuation system of the two joints can be modelled separately, in the same way as detailed in sections 5.2.1 to 5.2.3. For the load dynamics model of the mechanism, the exoskeleton has to be analyzed as a whole. The low limb exoskeleton can be treated as a serial robot and the well-established Lagrangian Formulation was adopted to calculate the actuated joint torque requirement from the kinematics of the exoskeleton as:

$$\mathbf{M}\ddot{\underline{\theta}} + \underline{V} + \underline{G} = \underline{\tau} \quad (6-2)$$

$$\text{or } \begin{bmatrix} M_{11} & M_{12} \\ M_{21} & M_{22} \end{bmatrix} \begin{bmatrix} \ddot{\theta}_1 \\ \ddot{\theta}_2 \end{bmatrix} + \begin{bmatrix} V_1 \\ V_2 \end{bmatrix} + \begin{bmatrix} G_1 \\ G_2 \end{bmatrix} = \begin{bmatrix} \tau_1 \\ \tau_2 \end{bmatrix} \quad (6-3)$$

The first term in (6-3) is the inertial component of the joint torques. The second term \underline{V} represents the Coriolis and centrifugal forces, which is followed by the gravitational component. The Lagrangian Formulation was adopted to calculate the symbolic representations of \mathbf{M} , \underline{V} and \underline{G} at any given instant of the exoskeleton operation.

Figure 6-12 was created to visualize the modelling representation. Two coordinate systems have been created. One is a base coordinate system, whose z-axis is co-axial with the hip joint of the exoskeleton, with its x-axis pointing horizontally in the direction a training subject will be facing and y-axis pointing up vertically. The other coordinate system's z-axis is co-axial with the knee joint with x-axis long the thigh segment. The centre of mass of the thigh and shank segments are also illustrated in the figure using the “” symbol. Equation (6-4) is the inertia matrix of segment i ($i = 1$ for thigh segment; $i = 2$ for shank segment) about its centre of mass. iI_i can be expressed with respect to the base coordinate system by the transformation in (6-5).

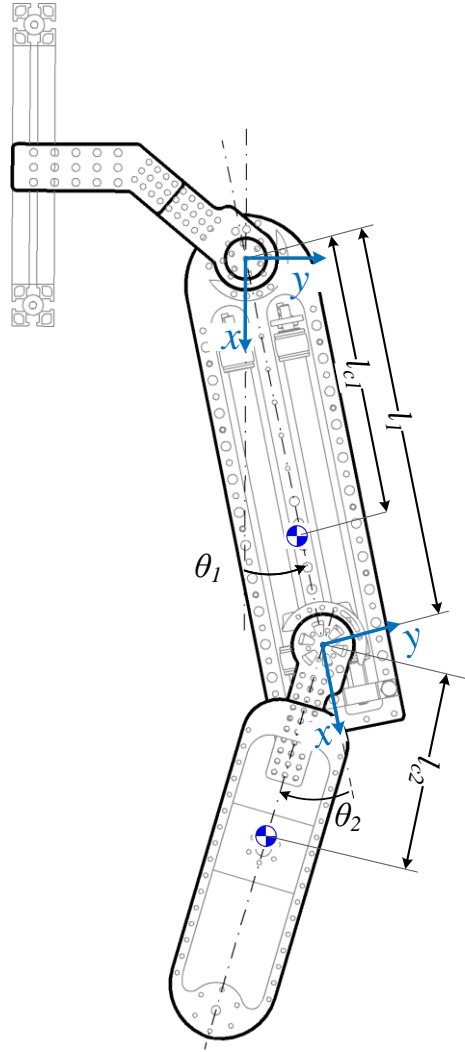


Figure 6-12 Illustrated side view drawing of the exoskeleton module for dynamics analysis of the mechanism. The z-axes of the two coordinate systems are both pointing out of the page.

$${}^i\mathbf{I}_i = \begin{bmatrix} I_{ix} & 0 & 0 \\ 0 & I_{iy} & 0 \\ 0 & 0 & I_{iz} \end{bmatrix} \quad (6-4)$$

$$\mathbf{I}_i = {}^0R_i {}^iI_i ({}^0R_i)^T \quad (6-5)$$

where 0R_i is the rotation matrix from COM of segment i to the base frame, which can be expressed as:

$${}^0R_1 = \begin{bmatrix} \cos \theta_1 & -\sin \theta_1 & 0 \\ \sin \theta_1 & \cos \theta_1 & 0 \\ 0 & 0 & 1 \end{bmatrix} \quad (6-6)$$

$${}^0R_2 = \begin{bmatrix} \cos(\theta_1 + \theta_2) & -\sin(\theta_1 + \theta_2) & 0 \\ \sin(\theta_1 + \theta_2) & \cos(\theta_1 + \theta_2) & 0 \\ 0 & 0 & 1 \end{bmatrix} \quad (6-7)$$

The kinetic energy of the entire exoskeleton system can thus be expressed as[187]:

$$K_e = \frac{1}{2} \dot{\underline{\theta}}^T \mathbf{M} \dot{\underline{\theta}} \quad (6-8)$$

where \mathbf{M} is an inertia matrix defined as:

$$\mathbf{M} = \sum_{i=1}^2 (\mathbf{J}_{vi}^T m_i \mathbf{J}_{vi} + \mathbf{J}_{\omega i}^T \mathbf{I}_i \mathbf{J}_{\omega i}) \quad (6-9)$$

where m_i is the mass of segment i ; J_{vi} and $J_{\omega i}$ are the Jacobian sub-matrices of segments i which can be calculated as:

$$\underline{J}_{v1}^1 = \underline{z} \times \underline{{}^1P_{c1}}, \quad \underline{J}_{v1}^2 = [0 \quad 0 \quad 0]^T \quad (6-10)$$

$$\underline{J}_{v2}^1 = \underline{z} \times \underline{{}^1P_{c2}}, \quad \underline{J}_{v2}^2 = \underline{z} \times \underline{{}^2P_{c2}} \quad (6-11)$$

$$\mathbf{J}_{vi} = \begin{bmatrix} \underline{J}_{vi}^1 & \underline{J}_{vi}^2 \end{bmatrix} \text{ with} \quad (6-12)$$

$$\mathbf{J}_{\omega 1} = \begin{bmatrix} 0 & 0 \\ 0 & 0 \\ 1 & 0 \end{bmatrix}; \quad \mathbf{J}_{\omega 2} = \begin{bmatrix} 0 & 0 \\ 0 & 0 \\ 1 & 1 \end{bmatrix}; \quad (6-13)$$

In (6-10) and (6-11), $\underline{{}^jP_{ci}}$ is a position vector of the centre of mass of segment relative to the coordinate system (for the base coordinate system and for the other).

$$\underline{{}^1P_{c1}} = [l_{c1} \cos \theta_1 \quad l_{c1} \sin \theta_1 \quad 0]^T \quad (6-14)$$

$$\underline{{}^1P_{c2}} = [l_{c2} \cos(\theta_1 + \theta_2) + l_1 \cos \theta_1 \quad l_{c2} \sin(\theta_1 + \theta_2) + l_1 \sin \theta_1 \quad 0]^T \quad (6-15)$$

$$\underline{{}^2P_{c2}} = \begin{bmatrix} l_{c2} \cos(\theta_1 + \theta_2) & l_{c2} \sin(\theta_1 + \theta_2) & 0 \end{bmatrix}^T \quad (6-16)$$

The potential energy stored in the exoskeleton with respect to the base coordinate system can be expressed as (6-17) with the vector of gravity coefficient $\underline{g} = [0 \quad g_c \quad 0]$.

$$U = -\sum_{i=1}^2 m_i \underline{g}^T \underline{{}^1P_{ci}} \quad (6-17)$$

The Lagrangian function of the mechanism is then defined in (6-18) and the actuation torques of the hip and knee joint can be calculation in (6-19), which can be re-arranged into matrix representation expressed in (6-3).

$$L = K_e - U \quad (6-18)$$

$$\frac{d}{dt} \left(\frac{\partial L}{\partial \dot{\theta}_i} \right) - \frac{\partial L}{\partial \theta_i} = \tau_i \quad \text{for } i = 1, 2 \quad (6-19)$$

The V and G terms of (6-3) can further be calculated as:

$$V_i = \sum_{j=1}^2 \sum_{k=1}^2 \left(\frac{\partial M_{ij}}{\partial \theta_k} - \frac{1}{2} \frac{\partial M_{jk}}{\partial \theta_i} \right) \dot{\theta}_j \dot{\theta}_k \quad \text{for } i = 1, 2 \quad (6-20)$$

$$G_i = -\sum_{j=1}^2 m_j \underline{g}^T \underline{J}_{vj}^i \quad \text{for } i = 1, 2 \quad (6-21)$$

The symbolic representations of the parameters in (6-3) are listed as below:

$$M_{11} = m_2 l_1^2 + 2m_2 \cos \theta_2 l_1 l_{c2} + m_1 l_{c1}^2 + m_2 l_{c2}^2 + I_{1z} + I_{2z} \quad (6-22)$$

$$M_{12} = I_{2z} + l_{c2} m_2 (l_{c2} + l_1 \cos \theta_2) \quad (6-23)$$

$$M_{21} = I_{2z} + l_c 2m_2 (l_c 2 + l_1 \cos(\theta_2)) \quad (6-24)$$

$$M_{22} = m_2 l_{c2}^2 + I_{2z} \quad (6-25)$$

$$V_1 = -l_1 l_{c2} m_2 \dot{\theta}_2^2 \sin \theta_2 - 2l_1 l_{c2} m_2 \dot{\theta}_1 \dot{\theta}_2 \sin \theta_2 \quad (6-26)$$

$$V_2 = l_1 l_{c2} m_2 \dot{\theta}_1^2 \sin\theta_2 \quad (6-27)$$

$$G_1 = (g_c m_2 (l_{c2} \cos(\theta_1 + \theta_2) + l_1 \cos\theta_1) + g_c l_{c1} m_1 \cos\theta_1) \quad (6-28)$$

$$G_2 = (g_c l_{c2} m_2 \cos(\theta_1 + \theta_2)) \quad (6-29)$$

It is also worth to note that the variable definitions used for the exoskeleton design and the rest of the thesis (shown in Figure 3-2) are different from the ones used in the dynamics modelling (shown in Figure 6-12). The following conversions are adopted for ease of further controller implementation:

$$\begin{cases} \theta_1 = \theta_h - 90^\circ \\ \theta_2 = -\theta_k \end{cases} ; \begin{cases} \dot{\theta}_1 = \dot{\theta}_h \\ \dot{\theta}_2 = -\dot{\theta}_k \end{cases} ; \begin{cases} \ddot{\theta}_1 = \ddot{\theta}_h \\ \ddot{\theta}_2 = -\ddot{\theta}_k \end{cases} ; \begin{cases} \tau_1 = \tau_h \\ \tau_2 = -\tau_k \end{cases} \quad (6-30)$$

Substitute (6-30) into (6-3), the model can then be expressed in (6-31).

$$\begin{bmatrix} M_{11} & -M_{12} \\ -M_{21} & M_{22} \end{bmatrix} \begin{bmatrix} \ddot{\theta}_h \\ \ddot{\theta}_k \end{bmatrix} + \begin{bmatrix} V_1 \\ -V_2 \end{bmatrix} + \begin{bmatrix} G_1 \\ -G_2 \end{bmatrix} = \begin{bmatrix} \tau_h \\ \tau_k \end{bmatrix} \quad (6-31)$$

For the controller implementation, two sets of state-space model representation of actuated joints were also constructed. The state-space variable (\underline{x}_j) control input (\underline{A}_j) and output (\underline{y}_j), vectors are calculated as:

$$\underline{x}_j = [\theta_j \quad \dot{\theta}_j \quad P_{Fj} \quad P_{Ej}]^T \quad (6-32)$$

$$\underline{A}_j = [A_{Fj} \quad A_{Ej}]^T \quad (6-33)$$

$$\underline{y}_j = [\theta_j \quad (P_{Fj} + P_{Ej})/2]^T \quad (6-34)$$

By re-arranging (6-31), the acceleration vector could be explicitly expressed for the development of the MIMO SM controllers, one for each of the actuated joints. The rest of the control development procedures were identical the MIMO SM controller for the knee joint mechanism elaborated in Section 5.4.1.

6.4 From average antagonistic PM pressure to joint compliance

Since GAREX does not have mechanism to feedback the real-time joint compliance or stiffness, joint compliance can only be predicted using the PM's dynamic force model. The joint stiffness S is calculated as:

$$\tau_j = (F_{Ej} - F_{Fj})r_j \quad \text{with } (i = F, E) \quad \text{and } (j = h, k) \quad (6-35)$$

$$S = \frac{\partial \tau}{\partial \theta} \quad (6-36)$$

When the MIMO SM controller is operating, the pressures of the flexor and extensor PM can be expressed as:

$$\begin{cases} P_F = P_{avg} + \Delta P_F \\ P_E = P_{avg} - \Delta P_E \end{cases} \quad (6-37)$$

here P_{avg} is the desired average antagonistic PM pressure; ΔP_F and ΔP_E are the difference between the actual pressures and the desired average antagonistic PM pressure of the flexor and extensor PMs. By substituting equations (4-2), (6-35) and (6-37) into (6-36), the joint compliance can be calculated as the reciprocal of the joint stiffness as:

$$\mathbb{C} = \frac{1}{S} = \frac{1}{2r^2 [2k_0 + 2k_1 P_{avg} + k_1 (\Delta P_F - \Delta P_E)]} \quad (6-38)$$

When the MIMO SM controller can perfectly track the desired average antagonistic PM pressure ($\Delta P_F = \Delta P_E$), the joint stiffness is linearly dependent on the set average pressure. With both k_0 and k_1 being positive constants, the compliance \mathbb{C}_j decreases as P_{avg} increases.

It is also noteworthy that the joint compliance calculated is purely based on the dynamic force model proposed in [43]. The model has been deemed to be inaccurate and subject to uncertainties, due to PM's highly nonlinear dynamics. If another modelling approach were adopted, the stiffness versus pressure and angular position relation could be different. For example, static force model by Chou and Hannaford [28] expresses the PM contractile force as:

$$F_{ij} = \left(\frac{3(l_0 - x_{ij})^2 - b^2}{4\pi n^2} \right) P_{ij} \quad (6-39)$$

where l_0 is the original length of the PM; b and n are constants related to the geometry of the PM. Based on this model, the desired compliance, when the average pressure can be tracked as expected ($\Delta P_F = \Delta P_E = \Delta P$) can be calculated as:

$$\begin{aligned} \mathbb{C} &= \frac{\pi n^2}{3r^2 \left[(-2l_0 + r(\theta_{E0} - \theta_{F0}))P_{avg} - r(\theta_{E0} + \theta_{F0})\Delta P + 2r\theta\Delta P \right]} \\ &= \frac{\pi n^2}{3r^2 \left[(-2l_0 + r(\theta_{E0} - \theta_{F0}))P_{avg} + (x_F - x_E)\Delta P \right]} \end{aligned} \quad (6-40)$$

It can be observed from (6-40) that the joint compliance is dependent on the joint position, average PM pressure and the pressure difference between the flexion and extension PMs. The differences in the two compliance expressions above indicates that joint compliance cannot be precisely derived from the PM models. There is also no mechanism in GAREX to measure the real-time compliance/stiffness magnitude and feedback it for control implementation. Therefore, it would be valuable to conduct experiment to prove that the proposed MIMO SM algorithm with close-loop average PM pressure control can effectively vary the joint compliance.

6.5 Experimental validation of the MIMO SM control system of GAREX

Two sets of experiments were designed to validate the system performance of GAREX. The first one is related to determining the capability of performing automating treadmill based gait rehabilitation training. The second aims to validate whether the proposed control strategy is able to adjust the assistance level during rehabilitation training. Healthy subjects with no current lower limb injury were recruited to conduct these experiments. Ethical approval for the experiments was granted by the University of Auckland Human Participants Ethics Committee (Ref. 014970). Written informed consent had been obtained from all the participants prior to conducting any experiments.

6.5.1 Robotic Gait Training Pilot

One healthy subject (male, 172 cm, and 68 kg) participated in the experiment that validated the robotic system's capability to provide gait rehabilitation training. During the preparation phase of the experiment, the subject was instructed to stand on the treadmill and a researcher measured the dimension of his lower limb and adjusted the exoskeleton according to the subject's anthropometric data. The researcher then securely strapped the subject's trunk and right leg to

the back support and exoskeleton respectively. It was made sure that the subject's hip and knee joints are coaxial with the respective joints of the exoskeleton.

During the experiment, programmed with the MIMO SM control system, GAREX guided the subject to walk in a predefined gait trajectory on the treadmill with a speed of 1.5 km/h. To conduct the experiment, the subject was asked to relax the leg strapped to the exoskeleton and let GAREX to guide its movement. The subject also adapted unactuated leg's movements to achieve stable walking on the treadmill. Four 2-minute experiments were conducted and in between two experiments there was a break of 2 minutes. In each experiment, the average PM pressures of the hip and knee joint were controlled to the same magnitude. The desired average pressures were in turn 160, 240, 320 and 400 KPa for the four experiments.

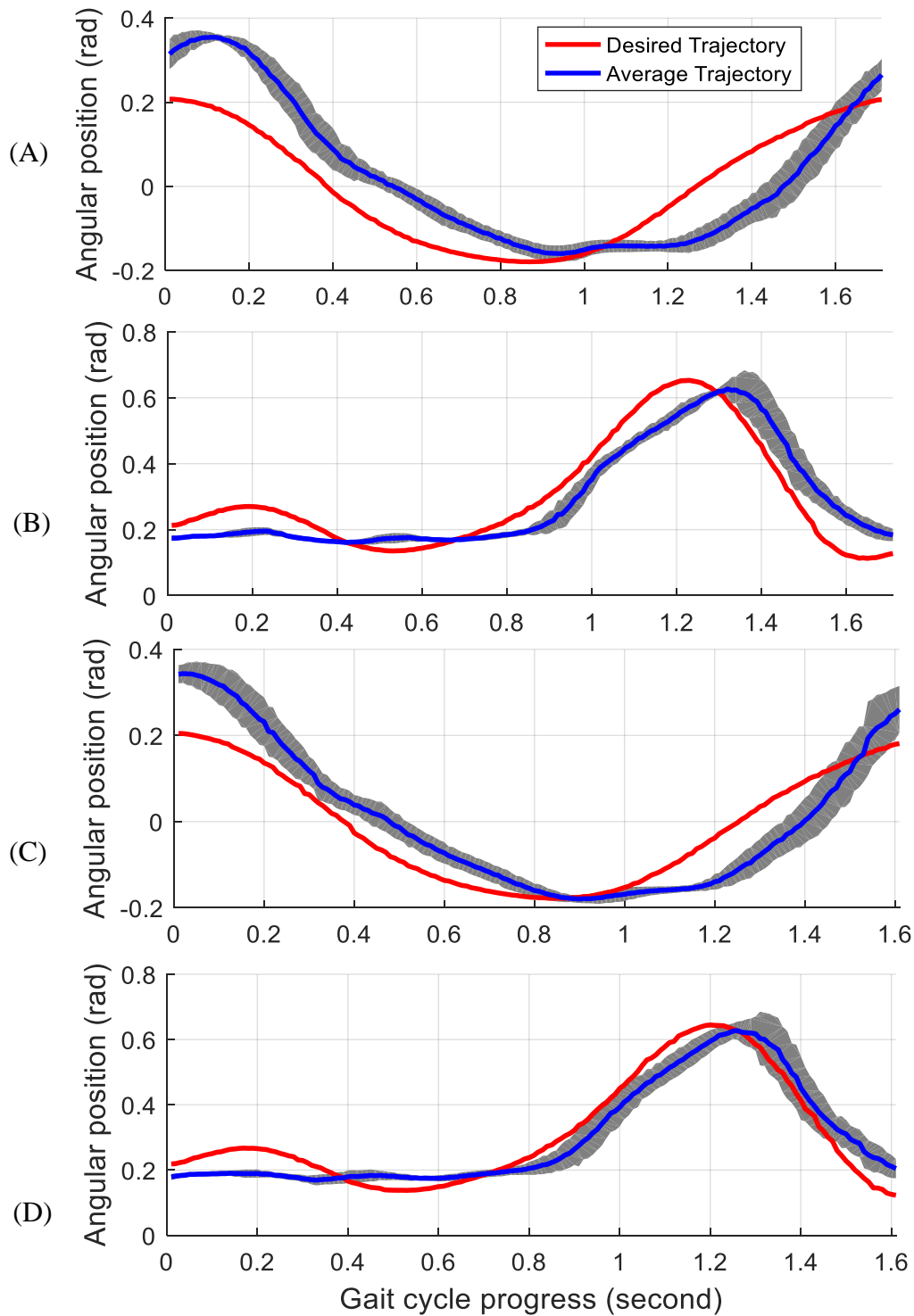


Figure 6-13 The comparison between the desired and actual gait trajectories of the two actuated joints during the validation experiments. The trajectories have been normalized to one gait cycle. The red lines are the predefined reference gait trajectory. The blue lines represent the average gait trajectories over the experimental period. The shaded area stands for the standard deviations of the average trajectories over the recorded gait cycles. (A): the hip joint trajectories with average PM pressure of the joint

regulated to 160 KPa. (B): the knee joint trajectories with average PM pressure of the joint regulated to 160 KPa. (C) and (D): the hip and joint trajectories when the average PM pressure of both joints were regulated to 240 KPa.

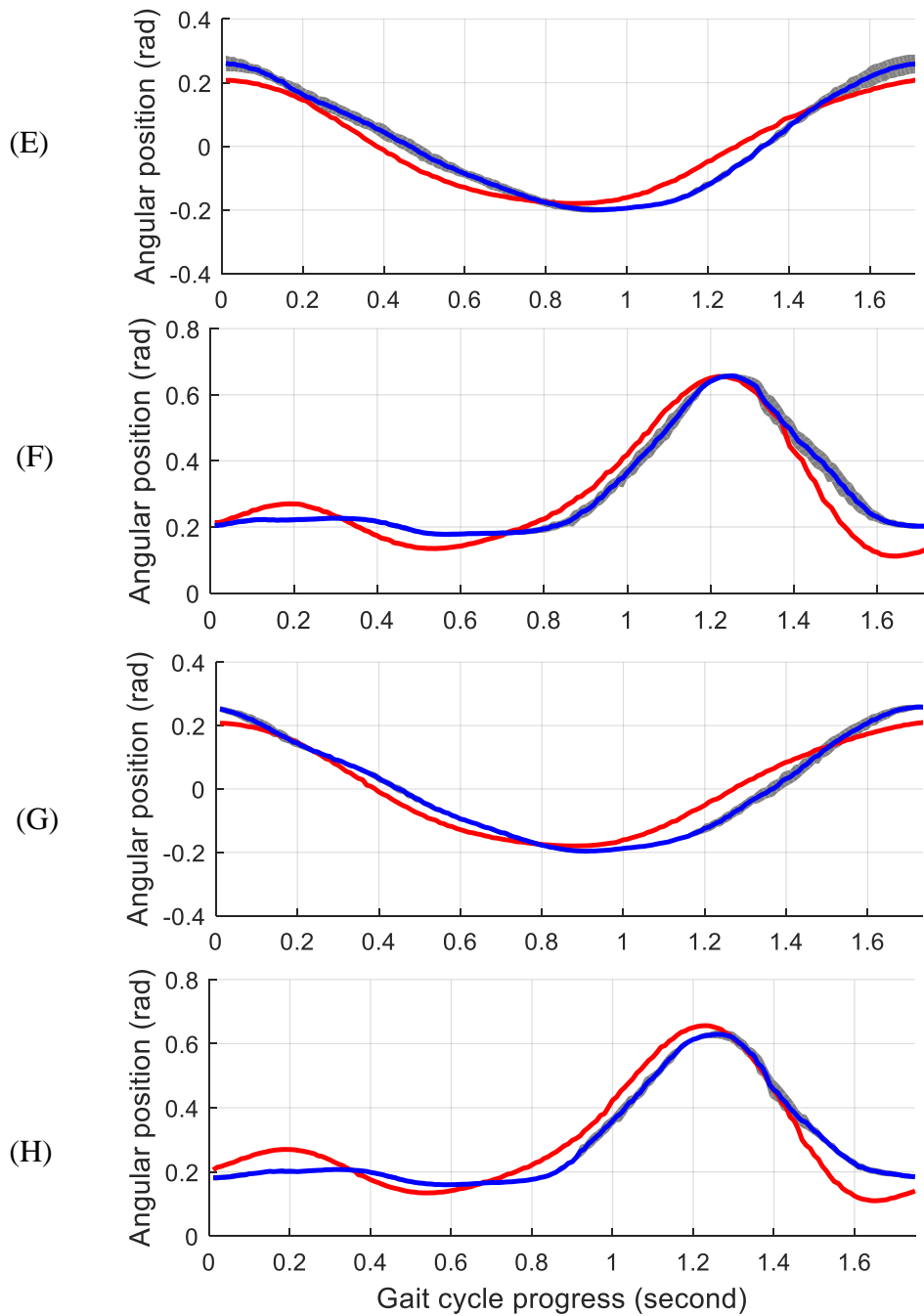


Figure 6-14 the same type of plots as in **Figure 6-13. (E) and (F): the hip and joint trajectories when the average PM pressure of both joints were regulated to 320 KPa. (G) and (H): the hip and joint trajectories when the average PM pressure of both joints were regulated to 400 KPa.**

The subject was able to walk on the treadmill comfortably with the guidance from GAREX in all four experimental conditions. The subject’s gait trajectories of the two actuated joints are presented in Figure 6-13 and Figure 6-14. The plots in red represent the desired joint space gait trajectory and the average gait trajectories over all the recorded gait cycles are plotted in blue. The standard deviations of the average trajectories are illustrated as the shaded areas. It can be observed from the figure that the controller was capable of tracking the desired gait trajectory in order to facilitate gait rehabilitation in all the experimental conditions. The trajectory tracking performance was evaluated with the root-mean-square error between the desired and actual trajectories and the results are listed in Table 6-1. It is obvious from the table that the RMS errors had a trend of decrease as the controlled average PM pressure increased. This is an indication that the exoskeleton became less compliant and gave the subject less freedom around the desired trajectory. To further validate whether the proposed controller is capable of changing the compliance of the exoskeleton, the second set of experiments were conducted.

It can also be observed from the table that at lower average antagonistic PM pressure, the hip joint has higher trajectory tracking error compared to the knee joint. However, at higher average antagonistic PM pressures the hip joint could better track its reference trajectory. Because of high inertia, more torque required to guide the hip joint to track desired trajectory. Therefore, at lower average pressure or higher joint compliance, the system could not provide sufficient torque for the hip joint. Compared to hip joint, the reference trajectory of the knee joint has a larger magnitude and hence it is generally more challenging for the controller to track for the controller.

Table 6-1 The RMS errors (rad) of both actuated joints under all four experimental conditions

	160KPa	240KPa	320KPa	400KPa
Knee	0.078	0.059	0.056	0.053
Hip	0.106	0.083	0.046	0.042

6.5.2 Validation of controllable compliance

The experiments were designed to validate that the developed MIMO SM controller is capable of tracking predefined gait trajectory and simultaneously adjusting the actuation compliance so as to modify the assistance provided. A total of 12 healthy subjects with no leg injuries participated in this set of experiments.

Before each subject started the experiment, the concept of compliance had been explained. Being more compliant means the subject has more freedom and less guidance from the exoskeleton during robotic training and vice versa. After the briefing, the experiment preparation was conducted and the procedure was identical to the previous experiment.

During a trial, a subject would conduct four experiments. Each of the experiment would last approximated 3 minutes. In between the two experiments there was a break of 2 minutes. Similar to the experiment described in Section 6.5.1, the subject was assisted by GAREX to walk on the treadmill at the speed of 1.5 km/h. The average PM pressures of the hip and knee joints were both controlled at 160, 240, 320 and 400 KPa during the four experiments.

Table 6-2 Compliance scores given by the 12 subjects for the experiments with four discrete average PM pressures.

	160 KPa	240 KPa	320 KPa	400 KPa
S1	1	2	3	4
S2	1	2	3	4
S3	1	2	4	3
S4	1	2	3	4
S5	1	4	3	2
S6	1	2	3	4
S7	1	3	2	4
S8	2	1	4	3
S9	1	2	3	4
S10	1	3	2	4
S11	1	3	2	4
S12	1	2	4	3

Each subject experienced the four experiments in a randomized order and he/she was not informed the controlled average pressure or the actuation compliance level of each experiment. Hence, the subject was asked to relax and let the exoskeleton to guide the leg movement for the first half of an experiment. In the second half, he/she was asked to actively walk with the assistance from the exoskeleton and/or try to walk in his/her preferred gait pattern disregarding the assistance from the exoskeleton, so that the subject would have the impression of the compliance of the exoskeleton. After the completing the first two and three trials, the subject would be asked to rank the compliance levels of the experiments he/she had completed. After finishing all four trials, the subject would be able to rank the compliance level each experiment with discrete score of 1, 2, 3 or 4, with 1 being most compliant and 4 being least compliant.

No matter what result was given after the four experiments, the researcher would ask the subject if he/she wished to repeat any of the experiments in order to help him/her refresh memory or eliminate any uncertainties. The subject could request up to two experiments to be repeated.

A total of 12 (10 males and 2 females) subjects of ages between 23 and 31 participated in the experiments. Heights of the subjects range from 164 to 188 cm and the weights range from 49 to 100 kg. Valid results were collected from all of the participants. Detailed compliant scores given by all the subjects for the four experimental conditions are listed in Table 6-2. For each controlled average pressure, the mean and variance of the compliance scores rated by the participants were calculated. Such results are summarized in the first two rows of Table 6-3. One-way Analysis of Variance (ANOVA) analysis was thought to be suitable for examining if there is any statistical difference between the means compliance scores under different experimental conditions.

Table 6-3 Statistical analysis result of the experiments on compliance. Top half of the table is showing the means and variances of the rated compliance levels for all the controlled average PM pressures. Both the original and logarithm transformed means and variances are listed. The bottom half of the table is illustrating all the possible between groups p-values of the Tukey’s test.

	Controlled Average PM Pressures			
	160KPa	240KPa	320KPa	400KPa
Mean	1.083	2.333	3.000	3.583
Variance	0.083	0.606	0.545	0.447
Mean Transformed	0.025	0.320	0.464	0.571
Variance Transformed	0.008	0.016	0.013	0.003
160 KPa		0.000	0.000	0.000
240 KPa			0.005	0.000
320 KPa				0.056
400 KPa				

To have a valid one-way ANOVA analysis, it was assumed that all the groups have equal variance has to be satisfied. Hence, Levene test was conducted to investigate the equality of variance of the experimental data. The test’s *p-value* of 0.032 rejected the null hypothesis that all four groups have equal variance. A commonly used logarithm transformation of the original experimental data was performed and the means and variances of the transformed data are listed in the third and fourth rows of Table 6-3. The Levene test of transformed results gave a *p-value* of 0.462, which means the assumption of equal variance is not violated.

The one-way ANOVA analysis was then performed on the on the transformed data. A *p-value* of 0.000 suggests a very strong evidence to reject the null hypothesis that all the samples have equal means. Multiple comparisons via Tukey’s test were also conducted to investigate whether there are statistical differences between all the combinations of two different groups. The analytical results again expressed by *p-values* are exhaustively listed in the second half of Table 6-3. As seen from the table, there are highly significant difference (*p-values* being 0.000) in means between groups whose average pressure levels are not adjacent. For adjacent groups, there is a very strong evidence for the difference in means between 160 and 240 KPa groups.

There is strong evidence for the difference in means between 240 and 400 KPa groups. However, there is not significant statistical difference in means between the 320 and 400 KPa groups.

The above statistical analysis further approves that there is negative correlation between the controlled average pressure of the PM actuation system and the exoskeleton compliance. However, the correlation is not linear. For the same difference interval in average pressure, the change in compliance is more significant when the average pressure is lower. Understanding such trend is important since further development of the GAREX system may require the automatic adaption of the compliance level based on the patient's performance or ability assessment during rehabilitation training.

6.6 Discussion and conclusions

Based on the model of the entire exoskeleton system, a MIMO SM controller was thus developed and tuned to deliver robust control performance. Currently, GAREX can comfortably guide the healthy subject to complete treadmill based gait experiments at a speed of 1.5 km/h, which similar the slower speeds have been adopted for clinical trials on a motor driven gait rehabilitation exoskeleton [188]. At the moment, the controlled bandwidth is limited by the pneumatic supply system. To further increase the bandwidth the following changes could be made: (1) increasing current pneumatic supply pressure (6 bar); (2) using larger diameter tubes and valves; (3) optimizing the exoskeleton design to further reduce its weight.

The means of using the average pressure to represent actuation compliance is not novel [22, 152]. Due to the system simplification with the pressure regulating valves, the joint space trajectory and average PM pressure controller were separated and the average PM pressure was adjusted through an open loop controller. The actuation compliance was again calculated from the average PM pressure using the force dynamics model of the PM. In literature, there were also no dedicated experiments to investigate if such compliance adjusting approach could vary the extent of guidance during robotic gait rehabilitation.

GAREX's MIMO control system includes the PM pressures as state variables and allows more direct manipulation of the average PM pressure compared to [22, 152]. A new experimental approach was adopted to validate the system capability on adjusting the compliance from participants' perception. One-way ANOVA statistical analysis conducted after the experiment indicated the control system is able to provide different levels of assistance via changing the

compliance when guiding the subjects to walk along the desired gait trajectories during rehabilitation training.

Chapter 7 FLCA Based Assist-as-needed Gait Rehabilitation for GAREX

Assist-as-needed (AAN) control strategies are regarded as one approach to improve effectiveness of gait rehabilitation trainings. GAREX's multi-input-multi-output (MIMO) sliding model (SM) control system can be used to adjust the assistance level provided during gait rehabilitation. To implement AAN concept, it still requires an algorithm to assess the active participation or effort of the training subject and adapt the amount of assistance according. For this purpose, a model-free fuzzy logic compliance adaptation (FLCA) controller was introduced to form a novel cascade control system. The FLCA controller was implemented and validated on the knee joint of GAREX. It adjusts the knee joint compliances according to the assessment of the subject's level of active participation once every gait cycle. The assessment is based on both the knee joint kinematic during the gait training as well as the knee joint interaction torque between the exoskeleton and the leg attached. The FLCA controller takes three inputs which are (1) the gait cycle root-mean-squared (RMS) values of the knee joint interaction torque between the exoskeleton and subject; (2) the gait cycle RMS error between the desired and actual knee joint trajectory; (3) the difference in RMS trajectory errors between the last and second last gait cycles. The output of the FLCA controller is the increment to the desired average PM pressure of the knee joint.

Experiments were conducted with three healthy subjects to investigate if the FLCA control system is able to manipulate the knee joint compliance based on the subject's participating effort. Each of the subjects was told to walk with various inputting forces to simulate different patient effort/capabilities in three experiments. Experimental results showed that the FLCA controller could effectively distinguish the capability/effort levels and adapt the knee joint compliance of the exoskeleton accordingly. The results also indicated FLCA and MIMO SM controllers collaborated well as a system to put the AAN concept into practice with GAREX.

7.1 Introduction

As reviewed in Chapter 2, patients' voluntary participation could lead to more effective rehabilitation training outcomes. Hence, assist-as-needed training strategies have been developed to encourage patients' active engagement in the training tasks. A number of previously developed AAN controller strategies on gait rehabilitation robots have also been reviewed in Section 2.3.3. In summary, mainly two types of implementations of the AAN concept have been identified. One is through adapting the desired speed or gait trajectory [59, 98] and other type is through impedance/admittance related control strategies [9, 23].

When developing the AAN control strategies, it is equally important to assess a patient's capability or participation as to adjust the assistance level provided by the rehabilitation robot. The most often used and easily implemented participation assessing method is via gait kinematics or more specifically derivations from the reference trajectories. Invariant impedance control controllers [15], force field controllers [67, 95] and impedance adaptation via gait velocities [189] all belong to this group.

The interaction force/torque between the exoskeleton and human lower limb has also been used to estimate the subject's participation level during gait rehabilitation. Jezernik et al. [98] developed gait pattern adaptive algorithms to online optimize the reference trajectory of the gait orthoses based on the patient's walking capability. Impedance adaptive controllers based on interaction force/torque measurement have also been reported in [9, 23]. The adaption algorithms in [98] and [23] rely on the models of the exoskeleton and/or the biomechanical properties of the human limb attached. The complexity of modelling work and the possible modelling inaccuracy make such controllers less practical in clinical scenarios.

Fuzzy logic provides an option for controlling complicated or nonlinear systems with uncertainties. Fuzzy logic controllers are developed based on system behaviours and usually do not require models of the systems. Benefitted from such properties, they have been widely used in the field of rehabilitation robotics, which the human factor is commonly regarded to be difficult to model accurately. Chang [158] reported an adaptive self-organizing fuzzy sliding mode trajectory control system for a PM driven 2-DoF serial robot manipulator. Xie and Jamwal [190] developed an iterative fuzzy controller for a PM driven parallel ankle rehabilitation robot. Besides trajectory control, fuzzy logic has also been utilized on controlling impedance/admittance magnitudes of various robotic rehabilitation systems. Tran et al [189] developed fuzzy logic based variable impedance controller for a lower limb exoskeleton. Different fuzzy rules have

been developed for the stance and swing phases to achieve optimized control results. Yang et al. [191] implemented a fuzzy logic tuner for the impedance controller of a cable-driven upper limb rehabilitation robot. Ayas and Altas [192] applied fuzzy logic adaptive admittance control to a parallel ankle rehabilitation robot. The fuzzy impedance adaption controllers in [189, 191] only utilized kinematic data as inputs to the fuzzy logic. The admittance controller in [192] on the other hand only used interaction force as the input.

In the previous chapters, the GAREX platform has been introduced, as well as the MIMO sliding mode control system that enables both task specific gait training and the control of the joint compliance. The controllable compliance hence allows the control of the assistance provided by the exoskeleton. This chapter will focus on the development of a new compliance adaptation algorithm that changes the joint compliance level based on the subject's level of active participation. A model-free fuzzy logic compliance adaption controller would be an ideal candidate for this application. To the author's best knowledge, fuzzy logic based compliance adaption has not been developed on rehabilitation robots driven by PM actuators.

This chapter is organized in the following order. Firstly, the improved hardware design with the human-exoskeleton interaction force sensing instrumentation will be presented. This is followed by the development process of the fuzzy logic compliance adaption algorithm. The next section will be on the experimental validation of the system with three healthy subjects. The discussion and conclusions will be presented at last.

7.2 The assessment of active participation

7.2.1 Interaction torque sensing

As mentioned in the introduction section of this chapter, interaction force/torque measurements have been utilized for the assessment of subjects' effort or active participation during robotic gait rehabilitation. A 6-axis load cell was also employed in this research for human robot interaction force sensing. It was installed between the shank segment of the exoskeleton and the brace for the human shank (As shown in Figure 7-1). Since the load cell is the only link between shank segments of the exoskeleton and the training subject, the sensed forces and torques are thus the interactive forces and torques. In this application, only the interaction knee joint torque in the sagittal plane is of the researcher's interest. It is also assumed that the shank segments of the exoskeleton and the attached human limb are always aligned. Therefore, the joint torque

can be calculated simply by the product of the interactive force along y-axis and its moment arm relative to the sagittal plane rotation of the knee joint.

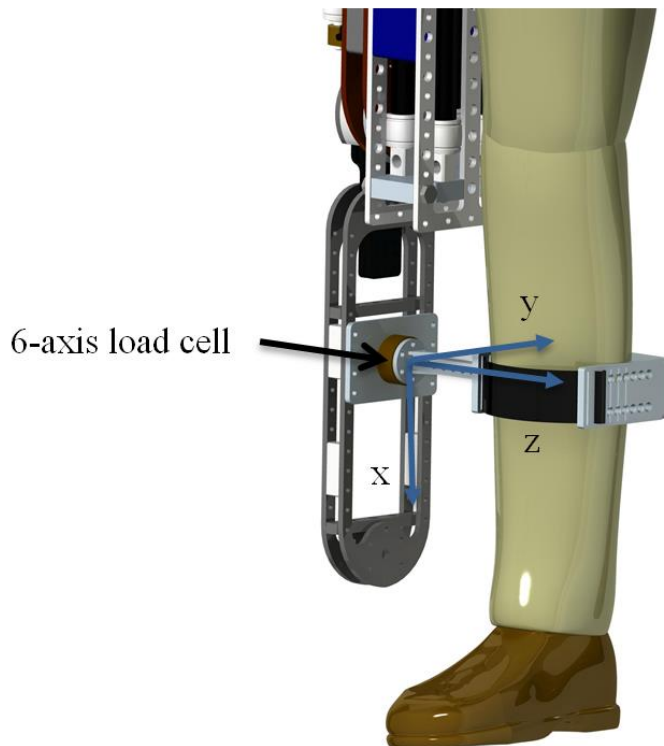


Figure 7-1 The 6-axis load cell for interaction force sensing.

7.2.2 Relation between interactive torque and subject participating level

It has been reported in the literature that the sensed interaction forces have been used as the indication of the subject's effort during rehabilitation training [9]. High interaction force was regarded as less effort from the subject to walk in desired gait pattern; hence the higher impedance was resulted to ensure the desired gait pattern can be achieved. In contrast, lower interaction force indicated more effort from the subject to synchronize his/her leg movement to the desired trajectories of the rehabilitation robot. Hence, lower impedance is adapted.

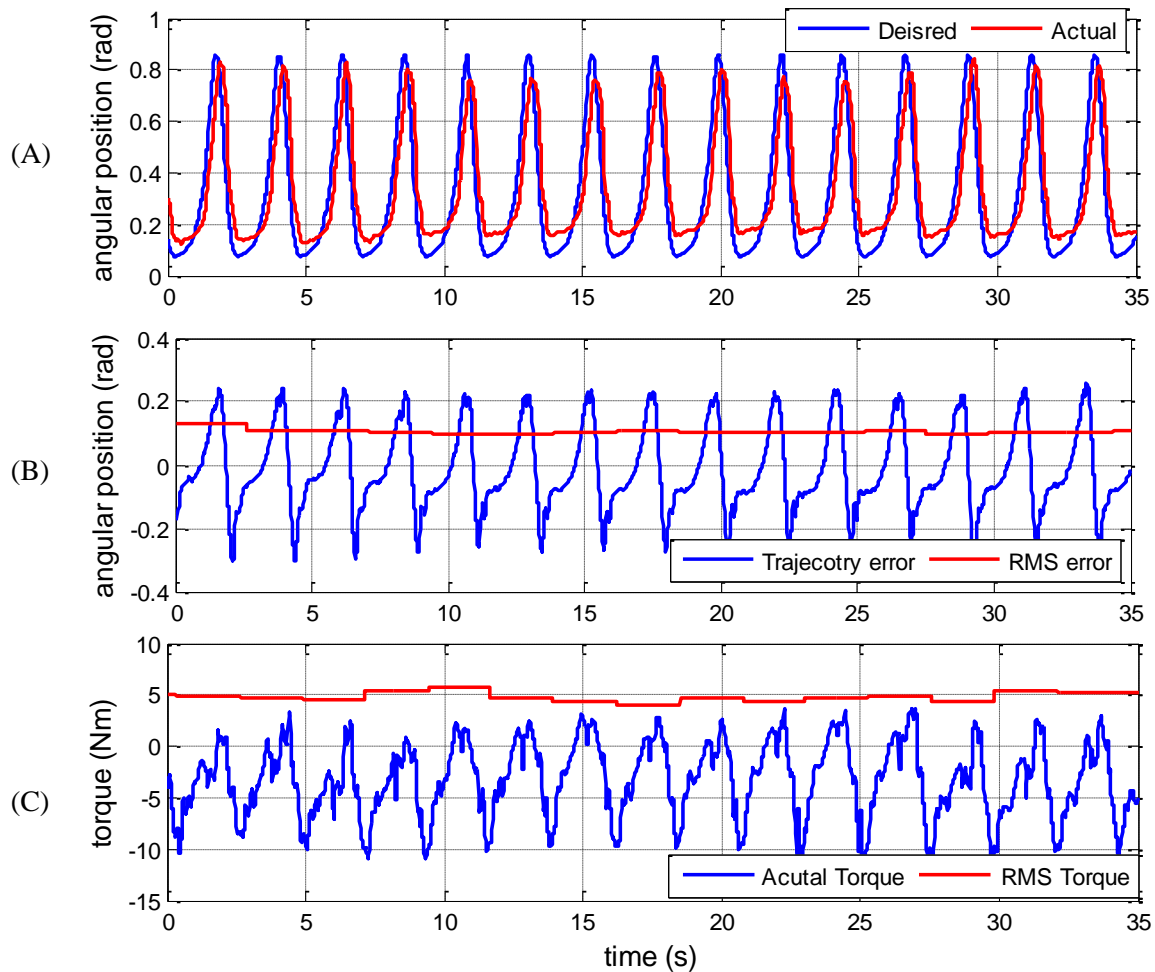


Figure 7-2 Experimental results when the subject was actively trying to follow the desired gait pattern. (A) Desired and actual knee joint trajectories versus time plot. (B) Plots of trajectory error and RMS trajectory error over every gait cycle. (C) Plots of interaction torque and RMS interaction torque over every gait cycle.

Experiments were designed to investigate how the subject's effort is reflected by the various sensor measurements of the system. The experiments were conducted with the help of a neurologically intact subject (male, 185 cm, 100 kg) with no lower limb injury. The MIMO SM controller presented in Chapter 6 was adopted to control the exoskeleton. Both the hip and knee joints of GAREX were actively controlled to guide the subject to walk on the treadmill at the speed of 1.5 km/h. The average PM pressures of the two actuated joints were regulated to 270 KPa. Different patient capabilities or participating levels were simulated by the subject in three experiments. In the first experiment, the subject was requested to actively engage the gait training by following the robotic guidance to walk in a desired trajectory. The second experiment simulated the no effort scenario. The subject tried to relax the leg attached to the exoskeleton as much

as possible let the exoskeleton provide torque required to produce the reference gait pattern. In the third experiment, stiff leg or undesired leg movements (spasms) were simulated. The subject was asked to slightly oppose the robotic guidance during the swing phase of every gait cycle. Experimental results of the three experiments are shown in Figure 7-2 to Figure 7-4.

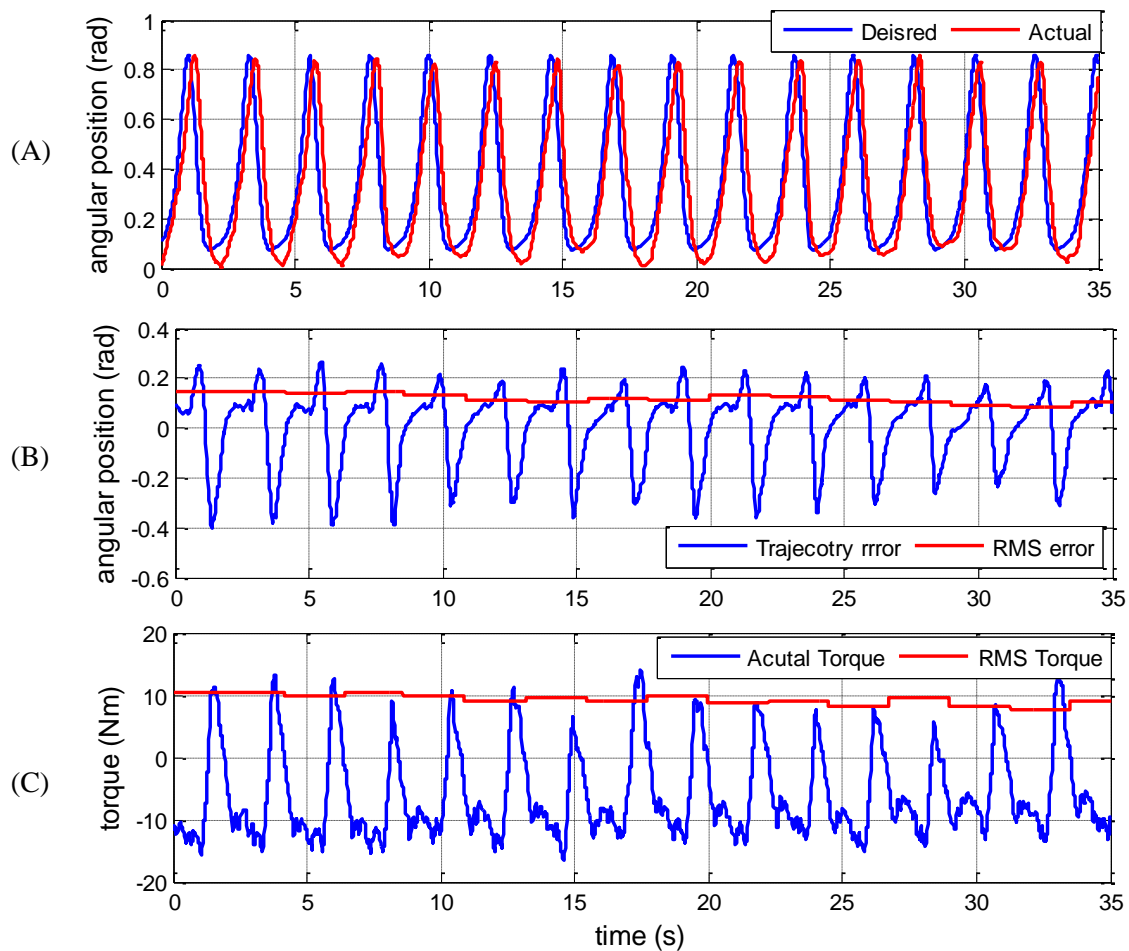


Figure 7-3 Experimental results when the subject was requested to relax the leg attached to the exoskeleton. (A) Desired and actual knee joint trajectories versus time plot. (B) Plots of trajectory error and RMS trajectory error over every gait cycle. (C) Plots of interaction torque and RMS interaction torque over every gait cycle.

Both the knee joint trajectory tracking performances and the interaction torque are plotted in Figure 7-2 to Figure 7-4. In order to compare the differences of the three experimental scenarios, RMS values of the trajectory tracking error and the interaction torque were calculated for every gait cycle period during the experiments and shown in the result plots. By analysing the results, it can be summarized that the subject's active participation or effort leads to better trajectory tracking accuracy and less RMS interaction torque over a gait cycle period compared to the experiment when the subject tried to relax and make no effort. On the other side, when the

subject deliberately opposed the guidance of the exoskeleton, larger overall trajectory error was resulted. The robotic system hence increased the control effort to drive the knee joint back to the desired trajectory, which thus led to higher interaction torque.

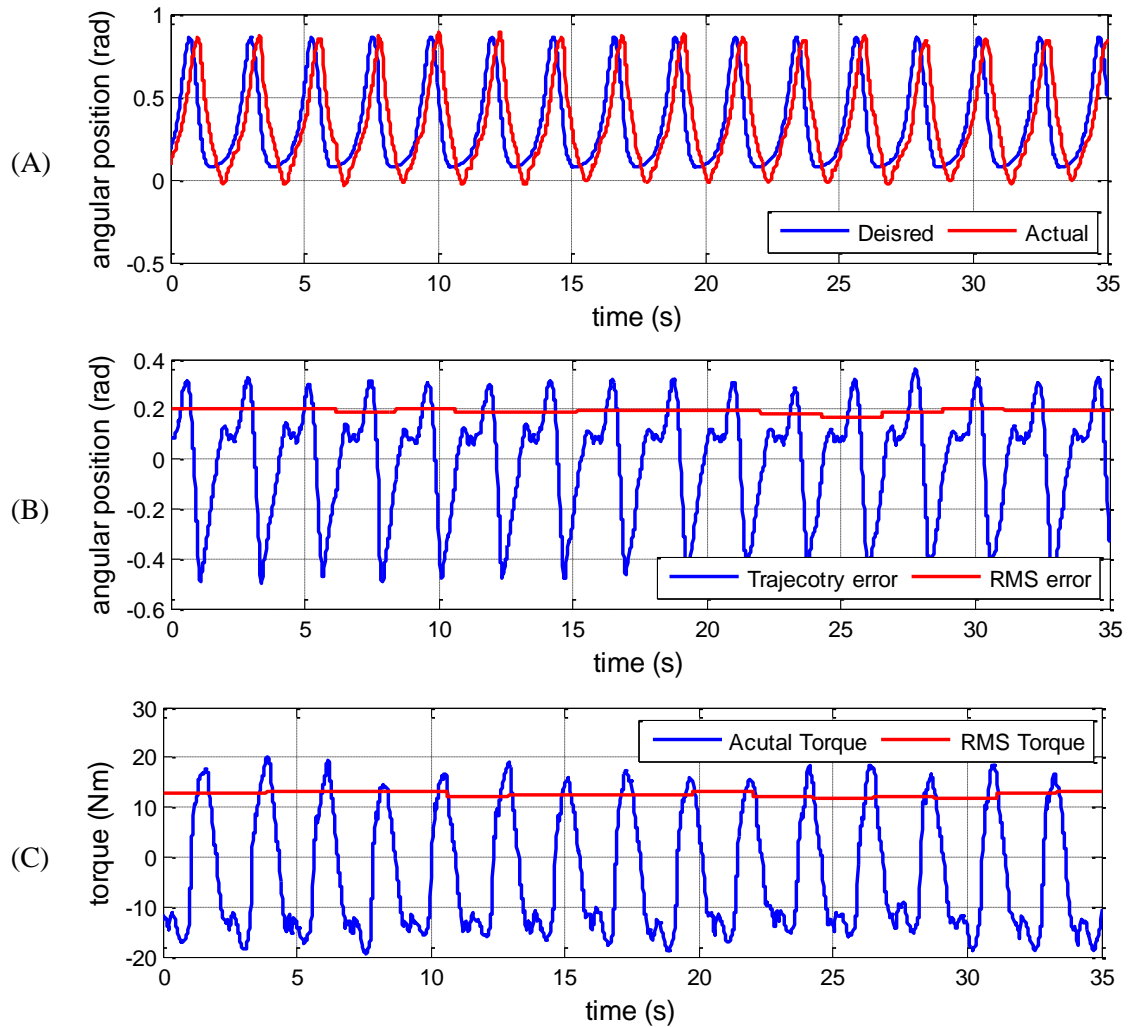


Figure 7-4 Experimental results when the subject was requested to slightly oppose the guidance of exoskeleton. (A) Desired and actual knee joint trajectories versus time plot. (B) Plots of trajectory error and RMS trajectory error over every gait cycle. (C) Plots of interaction torque and RMS interaction torque over every gait cycle.

7.3 Implementation of the FLCA controller

The goal of the adaption algorithm is to encourage active participation of training subjects by only providing as much assistance as he/she needed to walk in desired trajectories. From the experiments conducted in the last section, the general principles for compliance adaptation can be summarized as:

- (1) The interaction torque is **low** and the trajectory error is **low**. The subject is doing great and the exoskeleton is not doing much to help. Let the compliance level stay to where it is.
- (2) The interaction torque is **low** and the trajectory error is **high**. The subject cannot walk in the desired pattern and the system is not doing enough to help. Compliance needs to be reduced for more guidance.
- (3) The interaction torque is **high** and the trajectory error is **low**. The subject is going great with high assistance level from the exoskeleton. Compliance can be reduced to challenge the subject.
- (4) The interaction torque is **high** and the trajectory error is **high**. The subject cannot walk in the desired pattern but the exoskeleton has already been providing a lot of assistance. Let the compliance level stay to where it is for now.

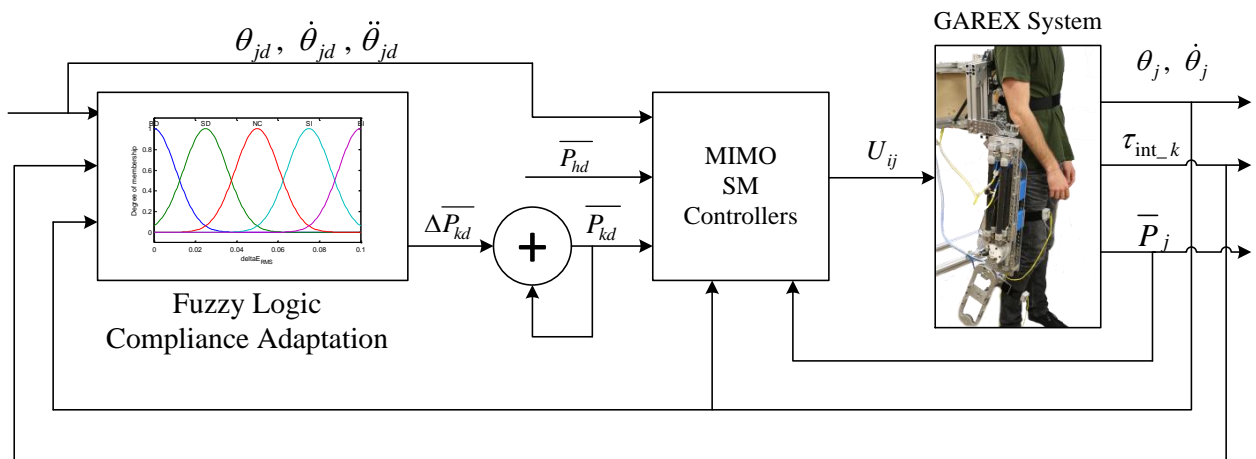


Figure 7-5 The fuzzy compliance adaptive control system block diagram of GAREX. In the figure $i = F, E$ and $j = h, k$; U_{ij} are the input to the plant or the voltages fed into the corresponding analogue valves; τ_{int_k} is the interaction torque of the knee joint; \bar{P}_j is the average pressure of the antagonistic PMs of the corresponding joint; the subscript d indicates desired value of a property and $\Delta \bar{P}_{kd}$ are the increment to the desired average pressure of the antagonistic PMs of the knee joint.

It is understood that any change in compliance will influence both the interaction torque and the trajectory tracking error. The change in interaction torque or trajectory error will affect each other. A fuzzy logic compliance adaptation controller was a good candidate to such complex system and hence developed to implement the AAN rehabilitation concept. The block diagram of the control system is show in Figure 7-5.

The frequency of the compliance adaptation processing was set to be gait cycle frequency of the exoskeleton. There are two main reasons for this decision. Firstly, the compliance adaptation is based on the subject's performance over a past period rather than at a certain instant. Hence, it is not necessary to run the compliance adaptation controller at the same frequency as the MIMO SM controller (100 Hz). Secondly, the trajectory error and interaction torque distributions over a gait cycle are not homogeneous. If the sampling periods contain different parts of a gait cycle, it is difficult to find standards to evaluate the subject's effort during those sampling periods. Hence, it is a good practice to set the sampling period to be integer multiples of the GC period. In this application, the sampling period was chosen to be same as the GC period.

There are three major stages of the fuzzy logic controller implementation. The first one is to define the inputs and output of the controller and perform fuzzification to acquire input and output membership functions. The RMS values of the knee joint trajectory error (θ_{k_RMS}) and the interaction torque ($\tau_{int_k_RMS}$) of the past GC are two of the inputs of the fuzzy logic controllers. The difference between the RMS trajectory errors of the current and the last gait cycles is calculated as the third input of the controller, shown in the following equation:

$$\Delta\theta_{k_RMS} = \theta_{k_RMS(n)} - \theta_{k_RMS(n-1)} \quad (7-1)$$

This input is utilized to reflect if the system's trajectory tracking performance is improving. The output of the controller is the increment ($\Delta\bar{P}_{kd}$) to the desired average pressure of the knee joint. The fuzzification of the inputs and out was through the membership functions shown in Figure 7-6 and Figure 7-7 . The crisp input and output values are converted into the linguistic variables and membership values. The fuzzy set of each input or output is determined using the membership functions which are normally distributed around its centre. There are three linguistic variables or membership functions (low, medium and high) each for the trajectory error and interaction torque inputs. The third input variable and the output variable each has five linguistic variables, which are BD (big decrease), SD (small decrease), NC (no change), SI (small increase) and BI (big increase). The centre value of the Gaussian shaped membership functions were tuned and finalized through experiments with the developed FLCA enabled control system. For certain input values, the membership degrees for the linguistic variables of each input can be calculated with membership functions as μ_{a_i} ($i = 1, 2, 3$), μ_{b_i} ($i = 1, 2, 3$), μ_{c_i} ($i = 1, 2, 3, 4, 5$) for inputs of the trajectory error, interaction torque and change in trajectory error respectively.

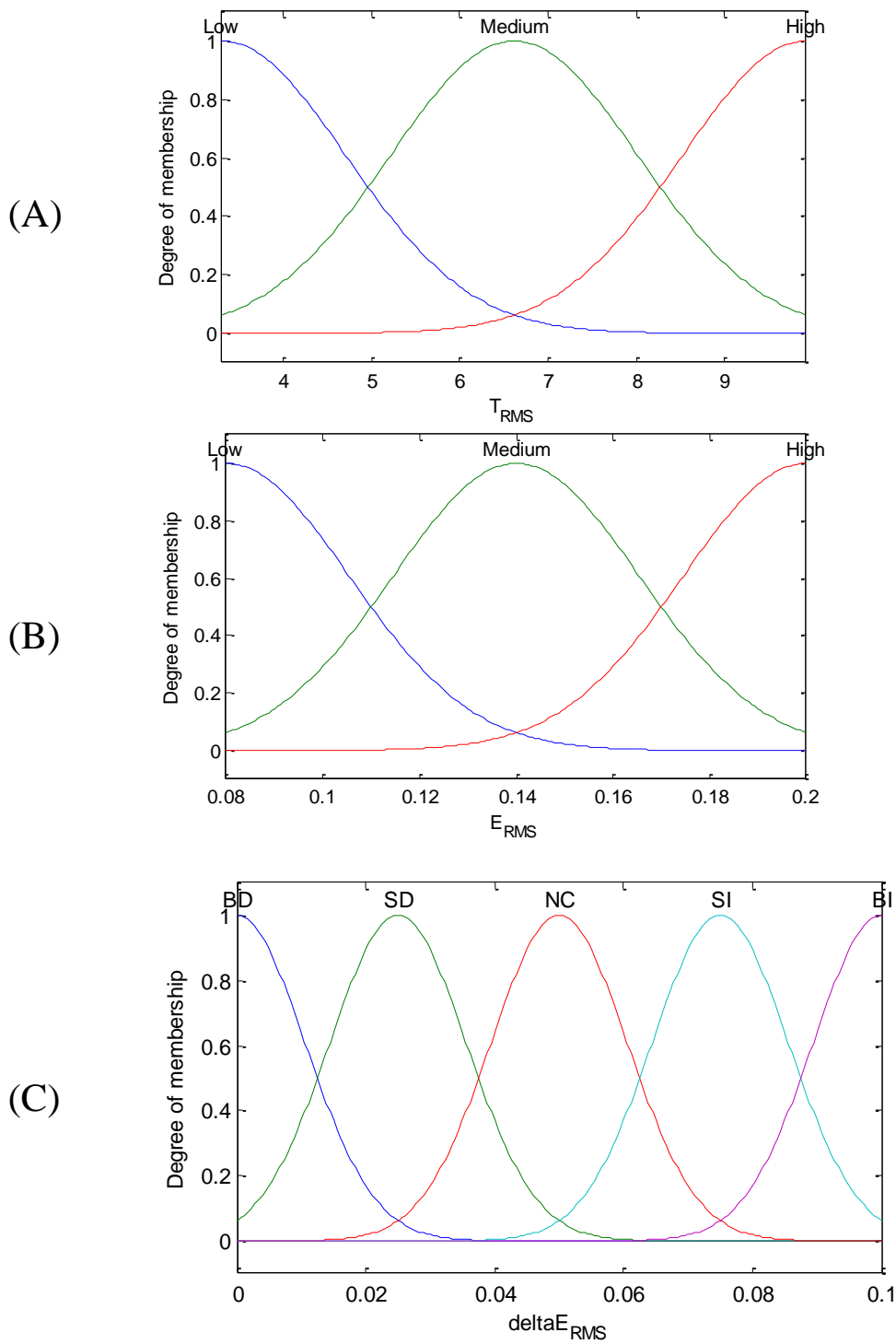


Figure 7-6 The membership functions of the input variables. (A) The RMS value of the interaction torque. (B) The RMS value of the tracking error. (C) The change of the tracking error.

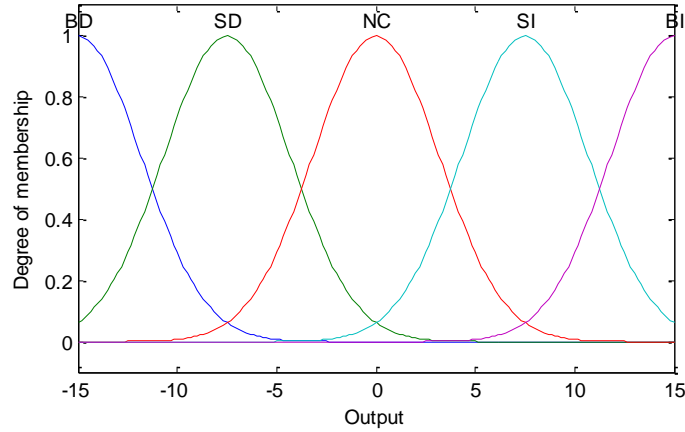


Figure 7-7 The output membership function of the FLCA controller

The stage after fuzzification is the inference process which generates the membership degrees of the output linguistic variables based on the fuzzified inputs. The key of the inference process is the development of the fuzzy rules. The fuzzy rules are to reflect the expectation of compliance adaptation by linking the linguistic variables with a combination of input linguistic variables. Table 7-1 exhaustively listed the fuzzy output generated by all 45 input combinations with 5 sub-tables. The fuzzy rules were first developed by the four principles stated in the beginning of this section and further tweaked through experiments. The well-known Mamdani's max-min method [193] is used for the inference process. From Table 7-1, it can be seen that certain amount of combinations of input linguistic variables that lead the same output linguistic variable. To calculate the membership degree of an output the linguistic variable, the membership degree resulted by each of the possible combinations is calculated first as:

$$\mu_{d_{-i(j)}} = \min(\mu_{a_{-x}}, \mu_{b_{-y}}, \mu_{c_{-z}}) \quad \text{with } (j = 1, 2, \dots, n) \quad (7-2)$$

where n is the number of possible combinations input linguistic variables that lead the i th output linguistic variable; $\mu_{a_{-x}}, \mu_{b_{-y}}, \mu_{c_{-z}}$ are the membership degrees of the input linguistic variables in that specific combination. The minimum of $\mu_{a_{-x}}, \mu_{b_{-y}}, \mu_{c_{-z}}$ is calculated and assigned to $\mu_{d_{-i(j)}}$. The membership degree of the output linguistic variables are calculated as the maximum of all the possible values ($\mu_{d_{-i(j)}}$):

$$\mu_{d_{-i}} = \max \left(\bigvee_{j \in (1, 2, \dots, n)} \mu_{d_{-i(j)}} \right) \quad (7-3)$$

The defuzzification stage maps the conversion from the degrees of the output membership function to the non-fuzzy controller output. The centre of area method is used for this process.

The controller was developed with help of the Fuzzy System Designer with the LabVIEW software package. The designed FLCA controller was programmed in LabVIEW and run on the myRIO real-time control platform.

Table 7-1 The rule tables for the FLCA. Since there are three input variables, each of the 3x3 table is for one membership function of the $\Delta\theta_{k_RMS}$ input.

$\tau_{int_k_RMS}$	θ_{k_RMS}		
	Low	Medium	High
Low	SD	NC	SI
Medium	SD	SD	SI
High	BD	SD	NC

$$\Delta\theta_{k_RMS} = BD$$

$\tau_{int_k_RMS}$	θ_{k_RMS}		
	Low	Medium	High
Low	NC	NC	SI
Medium	SD	NC	SI
High	BD	SD	SI

$$\Delta\theta_{k_RMS} = SD$$

$\tau_{int_k_RMS}$	θ_{k_RMS}		
	Low	Medium	High
Low	NC	SI	BI
Medium	SD	SI	SI
High	BD	NC	SI

$$\Delta\theta_{k_RMS} = NC$$

$\tau_{\text{int}_k_RMS}$	θ_{k_RMS}		
	Low	Medium	High
Low	NC	SI	BI
Medium	NC	SI	SI
High	SD	NC	SI

$\Delta\theta_{k_RMS} = SI$

$\tau_{\text{int}_k_RMS}$	θ_{k_RMS}		
	Low	Medium	High
Low	SI	SI	BI
Medium	NC	SI	BI
High	NC	SI	SI

$\Delta\theta_{k_RMS} = BI$

7.4 Experimental validation

Experiments were conducted with three healthy subjects (Subject A: male, 172 cm, 62 kg; Subject B: male, 185 cm, 100 kg; Subject C: male, 171 cm, 72 kg) with no lower limb injuries. Written consents have been obtained from all the participants prior to the experiments. To conduct the experiments, the subject was firstly fitted to GAREX which was adjusted according to the subject's anthropometric data. The subject performed a trial walk with robotic guidance for 5 minutes, so he could get used to the assisted walk with GAREX. After a rest of 5 minutes, the actual compliance adaptation experiments would take place. The subject was requested to behave differently in three experiments with GAREX. In the first experiment, the subject actively followed the guidance of the exoskeleton in order to walk in the desired trajectory. The experiment is designed to simulate the rehabilitation training scenario in which a patient makes good effort to actively participate in the training. In the second experiment, the subject tried to fully relax the leg attached to the exoskeleton and let GAREX provide the torque needed to produce the desired gait pattern. This experiment was designed to simulate the gait rehabilitation scenario when a patient is not capable of making active participation. In the last experiment, the subject was asked to oppose the guidance as much he could comfortably do, during the swing phase; and meanwhile he was still able to walk on the treadmill safely. The aim of this experiment was to simulate patients with stiff joints or spasm during robotic rehabilitation.

Each of the experiments lasted for 3 minutes and in between two experiments there was a rest period of 3 minutes.

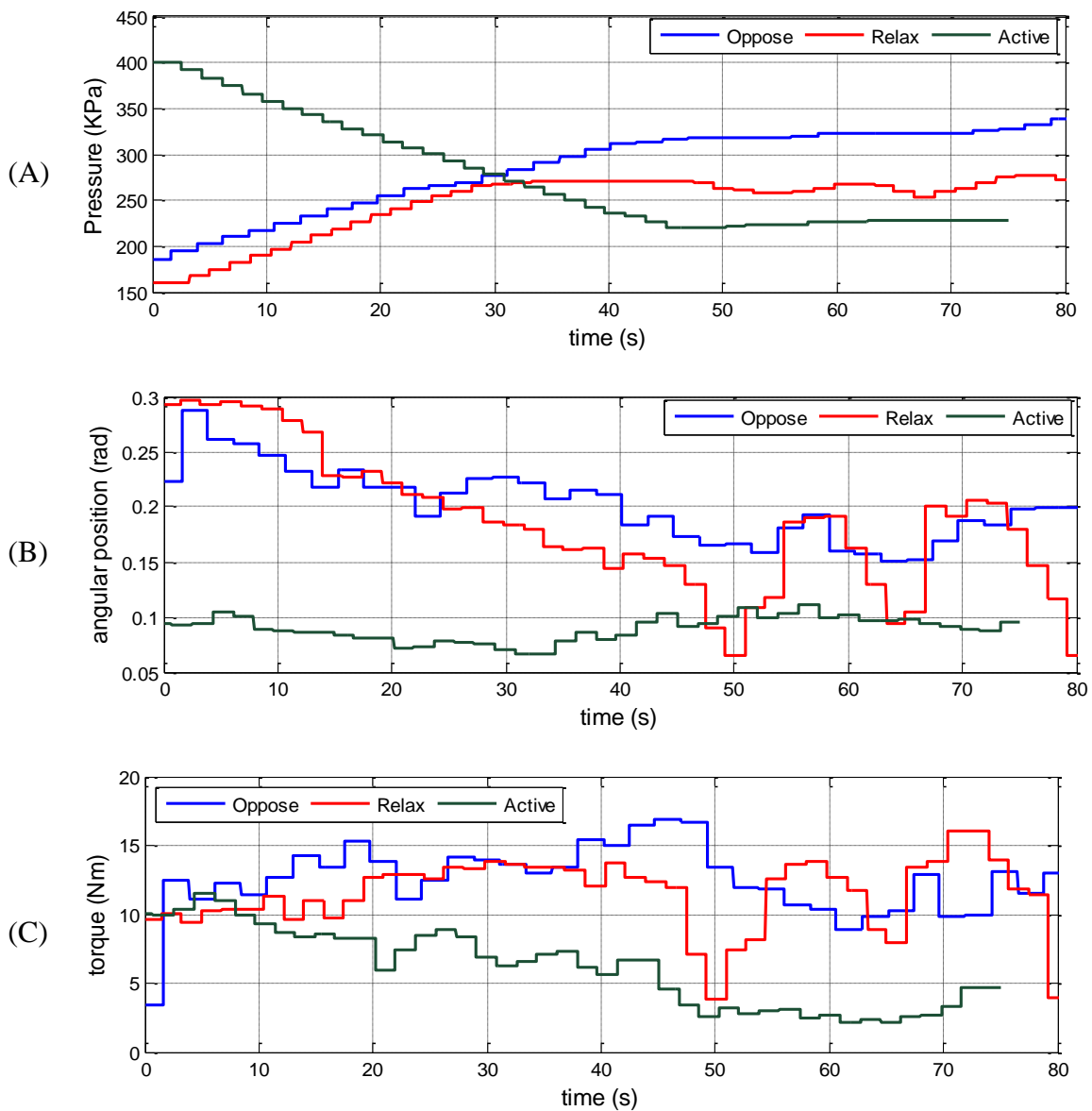


Figure 7-8 The experimental result plots for Subject A. (A) The desired knee joint average PM pressure versus time plots. (B) The GC RMS trajectory error versus time plot. (C) the GC RMS interaction torque versus time plots.

The experimental results of the three participants were shown in Figure 7-8 (Subject A), Figure 7-9 (Subject B) and Figure 7-10 (Subject C). For comparison purposes, the results of the experiments conducted by the same subject are shown in the same figure. Each of the figures contains three subplots. The output of the FLCA controller is represented by the P_{kd} plot. The controller inputs, which are the gait cycle RMS trajectory error and the gait cycle RMS interaction torque, are also shown in the figures. In order to ensure readability of the plots, only 80-

second segments of experiments are plotted. For each experiment, the starting point of the desired average pressure was chosen so the compliance adaptation processes could be visualized.

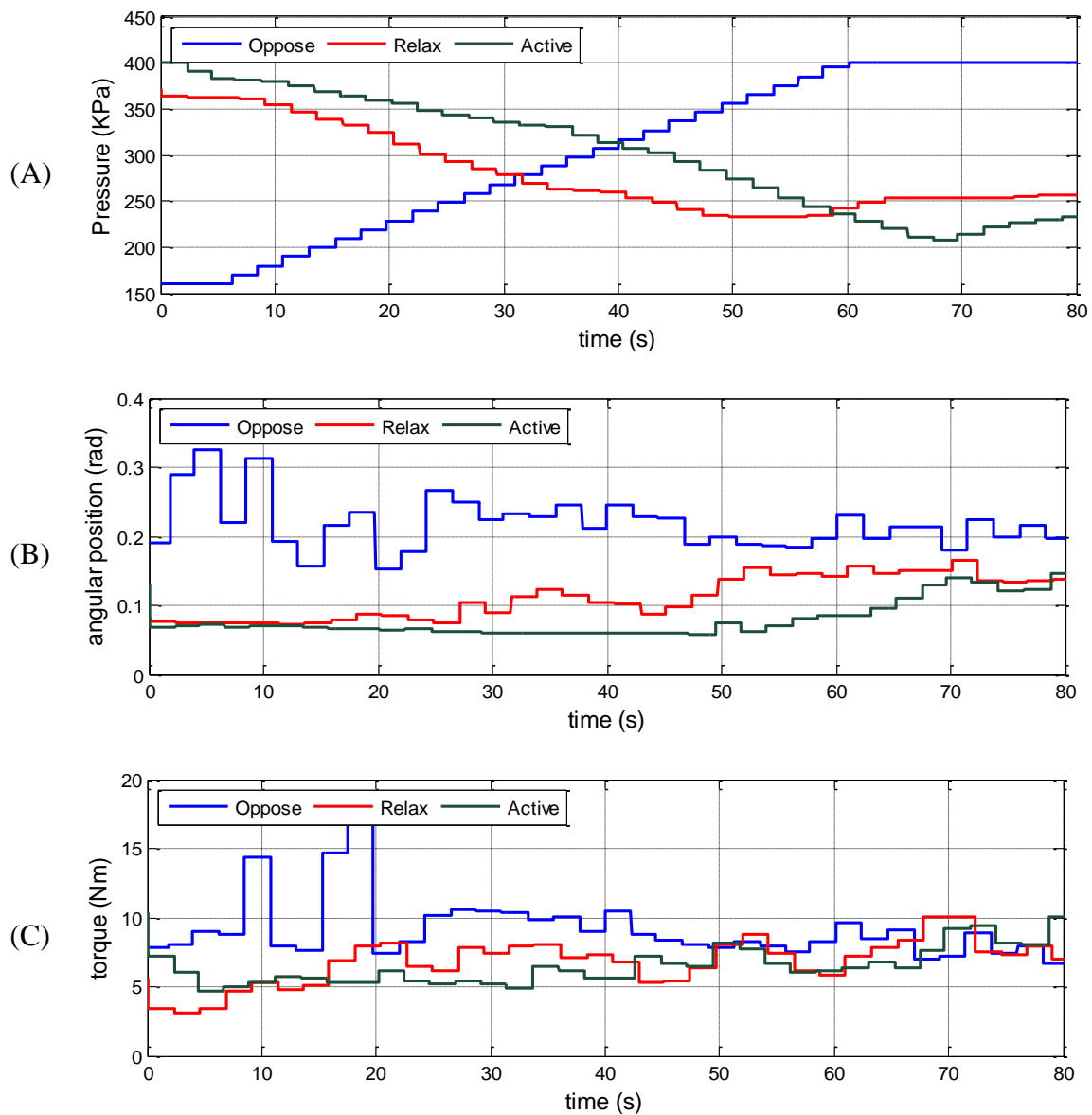


Figure 7-9 The experimental result plots for Subject B

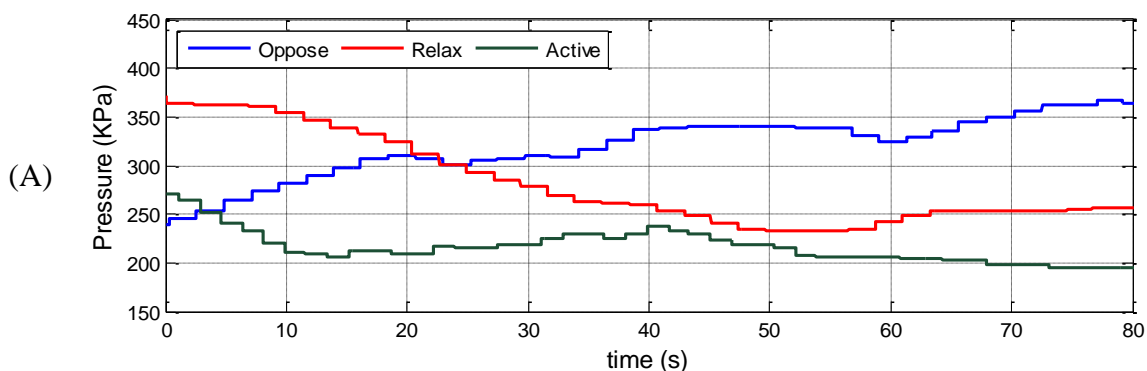
As stated in the adaptation rule, the compliance is supposed to be high when the active participation by the subject is detected. On the other hand, if the subject is not capable to follow the desired gait pattern. The compliance is supposed to be decreased in order to constrained subject's lower limb to the desired trajectory. To investigate if the control system can perform as expected, Figure 7-8-(A), Figure 7-9-(A) and Figure 7-10-(A) are analysed. After stable compliance had been achieved, actively following the desired trajectory resulted the highest compliances (lowest average PM pressure) for all the subjects. Compared to actively following, the

experiments with subject relaxing their legs attached to the exoskeleton resulted lower compliance levels. The lowest compliance was resulted by subjects deliberately opposing the robotic guidance. Such experimental results indicate that the control system performed to the overall expectation.

From the gait cycle trajectory error plots, it can be viewed that the magnitude of the trajectory error is generally positively correlated to the compliance level. However, the correlation is not obvious for the "Oppose" experiments conducted by Subject B and C. There are also relatively large magnitude variations in the "Oppose" experiments conducted by Subject A and Subject B, as well as the "Relax" experiment by Subject A. Different experiments conducted by the same subject were also compared. For Subject A and Subject B, the best overall trajectory tracking performance achieved in "Active" experiments, followed by the "Relax" experiments. The "Oppose" experiments scored largest overall tracking error. However, for Subject B, no obvious difference in tracking performance could be identified. These results indicated that it is not practical to perform compliance adaptation only based on the kinematics feedback.

Compared to the gait cycle RMS trajectory error, it is even less likely to only use the interaction torque to perform compliance adaption. As shown Figure 7-8-(C), Figure 7-9-(C) and Figure 7-10-(C), there are no obvious differences in $\tau_{int_k_RMS}$ between the three experimental conditions of the same subject. However, the inter-subject comparison shows some obvious differences. For Subject A, after the compliance levels adaption had been settled, the overall interaction torque in the "Active" experiment is much lower than the other two experiments. For Subject C, highest interaction torque was achieved by the "Active" experiment.

Through the analysis, it can be concluded that the controller is able to assess if subjects are actively participating in the trial and adjust the compliance level regardless that different subject may produce different input patterns when trying to make similar effort.



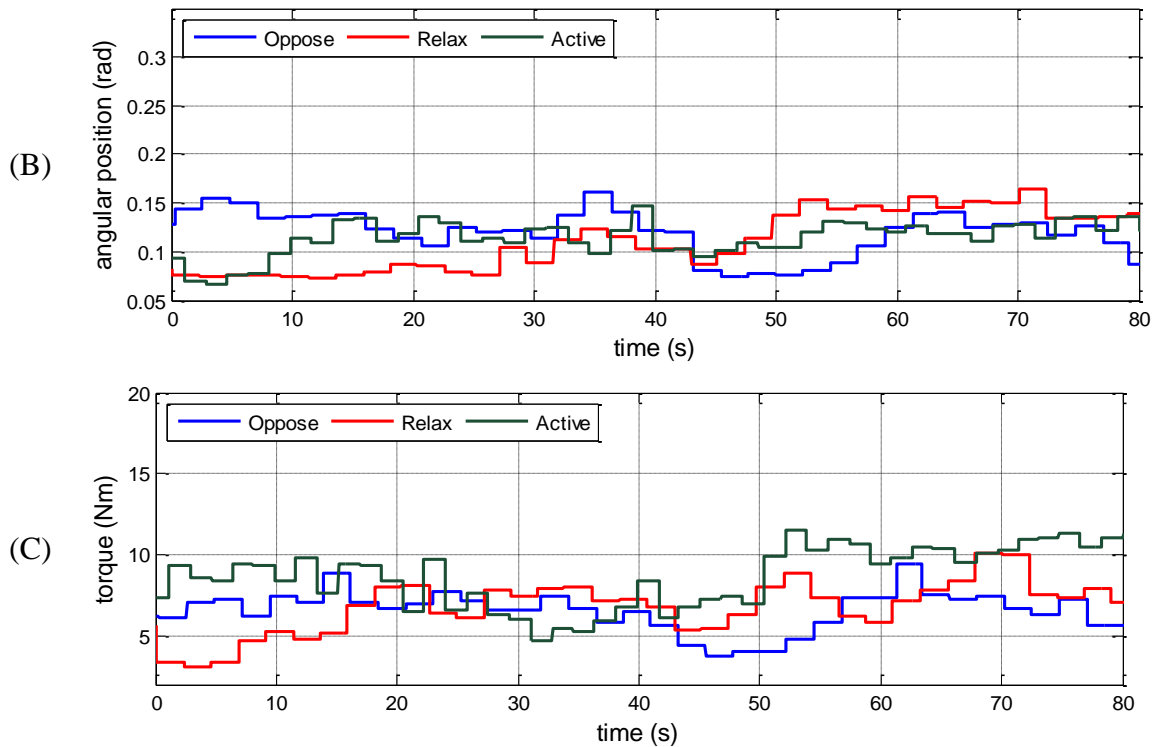
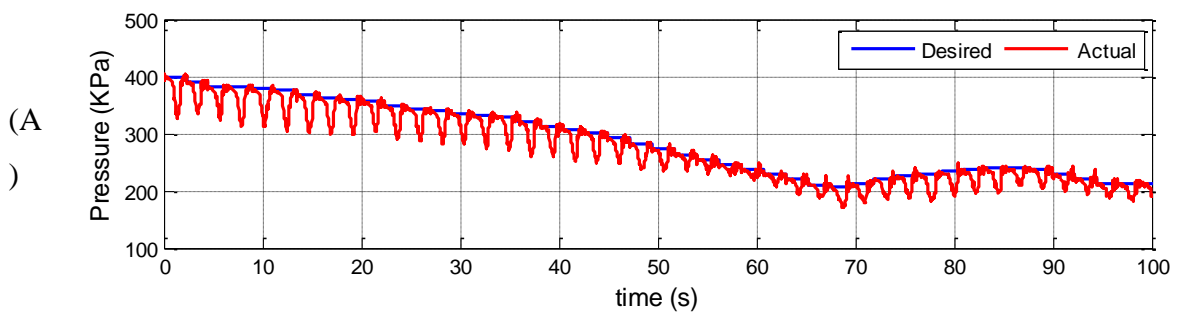


Figure 7-10 The experimental result plots for Subject C

The overall control system shown in Figure 7-5 is of a cascade control structure. The FLCA controller's output (\bar{P}_{kd}) is one of the inputs for the MIMO sliding model controller. It is necessary to investigate if the MIMO SM controller is able to track the desired average PM pressures. The tracking results of the three experiments conducted by Subject B are shown in Figure 7-11. As can be seen from the first two plots of the figure, the system was able to closely track the adapted \bar{P}_{kd} . However, for the "Oppose" experiment, the system was able to track the desired PM pressure for the first 20 seconds. After 20 seconds, the controller was unable to deliver satisfactory tracking performance. For the last five seconds, the control system managed to bring the average PM pressure back to its desired magnitude.



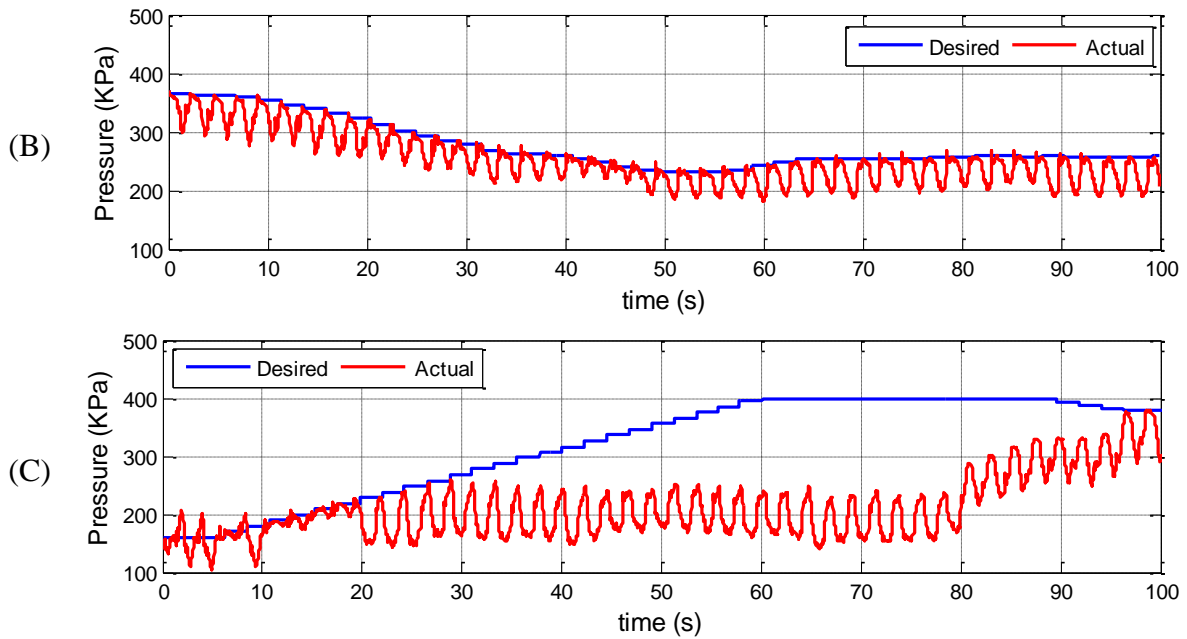


Figure 7-11 The desired and actual average PM pressures of the knee joint versus time plots for the three experiments conducted by Subject A. (A) “Active” experiment; (B) “Relax” experiment; (C) “Oppose” experiment.

The MIMO sliding model controller tuning could be one of the causes to the suboptimal control system performance. The MIMO SM controller needs to control the angular trajectory and the average PM pressure of an actuated joint simultaneously. Considering the safety and nature of robotic gait rehabilitation, angular trajectory tracking needs to be prioritized among the two control objectives. This was implemented by the tuning parameters that let angular trajectory tracking take the dominate role in the overall control actions. As a result, the large trajectory error in the “Oppose” experiment led to significant control action to drive the knee joint back to its desired position. The control action to maintain the average pressure thus became less effective. However, after the 90-second mark of Figure 7-11-(C), the desired average pressure started decreasing, which is an indication that the subject’s effort of opposing the guidance may have reduced. The angular position tracking could thus also be improved and the better average pressure regulation was resulted.

It can also be observed that the actual average PM pressure oscillated just below the desire value, even when the tracking was effective. Within the same gait cycle, the demand of control action to track the gait trajectory varies. For the knee joint, the trajectory over the swing phase is much more challenging for the controller than the stance phase. The average pressure tracking performance is somehow affected and hence the oscillations happen. Apart from controller

tuning strategy, the limited control system bandwidth could also be a cause of imperfect performance.

7.5 Discussion and conclusions

A fuzzy compliance adaptation controller was integrated with the existing MIMO sliding mode controller in order to implement the AAN concept with the GAREX system. The fuzzy controller adjusts the knee joint compliance of the exoskeleton based on the subject participation assessment through the gait kinematics and knee joint interaction torque. The FLCA controller does not require the model of the exoskeleton or the human biomechanics; therefore, it could be more practical in clinical settings.

The developed FLCA control system was experimentally validated with three healthy subjects. Each subject participated in experiments to simulate three different capability/effort levels of patients with gait problems. The experimental results indicated that the FLCA control system was able to distinguish the capability/effort levels and adapt the knee joint compliance of the exoskeleton accordingly. Experimental results also reveal that the MIMO SM controller was able to regulate the average PM pressure of the knee joint to the reference provided by the FLCA controller except when the subject was opposing the robotic guidance to create significant trajectory error.

Although effective compliance adaptation has been successfully achieved, there are still potential improvements that could be made to the control system. In terms of the controller implementation, the stance and swing phases of a gait cycle could be distinguished, because the torques of the two phases are considerably different (Figure 3-3). It would also be more meaningful to investigate the interaction torque of the two phases separately. A ground reaction force sensor can be used to distinguish the two phases. It can also be utilized together with the 6-axis load cell to more accurately estimate the knee joint interaction torque during the stance phase. With more accurate joint torque mapping over the entire gait cycle, the fuzzy controller could thus be updated for better control accuracy.

Further improvements of the experiments are also possible. Interviews with the participants revealed that the “Active” experiments were the easiest to conduct for all of them. They felt walking with GAREX is really similar to natural walking. All the subjects reported that it is difficult to fully relax the leg attached to GAREX and not participate at all, mainly because it is hard to have the robot support the body weight during the single stance phase on the attached

leg without the fear of falling. A possible solution could be the introduction of a body weight support system. For the “Oppose” experiments, it was observed that the magnitudes of trajectory error and interaction torque were varied among the subjects, because of their strength differences. In further studies, it may be worthy to provide visual feedback to the subject during the experiments, so the subjects could better follow the researcher’s instructions. This would help produce quantified participation levels of the subject for more in depth control performance evaluation.

Chapter 8 Conclusions

All the three main objectives of this research have been achieved. Firstly, a new robotic gait rehabilitation exoskeleton driven by PM actuators named GAREX was designed and built for the potential application in clinical settings. In this research, the robot makes a robust platform for control system implementation and experiments. Secondly, the sliding mode control strategies were developed and experimentally validated on GAREX. The newly proposed multi-input-multi-output (MIMO) sliding mode (SM) control system is able to not only track desired gait trajectories in task specific treadmill based gait trainings, but also control the compliance of the exoskeleton in order to provide different levels of assistance to the training subjects. Thirdly, the assist-as-needed concept was implemented with an intelligent control system, which consists of a fuzzy compliance adaptation controller and the MIMO SM controller. The pilot study conducted on healthy subjects proved that the control system was able to detect subjects' active effort or capability, in order to adjust the assistance provided accordingly.

This chapter recaps the work ducted and highlights the contributions made through the PhD research. Limitations of this research and insightful suggestions to future work directions are also discussed.

8.1 Impact and contributions

The goals of this PhD research have been on the development and control of the PM actuated GAREX system to deliver task specific and AAN gait rehabilitation training. The scientific contributions of the research are further elaborated as follow.

8.1.1 Robotic design of GAREX

A robotic gait rehabilitation exoskeleton has been designed and built as a solid platform to host the research and validation of more effective control strategies. PM actuators were adopted to actuate the sagittal plane rotations of exoskeleton's hip and knee joints. This specific type of actuators has intrinsic compliance that can be utilized by control strategies to vary the extents of guidance.

Only a handful of PM driven robotic gait rehabilitation devices have been reported in literature. To the author's best knowledge, none of them have been brought into the clinical trials. GAREX is also aimed to deliver task specific repetitive robotic gait rehabilitation in clinical applications. The task specific criterion imposes joint torque, range of motion and control bandwidth requirements to the exoskeleton design. There is a trade-off between the ROM and torque a PM actuated joint can provide. Detailed design analysis was conducted to verify the exoskeleton design. For clinical readiness, GAREX also has redundant safety implementations and anthropometric adaptability for most of the adult population.

8.1.2 A complete model of the PM actuated exoskeleton

The PM actuation system is highly nonlinear and subject to hysteresis behaviours. It is desirable to model the entire system in order to better understand the system and help upcoming controller implementation. The system model consists of four sequential sub-models, which are the flow dynamics of the valve, the pressure dynamics of the PMs, the force dynamics of the PMs and the load dynamics of the exoskeleton mechanism. In previously developed PM driven rehabilitation robots the first two sub-models had been ignored with the use of pressure regulating valves, which could lead to unpredictable transient behavior of the controlled PM pressure [194].

The model of the PMs needs to accommodate the dynamic PM operations during robotic gait rehabilitation. It was also noticed that there were no dynamic force models could adopted directly to the FESTO PMs actuating GAREX. As a result, a new dynamic modelling approach

has been developed based on the original model developed by Reynolds et al. [165] on conventional McKibben PMs. To better represent the behaviours of the FESTO PM used on GAREX, the model in [165] was modified to a piece-wise form. The new model not only fit well to the experimental data of the PMs on GAREX; it also covers a greater pressure range than the original model. Meanwhile, the new model is still in a simple form for further usage in model based control system development. Moreover, experimental and data processing procedures for calibrating the model parameters have been fully automated, so the model can be quickly adapted for PMs of different sizes.

8.1.3 Control systems of GAREX

The intrinsic compliance of PMs can be utilized to vary the extents of guidance. This is achieved by the novel application of a MIMO SM control system. It provides both trajectory tracking and average antagonistic PM pressure control for the actuated joints. In order to embrace all the modelling uncertainties, the MIMO SM controller was developed based on the complete system model of the exoskeleton. It was hypothesized that lower average PM pressure leads to more compliant joint mechanism and vice versa. The MIMO SM controller was initially implemented to the knee joint mechanism. Extensive experiments conducted on the sole robot and with a healthy subject proved the controller's simultaneous trajectory and average pressure tracking capability. Another set of experiments conducted on 5 healthy subjects demonstrated that the MIMO SM controller was able to adjust the joint compliance by controlling the average PM pressure.

After initial validation with the knee joint mechanism, the MIMO SM controllers were then implemented to both the hip and knee joints of GAREX to facilitate task specific gait rehabilitation. The pilot experiments showed that the exoskeleton could comfortably guide healthy subjects to complete treadmill based gait experiments, in a speed what was adopted for clinical trials on a motor driven gait rehabilitation robot. Such result revealed the potential of taking GAREX to the clinical trial stage in the near future.

Based on the literature review, there have not been any experiments to investigate the correlation between the joint compliance of the PM driven exoskeleton and the extent of assistance provided during gait rehabilitation. Hence, it was designed to have healthy subjects test the exoskeleton system at four different compliance levels in four experiments. Each of the subjects was asked to rate the assistance levels received in the four experiments from their perception. A total of 12 subjects conducted the experiments and the statistical analysis of the results

showed the successful manipulation of the assistance levels with the exoskeleton compliance adjusted by the MIMO SM controller.

The MIMO SM controller gives GAREX the means to provide various extents of assistance. To achieve AAN gait rehabilitation training with GAREX, model-free a fuzzy logic compliance adaptation controller was introduced to form a novel cascade control system with the MIMO SM controller. Experiments conducted by three healthy subjects showed that the FLCA controller could effectively distinguish the capability/effort levels and adapt the knee joint compliance of the exoskeleton accordingly. The FLCA and MIMO SM controllers collaborate as an intelligent control system to AAN concept into practice on GAREX.

8.2 Outlook and future work

The author recommends two tracks for future works. One track is to develop more sophisticated control strategies for more effective gait rehabilitation. Being intrinsically compliant, the GAREX system is a good platform for implementing and testing various control strategies especially those to facilitate AAN trainings. The following paragraphs will have more specific discussion on further work could be done to advance the control systems.

As mentioned in the previous chapters, integrating ground reaction force sensing capability into GAREX could open new possibilities for control strategy development. The stance and swing phases of a gait cycle can be easily identified with GRF sensing. A straight-forward possible development it is to have different joint compliances for the stance and swing phases. The knee and hip joints' torque requirements are much higher during the stance phase than the swing phase due to the need to support bodyweight. Therefore, the exoskeleton could be controlled to be stiff during the stance phase and compliance during the swing phase. The FLCA controller (Chapter 7) could also be modified to have different settings for the stance and swing phases.

Bio-signals, such as electromyography (EMG), could be integrated into control systems for detecting the patient's intention and for assessing the patient's abilities. One possible implementation is to use EMG as an indication of the patient's participation level and make it one of the inputs to the FLCA controller. For example, one potential idea for integrate EMG into GAREX's control system is to use the patient-specific EMG-driven neuromuscular model by Ma et al [195]. The EMG-driven neuromuscular model allows the patient's joint torque to be

calculated in real-time during robotic gait training. This would make system better estimate the patient's ability or participating level in order to benefit AAN control development.

The other track of future works is the further system development towards clinical trials or applications. The current exoskeleton design is still an engineering prototype mainly for conducting research. A few design factors can be modified to implement the applicable requirements for clinical trials. When designing the current exoskeleton, it was aimed to build a robust working system in a short period of time. As a result, the current exoskeleton is not optimal in terms of weight, durability and user-friendliness. One of the advantages of the PM actuators is being lightweight and reducing the inertia of the exoskeleton, which thus leads to the increase in the controlled joint trajectory bandwidth of the robotic system. The current exoskeleton was designed with flat aluminium parts and machined steel parts for robustness and quick fabrication, but it also led to a heavy exoskeleton. Hence, the weight of the current design could be significantly trimmed by careful material selection and design analysis.

In clinical setting, the preparation time for experiments needs to be as quick as possible. Currently, the exoskeleton has a modular design and can be adjusted to fit anthropometric data of most of the population. Details about the adjustability have been covered in Section 3.2 and Section 3.3. However, the adjustments require time-consuming procedures including bolting and unbolting. Hence, mechanisms that allow easy adjustment are also worth researching in the future.

To prepare GAREX for clinical trials, it is also necessary to integrate a body weight support (BWS) system. The BWS system not only ensures the safety and stability of patient during gait rehabilitation training, but also can be used as means of adjusting assistance level [66]. Therefore, it is valuable to investigate the cooperation between the GAREX and BWS systems. GAREX currently has a unilateral exoskeleton. Once the redesign of the hardware system is completed, GAREX could be extended to a bi-lateral system, which can facilitate gait training on a larger variety of patients than a unilateral system.

8.3 Publications

This research has generated the following publications with the PhD candidate as the first author:

Journal articles:

- Cao, J., Xie, S.Q., Das, R. and Zhu, G.L., 2014. Control strategies for effective robot assisted gait rehabilitation: the state of art and future prospects. *Medical engineering & physics*, 36(12), pp.1555-1566. DOI: 10.1016/j.medengphy.2014.08.005.
- Cao, J., Xie, S.Q., and Das, R., 2017. MIMO Sliding Mode Controller for Gait Exoskeleton Driven by Pneumatic Muscles. *IEEE Transactions on Control Systems Technology* (In press) DOI: 10.1109/TCST.2017.2654424
- Cao, J., Zhang, M., McDaid, A. and Xie, S.Q., 2017. Design and control of a compliant Robotic GAit Rehabilitation EXoskeleton (GAREX), *IEEE Transactions on Mechatronics* (Under review).

Conference Papers:

- Cao, J., Xie, S.Q., Zhang, M. and Das, R., 2014, December. A new dynamic modelling algorithm for pneumatic muscle actuators. In *International Conference on Intelligent Robotics and Applications* (pp. 432-440). Springer International Publishing.
- Cao, J., Xie, S.Q., McDaid, A. and Das, R., 2015, August. Sliding Mode Control of an Exoskeleton Gait Rehabilitation Robot Driven by Pneumatic Muscle Actuators. In *ASME 2015 International Design Engineering Technical Conferences and Computers and Information in Engineering Conference*. American Society of Mechanical Engineers.

Appendices

Appendix A: Ethics Approval

A-1 Consent Form

CONSENT FOR PARTICIPATION IN RESEARCH PROJECT

THIS FORM WILL BE HELD FOR A PERIOD OF 6 YEARS

Project title: Design Validation of the Robotic Exoskeleton for Assist-as-needed Gait Rehabilitation

Names of Researchers: Shane Xie, Andrew McDaid and Jinghui Cao

- I have read the Participant Information Sheet and understood the nature of the research and why I have been selected. I have had the opportunity to ask questions and have them answered to my satisfaction. I understand that the participation is entirely voluntary.
- I agree to take part in this research of a robotic exoskeleton for gait rehabilitation for a single session up to two hours.
- I understand the commercial sensitivity of the device and that I will not talk to anyone other than the researchers about the device.
- I understand that there is a possible chance of injury to my leg (stretching muscles, tendons and ligaments) or to my body if the device malfunctions to cause falling. The safety measures have been explained to me such as the emergency turn off switch and design safety features. Also that there is a first aid kit in the trial room and a staff member available to assist in any medical situations.
- I understand that if a physical injury results from this study, ACC cover and entitlements are not automatic and my claim will be assessed by ACC in accordance with the Accident Compensation Act 2001. If my claim is accepted, ACC must inform me of my entitlements, and must help me access those entitlements. Entitlements may include, but not be limited to, treatment costs, travel costs for rehabilitation, loss of earnings, and/or lump sum for permanent impairment. Compensation for mental trauma may also be included, but only if this is incurred as a result of physical injury. There will be no direct compensation from The University of Auckland to me.
- I **agree / do not agree** to be videotaped (cross out what does not apply).
- I understand that I can ask the videotaping to be paused.
- I **wish / do not wish** the video recordings to be used in publications, thesis and presentations (cross out what does not apply).

- I **wish / do not wish** to have the videotapes destroyed after the completion of the research (cross out what does not apply).
- I understand that I am able to withdraw at any time during the trial. All data will be kept traceable by coding system linking data to participants until after the deadline for withdrawing data has expired, so all the data will be removed. The end date for withdraw of data is 18/07/2018.
- I understand that I am not an anonymous participant but in any reports or publications the findings will be presented in such a way that does not identify me as the source.
- I understand that data collected will be securely stored and only the Principal Investigator or the researchers will be able to access this information.
- I understand that data and video recordings will be kept for the duration of the research project. My data will be deleted after six years. Video files will be stored on hard drives which only the researchers and supervisor have access to.
- I wish / do not wish to receive a copy of the summary of the results of this trial (cross out what does not apply). Recipient email address: _____

Name _____

Signature _____

Date _____

APPROVED BY THE UNIVERSITY OF AUCKLAND HUMAN PARTICIPANTS ETHICS COMMITTEE ON 18/07/2015, FOR 3 YEARS. REFERENCE NUMBER: 014970.

A-2 Advertising poster

Robotic Exoskeleton Trial Invitation

Dear fellow postgraduate student:

You are invited to an evaluation trial of robotic for gait rehabilitation. It will be a single session trial of up to two hours. In this trial, you will strap on the lower limb exoskeleton and perform a few passive and active tasks either sitting on a chair or walking on a treadmill.

Participants' safety is the priority for us. The researchers have designed the exoskeleton system with safety as paramount. Our researchers will keep monitoring during your trial and ensure everything is in the right order.

If you are interested in enjoying the experience of being an "Iron-man", please contact the researcher with the below email address. We will send you more detailed information and arrange a trial time.

Thank you.

Jinghui (Brian) Cao

PhD candidate in mechanical engineering

Email: jcao027@aucklanduni.ac.nz

A-3 Participant information sheet

PARTICIPANT INFORMATION SHEET

(Participants)

Project Title

Design Validation of the Robotic Exoskeleton for Assist-as-needed Gait Rehabilitation

Researcher Introduction

This research will be conducted by Jinghui Cao who received Bachelor of Engineering with First Class Honours in Mechatronics and is currently a PhD Candidate in the Department of Mechanical Engineering. The research is supervised by Prof Shane Xie and co-supervised by Dr Andrew McDaid, who is a Lecturer, both of the Department of Mechanical Engineering.

Project Description and Invitation

An exoskeleton type of robotic gait rehabilitation device is under development to provide effective gait training for patients post stroke or spinal cord injury. The development involves designing and building a robotic gait training exoskeleton, implementing patient's ability assessment mechanism and automatic control strategies to encourage participants' voluntary involvement during training.

In conventional manual body weight support treadmill training, therapists guides the patient's impaired leg(s) to achieve designed movements to accomplish the walking task over the treadmill. In this project, the robotic exoskeleton has been designed and built to automate the training process. The exoskeleton will drive both hip and knee joints to reproduce leg movement in the joint space. Novel actuators instead of electric motors will be adopted for actuation. These actuators will provide soft actuation between the robot and human leg(s) to ensure no excessive guiding movements applied to the leg(s).

This study on subject without any gait disorder is acting as a validation of concept and design for the whole research. It is aimed to (1) check wearing comfort of the robotic exoskeleton; (2) evaluate the gait assessment system for subject's level of participation; (3) test the developed robot control strategies.

You are invited to participate in this research by carrying out a series of exercises with a prototype of the robotic gait rehabilitation device. Potential participants in this research are individuals who are over the age of 16 and have no gait disorder or other disabilities.

As a participant, you will be shown the experimental setup and the operation of the prototype prior to your commitment to participation in this research. Your identity will be kept confidential from third parties.

Project Procedures

You will only be required to take part in one session to help the research team test the developed rehabilitation device and control strategies. The duration of the session is expected to span approximately two hours or less. The experimental trials will be carried out in the Mechatronics Laboratory (Research) at the University of Auckland.

Before the experimental trial begins, you will be given an explanation of the operation of the robotic devices, in particular the implemented safety features to allow termination of the robot operation should an emergency situation arise. A brief demonstration of the prototype rehabilitation device will also be given. Your age, gender, body height and weight, dimensions of lower limb segments will also be collected for future data analysis.

After the briefing and collection of your information (age, gender, height, weight, dimensions of the lower limb), one of your lower limbs will be strapped in place to the prototype device. During the experimental trial, you firstly will be asked to sit on a chair with the exoskeleton strapped on. The exoskeletons will perform exercise to your knee joint by guiding your shank to move in desired trajectory. Secondly you will be asked to actively walk at a self-selected speed with the exoskeleton unactuated on a treadmill. The sensors will record both kinematic and kinetic information. In the third part of the session, you will need to walk passively with the guidance of the exoskeleton device in a speed selected by the researcher(s). During this part of the trial, you should relax the limb with the exoskeleton strapped on the robotic device and allow the robot to move your limb along a predefined motion path. During this time, sensor based information will be also be logged. Furthermore, you will be required to move your leg actively with the guidance of the exoskeleton. In this step, the robotic exoskeleton will perform in the same way as the last step and you are encouraged to actively participate in the test by moving your leg to follow the predefined robotic movement. A number of sensors will be utilized throughout the process of the trial, including force, position pressure sensors and possibly surface electromyography (EMG) sensors. None of these sensors will be invasive as they attached to the exoskeleton or body surface only. Cameras and/or motion capture system may also be used to collect relative information. After the trial, a questionnaire will be presented to you to evaluate your experience of the experimental session.

During the session, should the level of discomfort exceed that of your liking, you can terminate the experimental trial by either indicating to the researcher or by using the emergency stop button provided.

Data Storage/ Retention/ Destruction/ Future Use

Data will be recorded during the trials via computer, including the measurements of: position, velocity and acceleration of the leg movements and interaction forces between the leg and exoskeleton, as well as the history of EMG. Video of the participant trials will be recorded and a questionnaire will be used at the end to evaluate the trial. Additionally, your age, gender and body weight will also be recorded. All such data will be stored electronically on a hard drive of a computer. The computer will be password protected and located in a key accessed. The data will be stored in such a way that a third party will not be able to identify you through the information stored on the data file. The information collected will be kept for a period of up to six years as reference for current and possibly future research, which include, but not limited to presentations, conference and journal papers, theses, and device calibration. When no longer required, such data files will be destroyed through permanent deletion.

Right to Withdraw from Participation

If the participants are not comfortable with the data collected, they can request to withdraw the data within one week from the end of the participation. The end date of data withdraw is 18/07/2018.

All data collected will be viewable for the participant for 24 hours after the trial, if he/she desire to do so. The participant can request to withdraw any data that they feel uncomfortable with the recorded data at that time. After which the data will only be available to the researcher and supervisors.

Use of Audio, Electronic or Other Media

Video recordings of the trial will be recorded, but the participant is able to request that the recording is to be stopped at any time during the trial.

The participant can review the video recording at the end and within 24 hours of the trial and request any editing that needs to be done for their satisfaction. After which only the researcher and supervisors are able to view the video. The video data will be used to improve the design and tuning the device for better results. The video recordings can also be used in publications, theses and presentations. However, participants can choose the video not to be used for these purposes.

Due to the commercial sensitivity of the gait rehabilitation platform, you will not be offered to a copy of the videos recorded.

Anonymity and Confidentiality

Your identity will be kept confidential from all third parties. If the data collected is used in publications, you will be referred to using a generic identifier such as “participant A”.

As videos or photographs recorded will contain items of clothing you are wearing at the time of the trial, anonymity may not be guaranteed. However, recordings will be performed in the manner as to minimise the risk of identification.

During the experiment your name will not be recorded. Instead a coding system (RGL000 – RGL999) will be used to linked experimental data and the questionnaire to a specific participant.

Distress and Discomfort

The robotic exoskeleton is designed with safety as paramount. In terms of hardware, mechanical stopping features have been designed to prevent hyper-extend of lower limb joints; stop buttons are accessible to both participants and researchers. Once a stop button is pressed, the actuation will be immediately terminated from various stages of the system in case of the malfunction of some part of the system. In terms of software, the designed user interface enables the researcher to real-time monitor the operation of the system to ensure everything is in the right order. Kinematic and forces parameter is also monitored by the software; should any parametric threshold is exceeded, the software will de-activate the actuators of the robot.

If the participant shows any distress or discomfort, the trial can be stopped immediately, until participant is willing to continue. The participant will have the access to an emergency shut off switch which allows immediate termination of the experiment should the participant becomes uncomfortable with the trial. If participant is unwilling to continue then the trial will be cancelled. The participants have the right to withdraw at any time during the trial. The researchers (supervisors and students) and physiotherapist will try to sort any discomfort with the device out. A first aid kit will be in the room while the trial is taking place.

Adverse Consequences and Compensation for Injury

Although many safety measures have been placed such as the emergency turn off switch and other designed safety features, there is still a possible chance of injury to participant's leg (stretching muscles, tendons and ligaments) or to their body if the device malfunctions to cause falling of the participant.

If physical injury results from your participation in this study, you should visit a treatment provider to make a claim to ACC as soon as possible. ACC covers and entitlements are not automatic and your claim will be assessed by ACC in accordance with the Accident Compensation Act 2001. If your claim is accepted, ACC must inform you of your entitlements, and must help you access those entitlements. Entitlements may include, but not be limited to, treatment costs, travel costs for rehabilitation, loss of earnings, and/or lump sum for permanent impairment. Compensation for mental trauma may also be included, but only if this is incurred as a result of physical injury. There will be no direct compensation from The University of Auckland to you.

Commercial sensitivity

There is a possibility that the developed gait rehabilitation device will be commercialized. As a result, you are asked not to talk about the device and the experiment to anyone other than the researcher and supervisors.

Closing Statement

If there is anything that you would like to discuss please contact one of the following

Researcher Jinghui Cao Email: jcao027@aucklanduni.ac.nz Phone: (09) 373-7599 extn. 87555	Supervisor Prof. Shane Xie Email: s.xie@auckland.ac.nz Phone: (09) 373-7599 extn. 88143
Co-supervisor Dr. Andrew McDaid Email: andrew.mcdaid@auckland.ac.nz Phone: +64 9 923 1898	Head of Department Prof. Brian Mace Email: b.mace@auckland.ac.nz Phone: (09) 373-7599 extn. 88148

For any concerns regarding ethical issue, you may contact the Chair, University of Auckland Human Participants Ethics Committee, The University of Auckland, Research Office, Private Bag, 92019, Auckland, 1142. Phone: (09)373 7599 ext.83711; email ro-ethics@auckland.ac.nz

APPROVED BY THE UNIVERSITY OF AUCKLAND HUMAN PARTICIPANTS ETHICS COMMITTEE
ON 18/07/2015 FOR 3 YEARS, REFERENCE NUMBER: 014970

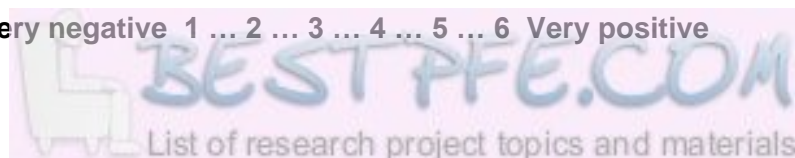
A-4 Questionnaire

Questionnaire for “Design Validation of the Robotic Exoskeleton for Assist-as-needed Gait Rehabilitation”

Participant identifier RGL-

- Question 1** I experienced discomfort during the trial.
Strongly disagree 1 ... 2 ... 3 ... 4 ... 5 ... 6 Strongly agree
- Question 2** I feel safe during the trial.
Strongly disagree 1 ... 2 ... 3 ... 4 ... 5 ... 6 Strongly agree
- Question 3** I still have freedom during the passive training. (Robot guiding training)
Strongly disagree 1 ... 2 ... 3 ... 4 ... 5 ... 6 Strongly agree
- Question 4** The robot is not limiting my walking during the free walking trial. (Robotic is not guiding)
Strongly disagree 1 ... 2 ... 3 ... 4 ... 5 ... 6 Strongly agree
- Question 5** The device looks attractive.
Strongly disagree 1 ... 2 ... 3 ... 4 ... 5 ... 6 Strongly agree
- Question 6** The device was noisy.
Strongly disagree 1 ... 2 ... 3 ... 4 ... 5 ... 6 Strongly agree
- Question 7** My hip movements are not obstructed during the trial.
Strongly disagree 1 ... 2 ... 3 ... 4 ... 5 ... 6 Strongly agree
- Question 8** The device is not obstructing my upper limbs' movements during the trial.
Strongly disagree 1 ... 2 ... 3 ... 4 ... 5 ... 6 Strongly agree
- Question 9** I believe train with this device will be interesting.
Strongly disagree 1 ... 2 ... 3 ... 4 ... 5 ... 6 Strongly agree
- Question 10** My overall impression of this device is

Very negative 1 ... 2 ... 3 ... 4 ... 5 ... 6 Very positive



Comments:

Issues that you had with the device during the trial

Potential issues that you believe could arise?

What would you suggest to improve?

Other comments on the device

APPROVED BY THE UNIVERSITY OF AUCKLAND HUMAN PARTICIPANTS ETHICS COMMITTEE
ON 18/07/2015 FOR 3 YEARS, REFERENCE NUMBER: 014970

References

- [1] stroke.org.nz. (January 12th, 2017). *Facts and fallacies*. Available: <http://www.stroke.org.nz/stroke-facts-and-fallacies>
- [2] V. L. Roger, A. S. Go, D. M. Lloyd-Jones, E. J. Benjamin, J. D. Berry, W. B. Borden, *et al.*, "Heart Disease and Stroke Statistics—2012 Update A Report From the American Heart Association," *Circulation*, vol. 125, pp. e2-e220, 2012.
- [3] P. W. Duncan, "Stroke disability," *Physical Therapy*, vol. 74, pp. 399-407, 1994.
- [4] W. H. Organization. (20, September). *The Atlas of Heart Disease and Stroke*. Available: http://www.who.int/cardiovascular_diseases/resources/atlas/en/
- [5] R. Bonita and R. Beaglehole, "Recovery of motor function after stroke," *Stroke*, vol. 19, pp. 1497-1500, 1988.
- [6] M. Kelly-Hayes, A. Beiser, C. S. Kase, A. Scaramucci, R. B. D'Agostino, and P. A. Wolf, "The influence of gender and age on disability following ischemic stroke: the Framingham study," *Journal of Stroke and Cerebrovascular Diseases*, vol. 12, pp. 119-126, 2003.
- [7] N. Sharma, J. Classen, and L. G. Cohen, "Neural plasticity and its contribution to functional recovery," in *Handbook of Clinical Neurology*. vol. 110, M. P. Barnes and D. C. Good, Eds., ed, 2013, pp. 3-12.
- [8] E. J. Plautz, G. W. Milliken, and R. J. Nudo, "Effects of repetitive motor training on movement representations in adult squirrel monkeys: role of use versus learning," *Neurobiology of learning and memory*, vol. 74, pp. 27-55, 2000.
- [9] R. Riener, L. Lunenburger, S. Jezernik, M. Anderschitz, G. Colombo, and V. Dietz, "Patient-cooperative strategies for robot-aided treadmill training: first experimental results," *Neural Systems and Rehabilitation Engineering, IEEE Transactions on*, vol. 13, pp. 380-394, 2005.
- [10] M. Pohl, C. Werner, M. Holzgraefe, G. Kroczeck, I. Wingendorf, G. Hoölig, *et al.*, "Repetitive locomotor training and physiotherapy improve walking and basic activities of daily living after stroke: a single-blind, randomized multicentre trial (DEutsche GANgrainerStudie, DEGAS)," *Clinical Rehabilitation*, vol. 21, pp. 17-27, 2007.
- [11] L. L. Cai, A. J. Fong, C. K. Otsoshi, Y. Liang, J. W. Burdick, R. R. Roy, *et al.*, "Implications of assist-as-needed robotic step training after a complete spinal cord injury on intrinsic strategies of motor learning," *The Journal of neuroscience*, vol. 26, pp. 10564-10568, 2006.
- [12] M. Lotze, C. Braun, N. Birbaumer, S. Anders, and L. G. Cohen, "Motor learning elicited by voluntary drive," *Brain*, vol. 126, pp. 866-872, 2003.
- [13] A. Kaelin-Lang, L. Sawaki, and L. G. Cohen, "Role of voluntary drive in encoding an elementary motor memory," *Journal of neurophysiology*, vol. 93, pp. 1099-1103, 2005.
- [14] H. Vallery, J. Veneman, E. van Asseldonk, R. Ekkelenkamp, M. Buss, and H. van Der Kooij, "Compliant actuation of rehabilitation robots," *Robotics & Automation Magazine, IEEE*, vol. 15, pp. 60-69, 2008.

References

- [15] J. F. Veneman, R. Kruidhof, E. E. G. Hekman, R. Ekkelenkamp, E. H. F. Van Asseldonk, and H. van der Kooij, "Design and Evaluation of the LOPES Exoskeleton Robot for Interactive Gait Rehabilitation," *Neural Systems and Rehabilitation Engineering, IEEE Transactions on*, vol. 15, pp. 379-386, 2007.
- [16] D. Aoyagi, W. E. Ichinose, S. J. Harkema, D. J. Reinkensmeyer, and J. E. Bobrow, "A Robot and Control Algorithm That Can Synchronously Assist in Naturalistic Motion During Body-Weight-Supported Gait Training Following Neurologic Injury," *Neural Systems and Rehabilitation Engineering, IEEE Transactions on*, vol. 15, pp. 387-400, 2007.
- [17] T.-Y. Choi and J.-J. Lee, "Control of manipulator using pneumatic muscles for enhanced safety," *Industrial Electronics, IEEE Transactions on*, vol. 57, pp. 2815-2825, 2010.
- [18] D. P. Ferris, J. M. Czerniecki, B. Hannaford, U. of Washington, and V. P. S. H. System, "An ankle-foot orthosis powered by artificial pneumatic muscles," *Journal of Applied Biomechanics*, vol. 21, p. 189, 2005.
- [19] S. Hussain, S. Q. Xie, P. K. Jamwal, and J. Parsons, "An intrinsically compliant robotic orthosis for treadmill training," *Medical Engineering & Physics*, vol. 34, pp. 1448-1453, 2012.
- [20] P. Beyl, K. Knaepen, S. Duerinck, M. Van Damme, B. Vanderborght, R. Meeusen, *et al.*, "Safe and Compliant Guidance by a Powered Knee Exoskeleton for Robot-Assisted Rehabilitation of Gait," *Advanced Robotics*, vol. 25, pp. 513-535, 2011.
- [21] S. Hussain, S. Q. Xie, and P. K. Jamwal, "Control of a robotic orthosis for gait rehabilitation," *Robotics and Autonomous Systems*, vol. 61, pp. 911-919, 2013.
- [22] S. Hussain, S. Q. Xie, and P. K. Jamwal, "Robust Nonlinear Control of an Intrinsically Compliant Robotic Gait Training Orthosis," *Systems, Man, and Cybernetics: Systems, IEEE Transactions on*, vol. 43, pp. 655-665, 2013.
- [23] S. Hussain, S. Q. Xie, and P. K. Jamwal, "Adaptive Impedance Control of a Robotic Orthosis for Gait Rehabilitation," *Cybernetics, IEEE Transactions on*, vol. 43, pp. 1025-1034, 2012.
- [24] S. Hussain, P. Jamwal, M. Ghayesh, and S. Xie, "Assist-as-Needed Control of an Intrinsically Compliant Robotic Gait Training Orthosis," *IEEE Transactions on Industrial Electronics*, vol. PP, pp. 1-1, 2016.
- [25] K. Kora, A. McDaid, and S. Xie, "Non-linear model-based Control for the Human-inspired Robotic Exoskeleton (HuREx) gait trainer," in *World Congress of the International Federation of Automatic Control, Cape Town, South Africa*, 2014.
- [26] T. Kitago and J. W. Krakauer, "Motor learning principles for neurorehabilitation," in *Handbook of Clinical Neurology*. vol. 110, M. P. Barnes and D. C. Good, Eds., ed, 2013, pp. 93-103.
- [27] J. H. Carr, R. B. Shepherd, J. Gordon, A. Gentile, and J. M. Held, *Movement science: Foundations for physical therapy in rehabilitation*: Aspen Publishers, 1987.
- [28] J. W. Krakauer, "Motor learning: its relevance to stroke recovery and neurorehabilitation," *Current opinion in neurology*, vol. 19, pp. 84-90, 2006.
- [29] R. A. Schmidt and T. D. Lee, *Motor control and learning: A behavioral emphasis*: Human Kinetics, 2011.

References

- [30] R. Nudo, "Adaptive plasticity in motor cortex: implications for rehabilitation after brain injury," *Journal of Rehabilitation Medicine-Supplements*, pp. 7-10, 2003.
- [31] N. A. Bayona, J. Bitensky, K. Salter, and R. Teasell, "The role of task-specific training in rehabilitation therapies," *Topics in stroke rehabilitation*, vol. 12, pp. 58-65, 2005.
- [32] C. H. Shea and R. M. Kohl, "Composition of practice: Influence on the retention of motor skills," *Research Quarterly for Exercise and Sport*, vol. 62, pp. 187-195, 1991.
- [33] R. Bogey and G. T. Hornby, "Gait training strategies utilized in poststroke rehabilitation: are we really making a difference?," *Topics in stroke rehabilitation*, vol. 14, pp. 1-8, 2007.
- [34] M. F. Levin, J. A. Kleim, and S. L. Wolf, "What do motor "recovery" and "compensation" mean in patients following stroke?," *Neurorehabilitation and Neural Repair*, vol. 23, pp. 313-319, 2009.
- [35] M. F. Levin, "Should stereotypic movement synergies in hemiparetic patients be considered adaptive?," *Behavioral and Brain Sciences*, vol. 19, pp. 79-80, 1996.
- [36] E. Taub, N. Miller, T. Novack, E. Cook 3rd, W. Fleming, C. Nepomuceno, *et al.*, "Technique to improve chronic motor deficit after stroke," *Archives of physical medicine and rehabilitation*, vol. 74, p. 347, 1993.
- [37] M. Alaverdashvili, A. Foroud, D. H. Lim, and I. Q. Whishaw, "" Learned baduse" limits recovery of skilled reaching for food after forelimb motor cortex stroke in rats: A new analysis of the effect of gestures on success," *Behavioural brain research*, 2008.
- [38] S. L. Ashburn, Ann, "The Bobath concept in stroke rehabilitation: a focus group study of the experienced physiotherapists' perspective," *Disability & Rehabilitation*, vol. 22, pp. 665-674, 2000.
- [39] S. Hesse, "Locomotor therapy in neurorehabilitation," *NeuroRehabilitation*, vol. 16, pp. 133-139, 2001.
- [40] C. M. Sackley and N. B. Lincoln, "Physiotherapy treatment for stroke patients: a survey of current practice," *Physiotherapy Theory and Practice*, vol. 12, pp. 87-96, 1996.
- [41] B. Bobath, *Adult hemiplegia: evaluation and treatment*: Butterworth-Heinemann Oxford, 1990.
- [42] M. P. Kilgard and M. M. Merzenich, "Cortical map reorganization enabled by nucleus basalis activity," *Science*, vol. 279, pp. 1714-1718, 1998.
- [43] J. Classen, J. Liepert, S. P. Wise, M. Hallett, and L. G. Cohen, "Rapid plasticity of human cortical movement representation induced by practice," *Journal of neurophysiology*, vol. 79, pp. 1117-1123, 1998.
- [44] L. G. Ungerleider, "Functional MRI evidence for adult motor cortex plasticity during motor skill learning," *Nature*, vol. 377, pp. 155-158, 1995.
- [45] B. Langhammer and J. K. Stanghelle, "Bobath or motor relearning programme? A comparison of two different approaches of physiotherapy in stroke rehabilitation: a randomized controlled study," *Clinical Rehabilitation*, vol. 14, pp. 361-369, 2000.
- [46] B. Langhammer and J. K. Stanghelle, "Bobath or motor relearning programme? A follow-up one and four years post stroke," *Clinical Rehabilitation*, vol. 17, pp. 731-734, 2003.

References

- [47] H. Barbeau, M. Wainberg, and L. Finch, "Description and application of a system for locomotor rehabilitation," *Medical and Biological Engineering and Computing*, vol. 25, pp. 341-344, 1987/05/01 1987.
- [48] S. Hesse, C. Bertelt, M. Jahnke, A. Schaffrin, P. Baake, M. Malezic, *et al.*, "Treadmill training with partial body weight support compared with physiotherapy in nonambulatory hemiparetic patients," *Stroke*, vol. 26, pp. 976-981, 1995.
- [49] S. Hesse, M. Malezic, A. Schaffrin, and K. Mauritz, "Restoration of gait by combined treadmill training and multichannel electrical stimulation in non-ambulatory hemiparetic patients," *Scandinavian journal of rehabilitation medicine*, vol. 27, p. 199, 1995.
- [50] G. Colombo, M. Joerg, R. Schreier, and V. Dietz, "Treadmill training of paraplegic patients using a robotic orthosis," *Journal of Rehabilitation Research and Development*, vol. 37, pp. 693-700, 2000.
- [51] L. Lunenburger, G. Colombo, and R. Riener, "Biofeedback for robotic gait rehabilitation," *Journal of NeuroEngineering and Rehabilitation*, vol. 4, 2007.
- [52] A. Koenig, X. Omlin, J. Bergmann, L. Zimmerli, M. Bolliger, F. Müller, *et al.*, "Controlling patient participation during robot assisted gait training," *Journal of NeuroEngineering & Rehabilitation (JNER)*, vol. 8, pp. 14-25, 2011.
- [53] D. G. Liebermann, A. S. Buchman, and I. M. Franks, "Enhancement of motor rehabilitation through the use of information technologies," *Clinical Biomechanics*, vol. 21, pp. 8-20, 2006.
- [54] S. Hesse and D. Uhlenbrock, "A mechanized gait trainer for restoration of gait," *Journal of Rehabilitation Research and Development*, vol. 37, p. 701.
- [55] H. Schmidt, C. Werner, R. Bernhardt, S. Hesse, and J. Krüger, "Gait rehabilitation machines based on programmable footplates," *Journal of NeuroEngineering & Rehabilitation (JNER)*, vol. 4, pp. 2-7, 2007.
- [56] H. Schmidt, S. Hesse, R. Bernhardt, and J. Krüger, "HapticWalker---a novel haptic foot device," *ACM Transactions on Applied Perception (TAP)*, vol. 2, pp. 166-180, 2005.
- [57] S. Hesse, A. Waldner, and C. Tomelleri, "Innovative gait robot for the repetitive practice of floor walking and stair climbing up and down in stroke patients," *Journal of NeuroEngineering & Rehabilitation (JNER)*, vol. 7, pp. 30-39, 2010.
- [58] J. Yoon and J. Ryu, "A novel locomotion interface with two 6-dof parallel manipulators that allows human walking on various virtual terrains," *The International Journal of Robotics Research*, vol. 25, pp. 689-708, 2006.
- [59] J. Yoon, B. Novandy, C. H. Yoon, and K. J. Park, "A 6-DOF gait rehabilitation robot with upper and lower limb connections that allows walking velocity updates on various terrains," *IEEE/ASME Transactions on Mechatronics*, vol. 15, pp. 201-215, 2010.
- [60] B. Novandy, J. Yoon, and A. Manurung, "Interaction control of a programmable footpad-type gait rehabilitation robot for active walking on various terrains," 2009, pp. 372-377.
- [61] M. Peshkin, D. A. Brown, J. J. Santos-Munne, A. Makhlin, E. Lewis, J. E. Colgate, *et al.*, "KineAssist: a robotic overground gait and balance training device," in *Rehabilitation Robotics, 2005. ICORR 2005. 9th International Conference on*, 2005, pp. 241-246.

References

- [62] A. Morbi, M. Ahmadi, and A. Nativ, "GaitEnable: An omnidirectional robotic system for gait rehabilitation," in *Mechatronics and Automation (ICMA), International Conference on Chengdu 2012*, pp. 936-941.
- [63] M. Bouri, Y. Stauffer, C. Schmitt, Y. Allemand, S. Gnemmi, R. Clavel, *et al.*, "The WalkTrainer (TM): A robotic system for walking rehabilitation," in *2006 IEEE International Conference on Robotics and Biomimetics, Vols 1-3*, ed, 2006, pp. 1616-1621.
- [64] P. Wang, A. H. McGregor, A. Tow, H. B. Lim, L. S. Khang, K. H. Low, *et al.*, "Rehabilitation Control Strategies for a Gait Robot via EMG Evaluation," in *2009 IEEE 11th International Conference on Rehabilitation Robotics, Vols 1 and 2*, ed, 2009, pp. 100-105.
- [65] P. Wang, K. H. Low, A. Tow, and P. H. Lim, "Initial System Evaluation of an Overground Rehabilitation Gait Training Robot (NaTure-gaits)," *Advanced Robotics*, vol. 25, pp. 1927-1948, 2011.
- [66] M. Frey, G. Colombo, M. Vaglio, R. Bucher, M. Jorg, and R. Riener, "A Novel Mechatronic Body Weight Support System," *Neural Systems and Rehabilitation Engineering, IEEE Transactions on*, vol. 14, pp. 311-321, 2006.
- [67] S. K. Banala, S. K. Agrawal, and J. P. Scholz, "Active Leg Exoskeleton (ALEX) for Gait Rehabilitation of Motor-Impaired Patients," in *Rehabilitation Robotics, 2007. ICORR 2007. IEEE 10th International Conference on*, 2007, pp. 401-407.
- [68] S. K. Banala, K. Seok Hun, S. K. Agrawal, and J. P. Scholz, "Robot Assisted Gait Training With Active Leg Exoskeleton (ALEX)," *Neural Systems and Rehabilitation Engineering, IEEE Transactions on*, vol. 17, pp. 2-8, 2009.
- [69] S. K. Banala, S. K. Agrawal, A. Fattah, V. Krishnamoorthy, W.-L. Hsu, J. Scholz, *et al.*, "Gravity-balancing leg orthosis and its performance evaluation," *Robotics, IEEE Transactions on*, vol. 22, pp. 1228-1239, 2006.
- [70] J. F. Veneman, R. Ekkelenkamp, R. Kruidhof, F. C. T. van der Helm, and H. van der Kooij, "A Series Elastic- and Bowden- Cable-Based Actuation System for Use as Torque Actuator in Exoskeleton-Type Robots," *International Journal of Robotics Research*, vol. 25, pp. 261-281, 2006.
- [71] R. J. Adams and B. Hannaford, "Control law design for haptic interfaces to virtual reality," *Control Systems Technology, IEEE Transactions on*, vol. 10, pp. 3-13, 2002.
- [72] D. Reinkensmeyer, J. H. Wynne, and S. J. Harkema, "A robotic tool for studying locomotor adaptation and rehabilitation," in *Engineering in Medicine and Biology, 2002. 24th Annual Conference and the Annual Fall Meeting of the Biomedical Engineering Society EMBS/BMES Conference, 2002. Proceedings of the Second Joint*, 2002, pp. 2353-2354 vol.3.
- [73] J. L. Emken, J. H. Wynne, S. J. Harkema, and D. J. Reinkensmeyer, "A robotic device for manipulating human stepping," *Robotics, IEEE Transactions on*, vol. 22, pp. 185-189, 2006.
- [74] D. Campolo, D. Accoto, D. Formica, and E. Guglielmelli, "Intrinsic constraints of neural origin: assessment and application to rehabilitation robotics," *Robotics, IEEE Transactions on*, vol. 25, pp. 492-501, 2009.
- [75] M. Wu, T. G. Hornby, J. M. Landry, H. Roth, and B. D. Schmit, "A cable-driven locomotor training system for restoration of gait in human SCI," *Gait & Posture*, vol. 33, pp. 256-260, 2011.

References

- [76] W. E. Ichinose, D. J. Reinkensmeyer, D. Aoyagi, J. T. Lin, K. Ngai, R. V. Edgerton, *et al.*, "A robotic device for measuring and controlling pelvic motion during locomotor rehabilitation," in *Engineering in Medicine and Biology Society, 2003. Proceedings of the 25th Annual International Conference of the IEEE*, 2003, pp. 1690-1693 Vol.2.
- [77] J. Wu, J. Gao, R. Song, R. Li, Y. Li, and L. Jiang, "The design and control of a 3DOF lower limb rehabilitation robot," *Mechatronics*, vol. 33, pp. 13-22, 2// 2016.
- [78] T. G. Sugar, J. He, E. J. Koeneman, J. B. Koeneman, R. Herman, H. Huang, *et al.*, "Design and control of RUPERT: a device for robotic upper extremity repetitive therapy," *IEEE Transactions on Neural Systems and Rehabilitation Engineering*, vol. 15, pp. 336-346, 2007.
- [79] J. Meuleman, J. Meuleman, E. H. F. v. Asseldonk, and H. v. d. Kooij, "Novel actuation design of a gait trainer with shadow leg approach," in *Rehabilitation Robotics (ICORR), 2013 IEEE International Conference on*, 2013, pp. 1-8.
- [80] D. J. Reinkensmeyer, D. Aoyagi, J. L. Emken, and J. A. Galvez, "Tools for understanding and optimizing robotic gait training," *Journal of rehabilitation research and development*, vol. 43, p. 657, 2006.
- [81] S. Hussain, "Design and assist-as-needed control of an intrinsically compliant robotic orthosis for gait rehabilitation," ResearchSpace@ Auckland, 2012.
- [82] D. Aoyagi, W. Ichinose, D. Reinkensmeyer, and J. Bobrow, "Human step rehabilitation using a robot attached to the pelvis," in *Proceedings of the 2004 American Society of Mechanical Engineers (ASME) International Mechanical Engineering Congress and Research Development and Design Exposition*, 2004, pp. 13-19.
- [83] J. Hidler, W. Wisman, and N. Neckel, "Kinematic trajectories while walking within the Lokomat robotic gait-orthosis," *Clinical Biomechanics*, vol. 23, pp. 1251-1259, 2008.
- [84] L. E. Kahn, P. S. Lum, W. Z. Rymer, and D. J. Reinkensmeyer, "Robot-assisted movement training for the stroke-impaired arm: Does it matter what the robot does?," *Journal of Rehabilitation Research and Development*, vol. 43, p. 619, 2006.
- [85] H. Vallery, R. Ekkelenkamp, M. Buss, and H. van der Kooij, "Complementary limb motion estimation based on interjoint coordination: Experimental evaluation," in *Rehabilitation Robotics, 2007. ICORR 2007. IEEE 10th International Conference on*, 2007, pp. 798-803.
- [86] H. Vallery, E. H. van Asseldonk, M. Buss, and H. van der Kooij, "Reference trajectory generation for rehabilitation robots: complementary limb motion estimation," *Neural Systems and Rehabilitation Engineering, IEEE Transactions on*, vol. 17, pp. 23-30, 2009.
- [87] L. M. Crespo and D. J. Reinkensmeyer, "Haptic guidance can enhance motor learning of a steering task," *Journal of motor behavior*, vol. 40, pp. 545-557, 2008.
- [88] L. Marchal-Crespo and D. J. Reinkensmeyer, "Review of control strategies for robotic movement training after neurologic injury," *Journal of NeuroEngineering and Rehabilitation*, vol. 6, p. 20, 2009.
- [89] M. K. Holden, "Virtual environments for motor rehabilitation: review," *Cyberpsychology & behavior*, vol. 8, pp. 187-211, 2005.

References

- [90] A. Mirelman, P. Bonato, and J. E. Deutsch, "Effects of training with a robot-virtual reality system compared with a robot alone on the gait of individuals after stroke," *Stroke*, vol. 40, pp. 169-174, 2009.
- [91] R. Banz, M. Bolliger, G. Colombo, V. Dietz, and L. Lünenburger, "Computerized visual feedback: an adjunct to robotic-assisted gait training," *Physical Therapy*, vol. 88, pp. 1135-1145, 2008.
- [92] A. Koenig, D. Novak, X. Omlin, M. Pulfer, E. Perreault, L. Zimmerli, *et al.*, "Real-time closed-loop control of cognitive load in neurological patients during robot-assisted gait training," *Neural Systems and Rehabilitation Engineering, IEEE Transactions on*, vol. 19, pp. 453-464, 2011.
- [93] A. Koenig, X. Omlin, L. Zimmerli, M. Sapa, C. Krewer, M. Bolliger, *et al.*, "Psychological state estimation from physiological recordings during robot assisted gait rehabilitation," *J. Rehabil. Res. Develop*, vol. 48, pp. 367-386, 2011.
- [94] N. Hogan, "Impedance control: An approach to manipulation: Part I applications," *Journal of dynamic systems, measurement, and control*, vol. 107, p. 17, 1985.
- [95] S. K. Banala, S. K. Agrawal, S. H. Kim, and J. P. Scholz, "Novel Gait Adaptation and Neuromotor Training Results Using an Active Leg Exoskeleton," *IEEE/ASME Transactions on Mechatronics*, vol. 15, pp. 216-225, 2010.
- [96] A. Duschau-Wicke, J. von Zitzewitz, A. Caprez, L. Lunenburger, and R. Riener, "Path Control: A Method for Patient-Cooperative Robot-Aided Gait Rehabilitation," *IEEE Transactions on Neural Systems and Rehabilitation Engineering*, vol. 18, pp. 38-48, Feb 2010.
- [97] S. Hussein, H. Schmidt, and J. Kruger, "Adaptive control of an end-effector based electromechanical gait rehabilitation device," in *Rehabilitation Robotics, 2009. ICORR 2009. IEEE International Conference on*, 2009, pp. 366-371.
- [98] S. Jezernik, G. Colombo, and M. Morari, "Automatic gait-pattern adaptation algorithms for rehabilitation with a 4-DOF robotic orthosis," *IEEE Transactions on Robotics and Automation*, vol. 20, pp. 574-582, Jun 2004.
- [99] S. Jezernik and M. Morari, "Controlling the human-robot interaction for robotic rehabilitation of locomotion," in *Advanced Motion Control, 2002. 7th International Workshop on*, 2002, pp. 133-135.
- [100] R. Banz, M. Bolliger, S. Muller, C. Santelli, and R. Riener, "A method of estimating the degree of active participation during stepping in a driven gait orthosis based on actuator force profile matching," *Neural Systems and Rehabilitation Engineering, IEEE Transactions on*, vol. 17, pp. 15-22, 2009.
- [101] I. Schwartz, A. Sajin, I. Fisher, M. Neeb, M. Shochina, M. Katz-Leurer, *et al.*, "The effectiveness of locomotor therapy using robotic-assisted gait training in subacute stroke patients: a randomized controlled trial," *PM & R : the journal of injury, function, and rehabilitation*, vol. 1, pp. 516-23, Jun 2009.
- [102] J. Hidler, D. Nichols, M. Pelliccio, K. Brady, D. D. Campbell, J. H. Kahn, *et al.*, "Multicenter randomized clinical trial evaluating the effectiveness of the Lokomat in subacute stroke," *Neurorehabilitation and Neural Repair*, vol. 23, pp. 5-13, Jan 2009.

References

- [103] M. F. Ng, R. K. Tong, and L. S. Li, "A pilot study of randomized clinical controlled trial of gait training in subacute stroke patients with partial body-weight support electromechanical gait trainer and functional electrical stimulation: six-month follow-up," *Stroke; a journal of cerebral circulation*, vol. 39, pp. 154-60, Jan 2008.
- [104] S. Fisher, L. Lucas, and T. A. Thrasher, "Robot-assisted gait training for patients with hemiparesis due to stroke," *Topics in stroke rehabilitation*, vol. 18, pp. 269-76, May-Jun 2011.
- [105] M. E. Tinetti, "Performance-oriented assessment of mobility problems in elderly patients," *Journal of the American Geriatrics Society*, 1986.
- [106] S. H. Peurala, I. M. Tarkka, K. Pitkänen, and J. Sivenius, "The Effectiveness of Body Weight-Supported Gait Training and Floor Walking in Patients With Chronic Stroke," *Archives of physical medicine and rehabilitation*, vol. 86, pp. 1557-1564, 2005.
- [107] S. H. Peurala, O. Airaksinen, P. Huuskonen, P. Jakala, M. Juhakoski, K. Sandell, *et al.*, "Effects of intensive therapy using gait trainer or floor walking exercises early after stroke," *Journal of Rehabilitation Medicine*, vol. 41, pp. 166-173, 2009.
- [108] B. Husemann, F. Müller, C. Krewer, S. Heller, and E. Koenig, "Effects of locomotion training with assistance of a robot-driven gait orthosis in hemiparetic patients after stroke a randomized controlled pilot study," *Stroke*, vol. 38, pp. 349-354, 2007.
- [109] W. H. Chang, M. S. Kim, J. P. Huh, P. K. W. Lee, and Y.-H. Kim, "Effects of Robot-Assisted Gait Training on Cardiopulmonary Fitness in Subacute Stroke Patients: A Randomized Controlled Study," *Neurorehabilitation and Neural Repair*, vol. 26, pp. 318-324, 2012.
- [110] T. G. Hornby, D. D. Campbell, J. H. Kahn, T. Demott, J. L. Moore, and H. R. Roth, "Enhanced gait-related improvements after therapist- versus robotic-assisted locomotor training in subjects with chronic stroke: a randomized controlled study," *Stroke; a journal of cerebral circulation*, vol. 39, pp. 1786-92, 2008.
- [111] K. P. Westlake and C. Patten, "Pilot study of Lokomat versus manual-assisted treadmill training for locomotor recovery post-stroke," *Journal of NeuroEngineering and Rehabilitation*, vol. 6, p. 18, 2009.
- [112] A. Mayr, M. Kofler, E. Quirbach, H. Matzak, K. Frohlich, and L. Saltuari, "Prospective, blinded, randomized crossover study of gait rehabilitation in stroke patients using the Lokomat gait orthosis," *Neurorehabilitation and Neural Repair*, vol. 21, pp. 307-14, Jul-Aug 2007.
- [113] S. Jezernik, R. Scharer, G. Colombo, and M. Morari, "Adaptive robotic rehabilitation of locomotion: a clinical study in spinally injured individuals," *Spinal Cord*, vol. 41, pp. 657-66, Dec 2003.
- [114] A. Duschau-Wicke, A. Caprez, and R. Riener, "Patient-cooperative control increases active participation of individuals with SCI during robot-aided gait training," *Journal of neuroengineering and rehabilitation*, vol. 7, pp. 43-43, 2010.
- [115] A. Schüick, R. Labruyère, H. Vallery, R. Riener, and A. Duschau-Wicke, "Feasibility and effects of patient-cooperative robot-aided gait training applied in a 4-week pilot trial," *Journal of NeuroEngineering & Rehabilitation (JNER)*, vol. 9, pp. 31-44, 2012.
- [116] B. Fleerkotte, J. Buurke, B. Koopman, L. Schaake, H. Kooij, E. F. Asseldonk, *et al.*, "Effectiveness of the Lower Extremity Powered ExoSkeleton (LOPES) Robotic Gait Trainer on Ability and Quality of Walking in SCI Patients," in *Converging Clinical and Engineering*

References

- Research on Neurorehabilitation*. vol. 1, J. L. Pons, D. Torricelli, and M. Pajaro, Eds., ed: Springer Berlin Heidelberg, 2013, pp. 161-165.
- [117] S. Srivastava, P.-C. Kao, S. H. Kim, P. Stegall, D. Zanotto, J. S. Higginson, *et al.*, "Assist-as-needed robot-aided gait training improves walking function in individuals following stroke," *IEEE Transactions on Neural Systems and Rehabilitation Engineering*, vol. 23, pp. 956-963, 2015.
- [118] M. K. Holden, K. M. Gill, M. R. Magliozzi, J. Nathan, and L. Piehl-Baker, "Clinical gait assessment in the neurologically impaired reliability and meaningfulness," *Physical Therapy*, vol. 64, pp. 35-40, 1984.
- [119] A. Shumway-Cook and M. H. Woollacott, *Motor control: theory and practical applications*: Lippincott Williams & Wilkins, 1995.
- [120] L. Prosser and A. Canby, "Further validation of the Elderly Mobility Scale for measurement of mobility of hospitalized elderly people," *Clinical Rehabilitation*, vol. 11, pp. 338-343, 1997.
- [121] K. Berg, "Measuring balance in the elderly: preliminary development of an instrument," *Physiotherapy Canada*, vol. 41, pp. 304-311, 1989.
- [122] D. Podsiadlo and S. Richardson, "The timed "Up & Go": a test of basic functional mobility for frail elderly persons," *Journal of the American geriatrics Society*, vol. 39, pp. 142-148, 1991.
- [123] J. F. Israel, D. D. Campbell, J. H. Kahn, and T. G. Hornby, "Metabolic costs and muscle activity patterns during robotic-and therapist-assisted treadmill walking in individuals with incomplete spinal cord injury," *Physical therapy*, vol. 86, pp. 1466-1478, 2006.
- [124] J. Rueterbories, E. G. Spaich, B. Larsen, and O. K. Andersen, "Methods for gait event detection and analysis in ambulatory systems," *Medical Engineering & Physics*, vol. 32, pp. 545-552, 2010.
- [125] M. K. Holden, K. M. Gill, and M. R. Magliozzi, "Gait assessment for neurologically impaired patients Standards for outcome assessment," *Physical Therapy*, vol. 66, pp. 1530-1539, 1986.
- [126] F. M. Collen, D. T. Wade, and C. M. Bradshaw, "Mobility after stroke: reliability of measures of impairment and disability," *Disability & Rehabilitation*, vol. 12, pp. 6-9, 1990.
- [127] S. Adams, R. Pickering, A. Ashburn, and N. Lincoln, "The scalability of the Rivermead Motor Assessment in nonacute stroke patients," *Clinical Rehabilitation*, vol. 11, pp. 52-59, 1997.
- [128] C. Collin, D. Wade, S. Davies, and V. Horne, "The Barthel ADL Index: a reliability study," *Disability & Rehabilitation*, vol. 10, pp. 61-63, 1988.
- [129] J. Sanford, J. Moreland, L. R. Swanson, P. W. Stratford, and C. Gowland, "Reliability of the Fugl-Meyer assessment for testing motor performance in patients following stroke," *Physical Therapy*, vol. 73, pp. 447-454, 1993.
- [130] G. Demeurisse, O. Demol, and E. Robaye, "Motor evaluation in vascular hemiplegia," *European neurology*, vol. 19, pp. 382-389, 1980.
- [131] N. Neckel, M. Pelliccio, D. Nichols, and J. Hidler, "Quantification of functional weakness and abnormal synergy patterns in the lower limb of individuals with chronic stroke," *Journal of NeuroEngineering and Rehabilitation*, vol. 3, p. 17, 2006.

References

- [132] N. D. Neckel, N. Blonien, D. Nichols, and J. Hidler, "Abnormal joint torque patterns exhibited by chronic stroke subjects while walking with a prescribed physiological gait pattern," *Journal of NeuroEngineering and Rehabilitation*, vol. 5, p. 19, 2008.
- [133] D. H. Sutherland, "The evolution of clinical gait analysis part III—kinetics and energy assessment," *Gait & Posture*, vol. 21, pp. 447-461, 2005.
- [134] J. J. Craig, "Introduction to robotics: mechanics and control," 2004.
- [135] A. Belli, P. Bui, A. Berger, A. Geysant, and J.-R. Lacour, "A treadmill ergometer for three-dimensional ground reaction forces measurement during walking," *Journal of Biomechanics*, vol. 34, pp. 105-112, 2001.
- [136] J. Hidler, "Robotic-assessment of walking in individuals with gait disorders," in *Engineering in Medicine and Biology Society, 2004. IEMBS'04. 26th Annual International Conference of the IEEE*, 2004, pp. 4829-4831.
- [137] A. J. del-Ama, J. C. Moreno, A. Gil-Agudo, A. de-los-Reyes, and J. L. Pons, "Online assessment of human-robot interaction for hybrid control of walking," *Sensors*, vol. 12, pp. 215-225, 2011.
- [138] M. H. Granat, D. J. Maxwell, C. J. Bosch, A. C. b. Ferguson, K. R. Lees, and J. C. Barbenel, "A body-worn gait analysis system for evaluating hemiplegic gait," *Medical Engineering & Physics*, vol. 17, pp. 390-394, 1995.
- [139] S. Galen, C. Clarke, D. Allan, and B. Conway, "A portable gait assessment tool to record temporal gait parameters in SCI," *Medical engineering & physics*, vol. 33, pp. 626-632, 2011.
- [140] K. Zhang, M. Sun, D. Kevin Lester, F. Xavier Pi-Sunyer, C. N. Boozer, and R. W. Longman, "Assessment of human locomotion by using an insole measurement system and artificial neural networks," *Journal of Biomechanics*, vol. 38, pp. 2276-2287, 2005.
- [141] H. Kazerooni, R. Steger, and L. Huang, "Hybrid control of the berkeley lower extremity exoskeleton (bleex)," *The International Journal of Robotics Research*, vol. 25, pp. 561-573, 2006.
- [142] P. H. Veltink, C. Liedtke, E. Droog, and H. van der Kooij, "Ambulatory measurement of ground reaction forces," *Neural Systems and Rehabilitation Engineering, IEEE Transactions on*, vol. 13, pp. 423-427, 2005.
- [143] C. Liedtke, S. A. Fokkenrood, J. T. Menger, H. van der Kooij, and P. H. Veltink, "Evaluation of instrumented shoes for ambulatory assessment of ground reaction forces," *Gait & Posture*, vol. 26, pp. 39-47, 2007.
- [144] T. Liu, Y. Inoue, and K. Shibata, "A wearable ground reaction force sensor system and its application to the measurement of extrinsic gait variability," *Sensors*, vol. 10, pp. 10240-10255, 2010.
- [145] L. Bueno, F. Brunetti, A. Frizera, and J. Pons, "Human-robot cognitive interaction," *Wearable Robots: Biomechatronic Exoskeletons*, vol. 1, pp. 87-126, 2008.
- [146] K. Kasaoka and Y. Sankai, "Predictive control estimating operator's intention for stepping-up motion by exo-skeleton type power assist system HAL," in *Intelligent Robots and Systems, 2001. Proceedings. 2001 IEEE/RSJ International Conference on*, 2001, pp. 1578-1583.

References

- [147] C. Lagoda, J. C. Moreno, and J. L. Pons, "Human-robot interfaces in exoskeletons for gait training after stroke: State of the art and challenges," *Applied Bionics and Biomechanics*, vol. 9, pp. 193-203, 2012.
- [148] V. Hömberg, "Neurorehabilitation approaches to facilitate motor recovery," *Handbook of clinical neurology*/edited by PJ Vinken and GW Bruyn, vol. 110, p. 161, 2013.
- [149] G. S. Sawicki and D. P. Ferris, "A pneumatically powered knee-ankle-foot orthosis (KAFO) with myoelectric activation and inhibition," *Journal of neuroengineering and rehabilitation*, vol. 6, p. 23, 2009.
- [150] X. Jin, X. Cui, and S. K. Agrawal, "Design of a cable-driven active leg exoskeleton (c-alex) and gait training experiments with human subjects," in *2015 IEEE International Conference on Robotics and Automation (ICRA)*, 2015, pp. 5578-5583.
- [151] C.-P. Chou and B. Hannaford, "Measurement and modeling of McKibben pneumatic artificial muscles," *IEEE Transactions on Robotics and Automation*, vol. 12, pp. 90-102, 1996.
- [152] T.-Y. Choi, B.-S. Choi, and K.-H. Seo, "Position and compliance control of a pneumatic muscle actuated manipulator for enhanced safety," *Control Systems Technology, IEEE Transactions on*, vol. 19, pp. 832-842, 2011.
- [153] P. Beyl, M. V. Damme, R. V. Ham, B. Vanderborght, and D. Lefeber, "Pleated Pneumatic Artificial Muscle-Based Actuator System as a Torque Source for Compliant Lower Limb Exoskeletons," *IEEE/ASME Transactions on Mechatronics*, vol. 19, pp. 1046-1056, 2014.
- [154] J. Cao, S. Q. Xie, R. Das, and G. L. Zhu, "Control Strategies for effective robot assisted gait rehabilitation: The state of art and future prospects," *Medical Engineering & Physics*, vol. 36, pp. 1555-1566, 2014.
- [155] P. Beyl, M. Van Damme, P. Cherelle, and D. Lefeber, "Safe and compliant guidance in robot-assisted gait rehabilitation using Proxy-based Sliding Mode Control," in *Rehabilitation Robotics, 2009. ICORR 2009. IEEE International Conference on*, 2009, pp. 277-282.
- [156] J. Perry, *Gait analysis : normal and pathological function* Thorofare, NJ : SLACK, c2010., 2010.
- [157] T.-S. Kuan, J.-Y. Tsou, and F.-C. Su, "Hemiplegic gait of stroke patients: The effect of using a cane," *Archives of Physical Medicine and Rehabilitation*, vol. 80, pp. 777-784, 1999/07/01 1999.
- [158] M.-K. Chang, "An adaptive self-organizing fuzzy sliding mode controller for a 2-DOF rehabilitation robot actuated by pneumatic muscle actuators," *Control Engineering Practice*, vol. 18, pp. 13-22, 2010.
- [159] G. Andrikopoulos, G. Nikolakopoulos, and S. Manesis, "Advanced Nonlinear PID-Based Antagonistic Control for Pneumatic Muscle Actuators," *IEEE Transactions on Industrial Electronics*, vol. 61, pp. 6926-6937, 2014.
- [160] J. H. Lilly and L. Yang, "Sliding mode tracking for pneumatic muscle actuators in opposing pair configuration," *IEEE Transactions on Control Systems Technology*, vol. 13, pp. 550-558, 2005.
- [161] J. Perry and J. M. Burnfield, "Gait analysis: normal and pathological function," 1992.

References

- [162] D. A. Winter, *Biomechanics and motor control of human movement*: John Wiley & Sons, 2009.
- [163] X. Shen, "Nonlinear model-based control of pneumatic artificial muscle servo systems," *Control Engineering Practice*, vol. 18, pp. 311-317, 2010.
- [164] D. J. Reinkensmeyer, J. L. Emken, and S. C. Cramer, "Robotics, motor learning, and neurologic recovery," *Annu. Rev. Biomed. Eng.*, vol. 6, pp. 497-525, 2004.
- [165] D. Reynolds, D. Repperger, C. Phillips, and G. Bandry, "Modeling the dynamic characteristics of pneumatic muscle," *Annals of Biomedical Engineering*, vol. 31, pp. 310-317, 2003.
- [166] V. L. Nickel, J. Perry, and A. L. Garrett, "Development of useful function in the severely paralyzed hand," *The Journal of Bone & Joint Surgery*, vol. 45, pp. 933-952, 1963.
- [167] K. Inoue, "Rubbertuators and applications for robots," in *Proceedings of the 4th international symposium on Robotics Research*, 1988, pp. 57-63.
- [168] D. G. Caldwell, N. Tsagarakis, and G. Medrano-Cerda, "Bio-mimetic actuators: polymeric pseudo muscular actuators and pneumatic muscle actuators for biological emulation," *Mechatronics*, vol. 10, pp. 499-530, 2000.
- [169] E. Kelasidi, G. Andrikopoulos, G. Nikolakopoulos, and S. Manesis, "A survey on pneumatic muscle actuators modeling," in *Industrial Electronics (ISIE), 2011 IEEE International Symposium on*, 2011, pp. 1263-1269.
- [170] B. Tondu and P. Lopez, "Modeling and control of McKibben artificial muscle robot actuators," *Control Systems, IEEE*, vol. 20, pp. 15-38, 2000.
- [171] J. Sarosi, "New approximation algorithm for the force of Fluidic Muscles," in *Applied Computational Intelligence and Informatics (SACI), 2012 7th IEEE International Symposium on*, 2012, pp. 229-233.
- [172] A. McDaid, K. Kora, S. Xie, J. Lutz, and M. Battley, "Human-inspired robotic exoskeleton (HuREx) for lower limb rehabilitation," in *Mechatronics and Automation (ICMA), 2013 IEEE International Conference on*, 2013, pp. 19-24.
- [173] D. G. Caldwell, G. A. Medrano-Cerda, and M. Goodwin, "Control of pneumatic muscle actuators," *IEEE Control Systems*, vol. 15, pp. 40-48, 1995.
- [174] P. Carbonell, Z. Jiang, and D. Repperger, "Nonlinear control of a pneumatic muscle actuator: backstepping vs. sliding-mode," in *Control Applications, 2001.(CCA'01). Proceedings of the 2001 IEEE International Conference on*, 2001, pp. 167-172.
- [175] S. W. Chan, J. H. Lilly, D. W. Repperger, and J. E. Berlin, "Fuzzy PD+I learning control for a pneumatic muscle," in *Fuzzy Systems, 2003. FUZZ '03. The 12th IEEE International Conference on*, 2003, pp. 278-283 vol.1.
- [176] T. D. C. Thanh and K. K. Ahn, "Nonlinear PID control to improve the control performance of 2 axes pneumatic artificial muscle manipulator using neural network," *Mechatronics*, vol. 16, pp. 577-587, 2006.
- [177] J. Huang, J. Qian, L. Liu, Y. Wang, C. Xiong, and S. Ri, "Echo state network based predictive control with particle swarm optimization for pneumatic muscle actuator," *Journal of the Franklin Institute*, vol. 353, pp. 2761-2782, 2016.

References

- [178] M. Van Damme, B. Vanderborght, R. Van Ham, B. Verrelst, F. Daerden, and D. Lefeber, "Proxy-based sliding mode control of a manipulator actuated by pleated pneumatic artificial muscles," in *IEEE International Conference on Robotics and Automation*, 2007, pp. 4355-4360.
- [179] K. Xing, J. Huang, Y. Wang, J. Wu, Q. Xu, and J. He, "Tracking control of pneumatic artificial muscle actuators based on sliding mode and non-linear disturbance observer," *IET control theory & applications*, vol. 4, pp. 2058-2070, 2010.
- [180] H. Aschemann and D. Schindele, "Sliding-mode control of a high-speed linear axis driven by pneumatic muscle actuators," *IEEE Transactions on Industrial Electronics*, vol. 55, pp. 3855-3864, 2008.
- [181] A. Sala, *Multivariable control systems an engineering approach*. London: London : Springer c2004., 2004.
- [182] J.-J. E. Slotine and W. Li, *Applied nonlinear control* vol. 199: Prentice-Hall Englewood Cliffs, NJ, 1991.
- [183] M. Smaoui, X. Brun, and D. Thomasset, "Systematic control of an electropneumatic system: integrator backstepping and sliding mode control," *IEEE Transactions on Control Systems Technology*, vol. 14, pp. 905-913, 2006.
- [184] K. D. Young, V. I. Utkin, and U. Ozguner, "A control engineer's guide to sliding mode control," *IEEE transactions on control systems technology*, vol. 7, pp. 328-342, 1999.
- [185] H. P. von Schroeder, R. D. Coutts, P. D. Lyden, and V. L. Nickel, "Gait parameters following stroke: a practical assessment," *Journal of rehabilitation research and development*, vol. 32, p. 25, 1995.
- [186] J. Hoogen, R. Riener, and G. Schmidt, "Control aspects of a robotic haptic interface for kinesthetic knee joint simulation," *Control Engineering Practice*, vol. 10, pp. 1301-1308, 2002.
- [187] L.-W. Tsai, *Robot analysis : the mechanics of serial and parallel manipulators / Lung-Wen Tsai*: New York : Wiley c1999., 1999.
- [188] K. P. Westlake and C. Patten, "Pilot study of Lokomat versus manual-assisted treadmill training for locomotor recovery post-stroke," *Journal of NeuroEngineering and Rehabilitation*, vol. 6, p. 18, 2009.
- [189] H. T. Tran, H. Cheng, H. Rui, X. Lin, M. K. Duong, and Q. Chen, "Evaluation of a Fuzzy-Based Impedance Control Strategy on a Powered Lower Exoskeleton," *International Journal of Social Robotics*, vol. 8, pp. 103-123, 2016.
- [190] S. Q. Xie and P. K. Jamwal, "An iterative fuzzy controller for pneumatic muscle driven rehabilitation robot," *Expert Systems with Applications*, vol. 38, pp. 8128-8137, 7// 2011.
- [191] J. Yang, H. Su, Z. Li, D. Ao, and R. Song, "Adaptive control with a fuzzy tuner for cable-based rehabilitation robot," *International Journal of Control, Automation and Systems*, vol. 14, pp. 865-875, 2016.
- [192] M. S. Ayas and I. H. Altas, "Fuzzy logic based adaptive admittance control of a redundantly actuated ankle rehabilitation robot," *Control Engineering Practice*, vol. 59, pp. 44-54, 2// 2017.
- [193] E. H. Mamdani and S. Assilian, "An experiment in linguistic synthesis with a fuzzy logic controller," *International journal of man-machine studies*, vol. 7, pp. 1-13, 1975.

References

- [194] S. Hussain, S. Q. Xie, and P. K. Jamwal, "Control of a robotic orthosis for gait rehabilitation," *Robotics and Autonomous Systems*, 2013.
- [195] Y. Ma, S. Xie, and Y. Zhang, "A patient-specific EMG-driven neuromuscular model for the potential use of human-inspired gait rehabilitation robots," *Computers in Biology and Medicine*, vol. 70, pp. 88-98, 3/1/ 2016.